NOTICE

The quality of this microform is heavily dependent upon the quality of the original thesis submitted for microfilming. Every effort has been made to ensure the highest quality of reproduction possible.

If pages are missing, contact the university which granted the degree.

Some pages may have indistinct print especially if the original pages were typed with a poor typewriter ribbon or if the university sent us an inferior photocopy.

Reproduction in full or in part of this microform is governed by the Canadian Copyright Act, R.S.C. 1970, c. C-30, and subsequent amendments.

AVIS

La qualité de cette microforme dépend grandement de la qualité de la thèse soumise au microfilmage. Nous avons tout fait pour assurer une qualité supérieure de reproduction.

S'il manque des pages, veuillez communiquer avec l'université qui a conféré le grade.

La qualité d'impression de certaines pages peut laisser à désirer, surtout si les pages originales ont été dactylographiées à l'aide d'un ruban usé ou si l'université nous a fait parvenir une photocopie de qualité inférieure.

La reproduction, même partielle, de cette microforme est soumise à la Loi canadienne sur le droit d'auteur, SRC 1970, c. C-30, et ses amendements subséquents.

Dynamics of Liquid Sloshing in Road Containers

Gennady Popov

A Thesis

in

The Faculty

of

Engineering

Presented in Partial Fulfilment of the Requirements

for the Degree of Doctor of Philosophy at

Concordia University

Montreal, Quebec, Canada

September 1991

ISBN 0-315-68710-X

ABSTRACT

DYNAMICS OF LIQUID SLOSHING IN ROAD CONTAINERS

Gennady Popov, Ph.D.
Concordia University, 1991

The behaviour of liquids in tanker vehicles, subjected to different road manoeuvres, has been identified as an important problem in the transportation of liquid cargoes and related industry. Some solutions of this problem are presented in this investigation. The analytical steady-state and numerical transient liquid responses are carried out for rectangular and circular cross-section containers undergoing a braking, acceleration, or a steady cornering manoeuvres. The solutions are obtained in terms of the main loading factors, such as the liquid forces, overturning moments, heights of the free surface, and the damped frequencies of liquid vibrations. The influence of the various input parameters on the liquid load is investigated.

A comprehensive nonlinear liquid slosh model, represented by the two-dimensional Navier-Stokes, the continuity, and the free-surface differential equations, is solved numerically in an Eulerian mesh using the finite difference methodology. A special attention is devoted to the boundary conditions implementation, for which purposes, the interpolation-reflection technique of the boundary conditions definition is developed for containers of an arbitrary shape. The dynamic slosh model is validated through the laboratory experimental testing and then is applied to investigate the liquid response in the partially filled rectangular and cylindrical circular containers. The transient

solutions are obtained for the variation of the input parameters in a wide range, which is significantly superior of that given by a linear slosh model. Within the applicability of the linear theory, the computed and theoretical results compare well, which together with experimental testing underscore a high degree of confidence in the simulation of a complicated sloshing problem.

A parametric study and following optimization analysis, carried out for steady-state liquid response, yield an optimal height for rectangular containers that minimizes the overturning moment in a wide range of input accelerations and show that the optimal container height is lying in the feasible designing region.

The present work provides a new information about the liquid behaviour in road containers and gives a powerful tool to investigate directional dynamics of vehicles carrying liquids.

ACKNOWLEDGEMENTS

The author is deeply grateful to his supervisors, Prof. T.S. Sankar and Prof. S. Sankar, for their continued guidance and encouragement during the course of this work.

The author is grateful to Dr. G.H. Vatistas for consultations and discussions related to fluid dynamics topics.

The author is grateful to Mrs. S. Nayak and Ms. A. Zimmerman for their sincere efforts in typing the manuscript.

The financial support of the CONCAVE Research Centre and the Department of Mechanical Engineering of Concordia University is thankfully acknowledged.

Finally, the author would like to express his appreciation of the devotion and understanding of his wife, Galina, during the course of this undertaking.

TABLE OF CONTENTS

LIST OF FIGURES

LIST OF TABLES

NOMENCLATURE

Dimensional Quantities

a	horizontal input acceleration
a_o	cross-sectional area of the container
a_ℓ	cross-sectional area occupied by the liquid
b	width of the container
D_o	diameter of cylindrical circular container, characteristic length
f_H, f_{HSS}	horizontal component of the force in transient and steady-state respectively
f_V, f_{VSS}	vertical component of the force in transient and steady-state respectively
g	gravitational acceleration
g_x, g_y	horizontal and vertical unit body forces respectively in rectilinear motion of the container
g_n	horizontal unit body force in the middle of the container in rotational motion
h_o	height of the container
h_{ss}	height of the liquid free surface in steady-state
h_{in}	initial fill level of the container
i,j,k	dimensions of the computational mesh, integers
L_o	characteristic length equal to the container length for longitudinal direction or to the width for transversal direction
m, m_{ss}	overturning moment in transient and steady-state respectively
p	pressure
P_o	characteristic pressure equal to the atmospheric pressure in transient and to $\rho g L_o$ in statics
R	radius of the track curvature

t	time
T_0	characteristic time
V_0	characteristic velocity
ν	kinematic viscosity of the liquid
ρ	mass density of the liquid
ω	angular velocity of the container
Ω	circular frequency of liquid vibration

Non-dimensional Quantities

A_0	cross-sectional area of the container
A_ℓ	cross-sectional area occupied by the liquid
C_{FH}, C_{FV}	dynamic coefficients of the horizontal and vertical forces equal to the ratios of the peak dynamic forces to the corresponding steady-state forces
C_M	dynamic coefficient of the overturning moment equal to the ratio of the peak dynamic moment to the steady-state moment
f	fill level as the ratio of the dimensional fill level to the characteristic length
F_H, $F_{H,SS}$	horizontal liquid forces in transient and steady-state
F_V, F_{VSS}	vertical liquid forces in transient and steady-state
G_x, G_y	unit body forces in horizontal and vertical directions respectively as the ratios of the corresponding dimensional body forces to the gravity acceleration
G_n	unit body force in the middle of the container in rotational motion as the ratio to the gravity acceleration
h	geometrical parameter for rectangular containers as the ratio of the container height to the characteristic length
H, H_{SS}	heights of the free surface as the ratios to the characteristic length in transient and steady-state
k	number of a compartment

K	normalized frequency of liquid vibration
K_{th}	normalized frequency of liquid vibration from the linear theory
M, M_{ss}	overturning moments in transient and steady-state as the ratios of the corresponding dimensional moment to the product of the liquid weight times the characteristic length
n	number of compartments of the container
P	pressure as the ratio of the dimensional pressure to the characteristic pressure in transient and to the product $\rho g L_0$ in steady-state
T	time as the ratio to the characteristic time
U,V	horizontal and vertical components of the flow velocities as the ratios to the characteristic velocity
X-Y	system of coordinates moving with the container
δ	track curvature parameter as the ratio of the radius of container rotation to the characteristic length
η-ξ	fixed system of coordinates located in the centre of rotation of the container
τ-n	local system of coordinates tangent-normal to the boundary

Nondimensional Groups

Eu	Euler number, $P_0/\rho V_0^2$
Fr	Froude number, V_0^2/gL_0
Re	Reynolds number, $V_0 L_0/\nu$
St	Strouhal number, $L_0/T_0 V_0$
Π	parameter linking the pressure in transient and in steady-state, $P/P_{ss} = \rho g L_0 / P_0 = 1/FrEu$

Note: the quantities listed above may be encountered in the text with additional subscripts or overscripts. For example, overscripts c and b, used with forces and moments, express these values for compartmented and baffled containers respectively. Wherever the new scripts are met, they are explained in the text.

CHAPTER 1

INTRODUCTION AND LITERATURE REVIEW

1.1 General

Dynamics of liquid motion in bulk transportation is unique in that the interaction of the liquid with the moving vehicle significantly affects the stability and controllability of the tank vehicle. The liquid motion in transporting containers, often called "sloshing", is a very important problem especially if it is related to toxic, flammable, and other dangerous liquids. The extensive statistical data, collected by the National Transportation Safety Board, the American Association of Automobiles, the U.S. Department of Transportation and other organizations, gives a clear view of the seriousness of the problem. For example, fatalities and damages related to transportation of dangerous liquids in the U.S.A. during 1979 [1] were: accident - 17,324; injuries - 941; damages - 14,733 in terms of millions of dollars; and fatalities - 18. Other sources indicate that a large number of road accidents are rollovers of the liquid carrying vehicles. By estimation from University of Michigan Transportation Research Institute, the number of single vehicle rollovers per year for all trucks of the tractor, semi-trailer type can reach in North America as many as 4,800 [2], while the statistics of Federal Highway Administration of DOT shows 2872 rollovers per year in non-collision accidents. The analysis of the road accidents involving single tank vehicle on Canadian roads during 1981-83 [3] shows that most of the accidents occurred while performing a cornering or lane change manoeuvre, when the liquid sloshing was considered as a major factor

contributing for the vehicle accident. Although the existing data is often incomplete and even contradictory, it identifies the problem of truck stability against a rollover, due to sloshing and other related factors, as an important issue.

A great number of investigations on liquid sloshing has been carried out since the sixties in different fields of application: space vehicles, large ground tanks and canals, cargo ships, and road vehicles. A variety of approaches to solve the sloshing problem due to different requirements, tank characteristics, and peculiarities of input disturbance gives different, sometimes contradictory, results which may not be directly applied to the road tanker design. The most important problem associated with the transport of liquid cargo is the problem of stability of the vehicle under a sudden manoeuvre such as straight-line braking, lane change, cornering, and simultaneous turning and braking. These manoeuvres, executed at limit performance of the vehicle, can lead to jackknifing, trailer swing, plow out or rollover of the latter, among which the rollover is the most dangerous mode of instability arising during the cornering, lane change, or braking in a turn manoeuvres.

During the last two decades, a significant effort has been made to develop analytical solutions, computer simulations, and experimental investigations to improve the performance of the vehicle transporting liquid cargo. One of the most general and logical approaches is to simulate the liquid motion with the Navier-Stokes and continuity equations together with the free-surface equation and appropriate boundary conditions. However, the analytical solution of such a system of nonlinear differential equations is not yet known. The existing

linear theories of sloshing are based on the assumptions of inviscid incompressible fluid, where a velocity potential exists, and on small amplitudes of fluid motion compared with container dimensions, often with the depth of the fluid. This leads to a significant simplification of the momentum equations which, upon introducing the velocity potential function, neglecting the viscous terms, and combining the resulting equations with the continuity equation, result in a linear second order Laplace's equation that can be solved analytically. The difficulties due to the free-surface equation are overcome either by neglecting the nonlinear terms under the assumption that the wave height and the fluid velocities are small or by linearization of this equation and eliminating the liquid height from the set. This gives rise to the linear or linearized sloshing theories respectively. In reality, the fluid motion may not be assumed small in amplitude. Moreover, strong nonlinearities introduced by the boundary conditions, when the wall shape drastically changes as for a rectangular tank, for example, and the damping, neglected in the linear theories, may have a significant role in the whole process. The complete nonlinear problems of a viscous liquid in road containers under different types of vehicle manoeuvre are not extensively investigated. Also, the questions related to the damped natural frequencies of sloshing and magnitudes of liquid forces and overturning moments are not answered yet.

The only effective means in reducing the slosh loading, actually accepted in the design, are the separating walls or baffles both used as cross-sectional walls and, therefore, being effective in longitudinal dynamics. The influence of separating walls is not studied enough, and the design concepts of compartmented and baffled tanks do not have a

solid theoretical basis. They are designed rather based on the strength analysis than on the stability considerations. The number of separating walls and baffles, as well as location and size of the baffle orifices are chosen intuitively and their effect on slosh load have not been studied in relation to road containers.

The lack of theoretical and experimental investigations of liquid cargo behaviour is due to difficulties of solutions of the governing equations and to the high risk of experimental limit performance studies. Most of the reported analytical and experimental studies on liquid motion are related to harmonic excitation of containers. The road vehicles, however, may be subjected to other types of excitation including accelerations or decelerations due to different manoeuvres, aerodynamical forces, and others. The effect of manoeuvre has to be investigated in terms of slosh loading parameters, such as forces and overturning moment, for different shapes of containers.

The behaviour of the coupled "liquid-vehicle" system is recognized as an important problem for vehicle stability. Despite this fact, there is only a limited number of investigations in this area. Mostly, the models of such a system include linear slosh models which are restricted in application due to inherent limitations of the linear theory. Thus, the development of a sufficiently accurate and reasonably complex nonlinear slosh model is seen to be very practical and important goal.

1.2 Literature Review

The area related to liquid motion in moving containers includes a great number of analytical and experimental studies emphasizing on different aspects of this problem. During the course of this

investigation, nearly fifty of the most important works has been reviewed in the two classifying groups. The first group includes physics of sloshing covering such subjects as flow patterns in containers, slosh loading parameters investigation, and development of slosh models. The second group concerns with numerical methods for solutions of the governing equations that are most widely used at the present time.

1.2.1 Physics of Sloshing

Probably the first and most complete study of sloshing problem, both theoretical based on linear approach and experimental, was conducted by Hutton in 1963 [4]. In this work, it has been shown that in some cases the linearized theory may correctly predict the liquid behaviour in a harmonically excited vertical cylindrical container. The theoretical and experimental results agree well if the amplitude of excitation is sufficiently small and the frequency of excitation is not in a narrow band of the resonance. It has been also observed three kinds of liquid motion: stable planar, unstable swirling, and stable nonplanar (rotary) motions which interchanged to each other while the frequency passes through the resonance. The theoretical analysis, based on the pure linear theory, gives only the steady planar harmonic motion for all frequencies except narrow resonance region for the harmonic excitation in one direction. Therefore, the experimentally observed nonplanar stable and unstable swirling motions are due to the nonlinear coupling between motions in different directions and to the viscous damping. Including the nonlinear effects on the free surface, Hutton has analytically obtained the rotary motion as well as the softening

effect for planar motion and the stiffening effect for nonplanar one. This study indicates that the coupling between liquid motions in different directions takes place through the free surface mainly, while the role of the viscosity and wall shape is of secondary significance. Thus, in partially filled containers, once induced planar motion may easily regenerate to a motion in other direction.

Further development of the sloshing problem was experimentally done by Abramson and other researchers in a series of investigations [5 - 10] in the middle sixties. They enlarged the scope of investigation using more combinations of excitation parameters and studying the force response of liquids in cylindrical and spherical tanks with separating walls. These studies have also shown the softening character of liquid sloshing and the presence of jump phenomena, as well as the unstable swirling and stable rotary motions while passing through the resonance. The large amplitude breaking wave has been observed near first-mode resonance; the wave, reaching a certain magnitude, breaks down and puts upper bound on its amplitude. This is accompanied by the change of the mode of vibration, and also, this limits lateral forces in the plane of excitation but creates forces in the direction perpendicular to excitation plane. The experimentally obtained liquid forces were compared with their analytical values from Hutton's theory. The difference does not exceed 15% for a sufficiently small excitation, equal approximately to 1% in terms of displacement with respect to the container diameter, that is, the analytical values are overestimated.

The approach similar to that used by Hutton has been employed by Moiseyev [11] to find the general solutions in terms of eigenvalues and eigenfunctions for free vibrations of the liquid and the liquid response

in terms of forced frequencies and velocity potential for forced vibrations basing the analysis on the linear approximation. The Moiseyev's theory cannot be, therefore, applied to the resonance region. One of the most important conclusions of this theory is that the sloshing frequencies are amplitude dependent, even in absence of damping. This fact has been confirmed by a number of experimental studies.

One approach to find the solutions of the sloshing problem is the use of the "water" wave theory. As an example of such a study, the shallow water wave theory was applied to compute the transient response of the liquid in a ground storage tank [12]. The linear wave theory yields the results very close to the experimental ones for sufficiently small liquid depth, between 10 and 30 % with respect to half of tank width, for nondimensional forcing amplitude of 0.005, and for excitation circular frequency around resonance. The good correlation is quite expected because of consistency of the input parameters with chosen theory. The deep water wave theory can also be applied to the slosh solution [13,14], however it will fail in the case of road containers with sufficiently high fill level when the interaction of the top container wall will destroy the waves and produce the liquid motion of a complex nature.

One of the basic characteristics of liquid motion in containers is natural frequencies. A number of studies dealt with this subject, but the most important results are summarized in Ref. [5] - (Abramson, 1966) and [15,16,17,18] - (Bauer, 1981, 1982, 1967, 1972). The natural frequencies are obtained from the solutions of the Laplace equation and the boundary conditions on rigid walls and free surface. The sets of

natural modal frequencies were found for different geometrical shapes of containers: rectangular, upright circular, and inverted parabolic by Bauer and others [17,18] and for horizontal cylindrical and spherical containers by Lamb [19], Budiansky [20], and Graham and Rodriguez [21]. These investigations show that natural frequencies strongly depend on the shape and fill level of the container. For rectangular containers, the frequencies increase with increasing of the fill level. They were first found by Lamb and lately generalized by Graham and Rodriguez in the form:

$$\Omega_m = \sqrt{(2m+1)\frac{\pi g}{L_0}\tanh\left[(2m+1)\frac{\pi h_0}{L_0}\right]}$$

where the integer m defines the order of the natural frequency and the corresponding mode for vibration in the direction of L_0. A similar expression can be obtained for frequencies associated with vibration in the direction perpendicular to L_0. For simultaneous vibrations in both directions, the motions will be coupled.

For a horizontal cylindrical container the natural frequencies were analytically investigated by Lamb and Budiansky and experimentally by McCarty and Stephens [22]. Lamb approximated the fundamental frequency by the Rayleigh's method for 50% filled container in terms of the gravity acceleration and container diameter as

$$\Omega_1 = 1.169\,(2g/D_0)^{1/2},$$

while Budiansky gave the approximate values for this frequency in terms of eigenvalues for nearly full, 50% filled, and nearly empty container as:

$$\Omega_1 = \left(2\lambda_1 \, g/D_0 \right)^{1/2}$$

where

$\lambda_1 \approx \pi/3 \left[f \, (1 - f) \right]^{1/2}$ nearly full container

$\lambda_1 \approx 1/3 \left(\frac{2}{\pi} - \frac{\pi}{8} \right)$ 50% filled container

$\lambda_1 = 1$ nearly empty container

and the fill level f is with respect to the container diameter.

The analytical and experimental frequencies correlate well for small vibrations of the liquid. The fundamental frequency in the transverse direction increases monotonically and slowly with the fill level for small f's and progressively faster with increase of the f. For the fill level tending to 1, the frequency reaches to infinity. The frequencies for higher modes have strongly pronounced maxima at $f \approx 0.5$

The natural frequencies in trapezoidal tanks with converging or diverging upward walls were investigated analytically by Bauer [15]. In the transverse direction for a converging tank, the frequencies increase with the fill level, while in a diverging tank they increase very rapidly for small f's and then remain almost constant. In the longitudinal direction, the frequencies for both trapesoidal tanks behave as in the case of the rectangular tank, i.e. they slowly increase with the fill level.

Most of the above considered results are based on linear theories of sloshing which give undamped frequencies and do not take into account the nonlinearities of the problem. The damping, neglected in these theories, may have a sufficiently weak influence on the magnitudes of

frequencies in the case of road containers since most of the transported liquids are characterized by small or moderate viscosity. The neglecting of nonlinear effects, such as, for example, introduced by interaction of the top and bottom container walls, may totally discredit the linear approach. Hence, a fluid slosh model taking into account the most important nonlinearities and including damping is needed to correctly predict the frequencies of liquid oscillation.

Much effort was made to investigate the interaction between liquids and separating walls [15,16] and [23 - 27]. The combined effect of the separating walls is as follows:

- reducing of the amplitude of liquid vibration in terms of the free-surface heights and, consequently, of slosh loading; and
- augmenting of natural frequencies compared with those of uncompartmented containers.

Usually, the separating walls are thin compared with main container walls and, therefore being elastic, they do not give the complete effect expected from them. This question was investigated by Bauer [16] on the example of the single elastic separating wall in rectangular and circular containers. His analysis shows that the coupled sloshing frequency is very close to the uncoupled frequency of the liquid vibration, which indicates that the wall stiffness is not an essential factor in affecting the sloshing process in a considered compartment.

The influence of number of baffles and the size of their orifices was studied by Partom [27] who numerically estimated the equivalent moment of inertia of a liquid in a vertical cylindrical container with radial separating walls. The calculations, based on the linear slosh theory, reveal that the role of partial separating walls is such that

their effect is significantly reduced if partitions are not full even by a small amount. This fact suggests that the baffled orifices in road containers must be kept closed during transportation in order to gain from the baffles as much as possible. Presently, the separating walls, being the only effective means in reducing the sloshing loads, are widely used in the design of liquid tankers. However, the present theories do not give a quantitative analysis of their influence on sloshing. The experimental results, obtained by Strandberg [28] showed the tremendous influence of the separating walls installed longitudinally in reduction of lateral sloshing loads. Despite this fact, the longitudinal partitions did not receive any attention from the manufacturers because of their additional weight and technological complexity.

Most of the studies, both theoretical and experimental, deal with the response of liquids subjected to harmonic disturbances. There are only a few which consider the sloshing under an arbitrary excitation. The earthquake sloshing in cylindrical water tanks undergoing an arbitrary ground motion was studied by Aslam et al. [29]. The comparison of analytical and experimental results showed a sufficiently good correlation between the both for a few first cycles of vibration. However with time, the discrepancy increases and, for an annular tank, for example, and for amplitude of liquid height at the inner wall, the computed height is as twice as small compared with the experimental one. This fact is doubtful since in the assumed linear theory the damping was neglected. Such a discrepancy can be attributed to a large amount of artificial or computational viscosity or to an incorrect treatment of the boundary conditions. In that study, it has also been found, both

analytically and experimentally, that the flexibility of the tank wall has little effect on the sloshing response which correlates quite well with the Bauer's investigation [16].

Summarizing the results of the previous research, it can be said that actually two theories of sloshing are used in the design of liquid tankers, i.e., the linear and the linearized. The latter includes nonlinearities of the free surface but does not include the damping and both theories give approximate values of sloshing parameters. Comparison with experiments shows that both theories predict quite accurately the slosh frequencies and less, or significantly less, accurately the slosh loading. Those theories can not be applied for sloshing near resonant frequencies nor for a sloshing with large amplitude.

The coupled problem associated with interaction of the sloshing liquid with the moving vehicle has been recognized as a crucial one in investigating of stability of the vehicle. Due to difficulties in obtaining solutions to this problem, there are, however, not many reported studies on this subject. One example of such an investigation is the report of Johns Hopkins University [30] where the numerical simulation technique, based on a three-dimensional linear slosh model, was used to study the limit performance of vehicles transporting liquids for variable fill level, cornering and braking manoeuvres, and compartmented and uncompartmented tanks. The main conclusions of this investigation are:

- The three-quarter full tank configuration is significantly less stable than all other configuration: (1/2, 3/4 and 7/8 fill levels have been investigated).

- The linearized assumptions of the slosh model may not be valid for limit manoeuvres.

That is, the authors admitted that a more accurate slosh model is needed for studying of the coupled problem characterized by a sufficiently strong sloshing.

Another approach for lateral stability analysis was used by Strandberg [28]. He combined the experimental and computer simulation techniques together. The slosh force in lateral direction was measured and recorded in a specially designed test set-up where the displacement of the container was simulated by a hydraulic servo-drive. Then, this force was used as an input to a hybrid computer software which solved a simplified vehicle model. Such a technique is very flexible in accounting for the slosh nonlinearities, but because of the vehicle model simplification, it restricts the degrees of freedom and, in principle, changes the motion of the system. Moreover, it does not provide the feedback between the liquid load and container body motions. Nonetheless, the results obtained are unique especially in connection with the role of longitudinal baffles. Introduction of the longitudinal baffles was, at that time, a new concept in the tank design first introduced by Lindström in 1976 [31]. The most important conclusions of the combined Lindström-Strandberg studies is that the circular cross-section tank is more stable than rectangular, elliptical, or super elliptical tanks because "the stability losses from the wider tank are larger than the gains from the lower center of gravity," and that the separating walls significantly increase the overturning and skidding stability. The practical recommendation given by Strandberg is that the compartment width must not exceed 0.6 m for a peak lateral acceleration

of 0.4 g's in order to provide a safe cornering or lane change manoeuvres.

A quasi-dynamic slosh model was developed and used to estimate the destabilizing effect of shifting cargo on the lateral stability of the tank vehicle by Sankar et al [32] and Ranganathan [33]. This approach assumes that the liquid moves in such a way that the free surface takes a position orthogonal to the total body force resulting from the gravity and lateral accelerations. The comparison of the results with those of an equivalent rigid cargo reveals that the liquid load shift depends upon the fill level, vehicle speed, and steer input and reaches a maximum at the fill level of 70%. An unfavourable combination of these parameters leads to a large magnitude of destabilizing forces that can cause the rollover of the vehicle. Although this approach does not predict the peak slosh loading, due to the liquid vibration, the computed mean values of the roll angle and estimation of the stability limits are in good agreement with the experimental results.

An approach based on a mechanical analogy which approximates the complicated sloshing by a simple equivalent mechanical system, usually by multi-degree of freedom system, has been very popular in the fifties and sixties [34 - 40]. The simplicity of the analogue equation allows to be easily combined with equations of vehicle motion for further analysis. But the complications, associated with definition of pendulum or spring-mass elements including their number, stiffnesses, and damping coefficients require the experimental investigations which, in principle, must be conducted for each specific problem. Too much in this matter depends on the researcher's experience and intuition since a good guess should be made prior to mathematical analysis and validation

of the equivalent system. Some good approximations have been made, for example, for the case of spherical container by Sayar [40] who returned to this problem a decade later (1981) and composed a mechanical system including a cubic spring for a pendulum mass which accurately simulates the slosh force for some values of the fill level but looses the accuracy for the other fillings. Thus, this method involves either experimental definition of the parameters of equivalent mechanical model or can be carried out by use of the linear slosh theory, but in this case, the approach looses its attractiveness since the linear analytical solutions are already available and the equivalent model, based on the linear theory, will have all limitations inherent by the theory.

All previous studies presented reveal the need for a more accurate mathematical model for fluid sloshing. Such a model can be represented by the incompressible Navier-Stokes and continuity equations together with the free-surface nonlinear equation and the appropriate boundary conditions along rigid walls and free surface. A brief discussion on the numerical techniques to solve this system of equations is presented in the next subsection.

1.2.2 Governing Equations and Methods of Solution

Various approaches and methods for solving of fluid flow problems are available. During the past few decades intensive research effort was made to develop efficient numerical procedures and to reduce excessive computer time. This is due to the fact that the exact theoretical analysis of partial differential equations of a flow is limited and has feasible solutions for the simplest cases of fluid motion. The set of governing equations includes the Navier-Stokes

equations, written with respect to the assumed system of coordinates, the continuity equation, and the free-surface equation which describes the kinematic condition at the free surface in terms of the free-surface velocities and slopes. The numerical solution of the set can be carried out separately for the Navier-Stokes and free-surface equations, however the latter imposes a constraint for the former because it defines the region where the Navier-Stokes equations have to be applied. The main difficulties in the solution of the whole system stem from the initial and boundary conditions. Usually, the initial conditions for a free-surface flow assume zero velocities for the entire flow and hydrostatic pressure distribution which corresponds to the initially motionless liquid. If, however, one intends to solve the problem from some specific state of the flow, a good guess has to be made which, in principle, is hardly possible. The boundary conditions at rigid wall can be either free- or no-slip type. Physically, the no-slip condition is correct, but in numerical calculation it may create an unrealistically large drag on the fluid. This question was investigated by Nichols and Hirt in 1971 [41] who found that depending on the flow Reynolds number, the conditions must be taken of one (free-slip for high Re) or another type. Some preliminary numerical study was undertaken in this investigation in order to verify this last statement which has been made heuristically. This matter will be discussed in Chapter 2.

The most broadly applicable computational methods to solve the Navier-Stokes equations are finite difference, finite element, and integral representation methods. The finite difference approach gives many techniques suitable to solve the viscous flow. If the governing equations are in the stream function-vorticity system, then the method

of Alternative Direction Implicit, ADI, of Peaceman and Rochford [42] or Successive Over-Relaxation, SOR, by Fox [43] and their later modifications described in [44,45] are more convenient. If the equations are used in the system of primitive variables, then the method of Implicit Continuous-fluid Eulerian, ICE, introduced by Harlow and Amsden [46] or its development, the Marker and Cell method, MAC, by Harlow and Welch [47] are more preferable. The history of computational fluid dynamics shows that no successful computation of problems with free surface has been accomplished in the stream function-vorticity formulation because of difficulties of boundary conditions imposition at the free surface.

Thus, the Marker and Cell method is now the most powerful technique to solve the sloshing problem. Lately, some modifications were brought to the MAC by their inventors [48], by Viecelli [49], by Chan and Street [50] and by other researchers. Amsden and Harlow introduced a simplified version of MAC, SMAC, where the pressure equation is not solved and the pressure itself is iterated to drive the velocities to the state when they satisfy the continuity condition. Viecelly has found a powerful technique of treating of curvilinear boundaries in a rectangular mesh by adjusting the pressure in the fictitious flow in such a way that the liquid is forced to move along the boundary. And Chan and Street introduced the Stanford University Modified MAC, SUMMAC, in which they improved the free surface-boundary treatment. One of the specific features of the MAC method is the use of a staggered grid. It has been shown by Patankar [51] that the staggered grid improves the computational stability of the central differences discretization by making disappear the difficulties due to the first derivatives

representing the convective terms.

The finite element approach is also successful for solving of many fluid flow problems. The methodology is based on minimizing of a related functional and the methods form two basic groups, i.e., conventional finite element methods, FEM, [52,53] and boundary element methods, BEM, [54]. These methods as well as the fluid-in-cell method, FLIC, were used by Washizu [54] to study liquid sloshing in a rectangular tank. Unfortunately, the correlation between these methods may not be established because the author used different input disturbances for the three cases of study. Nevertheless, it has been shown that all three numerical techniques can be successfully applied to the free-surface flow problem. Although the finite element methods have received a substantial development in the eighties, they did not remove all difficulties associated with finite difference methods. In particular, they did not essentially reduce the computer time, especially for problems with simple geometries, and did not increase the accuracy of solutions for problems with high Reynolds number. Some of the essential drawbacks of the finite element approach are its conceptional complexity and that fact that the variational principle may not necessarily exist for all differential equations of interest.

The integral representation approach in connection to the liquid flow problems was initiated, a decade and a half ago, by Wu [55]. This group of methods is based on the concept of fundamental solutions of differential equations and on the use of finite element technique. The governing equations are recast into the form of integral representations containing an integral over the fluid domain and an integral over the fluid boundary, then, they are solved by finite elements. These methods

are insensitive to the value of the Reynolds number in solving for the Navier-Stokes equations and are efficient in solving of two-dimensional flows without free surfaces. However, the free-surface flows significantly complicate the application of these methods and, in this case, the problem of the boundary condition at the free surface remains uncertain.

The analysis of the extensive research in computational fluid mechanics suggests that the choice of the numerical procedure for the sloshing problem should be based on the following:

i) Finite difference methodology: preferable for unsteady and nonlinear problems.

ii) Primitive variable formulation: easier and more conclusive in imposition of boundary conditions.

iii) Central difference discretization: higher order of accuracy of the finite difference representation comparing with one-side differences.

iv) Weighted upstream differencing: eliminates the computational instability proper to the central differences, however, reduces accuracy; a compromise between accuracy and stability has to be made.

v) Staggered grid: increases the computational stability.

As a particular method satisfying all these requirements, the Marker and Cell method appears to be the most suitable. There is no available computational procedure that could, however, work reliably and accurately with nonlinear sloshing problem characterized by the presence

of the time-varying free surface. Moreover, the methodology of applying of boundary conditions in staggered grids is not clearly defined at the present time. These and related questions will be considered in this investigation in the following chapters.

1.3 Scope of the Present Investigation

The objectives of the present research are to create a sufficiently accurate and reasonably complex mathematical and computer models for the sloshing problem, to develop the procedure for numerical solution, and to study the viscous liquid behaviour in road containers of different geometrical shapes subjected to road manoeuvres such as straight-line braking or accelerating and steady cornering. The transient responses of the liquid motion to a prescribed input are to be evaluated in terms of damped frequencies and amplitudes of slosh parameters, i.e., heights of the free surface, forces, and overturning moments. The analytical steady-state solutions are also a part of this investigation.

In Chapter 1, a detailed evaluation of the presently existing sloshing theories is made in order to establish the state-of-the-art of the problem. The various methods of numerical solutions and the choice of the Marker and Cell method are discussed.

In Chapter 2, the mathematical model of the sloshing problem is developed based on the two-dimensional incompressible Navier-Stokes, continuity, and free-surface equations. A dimensional analysis of the governing equations is also presented in this chapter. Such an analysis allows to extrapolate the computational results to the class of similar problems based on variation of the size, viscosity, density, and input acceleration. The various input and output parameters for the

sloshing problem are defined as well as the conversion of the non-dimensional parameters to the dimensional form. Also, the assumptions and limitations of the developed mathematical slosh model are discussed in this chapter.

In Chapter 3, the computer model of the sloshing problem is formulated. This includes the discretization of the governing equations in an Eulerian mesh carried out by central differences in space, with a weighted upstream differencing, and by forward differences in time. The boundary conditions on the flow variables are derived for free- and no-slip velocity conditions at the rigid wall and for free-slip condition at the free surface. The reflection type boundary conditions have been developed for arbitrary shaped boundary. This technique is called here interpolation-reflection of the boundary conditions. Finally, the computer code to solve the formulated sloshing problem is developed and some aspects of the numerical procedure are discussed.

In Chapter 4, a number of test runs of the computer program is carried out in order to specify the coefficients of upstream differencing and the order of interpolation of boundary conditions. The influence of these parameters on the numerical solution is discussed and the final choice of the boundary conditions is made. Also, the computer model of the sloshing problem is experimentally validated for the case of a rectangular container. The small scale model of a rectangular tank is tested on a specially created test set-up, where the lateral acceleration is simulated by an electro-hydraulic actuator. A good agreement between the experiment and the model is found.

The behaviour of the liquid motion in rectangular containers is studied in Chapter 5. The steady-state solutions are obtained

analytically by integrating the governing equations in static equilibrium. The solutions are given in terms of liquid heights, forces, and overturning moments as functions of the input parameters including the geometry of the container, fill level, and magnitude of input acceleration. The transient solutions are found numerically in terms of frequencies and amplitudes of main slosh variables. The computer results are compared with available data from the linear sloshing theory and a detailed discussion on those results is also presented.

In Chapter 6, the sloshing in horizontal cylindrical containers with circular cross-section is investigated in the form very similar to that of rectangular containers. An additional study is undertaken to show that in majority of practical cases, the nonhomogenous field of body forces existing in a liquid during the rotational motion may be reduced to a simpler homogeneous one of the rectilinear translational motion. The error, arising from such an approximation, is also estimated.

In Chapter 7, the solution to the sloshing problem in compartmented and baffled rectangular containers is presented. The effect of separating walls in reducing the slosh loads is investigated analytically for the steady-state motion and numerically for the transient case. The influence of the size and location of the baffled orifices and of the number of baffles is also studied in terms of the slosh frequencies and amplitudes of forces and overturning moments.

In Chapter 8, the analytical steady-state solutions are utilized to carry out an optimization study in searching for the optimal geometrical shape of a rectangular container. The overturning moment, chosen as the

objective function, is minimized in the feasible range of the container height and input acceleration parameters, and the sensitivity of the moment to the container height variation is analysed.

Finally, a discussion on the results, obtained in this investigation, conclusions and recommendations for future work are presented in Chapter 9.

CHAPTER 2

MATHEMATICAL MODELING OF THE LIQUID MOTION IN ROAD CONTAINERS

2.1 General

Road containers may be subjected to different forms of external excitation depending upon the types of vehicle manoeuvre which are generally classified into the following groups:

i) braking or accelerating,

ii) cornering,

iii) lane change.

iv) evasive or double lane change manoeuvre, and

v) cornering with braking.

In addition to the gravitational field, such manoeuvres produce in the liquid a field of unit body forces, which can be a constant or vary in time and homogeneous (for braking-accelerating) or nonhomogenous (for all the remaining manoeuvres) in space. For the purpose of clarity and generalization, the complicated fields of body forces may be represented by simpler forms. Thus, the braking and accelerating manoeuvres can be simulated by a step input acceleration in the longitudinal direction which creates a constant homogeneous force field in the liquid. The cornering, lane change and evasive manoeuvres can also be represented by a step input acceleration, or a combination of steps, but the force field that they engender, is a nonhomogenous one and will be a function of the local radius of turn. In the present investigation, two types of container motion are considered. The first one is that which arises under a step acceleration and is a rectilinear uniformly accelerated

motion representing the braking-accelerating manoeuvres. The second one is due to a step centrifugal acceleration simulating the vehicle steady-state cornering. These two motions, for brevity, will be called as rectilinear and rotational motions respectively of the container. It will be shown in the sections for steady-state solutions of Chapters 5 and 6 that the rotational motion can be, for majority of practical cases, replaced by the rectilinear one with a small and estimated error.

The two-dimensional (2-D) model of the liquid motion is formulated in this section to study the dynamics of sloshing in steady turn, when the anomalies of the initial phase of the manoeuvre are neglected, and in braking-accelerating manoeuvre, when the cross-section of the container is assumed to be rectangular.

2.2 Governing Equations for Transient and Steady-State Liquid Motion

The equations describing the 2-D flow in a container are the Navier-Stokes, the continuity, and the free-surface partial differential equations, that in conservative and nondimensional form are written as:

$$\left.\begin{aligned}
St\,\frac{\partial U}{\partial T} + \frac{\partial U^2}{\partial X} + \frac{\partial UV}{\partial Y} &= \frac{G_x}{Fr} - Eu\,\frac{\partial P}{\partial X} + \frac{1}{Re}\left(\frac{\partial^2 U}{\partial X^2} + \frac{\partial^2 U}{\partial Y^2}\right)\\
St\,\frac{\partial V}{\partial T} + \frac{\partial VU}{\partial X} + \frac{\partial V^2}{\partial Y} &= \frac{G_y}{Fr} - Eu\,\frac{\partial P}{\partial Y} + \frac{1}{Re}\left(\frac{\partial^2 V}{\partial X^2} + \frac{\partial^2 V}{\partial Y^2}\right)\\
\frac{\partial U}{\partial X} + \frac{\partial V}{\partial Y} &= 0\\
St\,\frac{\partial H}{\partial T} &= V - U\,\frac{\partial H}{\partial X}
\end{aligned}\right\} \qquad (2.1)$$

The boundary conditions necessary for completing the governing set of

equations, in the case of an arbitrary shape of the container are:

$$\left.\begin{array}{ll} P = P_0 & \text{on the free surface} \\ U_n = 0,\ V_n = 0 & \text{on the wetted wall for free-slip condition} \\ \left.\begin{array}{l} U_n = 0,\ V_n = 0 \\ U_\tau = 0,\ V_\tau = 0 \end{array}\right\} & \text{on the wetted wall for no-slip condition} \end{array}\right\} \quad (2.2)$$

The conditions given in the Eqn. (2.2) are written in terms of normal and tangential components of the U and V velocities with respect to the local system of coordinates, n-τ, with its origin lying on a wall point and with the n-axis being the inward normal to the wall, (Fig. 2.1). Such a form allows to treat separately the U and V boundary velocities which themselves are related to the X-Y coordinated system in which a container body is situated in the first quadrant in such a way that X- and Y- axes touch the container at least in one point each. In a specific case of a rectangular container, when the n-τ coordinates coincide in directions with X-Y coordinates, the former are dropped to avoid redundancy.

The nondimensional groups, included in Eqns. (2.1), are the Strouhal, St, Froude, Fr, Euler, Eu, and Reynolds, Re, numbers expressed in terms of characteristic values of the flow and physical properties of the liquid as:

$$St = \frac{L_0}{T_0 V_0}, \quad Fr = \frac{V_0^2}{gL_0}, \quad Eu = \frac{P_0}{\rho V_0^2}, \quad Re = \frac{V_0 L_0}{\nu} \qquad (2.3)$$

The nondimensional equations, Eqns. (2.1), together with the

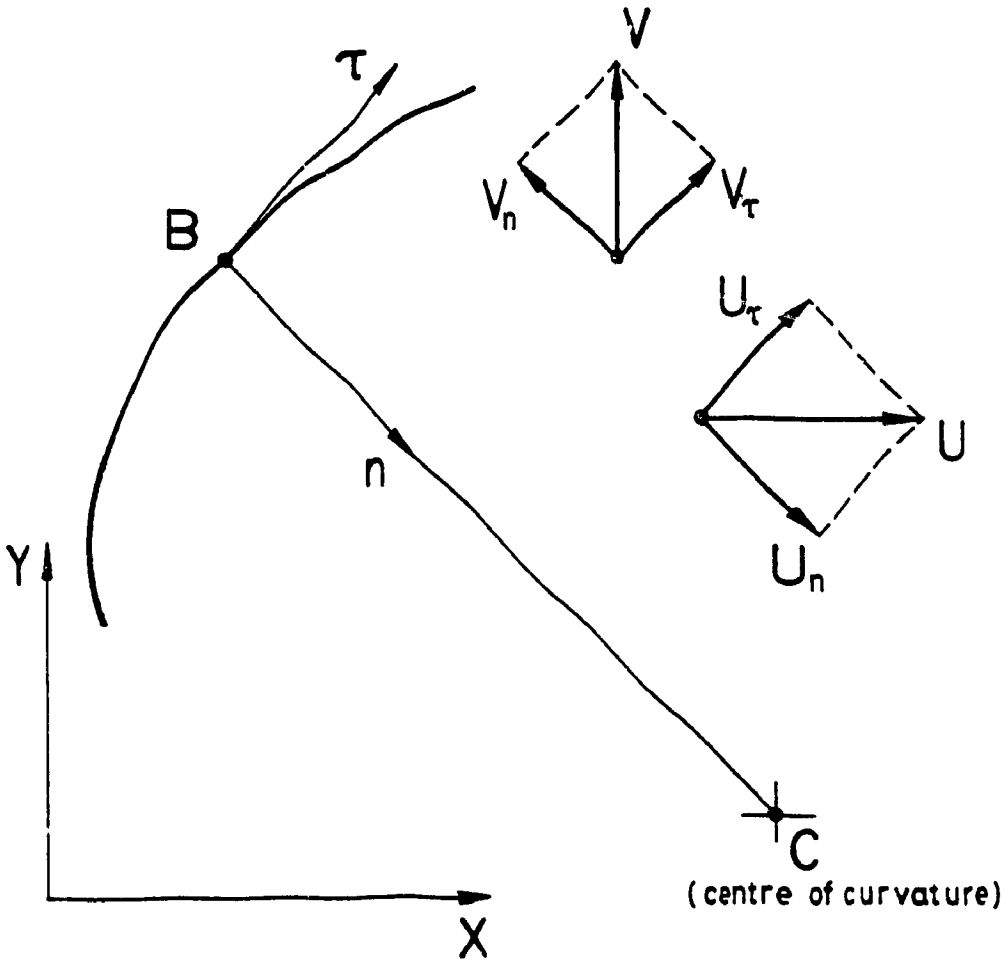

At the boundary point B:

$U_n = 0,\ V_n = 0$ for free-slip condition

$U_n = 0,\ V_n = 0$
$U_\tau = 0,\ V_\tau = 0$ } for no-slip condition

Fig.2.1. Velocity components and systems of coordinate

boundary conditions, Eqns. (2.2) describe a class of similar liquid flows, provided that the geometrical similarity of container's walls and the similarity of applied external forces (G_x and G_y) is maintained. The four nondimensional numbers in Eqns. (2.3), that must be equal for similar flows, constitute the necessary conditions for similarity. The sufficient condition for similarity is, however less than four and it can be established by considering the specifics of the flow. This can be done through further alteration of the governing equations by defining the characteristic values of the flow parameters in the following manner:

$$\left.\begin{aligned} &\underline{\text{characteristic length}},\ L_0, \text{ is the length of the container in the direction of applied excitation,} \\ &\underline{\text{characteristic time}},\ T_0 = \sqrt{L_0 / g}\ , \\ &\underline{\text{characteristic velocity}},\ V_0 = \sqrt{g\, L_0}\ , \\ &\underline{\text{characteristic pressure}},\ P_0 = \rho\, V_0^2\ . \end{aligned}\right\} \qquad (2.4)$$

Substituting the characteristic values into the expressions in Eqns. (2.3), makes the St, Fr, and Eu numbers identically equal to 1 and the $Re = g^{1/2} L_0^{3/2}\ \nu^{-1}$. Now, the sufficient number of parameters defining the similar flows becomes equal to two, i.e. G_x and Re while the $G_y = -1$ is excluded if the gravitational acceleration is assumed to be a constant. The additional defining parameter, the fill level f, results from the geometrical similarity and must be the same for similar flows.

For the steady-state response, when the sloshing is absent and

therefore all fluid velocities vanish, the Eqns. (2.1) reduce to the following hydrostatic equations:

$$\frac{\partial P_{ss}}{\partial X} = G_x \quad \text{and} \quad \frac{\partial P_{ss}}{\partial Y} = G_y \tag{2.5}$$

2.3 Dimensional Analysis of the Sloshing Problem

The numerical integration of the nondimensional governing equations is carried out for a given set of the defining parameters. Once the solution is known, the nondimensional analysis allows to extrapolate a further solution to other values of the input parameters. This can be done through the dimensional analysis of these equations. All parameters and variables of the sloshing problem may be collected in the following groups:

$$\ell_i \ , \ a_i, \ \rho_i, \ \nu_i \text{ and } t_i, \ v_i, \ p_i, \ f_i, \ m_i \tag{2.6}$$

where the nine listed groups of dimensional quantities represent the lengths, accelerations, mass densities, viscosities, times, velocities, pressures, forces, and moments proper to the problem, respectively. The frequencies are omitted, since they may be expressed by the inverse values of the corresponding time periods.

The list (2.6) may be rewritten in terms of the corresponding characteristic values of the parameters and variables involved as:

$$L_0, \ g, \ \rho, \ \nu \text{ and } T_0, \ V_0, \ P_0, \ F_0, \ M_0 \tag{2.7}$$

where the characteristic values are the container width, gravity

acceleration, density and viscosity of the most dense or viscous liquid (if more than one liquid is involved); time, velocity, and pressure, as they are defined in Exp.(2.4); and the force and moment, which are defined in the following manner:

$$F_0 = \rho g L_0^3 \quad \text{and} \quad M_0 = \rho g L_0^4$$

Then, two unsteady viscous incompressible flows in horizontally accelerated containers are similar, if the following conditions hold:

$$\left.\begin{aligned} &\frac{\ell_i}{L_0} = \text{idem}, \ \frac{a_i}{g} = \text{idem}, \ \frac{\rho_i}{\rho} = \text{idem}, \ \frac{\nu_i}{\nu} = \text{idem}, \\ &\frac{t_i}{T_0} = \text{idem}, \ \frac{V_i}{V_0} = \text{idem}, \ \frac{p_i}{P_0} = \text{idem}, \ F_i = \text{idem}, \ M = \text{idem} \end{aligned}\right\} \tag{2.8}$$

$$\text{and} \quad St = \text{idem}, \ Fr = \text{idem}, \ Eu = \text{idem}, \ Re = \text{idem} \tag{2.9}$$

The conditions in Eqns. (2.8) and (2.9) include geometric, kinematic, and dynamic similarity; the similarity of the fill levels is maintained by the first term in Eqns. (2.8).

Introducing the scaling factors as

$$K_L, \ K_g, \ K_\rho, \ K_\nu, \ K_T, \ K_V, \ K_P, \ K_F, \ K_M, \tag{2.10}$$

that represent the ratios of the corresponding parameters and variables of the two compared flow, the expressions (2.8) and (2.9) may be rewritten in the form:

$$\frac{K_L}{K_T K_V} = 1, \quad \frac{K_V^2}{K_g K_L} = 1, \quad \frac{K_p}{K_\rho K_V^2} = 1, \quad \frac{K_V K_L}{K_\nu} = 1,$$

$$\frac{K_F}{K_\rho K_g K_L^3} = 1, \quad \frac{K_M}{K_\rho K_g K_L^4} = 1 \qquad (2.11)$$

This system, containing 6 equations and 9 variables, can be only solved if three of the scaling factors are defined a priori, and they must be chosen from the list of parameters defining the flow, i.e., K_L, K_g, K_ρ, and K_ν. Some special cases of similarity are considered in the following subsections.

2.3.1 Container Size Variation, K_L = var, $K_g = K_\rho = 1$

This case corresponds to fixed values of the input acceleration and mass density of the liquid. The solution of Eqns. (2.11) yields:

$$K_\nu = K_L^{3/2}, \; K_T = K_L^{1/2}, \; K_V = K_L^{1/2}, \; K_P = K_L,$$
$$K_F = K_L^3, \; K_M = K_L^4, \text{ and } K_\Omega = K_L^{-1/2} \qquad (2.12)$$

The flows in two similar containers of different size may be similar if only the viscosity of liquids differ by $K_L^{3/2}$ times. Then the resulting parameters for the flow in a bigger container ($K_L > 1$) change in the following manner: the period of the liquid oscillations and all the velocities will increase by $K_L^{1/2}$ times, the pressure, forces and moment increase by the first, third, and fourth powers of the size change respectively, and the frequency of oscillation decreases by $K_L^{-1/2}$ times. Thus, it is not necessary to vary the size of the container, since a

solution for any container size may be obtained by a simple recalculation of the solution for one fixed size according to the expressions in Eqns.(2.12). It has to be noted that if the viscosity is kept unchanged, then the complete similarity is not possible due to a contradiction between the second and fourth expressions in Eqns. (2.11), which represent the Fr and Re numbers. In this case, only the similarity either by Fr or by Re can be maintained.

In general, only two scaling factors from the four defining ones can be set equal to 1 with the third factor varying. If three factors are set equal to 1, then one of the expressions in Eqns. (2.11) becomes inconsistent with the remaining expressions, and it must be rejected with the consequence of unsatisfying of the corresponding criterion of similarity.

2.3.2 Viscosity Variation, K_ν = var, $K_g = K_\rho = 1$

The expressions in Eqns. (2.11) for this case yield:

$$K_L = K_\nu^{2/3}, \quad K_T = K_\nu^{1/3}, \quad K_V = K_\nu^{1/3}, \quad K_P = K_\nu^{2/3}, \quad K_F = K_\nu^2,$$

$$K_M = K_\nu^{8/3}, \text{ and } K_\Omega = K_\nu^{-1/3} \qquad (2.13)$$

When the viscosity of two flows is different, the complete similarity is possible if the sizes of containers differ by $K_\nu^{2/3}$ and for the flow with greater viscosity ($K_\nu > 1$) the time period of oscillations and all the velocities will increase by $K_\nu^{1/3}$ times. The pressure, forces, and moment will also increase proportionally to two third, square, and eight third powers of the viscosity change, while the frequency of oscillations will be lowered by $K_\nu^{-1/3}$ times.

2.3.3 Density Variation, K_ρ = var, $K_g = K_\nu = 1$

This case corresponds to two liquids with different mass densities and equal viscosities and subjected to the same acceleration. The expressions 2 and 4 in Eqns. (2.11) imply that the container size should not be changed to maintain the similarity. Hence, Eqns. (2.11) give:

$$K_L = 1, \quad K_T = K_V = K_\Omega = 1, \quad K_p = K_F = K_M = K_\rho \tag{2.14}$$

It can be seen that velocities and frequencies are invariant to the density change in a container of fixed size, and the pressure, forces, and moment are proportional to the density change. Thus, the density is not a parameter defining the flow.

2.3.4 Acceleration variation, K_g = var, $K_\rho = K_\nu = 1$

The solution of Eqns. (2.11) for the same liquid subjected to different accelerations is obtained in the form:

$$K_L = K_g^{-1/3}, \quad K_T = K_g^{-2/3}, \quad K_\nu = K_g^{1/3}, \quad K_P = K_g^{2/3}, \quad K_F = 1$$

$$K_M = K_g^{-1/3}, \quad K_\Omega = K_g^{-1/3} \tag{2.15}$$

that states that if the input acceleration is varied then the container size must be changed by $K_g^{-1/3}$ times in order to obtain a similar flow. The dimensional theory does not specify the acceleration expressed by K_g factor. It can be any input acceleration i.e. either horizontal or vertical (gravitational) acceleration each of which enters only into one of the momentum equations and they are mutually independent. The Froude

number includes only the gravitational acceleration, while G_x and G_y represent the input accelerations in the horizontal and vertical directions. In a specific case of road containers, the gravitational acceleration may be assumed constant and the G_y, for the considered uncoupled problem equals to -1. Therefore, the results obtained in this subsection for the forces and moment must be attributed only to the horizontal component of the liquid force and to that part of the overturning moment which is due to this force, assuming the K_{G_x} value istead of K_g. It can also be said that the change in the gravitational acceleration does affect only the second momentum equation, while the change in G_x affects only the first one. Thus, the lateral input acceleration, G_x, is a defining parameter for the sloshing problem.

2.4. Definition of Input and Output Slosh Parameters

The liquid motion inside an accelerated container is dictated by the acceleration of container body, size and shape of the container including also the fill level, and by the properties of the liquid. As it has been discussed in the previous section, the size and the viscosity of the liquid are represented by the more general parameter, the Reynolds number, and the density of the liquid, represented by the Euler number, ceases to be a defining parameter and the Eu itself becomes a function of Re. In the case of a rotational motion, the additional parameter, characterizing the track curvature, appears. Thus, the set of nondimensional input parameters is as follows:

i) Input acceleration, $G_x = -a/g$ for the rectilinear motion and $G_n = \omega^2 R/g$ for rotational motion.

ii) Height of the container, $h = h_o / L_o$ for rectangular containers and

h=1 for circular cross-section containers.

iii) Fill level, $f = h_{in} / L_o$.

iv) Number of compartments for compartmented and baffled containers, n.

v) Track curvature, $\delta = R/L_o$.

vi) Reynolds number, $Re = V_o L_o/\nu$.

The solution of the hydrodynamic equations is carried out in terms of the pressures, velocities, and heights of the free surface as functions of the time and space coordinates. The loading slosh parameters, defined as horizontal and vertical forces and overturning moment, all driven to the point "O", Fig. 2.2, are found by numerical integration of the pressure along the wetted walls of the container as

$$F_H = \delta Y \sum_{j=2}^{m} (P_{jr} - P_{jl}),\ F_V = \delta X \sum_{i=2}^{n} (P_{ib} - P_{it}),\ M = F_H Y_H - F_V S_V \qquad (2.16)$$

where the displacement of the forces from the point "O" are

$$Y_H = \frac{\partial Y \sum_{j=2}^{m} (P_{jr} - P_{jl})\ Y_j}{F_H},\ S_V = \frac{\partial X \sum_{i=2}^{n} (P_{ib} - P_{it})\ X_i}{F_V} - \frac{1}{2} \qquad (2.17)$$

and the subscripts r, l, b, and t are referred to the right, left, bottom, and top portions of the wall respectively. The forces of friction, due to the shear stress of the liquid, are neglected because of their very small values comparing with the normal stress forces, that is correct for flows with high Re-number which is appropriate for this investigation. Since the pressures in the numerical code are computed in the middle of each cell, they are extrapolated to the wall in order to get their values included in the Eqns. (2.16). The extrapolation technique is considered in the next chapter.

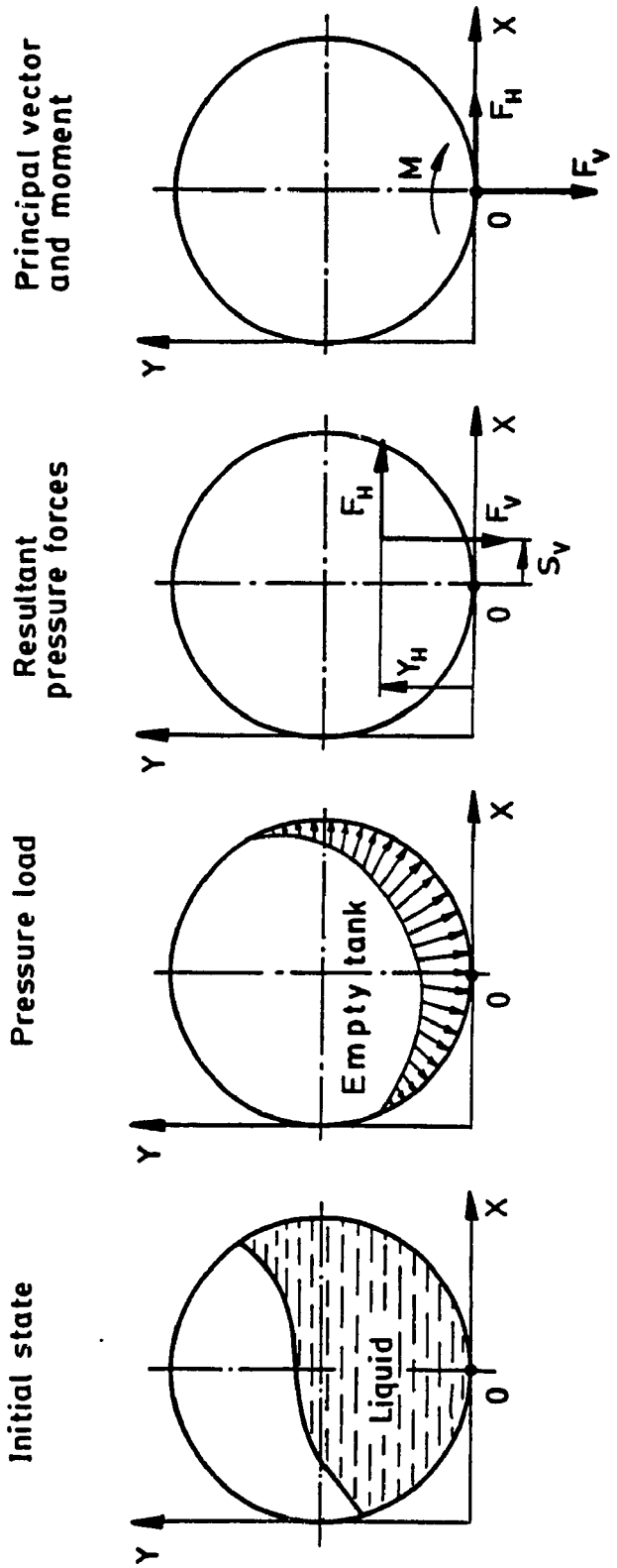

Fig.2.2. Slosh forces and overturning moment driven to the central bottom point of the container

The dynamic coefficients for forces and moments, representing the ratios of the dynamic peak values to the corresponding steady-state values, are designated as

$$C_{FH} = \frac{F_H}{F_{HSS}}, \quad C_{FV} = \frac{F_V}{F_{VSS}}, \quad C_M = \frac{M}{M_{SS}} \tag{2.18}$$

and the damped natural frequencies of liquid oscillations are normalized with respect to the total unit body force as

$$K = \Omega \Big/ \left[\frac{g}{L_0} \left(1 + G_X^2 \right)^{1/2} \right]^{1/2} \tag{2.19}$$

2.5 Conversion of the Slosh Parameters to Dimensional Form

The nondimensional slosh forces, computed in this investigation as their ratios to the liquid weight, and the moment, computed as the ratio to the product "liquid weight times characteristic length", all per unit width of the container, can be converted to the dimensional form, as well as the area occupied by the liquid, by means of the following expressions, where the width of the container is b:

$$\left.\begin{aligned} a_0 &= L_0^2 A_0 \\ f_H &= \rho g a_0 b F_H \\ f_V &= \rho g a_0 b F_V \\ m &= \rho g a_0 b L_0 M \end{aligned}\right\} \tag{2.20}$$

These expressions are valid both for the steady-state and transient responses, and the characteristic length for a circular cross-section container is equal to its diameter.

2.6 Assumptions and Limitations of the Slosh Model

The main assumptions made in the development of the slosh model together with the limitations may be stated as follows:

i) The liquid flow inside a container is assumed to be incompressible. This assumption implies a very high degree of accuracy since the compressibility effect of the flows with free surfaces is known to be negligibly small.

ii) The two-dimensional model of the liquid flow, adopted in this investigation, can sufficiently describe the liquid sloshing response in steady turning manoeuvre for any cross-sectional shape of the container and in braking-accelerating manoeuvre only for rectangular containers. The more complicated manoeuvres, such as simultaneous braking and cornering, can be represented only by a three-dimensional slosh model that can be developed by adding the additional dimension to the velocities, pressures, and liquid heights arrays. Such an extension is seen as a straightforward procedure.

iii) The surface tension and capillarity effect are neglected. This assumption is quite accurate because the lengths of the capillary waves are very small, usually a few centimeters, comparing with gravitational waves of the liquid. For example, for water and air, the capillary wave length is of the order of 1.8 cm [14].

iv) It is assumed that the unit body forces are constant and homogeneous. The first part of this assumption implies that the step input acceleration approximates the cornering manoeuvre which is usually characterized by a very steep ramp in the initial phase of the manoeuvre. In the case of braking-accelerating this assumption is even

more realistic since the brakes are often applied suddenly. Thus, the more severe case of sloshing is considered. The second part assumes that the centrifugal acceleration is independent of the local radius of turn. Such an assumption can be made only if the size of the container is small with respect to the radius of the turn which is the case in the present problem. This assumption, however, will be validated in Chapters 5 and 6 during the derivations of steady-state responses.

v) The container wall is considered to be absolutely rigid and therefore the coupling effect of the liquid-wall interaction is neglected. It has been shown by different authors that such a coupling, though affects the coupled frequencies of the wall vibrations, has almost no influence on the liquid vibrations, and therefore in estimating of the slosh loading, the walls can be considered rigid.

vi) In the case of compartmented and baffled containers, the separating walls are assumed evenly distributed. This assumption holds for the steady-state and transient responses throughout this investigation. However, uneven distribution of partitions can be easily introduced for the case of transient response, but in the case of steady-state response, new derivations are needed.

vii) Identical fill level in all compartments of multisectional containers has been considered, which is not an assumption as a matter of fact, but rather a specific case under consideration. As in the previous case, the assumed model can be easily extended for the transient solution to different fill levels in a compartmented tank.

viii) The liquid forces exerted by the liquid on container walls are computed in this study based only on the normal stress or on the hydrodynamic pressure, while the friction forces due to the shear stress

are neglected. This assumption is well founded for a flow with high Re-number. A rough estimation of the friction force shows that it is 3 to 5 orders of magnitude smaller than the pressure forces if the Re is in the range 10^2 - 10^7. However, for very viscous flows, that are not considered in this investigation, the friction force must be taken into account.

ix) The initial conditions for the numerical solution of the governing equations assume the liquid to be initially at rest. This assumption is a necessary one since it is very difficult to guess the velocity and pressure fields if other then zero-initial conditions are considered. An incorrectly assumed initial state of the flow may became a strong source of computational instability.

x) It is also necessary to mention that the model cannot be used for study of liquid motion under very severe sloshing conditions characterized by such input acceleration that creates a breaking wave or leads to separation of the liquid into parts. A solution of such a flow faces many difficulties related to rearranging of boundary conditions to solve the motion of liquid parts and it will result in enormously increased computational time.

2.7 Summary

In this chapter, the mathematical model of the liquid sloshing in road containers is described. The liquid motion in containers under typical road manoeuvres is simulated by the Navier-Stokes, continuity, and the free-surface differential equations, which include the most important nonlinearities appropriate to the problem under consideration.

The dimensional analysis of the governing equations is presented

for extrapolating the computational results for more extensive range of input parameters.

The input and output slosh parameters are defined and the vehicle manoeuvres, such as steady cornering and braking-accelerating, are simulated by simplified motions.

The assumptions and limitations of the proposed model are summarized together with the possible modifications which will allow the extension of the model for treating more complicated cases of the sloshing.

CHAPTER 3

FORMULATION OF THE COMPUTER MODEL OF SLOSHING

3.1 Description of the Marker-and-Cell Numerical Technique

The numerical method to solve the equations of liquid motion chosen in this study is the Marker-and-Cell (MAC) method [41,46-49] generally characterized by the following features:

i) The use of primitive variables, i.e. velocities, pressure, and heights of the free surface.

ii) The finite difference approximation of the differential equations is made by use of the forward differences in time and central differences in space. Such a scheme, often computationally unstable, is made stable by applying the upstream differencing technique to the central difference formulae. The over-relaxation is used to increase the rate of computational convergence.

iii) The use of staggered grid, usually implied by the MAC-method, increases the computational stability by reducing the difficulties related to the convective terms of the Navier-Stokes equations. A cell of typical staggered grid is shown in Fig. 3.1, where it can be seen that the velocities are applied at the sides of the control volume (or a cell) and the pressure in the middle of a cell.

iv) The markers, used in the original MAC-method to define the trajectories of liquid particles including those which belong to the free surface, are dropped because the free-surface position is calculated directly from the equation of the free surface after the velocity field is computed from the momentum equations and specified through the velocities and pressure iterations.

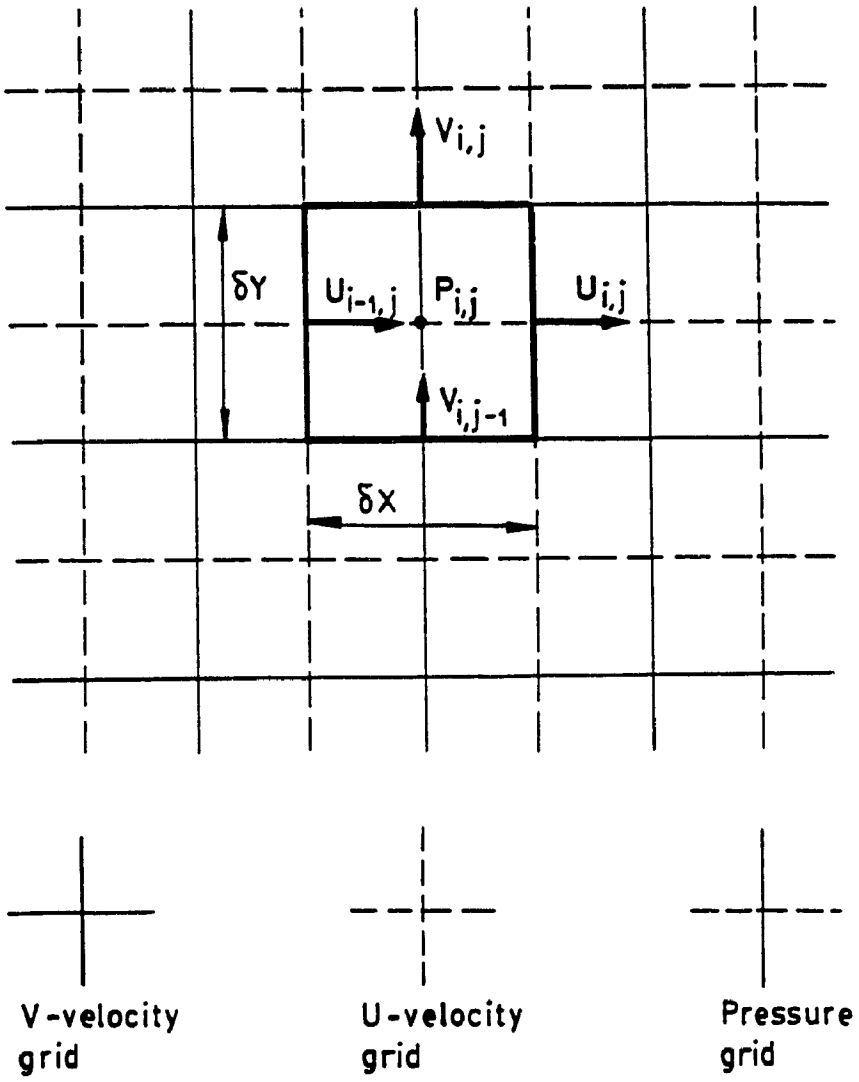

Fig.3.1. Staggered computational grid

3.2 Discretization of the Governing Equations

The partial differential equations (2.1) are approximated by the corresponding finite-difference equations in accordance with the statements mentioned in the previous section in the following manner:

X-momentum equation

$$U^{K+1}_{i,j} = U^{K}_{i,j} + \frac{\delta T}{St}\left\{-\frac{Eu}{\delta X}\left(P^{K}_{i+1,j} - P^{K}_{i,j}\right) + \frac{G_x}{Fr} - \frac{1}{4\delta X}\left[\left(U^{K}_{i,j} + U^{K}_{i+1,j}\right)^2\right.\right.$$

$$+ \alpha\left|U^{K}_{i,j} + U^{K}_{i+1,j}\right|\left(U^{K}_{i,j} - U^{K}_{i+1,j}\right) - \left(U^{K}_{i-1,j} + U^{K}_{i,j}\right)^2 - \alpha\left|U^{K}_{i-1,j} + U^{K}_{i,j}\right|$$

$$\left.\times\left(U^{K}_{i-1,j} - U^{K}_{i,j}\right)\right]$$

$$- \frac{1}{4\delta Y}\left[\left(V^{K}_{i,j} + V^{K}_{i+1,j}\right)\left(U^{K}_{i,j} + U^{K}_{i,j+1}\right) + \alpha\left|V^{K}_{i,j} + V^{K}_{i+1,j}\right|\left(U^{K}_{i,j} - U^{K}_{i,j+1}\right)\right.$$

$$\left. - \left(V^{K}_{i,j-1} + V^{K}_{i+1,j-1}\right)\left(U^{K}_{i,j-1} + U^{K}_{i,j}\right) - \alpha\left|V^{K}_{i,j-1} + V^{K}_{i+1,j-1}\right|\left(U^{K}_{i,j-1} - U^{K}_{i,j}\right)\right]$$

$$\left. + \frac{1}{Re}\left[\frac{1}{\delta X^2}\left(U^{K}_{i+1,j} - 2U^{K}_{i,j} + U^{K}_{i-1,j}\right) + \frac{1}{\delta Y^2}\left(U^{K}_{i,j+1} - 2U^{K}_{i,j} + U^{K}_{i,j-1}\right)\right]\right\} \qquad (3.1)$$

Y-momentum equation

$$V_{i,j}^{K+1} = V_{i,j}^{K} + \frac{\delta T}{St}\left\{ \frac{Eu}{\delta Y}\left(P_{i,j+1}^{K} - P_{i,j}^{K}\right) + \frac{G_y}{Fr} - \frac{1}{4\delta X}\left[\left(U_{i,j}^{K} + U_{i,j+1}^{K}\right)\right.\right.$$

$$\times\left(V_{i,j}^{K} + V_{i+1,j}^{K}\right)$$

$$+ \alpha\left|U_{i,j}^{K} + U_{i,j+1}^{K}\right|\left(V_{i,j}^{K} - V_{i+1,j}^{K}\right) - \left(U_{i-1,j}^{K} + U_{i-1,j+1}^{K}\right)$$

$$\times\left(V_{i-1,j}^{K} + V_{i,j}^{K}\right)$$

$$\left. - \alpha\left|U_{i-1,j}^{K} + U_{i-1,j+1}\right|\left(V_{i-1,j}^{K} - V_{i,j}^{K}\right)\right] - \frac{1}{4\delta Y}\left[\left(V_{i,j}^{K} + V_{i,j+1}^{K}\right)^{2}\right.$$

$$+ \alpha\left|V_{i,j}^{K} + V_{i,j+1}^{K}\right|\left(V_{i,j}^{K} - V_{i,j+1}^{K}\right) - \left(V_{i,j-1}^{K} + V_{i,j}^{K}\right)^{2}$$

$$\left. - \alpha\left|V_{i,j-1}^{K} + V_{i,j}^{K}\right|\left(V_{i,j-1}^{K} - V_{i,j}^{K}\right)\right]$$

$$\left. + \frac{1}{Re}\left[\frac{1}{\delta X^{2}}\left(V_{i+1,j}^{K} - 2V_{i,j}^{K} + V_{i-1,j}^{K}\right) + \frac{1}{\delta Y^{2}}\left(V_{i,j+1}^{K} - 2V_{i,j}^{K} + V_{i,j-1}^{K}\right)\right]\right\} \qquad (3.2)$$

Continuity (divergence) equation

$$D_{i,j}^{K+1} = \frac{1}{\delta X}\left(U_{i,j}^{K+1} - U_{i-1,j}^{K+1}\right) + \frac{1}{\delta Y}\left(V_{i,j}^{K+1} - V_{i,j-1}^{K+1}\right) \qquad (3.3)$$

Free - surface equation

$$H_i^{K+1} = H_i^K + \frac{\delta T}{St}\left\{ \bar{V}_i^{K+\frac{1}{2}} - \frac{1}{2\delta X}\left[\bar{U}_i^{K+\frac{1}{2}} H_{i+1}^K + \gamma \left|\bar{U}_i\right|^{K+\frac{1}{2}} \left(H_i^K - H_{i+1}^K\right) \right.\right.$$

$$\left.\left. - \bar{U}^{K+\frac{1}{2}} H_{i-1}^K - \gamma \left|\bar{U}_i\right|^{K+\frac{1}{2}} \left(H_{i-1}^K - H_i^K \right)\right]\right\} \qquad (3.4)$$

where the free-surface velocities are expressed as

$$\bar{V}^{K+\frac{1}{2}} = \frac{1}{2}\left(V_{1,JT}^{K+1} + V_{1,JT}^K \right)$$

$$\bar{U}^{K+\frac{1}{2}} = \frac{1}{4}\left(U_{i-1,JT}^{K+1} + U_{1,JT}^{K+1} + U_{i-1,JT}^K + U_{1,JT}^K \right) \qquad (3.5)$$

and α and γ are the coefficients of upstream differencing varying between 0 and 1. If $\alpha = \gamma = 0$, then the discretization corresponds to the pure central difference scheme; if $\alpha = \gamma = 1$, then the difference equations reduce to full upstream form; and if α and γ are between 0 and 1, then some amount of donor cell fluxing is introduced. The partial and full upstream differencing introduces a false diffusion that is directly following from the Taylor-series expansion of the differential equations, which is true if the space increments δX and δY are very small. For large values of δX and δY, or in the cases of sufficiently rough computational meshes, the Taylor-series analysis is misleading [51] and the upstream differencing gives more reasonable results.

The free-surface velocities, entering the free-surface equation, are averaged in time between the (k+1) and k-th time levels, and those are more accurate than usually taken values at the (k+1) level. Also, they are computed for the JT-cell layer that is slightly below of the

free surface, i.e. they are not extrapolated outside from the flow. The calculations show that velocities in liquid increase in the direction from the bottom of the container to the free surface, and because of this, it seems more reasonable to extrapolate the free surface velocities. However, it leads to slightly divergent oscillation of the free-surface heights that is physically incorrect even for zero-viscosity flow. This fact may be attributed to some local effects at the free surface, such as surface tension and interaction of the free surface with ambient air, which are not taken into account by the present model. Therefore, it has been found reasonable to keep the velocities at the free surface equal to those in the liquid near the free surface. This question will be discussed in detail in Chapter 4 while validating the computer model.

3.3. Boundary Conditions

The boundary value problem, stated in Eqns.(2.1) requires a definition of the boundary conditions for all variables, i.e. U,V,P, and H. The boundary conditions given by expressions (2.2) are consistent with the corresponding differential equations, when they are defined exactly at the boundary including the rigid wall and the free surface. When the finite difference analogue to the original differential equations is solved in a staggered grid, then the boundary grid points may fall either inside or outside of the flow and belong, in the second case, to so-called fictitious flow.

The definition of the boundary points can be made by the prior classification of cells into three groups: completely filled by liquid, partially filled, and empty cells as it is shown in Fig. 3.2 for the

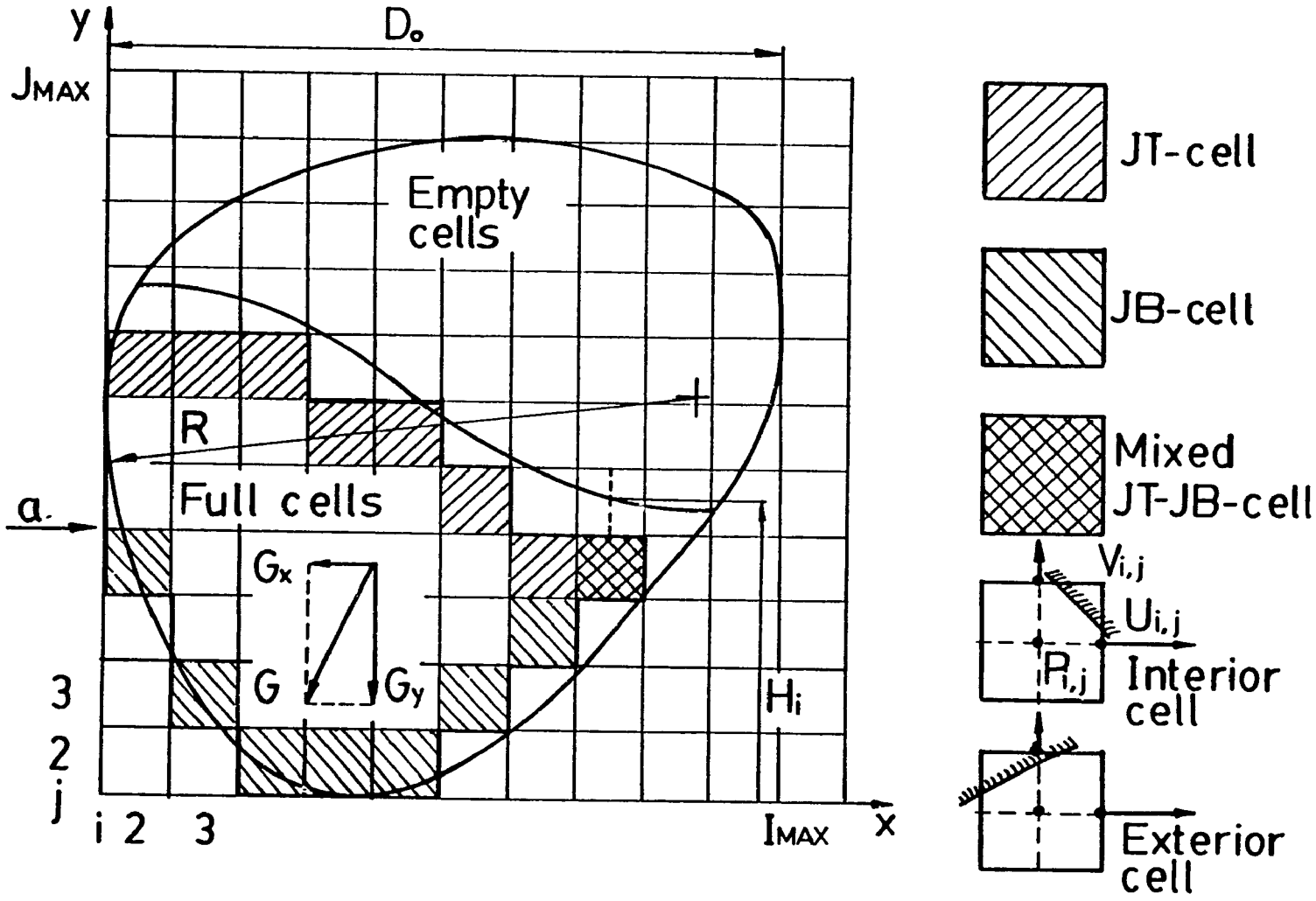

Fig.3.2. Container geometry and computational mesh arrangement

more general case of an arbitrary shape container. The interior cells, either physically full or partially filled, constitute the real flow domain and their velocities must be inside the flow boundary. If at least one of the velocities is outside, then the cell is exterior. The outward layer of interior cells is formed by the JT-cells belonging to the free surface, JB-cells pertaining to the rigid wall at the container bottom, simply interior cells located in the gap between the JT-and JB-cells, and mixed JB-JT-cells as it is shown in Fig. 3.2. The very next layer of cells surrounding the interior cells is the boundary layer. The equations of the flow are solved only over the interior cell domain and the boundary values of the flow parameters are computed for the boundary layer cells.

The problem under present study needs the definition of the boundary conditions for the following flow variables:velocity components of the liquid, U and V, the pressure, P, at the rigid wall and free surface, and the liquid height, H, in two points of the free surface. The velocity boundary conditions on the rigid wall may be either free-slip or no-slip. The choice of one or another condition may be based on the thickness of the boundary layer formed along the wall, as it is suggested in [41] where the free-slip condition is recommended for high Re values, when the boundary layer thickness is small comparing with the cell size, and the no-slip condition for low Re. The free-slip condition is often called reflection boundary condition which assumes the tangential velocity and the pressure to be even functions of the normal distance from the wall and the normal velocity to be an odd function of the same distance. In the present investigation, the term reflection is generalized in the way that both free-slip and no-slip

conditions are treated as reflection-type conditions assuming the even symmetry for free-slip and odd symmetry for no-slip. Also, the extrapolation or interpolation technique to compute the boundary velocities is developed basing on the first or second order Newton's interpolation for unequal intervals assuming one or two internal nodes plus the node lying on the wall for the no-slip condition and zero or first order, also with one or two internal nodes but without the wall node, for the free-slip condition. The different order of extrapolation for the velocity components is due to the fact that the influence of the wall on the tangential component of a velocity in the free-slip condition is absent and also in order to keep the same number of cell-velocities defining the boundary value. With this technique of defining of the boundary velocity, the conventional reflection type is obtained as a particular case by assuming zero order extrapolation for the tangential component and first order for the normal one.

The second order interpolation and the reflection of the boundary velocity is illustrated in Fig. 3.3, for the free-slip condition where the internal nodes of the real flow are designated as points 1 and 2 and the boundary node by B which is located in the fictitious flow. The point B' is the reflection of the boundary point B back to the real flow. The normal velocity distribution, shown in the first graph of this figure, is oddly symmetric with respect to the origin of the n-τ system of coordinates that is correct for the free-slip condition, at least in the neighborhood of the wall. The boundary velocity, V_{nB}, located in the point B can be either simply extrapolated from the real flow, as it is shown by the dotted line, or interpolated in the point B' and then reflected to the point B. It can be seen from the picture,

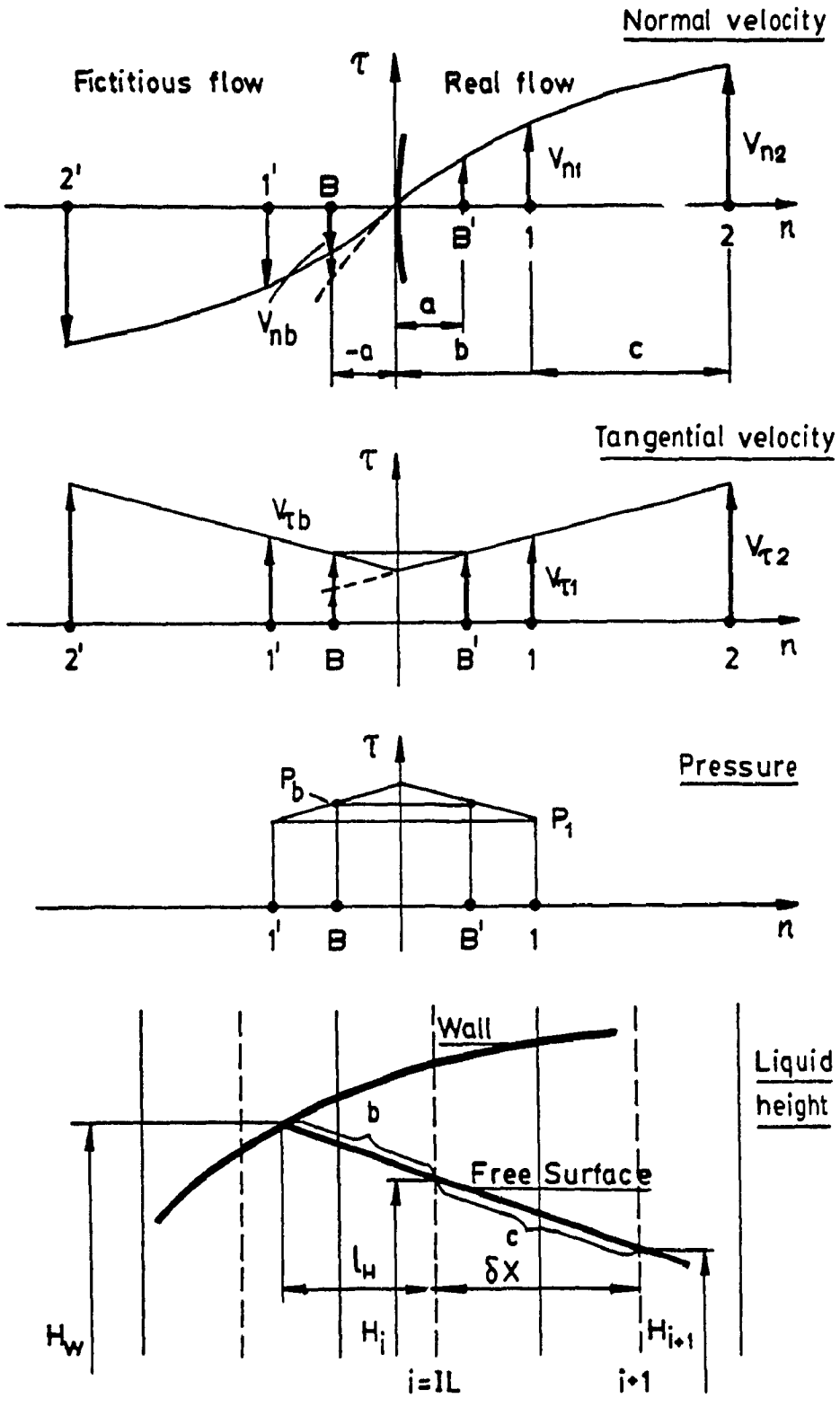

Fig.3.3. Interpolation-reflection type boundary condition

that these different approaches give different results; the boundary velocity computed by simple extrapolation is overestimated, if the velocity profile is convex, or underestimated, if this profile is concave, comparing with interpolation-reflection procedure. It seems that interpolation-reflection method gives more realistic result since it is consistent with the symmetry principal, while the extrapolation assumes the extension of the real flow beyond the physical border which has no any reasonable basis. The second graph of Fig. 3.3 shows the definition of the tangential boundary velocity using the same interpolation-reflection principal which results in the linear interpolation but uses the same number of the internal nodes since the node at the wall does not participate.

In a real situation, the boundary point B may fall inside the wall, then a simple interpolation with no reflection has to be made. For the no-slip condition, the tangential velocity is treated in exactly the same manner as the normal one and this results in the same order interpolation for both velocity components. At the free surface, the boundary velocities are defined by using zero or first order extrapolation technique, since only the free-slip condition is possible.

The boundary pressure at rigid wall is computed from the simplified momentum equation written for the direction normal to the wall, which results in linear pressure distribution in the neighbourhood of the wall. Hence, the boundary pressure is adjusted by the amount that depends on the slope of the wall and the instantaneous value of the total body force in the node, from where the pressure is linearly interpolated or extrapolated along the n-axis. At the free surface, the pressure is maintained equal to the ambient air pressure, while the

routine for the boundary pressure calculation remains the same.

Different definitions for the boundary liquid heights are considered in this study. They include first and second order interpolation as well as a special development of the reflection principal carried out in subsection 3.3.4 for a particular case of rectangular container. The final choice of the boundary conditions will be made in Chapter 4 while validating the computer model of sloshing.

3.3.1 Boundary Velocities at the Rigid Wall

The calculation of a boundary velocity involves different cell-velocities depending on the slope of the n-axis. Possible configurations of the grid points involved are shown in Fig. 3.4 for one quarter of the Y-X plane, where for Configuration 1, the line, traced from the boundary point B normally to the wall, intersects the grid lines at points 1 and 2. The four configurations are established for two-node interpolation, and in general, the number of configurations depends on the order of interpolation: the higher is the order of interpolation the more configurations are to be defined. The velocities at the nodes 1 and 2 are defined by interpolation between the nearest cell velocities, for example for Configuration 1, V_1 is found using V_3 and V_6, and V_2 using V_4 and V_7. For the remaining three quarters, the configurations are symmetrical and, therefore, the derivation of the boundary velocities may be carried out only for the four shown configurations. The grids for the U-velocity and pressure may be constructed in the similar manner.

The definition of the boundary velocities starts with breaking of the rigid boundary into portions corresponding to the given

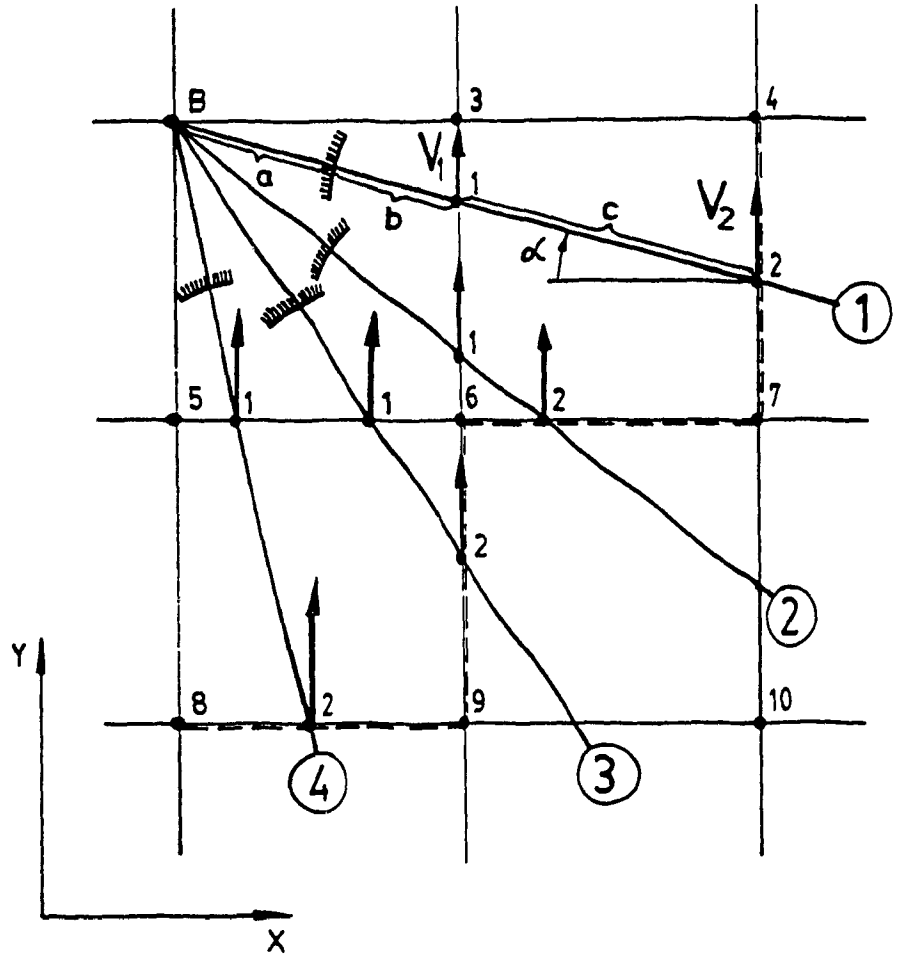

Fig.3.4. Configurations of the grid points for V velocity with two internal nodes

configurations, which are defined in Table 3.1. Then, the weighting coefficients, accounting for the contribution of participating cell-velocities, are computed separately for U and V velocities for each configuration and for free-slip or no-slip conditions, applied to the velocity of interest. The derivation of the weighting coefficients is given in Appendix I, while Fig. 3.5 illustrates such a derivation for V boundary velocity for the case of the free-slip condition, and the weighting coefficients are listed in Table 3.2 for the first order extrapolation and in Table 3.3 for the second order.

In these tables, the quantities entering the weighting coefficients, η's, are defines as:

$$\alpha = \arctan\left(\frac{B}{A}\right)$$
$$\ell = (R\cos\alpha - A) \,/\, L_o \qquad (3.6)$$
$$m = \frac{\delta Y}{\delta X \,|\tan\alpha|}$$

where the lengths, ℓ, A, and B, the radius of the wall curvature, R, and the angle α are different for U and V velocities and must be computed in the corresponding grids. In Fig. 3.5 they are shown as for V velocity with v subscript.

Considering the free-slip second order V velocity case, it follows from Fig, 3.5 that the normal component of the V velocity in the point B, V_{nB}, and the corresponding tangential component, $V_{\tau B}$, form angles γ and $(\beta-\alpha)$ respectively with the total vector of the boundary velocity, V_{Bt}. The boundary value of the velocity, V_B, defined as a projection of the total vector, V_{Bt}, on the Y-axis, forms the angle α with $V_{\tau B}$. Thus, the expressions defining the boundary velocity can be written as:

Table 3.1. Definition of boundary velocity configurations

Configuration	Angle α
1	$0 \le \alpha < \text{Arctan}\left(\frac{\delta Y}{2\delta X}\right)$
2	$\text{Arctan}\left(\frac{\delta Y}{2\delta X}\right) \le \alpha < \text{Arctan}\left(\frac{\delta Y}{\delta X}\right)$
Transitional 2 to 3	$\alpha = \text{Arctan}\left(\frac{\delta Y}{\delta X}\right)$
3	$\text{Arctan}\left(\frac{\delta Y}{\delta X}\right) < \alpha < \text{Arctan}\left(\frac{2\delta Y}{\delta X}\right)$
4	$\text{Arctan}\left(\frac{2\delta Y}{\delta X}\right) \le \alpha \le \frac{\pi}{2}$

Table 3.2. Interpolation-reflection type rigid wall boundary velocities by the first order interpolation of the normal velocity component for free-slip condition

	Normal component $V_{nB} = \left(\sum \eta_i V_i\right) \sin\alpha$ $U_{nB} = \left(\sum \eta_i U_i\right) \cos\alpha$	Tangential component $V_{\tau B} = \left(\sum \eta_i V_i\right) \cos\alpha$
1 and 2	$\eta_3 = \frac{\ell\,(m-1)}{m\,(\delta X + \ell)}$; $\eta_6 = \frac{\ell}{m\,(\delta X + \ell)}$	$\eta_3 = \frac{m-1}{m}$; $\eta_6 = \frac{1}{m}$
3 and 4	$\eta_5 = \frac{\ell\,(1-m)}{m\delta X + \ell}$; $\eta_6 = \frac{m\,\ell}{m\delta X + \ell}$	$\eta_5 = 1 - m$; $\eta_6 = m$

Table 3.3. Interpolation-reflection type rigid wall boundary velocities by the second order interpolation of the normal velocity component for free-slip condition

Configur. No.	Normal component $V_{nB} = \left(\sum \eta_i V_i \right) \sin \alpha$ $U_{nB} = \left(\sum \eta_i U_i \right) \cos \alpha$	Tangential component $V_{\tau B} = \left(\sum \eta_i V_i \right) \cos \alpha$ $U_{\tau B} = \left(\sum \eta_i V_i \right) \sin \alpha$
1	$\eta_3 = \frac{2\ell(m-1)}{m\delta X}$; $\eta_4 = -\frac{\ell(m-2)(\delta X+2\ell)}{m\delta X\,(2\delta X+\ell)}$; $\eta_6 = \frac{2\ell}{m\delta X}$; $\eta_7 = -\frac{2\ell\,(\delta X+2\ell)}{m\delta X\,(2\delta X-\ell)}$	$\eta_3 = \frac{2(m-1)(\delta X-\ell)}{m\delta X}$; $\eta_4 = -\frac{(m-2)(\delta X+2\ell)}{m\delta X}$ $\eta_6 = \frac{2(\delta X+\ell)}{m\delta X}$; $\eta_7 = -\frac{2(\delta X-2\ell)}{m\delta X}$
2	$\eta_3 = \frac{\ell(m\delta X+2\ell)}{m\delta X(\delta X+\ell)}$; $\eta_7 = -\frac{\ell\,(\delta X-2\ell)}{\delta X\,(m\delta X+\ell)}$; $\eta_6 = \frac{\ell}{\delta X(m-1)}\left[\frac{m\delta X+2\ell}{m(\delta X-\ell)} - \frac{(2-m)(\delta X+2\ell)}{m\delta X-\ell}\right]$	$\eta_3 = \frac{m\delta X+2\ell}{m\delta X}$; $\eta_4 = -\frac{\delta X+2\ell}{\delta X}$; $\eta_6 = \frac{m\delta X - m(2-m)(\delta X+2\ell)+2\ell}{m(m-1)\delta X}$
3	$\eta_5 = \frac{\ell(\delta X+2\ell)}{\delta X(m\delta X+\ell)}$; $\eta_9 = -\frac{\ell(m\delta X-2\ell)}{m\delta X(\delta X-\ell)}$; $\eta_6 = \frac{\ell}{\delta X(1-m)}\left[\frac{m(\delta X+2\ell)}{m\delta X+\ell} - \frac{(2m-1)(m\delta X-2\ell)}{m(\delta X-\ell)}\right]$	$\eta_5 = \frac{\delta X+2\ell}{\delta X}$; $\eta_9 = -\frac{m\delta X+2\ell}{m\delta X}$; $\eta_6 = \frac{m^2(\delta X+2\ell) - (2m-1)(m\delta X+2\ell)}{m(1-m)\delta X}$
4	$\eta_5 = \frac{2\ell(1-m)}{m\delta X}$; $\eta_6 = \frac{2\ell}{\delta X}$; $\eta_8 = -\frac{\ell(1-2m)(m\delta X-2\ell)}{m\delta X\,(2m\delta X+\ell)}$; $\eta_9 = -\frac{2\ell(m\delta X+2\ell)}{\delta X(2m\delta X+\ell)}$	$\eta_5 = \frac{2(1-m)(m\delta X+\ell)}{m\delta X}$; $\eta_6 = \frac{2(m\delta X+\ell)}{\delta X}$ $\eta_8 = -\frac{(1-2m)(m\delta X+2\ell)}{m\delta X}$; $\eta_9 = -\frac{2(m\delta X+2\ell)}{\delta X}$
2 to 3	$\eta_6 = \frac{2\ell}{\delta X}$; $\eta_{10} = -\frac{\ell(\delta X-2\ell)}{\delta X(2\delta X-\ell)}$	$\eta_6 = \frac{2(\delta X+\ell)}{\delta X}$; $\eta_{10} = -\frac{\delta X+2\ell}{\delta X}$

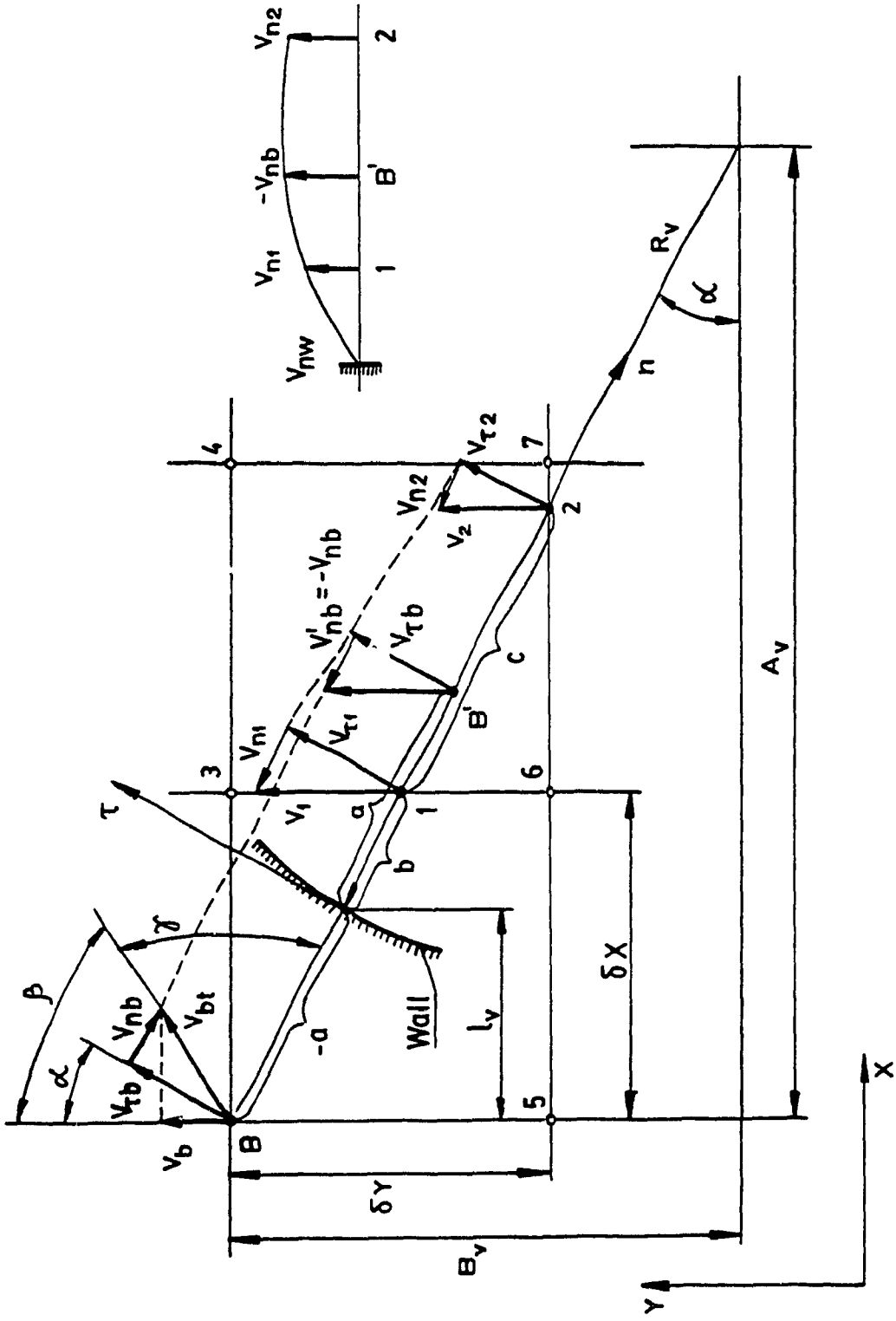

Fig.3.5. Derivation of the boundary V velocity for free-slip condition

$$V_{Bt} = \sqrt{V_{nB}^2 + V_{\tau B}^2}$$

$$V_B = V_{Bt} \cos\beta \qquad (3.7)$$

$$\gamma = \arctan\left(\frac{V_{\tau B}}{V_{nB}}\right)$$

Since $\beta - \alpha + \gamma = \frac{\pi}{2}$, the expression for $\cos\beta$ can be developed in the following manner:

$$\cos\beta = \sin(\gamma - \alpha) = \sin\left[\arctan\left(\frac{V_{\tau B}}{V_{nB}}\right)\right]\cos\alpha - \cos\left[\arctan\left(\frac{V_{\tau B}}{V_{nB}}\right)\right]\sin\alpha$$

$$= \frac{V_{\tau B}.\cos\alpha}{\sqrt{V_{\tau B}^2 + V_{nB}^2}} - \frac{V_{nB}.\sin\alpha}{\sqrt{V_{\tau B}^2 + V_{nB}^2}} = \frac{1}{V_{Bt}}\left(V_{\tau B}\cos\alpha - V_{nB}\sin\alpha\right),$$

and the boundary V velocity can be expressed as

$$V_B = V_{\tau B}\cos\alpha - V_{nB}\sin\alpha \qquad (3.8)$$

Expressing the values of the $V_{\tau B}$ and V_{nB} in the general form as

$$V_{\tau B} = \left(\sum \eta_i V_i\right)_\tau \cos\alpha \quad \text{and} \quad V_{nB} = \left(\sum \eta_i V_i\right)_n \sin\alpha$$

and substituting these values into the Eqn. (3.8) yields

$$V_B = \left(\sum \eta_i V_i\right)_\tau \cos^2\alpha - \left(\sum \eta_i V_i\right)_n \sin^2\alpha \qquad (3.9)$$

$$\text{where } \alpha = \arctan\left(\frac{B}{A}\right)$$

Thus, the Eqn. (3.9) gives explicitly the boundary V velocity for free-slip condition and for any of the four configurations, provided that the weighting coefficients are known from Table 3.3 and the angle α is defined as it is shown in Eqn. (3.9) or by any other way for the given shape of the container wall.

For the U velocity, free-slip condition, and second order of extrapolation, the angles β and γ can be redefined in the following way: β is the angle between the total boundary velocity vector, U_{Bt}, and the X- axis and γ is the angle between U_{Bt} and the tangential component, $U_{\tau B}$. Then the boundary U velocity, U_B, defined as the projection of the U_{Bt} on the X -axis, is expressed with exactly the same expression as V_B, i.e. by Eqn. (3.9). Hence, the Eqn. (3.9) gives the boundary values for both U and V velocities for the free-slip condition and the second order of extrapolation. It has to be noted, though the expressions for U_B and V_B are identical, the computed values of those velocities will be different because of the staggered grid.

Now consider the no-slip condition for the second order extrapolation, when both components of either V or U are defined similarly. In this case

$$\alpha - \beta + \gamma = \frac{\pi}{2} \tag{3.10}$$

where β and γ are formed by the total vector, V_{Bt}, with the V_B and V_{nB} velocities respectively. Then, the Eqns. (3.7) hold and the expression for cos β gives:

$$\cos\beta = \sin(\alpha+\gamma) = \sin\alpha \cos\left[\arctan\left(\frac{V_{\tau B}}{V_{nB}} \right)\right] + \cos\alpha \times$$

$$\sin\left[\arctan\left(\frac{V_{\tau B}}{V_{nB}} \right)\right] = \frac{1}{V_{Bt}} \left(V_{\tau B} \cos\alpha + V_{nB} \sin\alpha \right)$$

Taking into account that in the following expressions

$$V_{\tau B} = \left(\sum \eta_i V_i \right)_\tau \cos\alpha \qquad \text{and} \qquad V_{nB} = \left(\sum \eta_i V_i \right)_n \sin\alpha$$

the weighting coefficients for both components are identical, because of the same order of extrapolation, the expression for the cosβ becomes:

$$\cos\beta = \frac{\sum \eta_i V_i}{V_{Bt}} \left(\cos^2\alpha + \sin^2\alpha \right) = \frac{\sum \eta_i V_i}{V_{Bt}}$$

where $V_{Bt} = \sqrt{V_{nB}^2 + V_{\tau B}^2} = \left(\sum \eta_i V_i \right) \sqrt{\sin^2\alpha + \cos^2\alpha} = \sum \eta_i V_i$

Finally, substitution of the last expression into the previous one for the $\cos\beta$ gives

$$\cos\beta = 1 \quad \text{or} \quad \beta = 0^0 \tag{3.11}$$

This has proved that if a velocity components are interpolated with the same order for no-slip condition, then the total vector of the boundary velocity, V_{Bt}, coincides in direction and magnitude with the boundary velocity, V_B. In other words, it is not necessary to split a velocity into the two components but rather to interpolate and reflect it. Because of this fact, the boundary velocity can be computed as

$$V_B = \sum \eta_i V_i \tag{3.12}$$

The expression (3.12) holds for U_B velocity as well and, in general, it holds for any velocity in the X-Y plane. However, the weighting coefficients for U and V velocities are different because of the staggered grid, and they can be taken from Tables 3.2 - 3.3 for the normal component, either for U_{nB} or V_{nB}, depending on the boundary velocity of interest and the order of interpolation.

3.3.2 Boundary Velocities at the Free Surface

At the free surface, the shear stress is absent in accordance with the neglected local free-surface effects. Also, the reflection principle does not hold since the so-called fictitious flow is an extension of the real flow beyond the free surface. In this case, the boundary velocity can be extrapolated outside using an order of extrapolation between zero and two that, in principle, must be confirmed by a preliminary investigation as it is considered in Chapter 4. The weighting coefficients, η's, can be taken from Table 3.2 for zero order extrapolation and from Table 3.3 for the first order both for the tangential components, but in the second case the length ℓ given in Eqn. (3.6) is to be a positive value if the point B is located outside of the wall and a negative one, as it is in this table, if the point B is located inside.

The essential difference in boundary conditions for the rigid wall and free surface is that that in the case of the rigid wall the weighting coefficients are computed only in the beginning of the computer program, while in the case of the free surface, the coefficients must be calculated for each time step because of the change of the free-surface position. Therefore, the angle α must be redefined for this case as:

$$\alpha = \arctan\left(\frac{\delta X}{H_{i-1} - H_i}\right) \quad \text{for the negative slope of the free surface}$$

$$\alpha = \arctan\left(\frac{\delta X}{H_{i+1} - H_i}\right) \quad \text{for the positive slope}$$

where the boundary or B-cell is the i-cell.

In order to avoid the definition of the radius of curvature of the free surface, the free surface is approximated by a straight line between the

two cells involved. Then, the length ℓ can be expressed as:

$$\ell = \left(H_B - H_i \right) \sin\alpha \cos\alpha \qquad (3.14)$$

where H_B is the height (or Y-coordinate) of the boundary node B.
It has to be noted, that because of the staggered grid, the heights in Eqns. (3.13) and (3.14) are different for U and V velocities. For the V velocity, they coincide with the computed H_i's while for the U velocity, they are shifted by $-\delta X/2$ distance and must be averaged between the two surrounding values.

The extrapolation of both the V and U boundary velocities may appear to be too free and introduce some arbitrariness in the boundary conditions definition, especially in the case of a coarse mesh. Then, only one, for example, V boundary velocity can be found by extrapolation while the second one is to be defined from the continuity condition. The continuity, in general, is not satisfied for a free surface cell because of a positive or negative liquid flux into or out of the cell. This is true when a partial cell, bounded by the free surface, is considered. If however, the complete cell composed by the real and fictitious parts is examined, then the continuity condition may be demanded on that basis that this cell is a continuation of the flow for which the continuity must be satisfied in every cell, and the free surface is believed to be some fictitious separating surface moving in space with local velocities of the flow. In this case, the continuity equation gives for the boundary U velocity the following expression

$$U_{i,j} = U_{i-1,j} - \frac{\delta X}{\delta Y} \left(V_{i,j} - V_{i,j-1} \right) \qquad (3.15)$$

which is explicit while sweeping in the mesh from left to right and providing that the most left $U_{i-1,j}$ is defined from the rigid wall boundary condition and the V velocities are computed a priori. The final choice of the boundary condition at the free surface is made in Chapter 4 through comparison of the computed and experimental results of the liquid motion in a test container.

3.3.3 Pressure Boundary Conditions

The boundary pressure at rigid wall can be computed from the momentum equation, written for a wall point in the direction normal to the wall, which can be brought to the following simple form:

$$\frac{\partial P}{\partial n} = \frac{1}{Eu\ Fr}\left(\pm G_x \cos\alpha \pm G_y \sin\alpha\right) + \frac{1}{Re\ Eu}\frac{\partial^2 V_n}{\partial n^2} \qquad (3.16)$$

In this equation, the Re number is large for the free-slip condition and the second derivative of the normal velocity is small for the no-slip condition. Therefore, the viscous term can be neglected without introducing a significant error. Then, the pressure derivative can be expressed from Fig. 3.6 a, as

$$\frac{\partial P}{\partial n} = \frac{P_1 - P_B^1}{b - a}, \qquad (3.17)$$

and the resulting boundary pressure is found to be

$$P_B = P_B^1 = P_1 - \frac{b - a}{Eu\ Fr}\left(\pm G_x \cos\alpha \pm G_y \sin\alpha\right) \qquad (3.18)$$

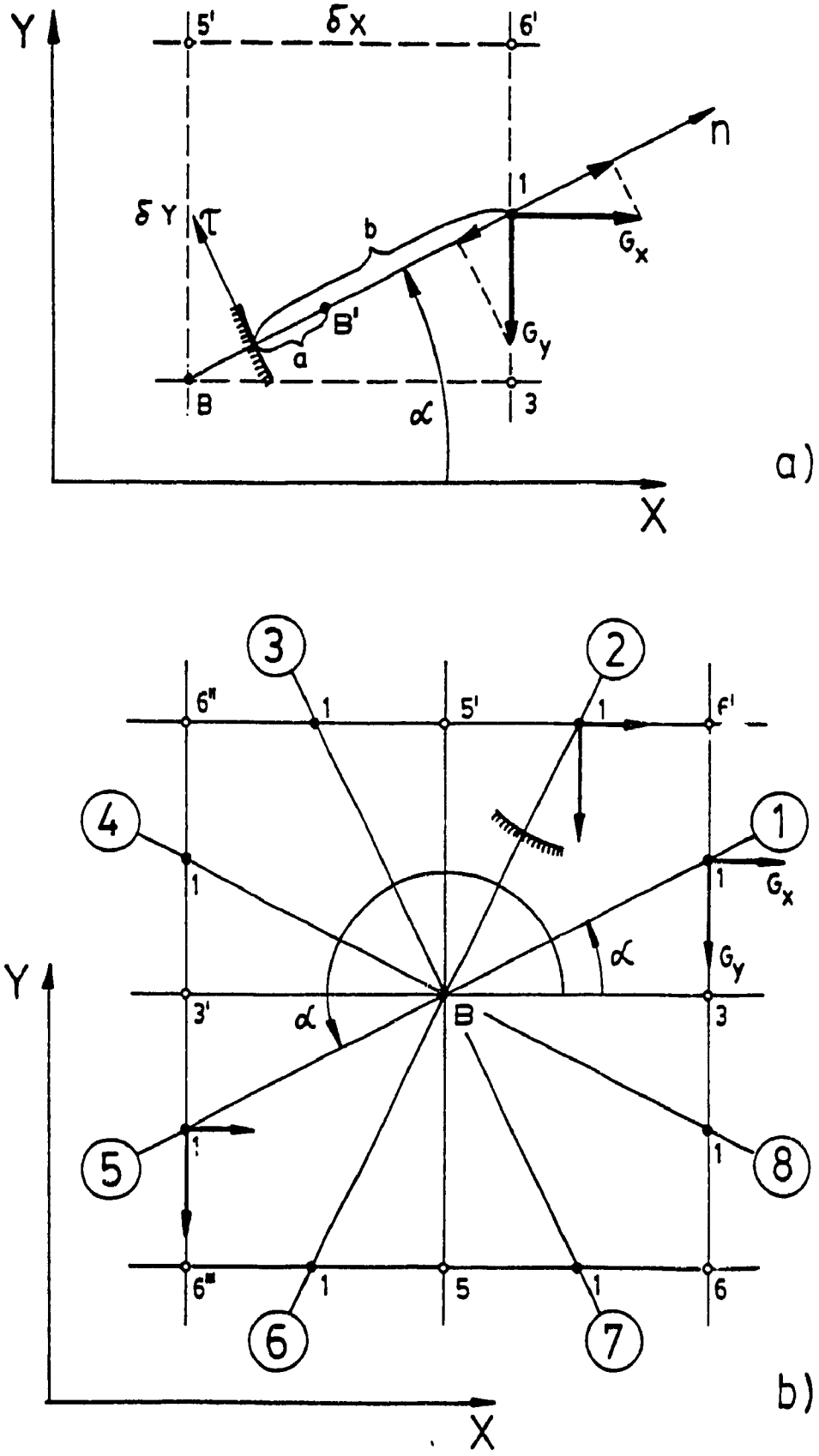

Fig.3.6. Derivation of the pressure boundary condition, a), and the corresponding configurations, b)

where the distance a is between the nodes 1 and B and the pressure at node 1, P_1, is found by interpolation between the nearest cell-pressures as it is shown in Fig. 3.6 b for each of the possible 8 configurations. The configurations are defined by the angle α formed by the inward normal n with X -axis, and they are listed in Table 3.4 together with the expressions for the boundary pressure. The assumptions made for the boundary pressure definition led to a linear pressure distribution along the normal line in the vicinity of the wall that is expressed by the second term of Eqn. (3.18). This correction term, introducing a partially hydrostatic pressure distribution near the wall, does not assume the hydrostatic condition since the boundary pressure also includes the cell pressures which are the total pressure values.

The boundary pressure on the free surface can be computed using the condition similar to no-slip condition for a velocity at rigid wall. This assumes a constant pressure at the free surface (equal to atmospheric pressure, in the case of an unpressurized tank) that is correct if the surface tension and the interaction of the free surface with the ambient air are neglected. Then, the boundary pressure is found by extrapolation of the first or second order depending on the order of extrapolation of the velocity. The configurations for pressure grid at the free surface are defined similarly to a velocity grid, see Fig. 3.4, and the boundary pressure is expressed as

$$P_B = \sum \eta_i P_i \qquad (3.19)$$

where the weighting coefficients can be taken from Table 3.2 for the

Table 3.4. Boundary pressure at rigid wall

Configuration	Configuration definition	Boundary pressure
1	$0 \le \alpha < \arctan\left(\frac{\delta Y}{\delta X}\right)$	$P_B = \frac{m-1}{m} P(3) + \frac{1}{m} P(6') + \frac{\delta X + 2\ell}{EuFr}\left(-G_x - G_y \tan\alpha\right)$
2	$\arctan\left(\frac{\delta Y}{\delta X}\right) \le \alpha < \frac{\pi}{2}$	$P_B = (1-m)P(5') - mP(6') + \frac{\delta Y + 2\ell \tan\alpha}{EuFr}\left(-\frac{G_x}{\tan\alpha} - G_y\right)$
3	$\frac{\pi}{2} \le \alpha < \frac{\pi}{2} + \arctan\left(\frac{\delta Y}{\delta X}\right)$	$P_B = (1-m)P(5') + mP(6'') + \frac{\delta Y - 2\ell \tan\alpha}{EuFr}\left(-\frac{G_x}{\tan\alpha} - G_y\right)$
4	$\frac{\pi}{2} + \arctan\left(\frac{\delta X}{\delta Y}\right) \le \alpha < \pi$	$P_B = \frac{m-1}{m} P(3') - \frac{1}{m} P(6'') + \frac{\delta X + 2\ell}{EuFr}\left(G_x + G_y \tan\alpha\right)$
5	$\pi \le \alpha < \pi + \arctan\left(\frac{\delta Y}{\delta X}\right)$	$P_B = \frac{m-1}{m} P(3') - \frac{1}{m} P(6''') + \frac{\delta X + 2\ell}{EuFr}\left(G_x + G_y \tan\alpha\right)$
6	$\pi + \arctan\left(\frac{\delta Y}{\delta X}\right) \le \alpha < \frac{3\pi}{2}$	$P_B = (1-m)P(5) + mP(6'') + \frac{\delta Y - 2\ell \tan\alpha}{EuFr}\left(\frac{G_x}{\tan\alpha} + G_y\right)$
7	$\frac{3\pi}{2} \le \alpha < \frac{3\pi}{2} + \arctan\left(\frac{\delta X}{\delta Y}\right)$	$P_B = (1-m)P(5) + mP(6) + \frac{\delta Y + 2\ell \tan\alpha}{EuFr}\left(\frac{G_x}{\tan\alpha} + G_y\right)$
8	$\frac{3\pi}{2} + \arctan\left(\frac{\delta X}{\delta Y}\right) \le \alpha < 2\pi$	$P_B = \frac{m-1}{m} P(3) + \frac{1}{m} P(6) + \frac{\delta X + 2\ell}{EuFr}\left(-G_x - G_y \tan\alpha\right)$

first-order extrapolation and from Table 3.3 for the second order for the normal velocity component in both cases. The quantities, entering the weighting coefficients and given in Eqns. (3.6), must be computed in the pressure grid.

3.3.4 Free-Surface Height Boundary Conditions

The reflection principle, employed for the boundary velocities and pressure, can be extended for the free-surface boundary height only in the simplest case when the container wall is perpendicular to the X-axis if the height of the free surface is defined as Y-coordinate. This is due to a specific meaning of the height variable which demand the same datum for its measurement. Thus, for the vertical walls of a rectangular container, the datum for real and fictitious flows' heights is always the X-coordinate, and in this case, the assumption of symmetry leads to symmetrical heights with respect to the wall. In any other case, the free-surface height, or some distance characterizing the location of a free-surface point, must be referred from a datum which has to be somehow reflected into the fictious flow. This may involve a complicated transformation of the flow domain, and the flow itself must be solved in the corresponding system of coordinates.

In order to avoid those complications, the boundary height calculation adopted in this investigation is made in the point of intersection of the free surface and the wall, instead of centre lines of the mesh columns, by simple extrapolation of the second or first order, as it is shown in the last graph of Fig. 3.3. Hence, for the linear extrapolation, the boundary height computed at the wall point can be expressed as:

$$H_w = \left(1 + \frac{\ell}{\delta X}\right) H_i - \frac{\ell}{\delta X} H_{i+1} \qquad (3.20)$$

where ℓ can be easily defined for the two points of intersection of the free surface and wall provided that the wall shape is known.

Such an approach requires a redefinition of the finite difference formulae for the free-surface equation, given in Eqn. (3.4), for the two mentioned points because of unequal distances between the grid points. The modified discretized equations are given in Eqns. (3.21) for the left and right points of intersection or for the IL and IR columns respectively:

$$H_i^{K+1} = H_i^K + \frac{\delta T}{St}\left\{\bar{V}_i^{K+\frac{1}{2}} - \bar{U}_i^{K+\frac{1}{2}}\left[\frac{H_{i+1}^K - H_{i-1}^K}{\delta X + \ell_H} + \gamma\left(\frac{H_i^K - H_{i-1}^K}{\delta X + \ell_H} + \frac{H_i^K - H_{i+1}^K}{2\delta X}\right)\right]\right\}$$

$$H_i^{K+1} = H_i^K + \frac{\delta T}{St}\left\{\bar{V}_i^{K+\frac{1}{2}} - \bar{U}_i^{K+\frac{1}{2}}\left[\frac{H_{i+1}^K - H_{i-1}^K}{\delta X + \ell_H} + \gamma\left(\frac{H_i^K - H_{i-1}^K}{2\delta} + \frac{H_i^K - H_{i+1}^K}{\delta X + \ell_H}\right)\right]\right\} \qquad (3.21)$$

where: in the first equation i = IL and $H_{i-1} = H_w$,

in the second equation i = IR and $H_{i+1} = H_w$,

and velocities with bars are those at the free surface.

In the beginning of this section, it has been mentioned that in the case of a rectangular tank, the boundary condition on the liquid height can be, for vertical walls only, developed based on the principle of flow reflection. Although this approach has a limited application, i.e.

the interference of the free surface with horizontal walls is not allowed, it has shown very good result for small amplitude liquid oscillation which will be discussed in Chapter 4. The idea of this approach is based on the assumption that at the time level, k, the real and fictitious flows are symmetrical with respect to the wall in terms of the liquid heights and slopes of the free surface, while the velocities are subjected to odd or even symmetry depending on either no-slip or free-slip condition is accepted, see Fig. 3.8. At the time (k+1), the symmetry is disturbed for the no-slip velocity conditions but it remains for the free-slip condition. The boundary height can be then derived (the derivation is given in Appendix II) from the free-surface equation, Eqn. (2.1), for the no-slip and free-slip conditions respectively in the form:

$$H_B^{K+1} = H_2^{K+1} - \frac{2\delta T}{St}\bar{V}_2^K$$

$$H_B^{K+1} = H_2^{K+1} \qquad (3.22)$$

From these equations, it can be seen that no-slip velocity condition leads to cancellation of the spatial derivative term because of assumed symmetry of the real and fictitious flows while the free-slip conditions results in even simpler expression where both the time and spatial derivatives are cancelled. It has to be noted that the symmetry condition for the flow is organized at the beginning of each time step.

3.4 The Pressure-Velocity Iteration Procedure

The discretized momentum equations, Eqns. (3.1) and (3.2) are solved numerically only once at each time step and such a solution does

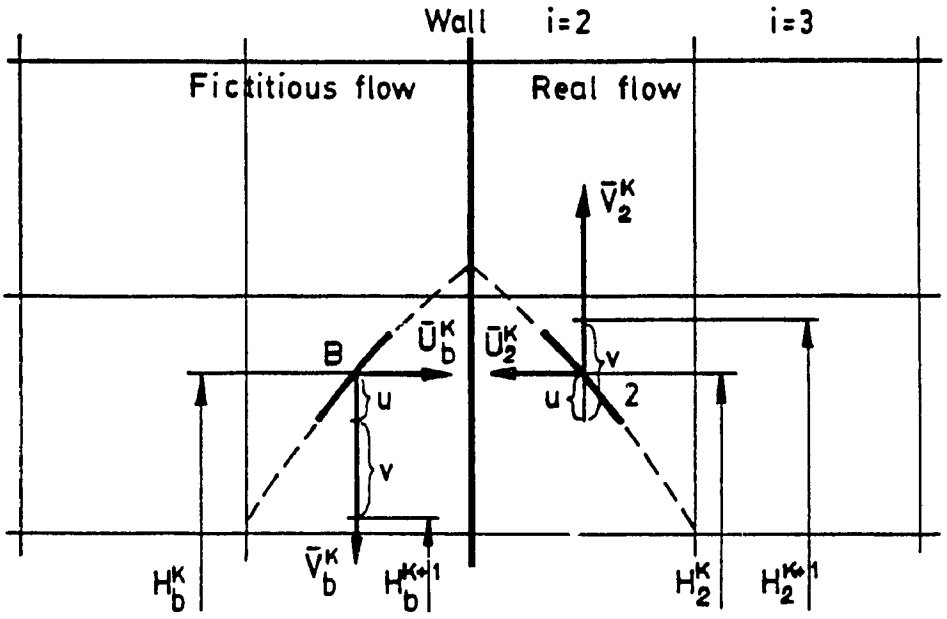

Fig.3.7. Liquid height reflection type boundary condition

not satisfy, in general, the continuity condition. The obtained values of the cell velocities and pressures are then specified by iterating the continuity or divergence equation. The velocity divergence, D, given in Eqn. (3.3) is computed for each fluid cell and the pressure is adjusted to drive the divergence to some prescribed small value defined by the tolerance which in this study was taken equal to 10^{-5}. The pressure change in a cell for each iteration is calculated as

$$\delta P = - \frac{\omega \, St \, D}{2\delta T \, Eu \left(\frac{1}{\delta X^2} + \frac{1}{\delta Y^2} \right)} \tag{3.23}$$

where the over-relaxation factor ω is used to accelerate the convergence of the iteration. It has been optimized for each narrow class of solved problems distinguished by the shape of the container and the fill level. Typically, it has been varied between 1.8 and 1.9. Then, the new parameters of the flow are

$$P_{i,j} = P_{i,j} + \delta P \qquad V_{i,j} = V_{i,j} + \frac{\delta T \, Eu}{\delta X \, St} \delta P$$

$$U_{i,j} = U_{i,j} + \frac{\delta T \, Eu}{\delta X \, St} \delta P \qquad V_{i,j-1} = V_{i,j-1} - \frac{\delta T \, Eu}{\delta X \, St} \delta P \tag{3.24}$$

$$U_{i-1,j} = U_{i-1,} - \frac{\delta T \, Eu}{\delta X \, St} \delta P$$

These new values participate in the next iteration until the desired accuracy is reached. The last computed values of velocities and pressure serve to calculate the fluid heights, forces, and overturning moments, and after this a new time cycle is done. This technique, introduced by Hirt [56], is reliable and computationally economical compared with direct iteration of the momentum equations.

3.5 Development of the Computer Code

The computational procedure, briefly described above, is considered in detail in the present subsection. The flow-chart of the computer code given in Fig. 3.8 can be summarized in the following manner:

i) The constant parameters of the problem including the definition of the container shape are defined first in blocks 1 and 2.

ii) The initial conditions, prescribing zero velocity and hydrostatic pressure distribution, are set in block 3. The initial conditions are defined in overlapping fluid region that include the boundary cells, thereby the boundary conditions for the first time step are automatically included.

iii) The discretized momentum equations are solved without iterations in block 4.

iv) The boundary conditions on velocities and pressures are set in block 5.

v) The previously obtained velocities and pressures are iterated utilizing the over-relaxation techniques, blocks 6,7,8, until the convergence is reached.

vi) The heights of the free surface are computed using the final values of the velocities for the current time step. However, due to incomplete iterations, these heights are approximate and the error can accumulate with time. Therefore, the correction of the heights has to be done by comparing the current volume of the liquid with the initial one and equally sharing the surplus or deficit of the volume between the

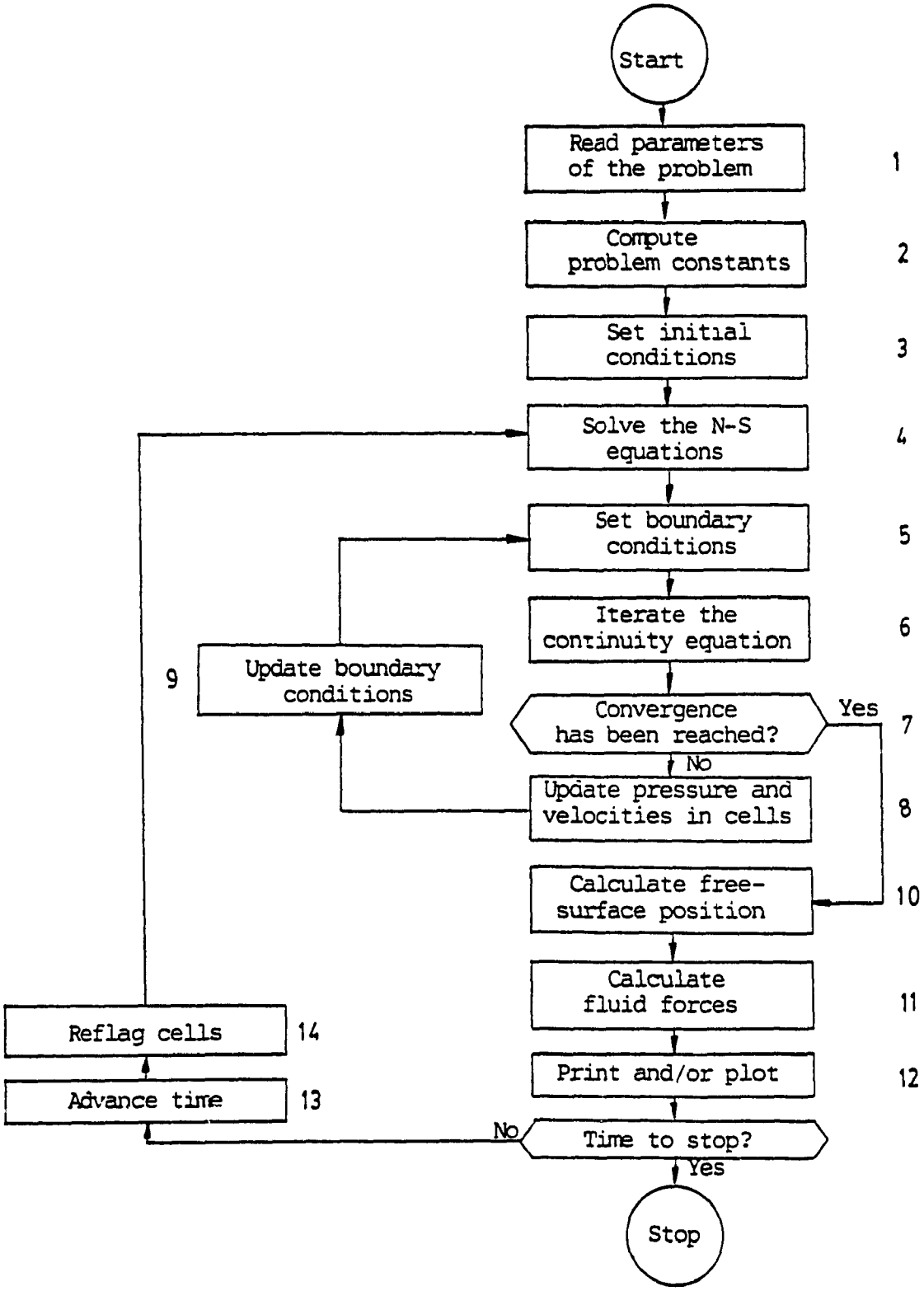

Fig.3.8. The numerical procedure for obtaining transient solutions

columns having the free surface. Because of this fact, the algorithm of the block 10 includes the following:

a) compute new free-surface position,

b) compute liquid heights at walls, HL and HR,

c) set BC's on H,

d) correct liquid heights,

e) update array by calculating IL, IR, and JT-cells,

f) update HL and HR,

g) update BC's on H.

vii) The forces and moment acting on the container body are calculated by integrating the pressure that is previously extrapolated from the centres of cells to the wall, block 11.

viii) By this step, all calculations associated with the current time step are accomplished and the solution can be marched in time. The preparation for the next time step is done in blocks 13 and 14 where the time is advanced by δT and the repackage of the flow parameters, i.e. velocities and heights, is made by giving them the status of old values.

ix) Finally, the solution is passed to the block 4, from where a new sequence of similar operations is carried out.

3.6 Summary

In this chapter, the computer model representing the liquid sloshing in road containers is described. The main attention is given to the definition of the boundary conditions of the problem stressing on the consistency of their imposition for different variables of the flow.

The boundary conditions are defined using the reflection principle and the interpolation technique of different orders of accuracy is developed in a general manner for containers of arbitrary shape. The final choice of the boundary conditions will be made in Chapter 4 after comparison of the numerical solutions with the results of physical testing.

The computational procedure is discussed in detail and all computational steps are summarized. The computer model of the sloshing phenomena is general enough to suit for solutions in a wide range of shapes of liquid tankers. The peculiarity, due to some specific conditions of baffled containers, will be discussed in Chapter 7.

CHAPTER 4

EXPERIMENTAL VALIDATION OF THE COMPUTER MODEL

4.1 General

The computer model of sloshing phenomena developed in the previous chapter allows some freedom in assignment of the boundary conditions imposed on the flow variables, and therefore, the final choice of the boundary conditions should be made on the basis of acceptable agreement between the experimental and computational results. On the other hand, the accuracy of the numerical solution being a function of the spatial and time increments can be checked through the computational experimentations since an analytical methodology is lacking for the nonlinear flow equations. Because of these facts, the objectives of the present chapter are:

i) Tuning of the computer program by appropriate choice of the boundary conditions by employing the physical experimentation.

ii) Estimation of the error of the finite difference analogue through the computational testing.

The question what must be done first, either physical or computation testing, is difficult to be solved without having a prior information about the behaviour of the computational procedure because of the coupled nature of the boundary conditions and discretization of the flow. Numerous computer runs have revealed that the correct imposition of the boundary conditions is of primary importance for a successful numerical calculation. The incorrect boundary conditions very often led to computational instability while the space and time

increments, provided that the time step is not too large, do not result in instability. That is why, the physical experiment precedes the computational testing.

The experiment was carried out in a small scale rectangular tank made from plexiglas and subjected to a prescribed input acceleration, which has been created by means of an electro-hydraulic actuator. As a criterion for comparison of the real and computed flows, the height of the free surface at the left vertical tank wall has been chosen under the assumption that if the correlation between heights in similar points is good, then the flow velocities and pressures are computed correctly. The arrangement of the experimental set-up is described in the following subsection.

4.2 Experimental Set-up and Procedure

The experimental set-up, shown in Fig. 4.1, consisted of the model tank of size 0.8 m x 0.57 m in height filled with water and mounted on a horizontal platform with low friction linear ball bearings. An electrohydraulic actuator fixed horizontally was used to generate the motion of the tank in the horizontal plane. The displacement and acceleration of the tank as well as the force developed in the link between the tank and actuator were recorded by means of corresponding transdusers. The liquid free-surface oscillations were recorded using a video camera -Sony Handicam with an incorporated digital timer having 1 sec. resolution time and making 30 frames per second. The time step used for comparison of results was 0.1 sec. which was obtained by shifting the magnetic tape by 3 frames at a time.

The input acceleration is of the type "accelerating-braking" as

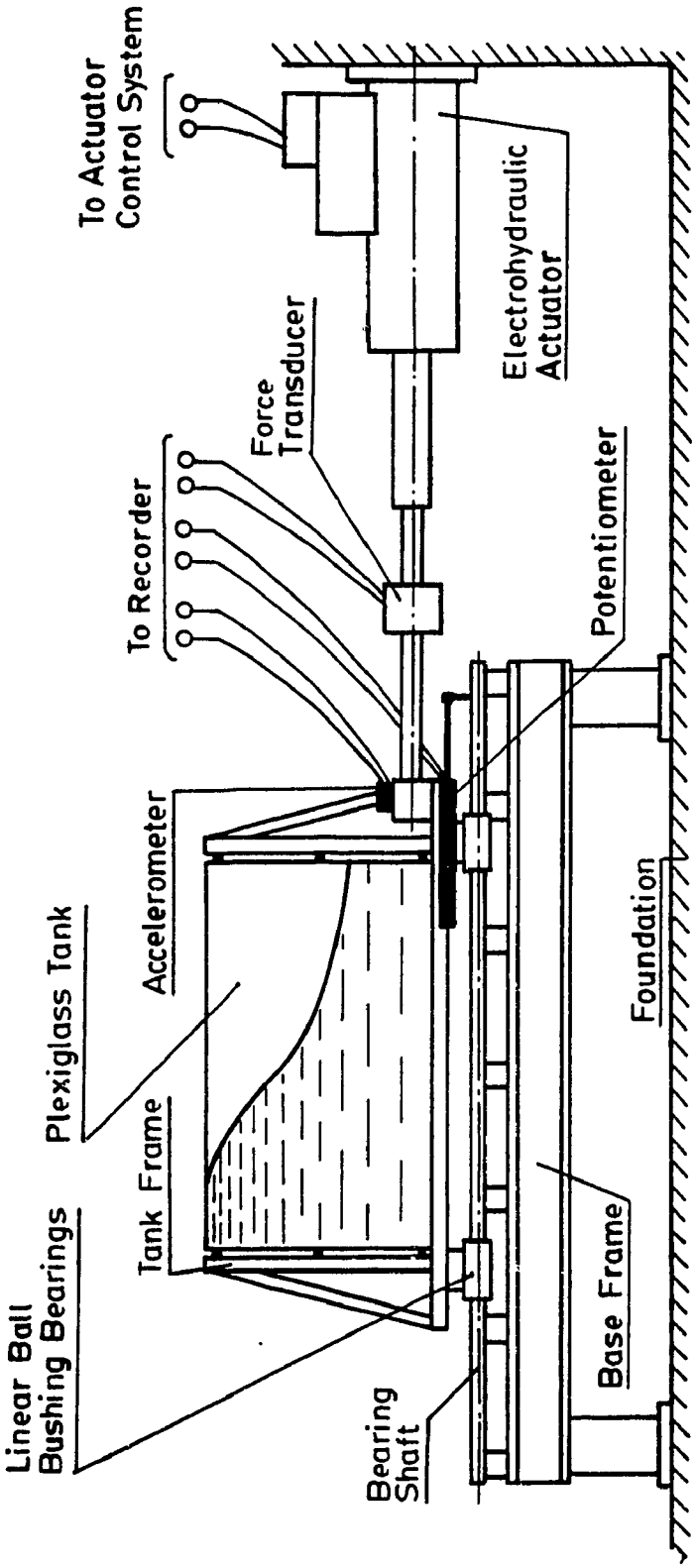

Fig.4.1. The experimental set-up

shown in Fig. 4.2 together with the corresponding displacement. The short duration signal, of about 1 sec. long, was applied to the liquid tank because of the limited stroke of the hydraulic actuator. The total observation time was 8 sec. that included the time of the free vibration after the input signal has been cancelled. The oscillation of the free-surface height at the left wall of the tank is shown by circles in Fig. 4.3, where the solid line gives the oscillation computed in the same tank under the exactly similar conditions and for the final choice of the boundary conditions for which the correlation has been found satisfactory.

4.3 Discussion on the Experimental Results

The final choice of the boundary conditions giving sufficiently close agreement with the experiment, shown in Fig. 4.3, has been achieved through numerous trials of the computer model with different definition of the boundary conditions, variation of the upstream differencing coefficients, and variation of the cell size. The study of this problem is summarized by classifying the directions of the search into the following groups:

i) Type of the boundary condition, which can be either free-slip or no-slip condition.

ii) Method of calculation of boundary condition, which can be either direct extrapolation or interpolation-reflection.

iii) Order of interpolation or extrapolation of the boundary condition that can be zero, first, or second.

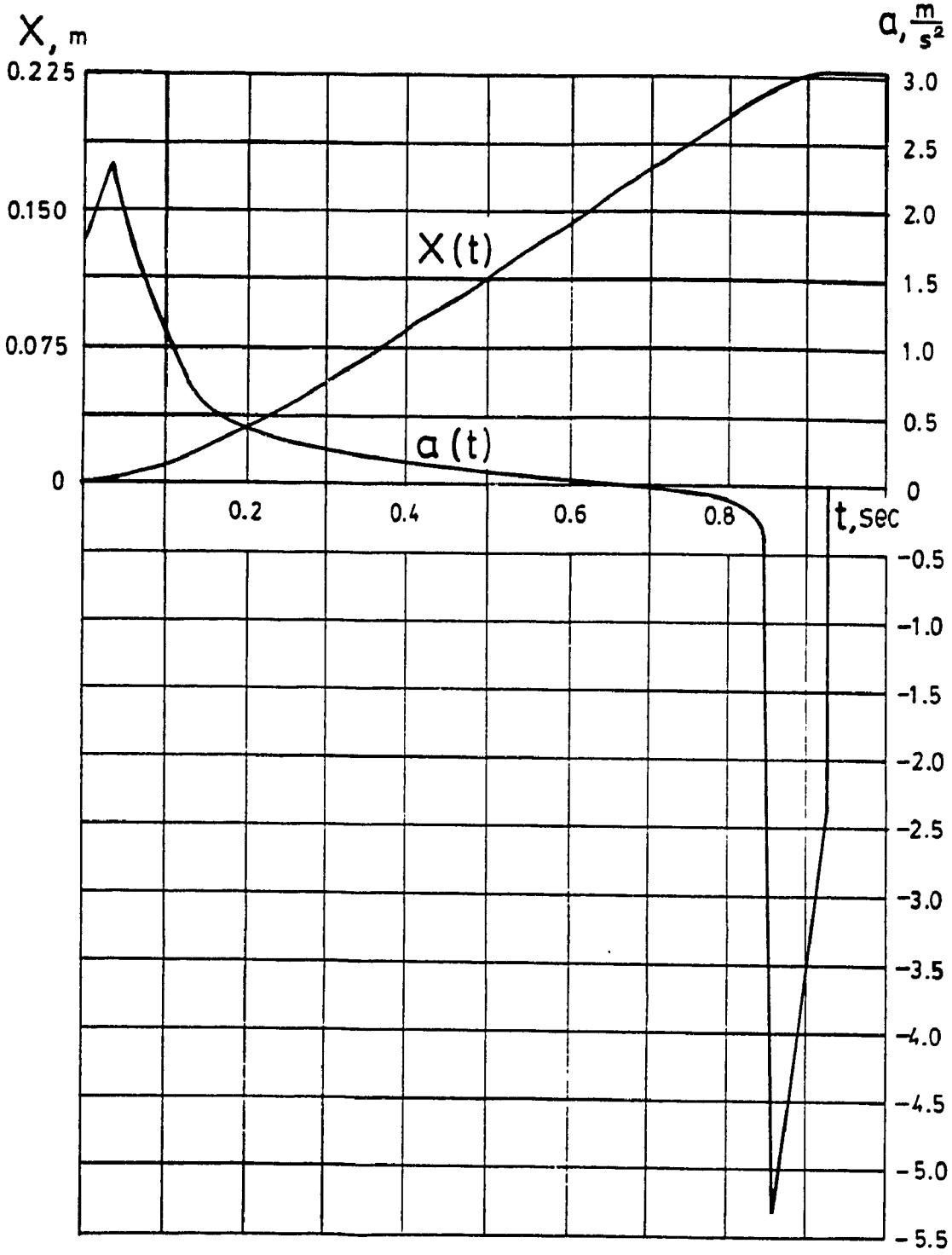

Fig.4.2. Input acceleration and the corresponding displacement histories for experimental testing

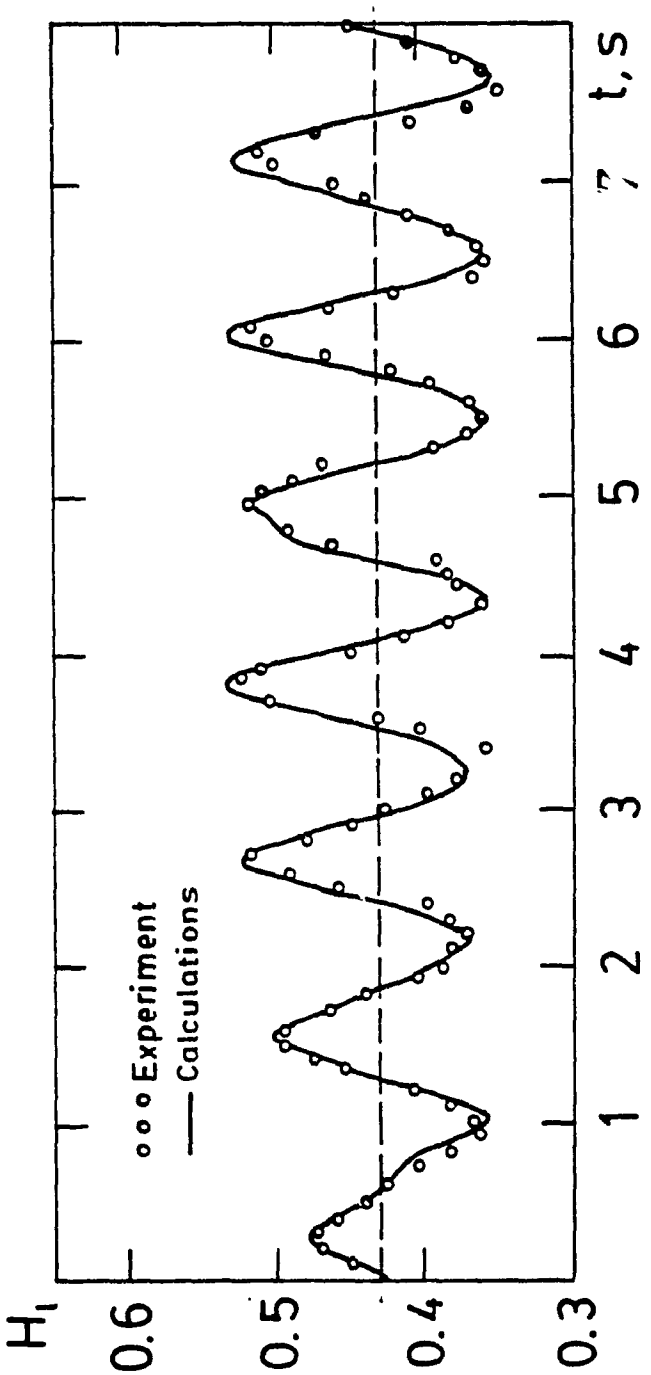

Fig.4.3. Computed and experimental heights of the free surface near the left wall of the model tank

iv) Specification of the upstream differencing coefficients which can vary between 0 and 1.

v) Influence of the cell size on the accuracy of calculation.

The free-slip and no-slip conditions have been studied on the example of a cylindrical container and then applied to other cases of study. This investigation has shown that for high values of the Re number, i.e. greater then 10^5, the solutions for both types of boundary conditions are very close and if Re is decreased, then solutions diverge displaying more realistic results for the no-slip condition at all times.

The extrapolation and interpolation-reflection technique have been tried for the model rectangular tank. The direct extrapolation results in divergent oscillations of the liquid heights near the vertical wall for high values of the Re, i.e. 10^5 and greater. This is physically incorrect and, in principle, should not happen at any Re number. It seems, the extrapolation overestimates the liquid velocities, especially in the region of the free-surface, and therefore must be rejected, no matter whether the discrepancy is attributed to the overestimation or to some local free-surface effects which are not taken into account by the present model. The interpolation-reflection type boundary condition, in contrast, do not give the divergent oscillation even for very low viscosity liquid like water.

It is usually assumed that higher order of interpolation is more accurate and this has been confirmed by the test runs for rigid wall boundary conditions. However, the second order interpolation failed in some cases when the sharp wave was formed near the vertical wall and the wave peak was resolved only by one column of cells. Therefore, less

accurate but more reliable with a coarse mesh first order interpolation was adopted in this study. In the case of a fine mesh, the second order should be used. However, the judgment whether the mesh is coarse or fine should be made in each specific case, based on trial runs. For example, the mesh used for the model tank, composed of 20x12 cells including the boundary cells, has been considered as a coarse mesh.

At the free surface, better results are obtained with zero order extrapolation of the boundary velocity, which corresponds to the Neumann type of boundary condition by setting the velocity gradient through the free surface equal to zero. This partially takes into account the neglected local free-surface effects, such as the surface tension and interaction of the liquid wave with the ambient air. For that reason, the zero order velocity extrapolation has been used in this investigation.

The upstream differencing coefficients were taken equal both in momentum and free-surface equations and their values were chosen to provide a stable calculation for a considered class of problem defined basically by the geometry of the container. The strongest factor affecting the minimum value of the coefficients is the level of the input acceleration which characterizes the intensity of sloshing. In order to make a consistent comparison of the numerical results, the fixed maximum values of the upstream differencing coefficients were adopted for calculation within each class of problem. Those values have been established as 0.7 for circular cross-section containers and 1.0 for rectangular containers. The higher value for rectangular containers is explained by their various geometry and stronger sloshing compared to circular containers, especially if the fill level exceeds 50%.

The influence of the cell size on the accuracy of calculation was investigated by the numerical experimentation with the rectangular container. The solutions have been obtained with meshes of 10 x 10, 25 x 25, and 40 x 40 cells, see Fig. 4.4, where the results are given by circles, solid line, and crosses respectively for one period of oscillation. The difference in peak value of the liquid height near vertical wall between 40 x 40 and 25 x 25 meshes is about 2%, while the same difference between 40 x 40 and 10 x 10 meshes is about 5%. Besides the difference in amplitude, the small phase shift exists between the most accurate refined mesh and the most coarse mesh, that is of the order of 4% with respect to the period of oscillation. Though this method does not give the discretization error, it provides, however, with the trend of the error behaviours. It follows from the previous consideration that the difference between a sufficiently fine, 40 x 40, and sufficiently coarse, 10 x 10, meshes is not large and a coarse mesh can be used for studying of the sloshing problem.

4.4 Final Selection of the Boundary Conditions

Summarizing the results of preliminary investigation, the boundary conditions employed in this study can be described in the following manner:

i) At the rigid wall, the first order no-slip interpolation-reflection boundary conditions are most suitable for the adopted coarse grids.

ii) At the free surface, the zero-order extrapolated or interpolated boundary conditions on velocities and first-order boundary conditions on pressure are used in order to

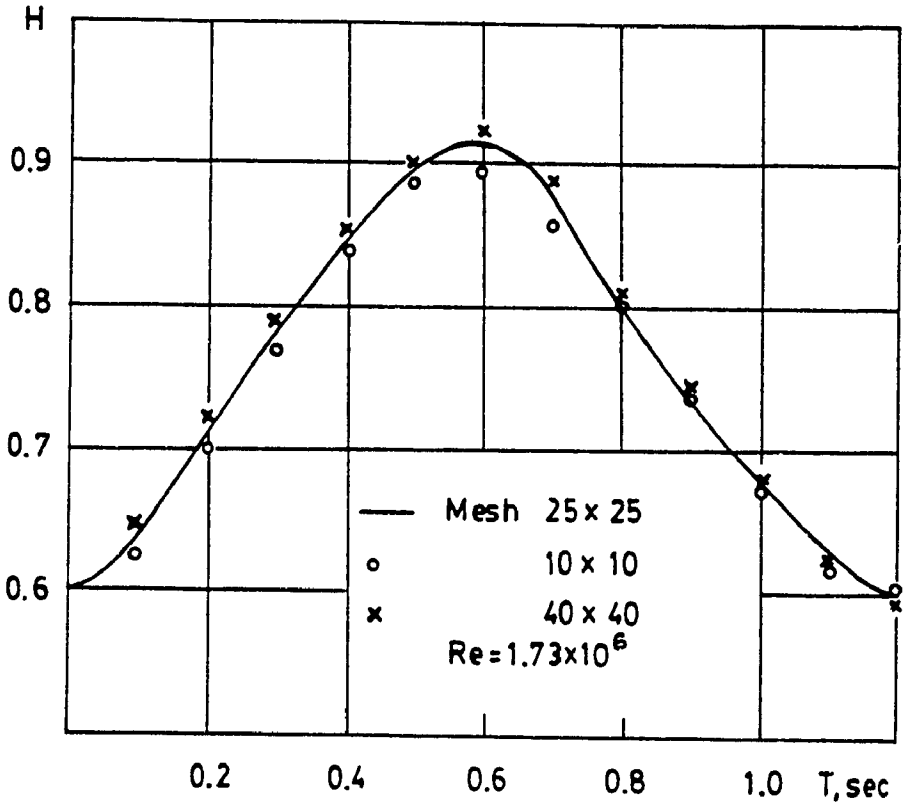

Fig.4.4. Influence of the cell size oh the liquid height calculation

compensate the free-surface local effects missed by the present model.

iii) For the height boundary conditions, the irregular mesh with the boundary height at the intersection of the free surface and wall is to be used. Consequently, the Eqns. (3.20) and (3.21) are to be employed in all cases except for the case of vertical walls of a rectangular container when the reflection type boundary condition, first of Eqn. (3.22), gives more accurate results.

The special boundary conditions due to baffles' orifices in compartmented containers will be considered in Chapter 7.

4.5 Summary

In this chapter, the model of liquid sloshing, developed in Chapters 2 and 3, has been experimentally validated. In particular, the boundary conditions have been selected on the basis of the best possible correlation with experimental results. The influence of the cell size and coefficients of upstream differencing has been also investigated. In such a way refined computer model of sloshing was used to study the sloshing characteristics for rectangular, circular, and compartmented and baffled containers which is discussed in the following chapters.

CHAPTER 5

STEADY-STATE AND TRANSIENT RESPONSES OF LIQUID SLOSHING IN RECTANGULAR CONTAINERS

5.1 General

In this chapter, the steady-state and transient responses of the liquid motion in rectangular containers subjected to a step input lateral acceleration are studied. Although a rectangular cross-section is not used in the road tanker design, it serves as a good approximation for modified rectangular containers which differ from purely rectangular ones by small roundings in the corners. The steady-state responses are obtained by solving the hydrostatic equations for two types of the container motion, simulating the straight line braking and the steady turn of a tank vehicle. It is shown that these two cases can be described by the same solution, which actually simulates the first case (braking) and is sufficiently accurate in the second case for majority of practical combinations of input parameters. The error resulting in the simulation of the second case is estimated and appears to be small.

The transient responses are obtained using numerical simulation of the liquid motion on the digital computer, Cyber 830 D. The computer model of the sloshing phenomena, described in Chapter 3, includes all essential nonlinearities of the problem and is seen to be sufficiently accurate in predicting the dynamic behaviour of the liquid motion. The solutions are carried out in terms of the free-surface heights, liquid forces and overturning moments, and the natural damped frequencies of liquid vibrations.

5.2 Steady-State Solutions

The steady-state solution is of the interest, when vibration of the liquid motion is strongly damped (highly viscous liquid) or when a tank vehicle manoeuvre occurring under a constant lateral acceleration is sufficiently long in time. Also, the steady-state solution provides information for understanding the phenomenon of liquid behaviour in general, as well as it eliminates the excessive computer time needed to bring the transient solution to the steady-state.

In this section, two types of the container motion are considered, i.e. the rectilinear motion which simulates the braking-accelerating manoeuvre and the rotational motion which represents the steady turn as it has been discussed in Section 2.1.

5.2.1 Rectilinear Motion of a Container

The non-dimensional hydrostatic equations for a 2-D problem are

$$G_x = \frac{\partial P_{ss}}{\partial X} \; ; \qquad G_y = \frac{\partial P_{ss}}{\partial Y} \tag{5.1}$$

where the unit body forces G_x and G_y are constant and coordinate-independent. The total differential for pressure in static equilibrium and the equation of isobars are

$$dP_{ss} = G_x\, dX + G_y\, dY \; ; \qquad G_x\, dX + G_y\, dY = 0 \tag{5.2}$$

Integration of Eqns.(5.2) yields:

$$P_{ss} = G_x (X-X_o) - Y + Y_o \; ; \qquad Y = Y_o + G_x (X-X_o) \tag{5.3}$$

where X_o, Y_o are coordinates of a point with known pressure. Depending on the combination of the geometrical parameter, h, filling parameter, f, and the level of the input acceleration, G_x, the liquid free surface can take a position, or Configuration 1, 2, 3 or 4,as it is shown in Fig.5.1. Configuration 1 takes place when the free surface intersects the side walls of the container; Configuration 2 appears if the free surface passes through one side wall and the upper wall; Configuration 3 exists when the free surface passes through the bottom and one side wall; and Configuration 4 takes place when the free surface intersects the top and bottom walls. The free-surface equations can be found from the second expression of Eqn. (5.3) by specifying the coordinates X_o, Y_o of one of the two points of intersection of the free surface with the container wall. This can be done by equating the area currently occupied by the liquid to the initial area. The resulting expressions for the free-surface equations for the different configurations are given in Table 5.1.

The horizontal and vertical forces, being the ratio of their dimensional values to the liquid weight, are expressed as:

$$F_{HSS} = G_x \; ; \qquad F_{VSS} = G_y = -1 \tag{5.4}$$

and the overturning moment with respect to the middle bottom point 'O' of the container is taken as the ratio of the dimensional moment to the product of the weight and L_o, or to the quantity $\rho g L_o^2 h_{in}$, and is given

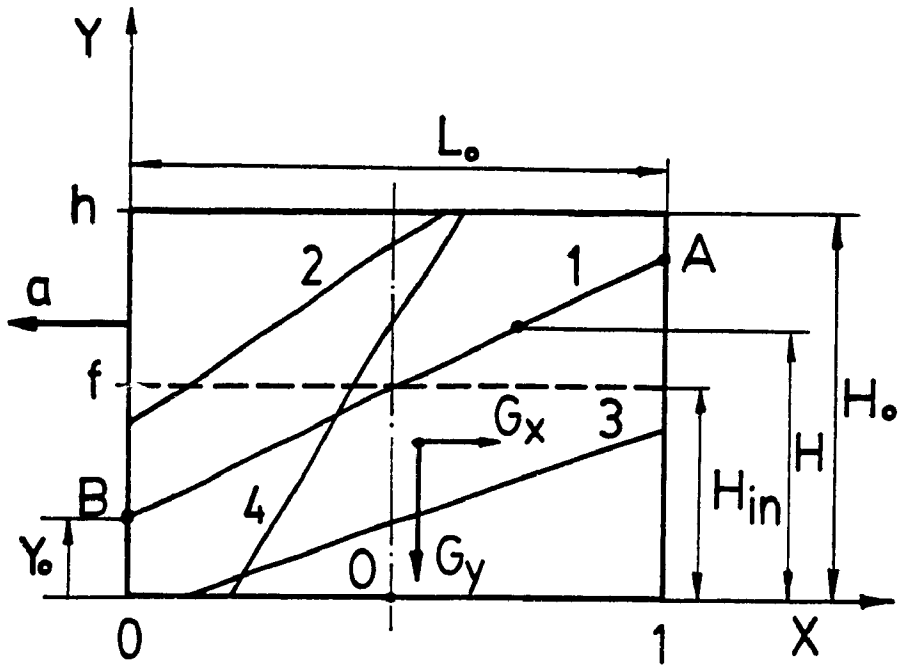

Fig.5.1. Schematics and configurations for rectilinear motion of a rectangular container

Table 5.1. Free-surface equations and configurations' definition for steady-state response in rectilinear motion

Configuration	G_x	Free-surface equations	General condition on Y(X)	Condition from the free-surface equations	Condition on G_x
1	$G_x>0$	$Y_{ss} = G_x X + f - \frac{G_x}{2}$	$Y(0)\geq 0$ $Y(1)\leq h$	$\frac{\lvert G_x\rvert}{2} + f - h \leq 0$	$\lvert G_x\rvert \leq 2(h-f)$
	$G_x<0$		$Y(0)\leq h$ $Y(1)\geq 0$	$f - \frac{\lvert G_x\rvert}{2} \geq 0$	$\lvert G_x\rvert \leq 2f$
2	$G_x>0$	$Y_{ss} = G_x X + h - A$	$Y(0)\geq 0$ $Y(1)\geq h$	$\lvert G_x\rvert - A \geq 0$	$\lvert G_x\rvert \geq 2(h-f)$
	$G_x<0$	$Y_{ss} = G_x(X-1) + h - A$ $A = \sqrt{2(h-f)\lvert G_x\rvert}$	$Y(0)\geq h$ $Y(1)\geq 0$	$h - A \geq 0$	$\lvert G_x\rvert \leq \frac{h^2}{2(h-f)}$
3	$G_x>0$	$Y_{ss} = G_x (X-1) + B$	$Y(0)\leq 0$ $Y(1)\leq h$	$B - h \leq 0$	$\lvert G_x\rvert \leq \frac{h^2}{2f}$
	$G_x<0$	$Y_{ss} = G_x X + B$ $B = \sqrt{2f\lvert G_x\rvert}$	$Y(0)\leq h$ $Y(1)\leq 0$	$B - \lvert G_x\rvert \leq 0$	$\lvert G_x\rvert \geq 2f$
4	$G_x>0$	$Y_{ss} = G_x(X - 1 + \frac{f}{h}) + \frac{h}{2}$	$Y(0)\leq 0$ $Y(1)\geq h$	$\frac{\lvert G_x\rvert f}{h} - \frac{h}{2} \geq 0$	$\lvert G_x\rvert \geq \frac{h^2}{2f}$
	$G_x<0$	$Y_{ss} = G_x(X - \frac{f}{h}) + \frac{h}{2}$	$Y(0)\geq h$ $Y(1)\leq 0$	$\frac{\lvert G_x\rvert f}{h} - \lvert G_x\rvert + \frac{h}{2} \leq 0$	$\lvert G_x\rvert \geq \frac{h^2}{2(h-f)}$

in Table 5.2. The values of the moment for a completely filled container can be obtained from the expression for Configuration 2 and for an empty container from Configuration 3 in the form:

$$M_{ss} = \frac{h\,G_x}{2} \qquad \text{for 100\% fill level} \qquad (5.5)$$

$$M_{ss} = \pm\frac{1}{2} \qquad \text{for 0\% fill level}$$

Obviously, the moment must be zero for an empty tank, and its dimensional value does so because of $h_{in} = 0$. But in this particular non-dimensional form, it is equal to $\pm\frac{1}{2}$, depending on the sign of G_x The influence of the input acceleration on the magnitude of the moment is illustrated in Fig.5.2. It can be seen that for low height containers, the moment is a nonlinear function of G_x. With increasing of the h, the function becomes more linear and more steep. The behaviour of the moment with the fill level variation is shown in Fig.5.3. It can be seen that the moments start from $\frac{1}{2}$ at f=0 and decrease to the values corresponding to f=100% stated in Eqn.(5.5). They drop rapidly for small values of G_x and then remain almost constant. For high levels of the input accelerations, greater than G_x=1, the functions display maxima and drop to the level corresponding to fully filled containers. The influence of the geometrical parameter, h, is given in Fig.5.4. Depending on the fill level, the moment either drops or rises from the values defined for Configuration 4 as

$$M_{ss} = \pm\frac{h-f}{2f} \qquad (5.6)$$

Table 5.2. Overturning moments for steady-state response in rectilinear motion

Configuration	Moment equation cw direction is positive sign + for $G_x > 0$ sign - for $G_x < 0$
1	$M_{ss} = \frac{G_x}{2}\left(f + \frac{G_x^2}{12f} + \frac{1}{6f}\right)$
2	$M_{ss} = \frac{h-f}{f}\left[\pm\frac{1}{2} - hG_x + \frac{h^2 G_x}{2(h-f)} - \frac{AG_x}{3}\left(\frac{1}{G_x^2} - 1\right)\right]$
3	$M_{ss} = \pm\frac{1}{2} - \frac{BG_x}{3}\left(\frac{1}{G_x^2} - 1\right)$
4	$M_{ss} = \pm\left(\frac{1}{2} - \frac{f}{2h} - \frac{h^3}{12f} - \frac{h^3}{24f\,G_x^2}\right) + \frac{hG_x}{2}$

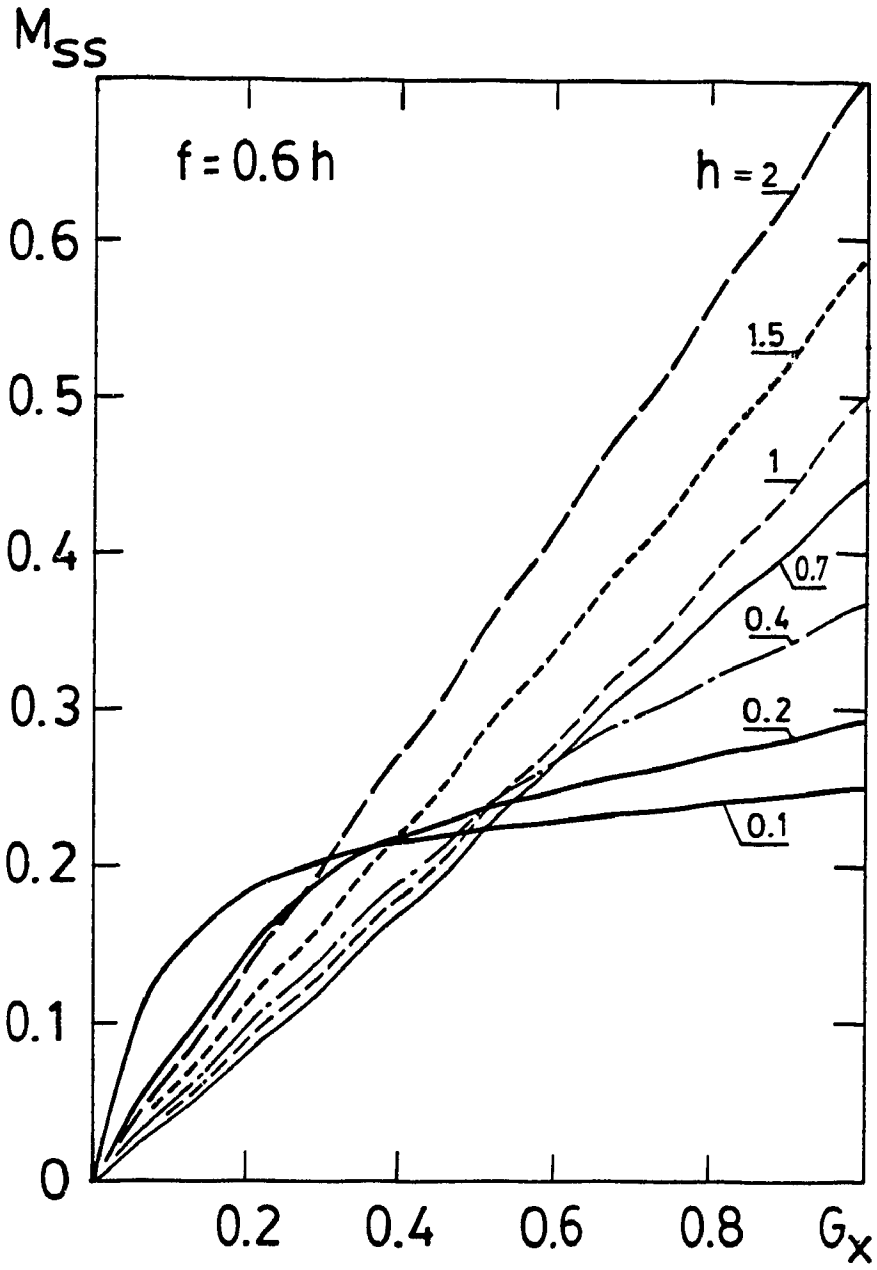

Fig.5.2. Steady-state overturning moment as function of the input acceleration

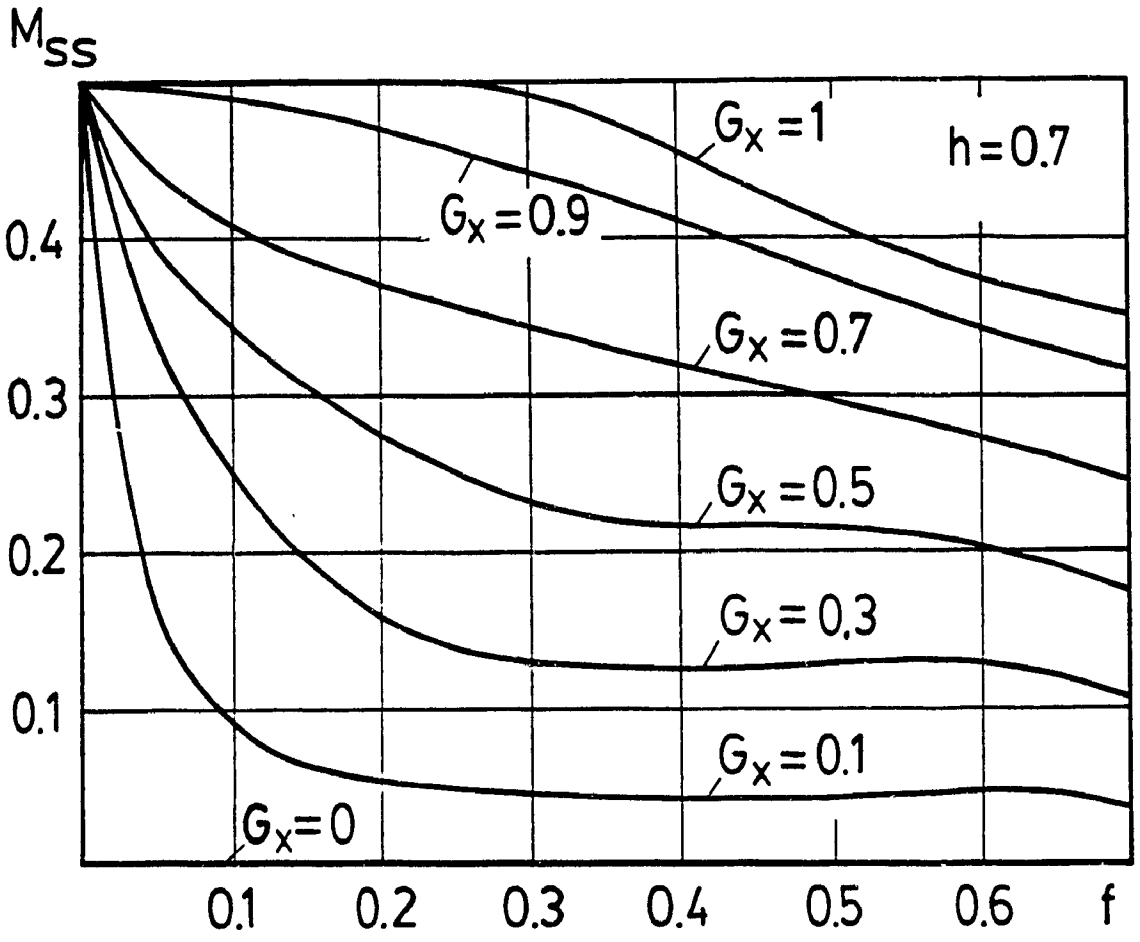

Fig.5.3. Steady-state overturning moment as function of the fill level

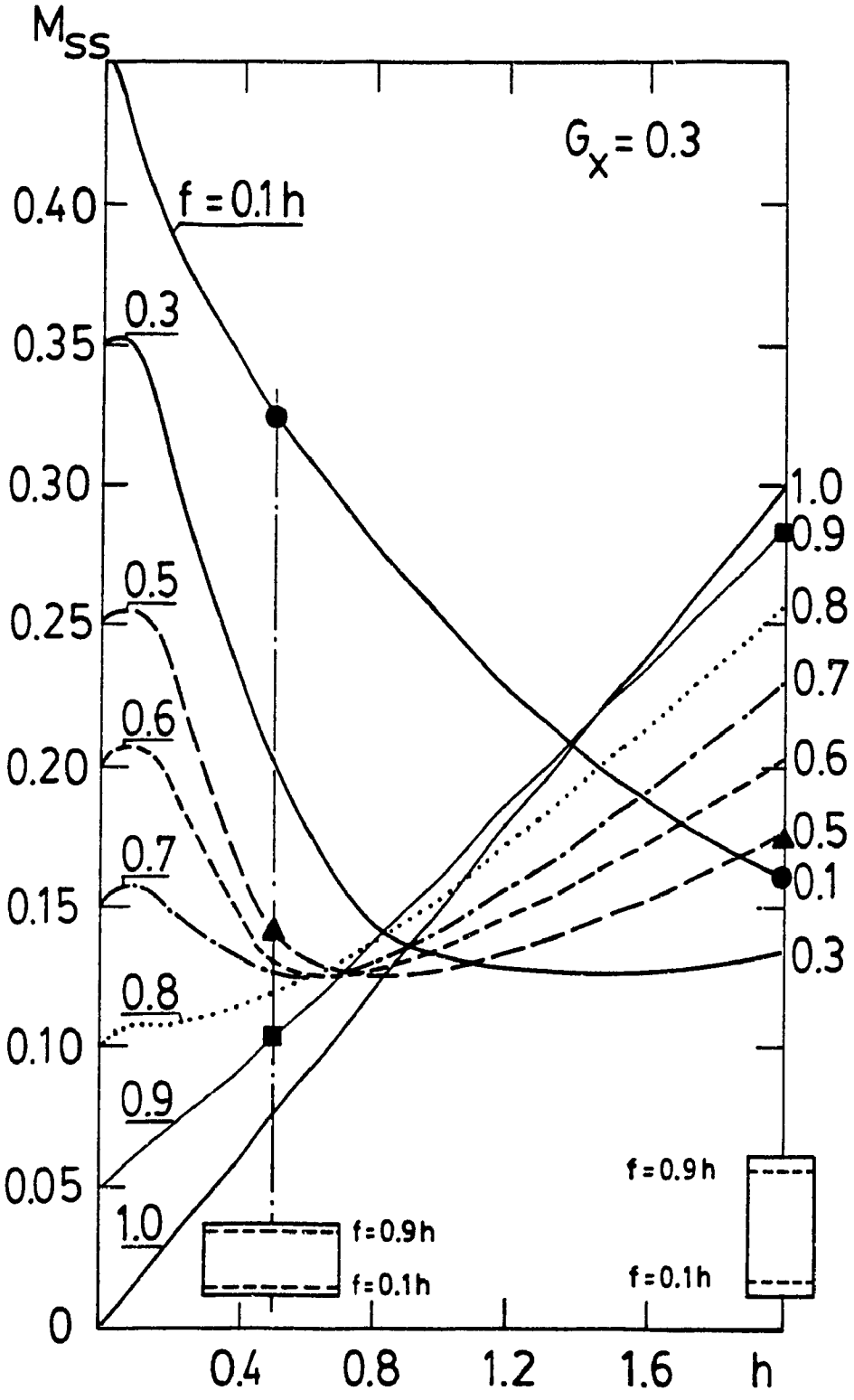

Fig.5.4. Steady-state overturning moment as function of the container height

For fill levels below 80%, the functions have minima occurring at different values of h, and for fillings above 80% the functions approach the straight line corresponding to a 100% filled container. A comparison of two containers having h's equal to 0.5 and 2.0 is shown in Fig.5.4 to clarify the behaviour of M_{ss}. For small f's, see circles on vertical lines at h=0.5 and 2.0, it is advantageous to have a container with greater height, h=2.0, while for f=0.9 h, a container with smaller height is preferable. For instance, the fill level corresponding to a minimum value of M_{ss} is approximately equal to 0.6h for G_x=0.3, while for greater G_x's it decreases. By expressing the functions for the moment in a dimensional form will affect the positions of minima of moments, however, these minima will still exist and depend on the container height as well as on the input acceleration and fill level parameters. That is, the optimization of the container shape is a feasible and important practical problem.

5.2.2 Rotational Motion of a Container

The hydrostatic equations for a steady rotation of the container around some vertical axis remain the same as in Eqn (5.1) but the horizontal body force is now dependent on the X or ξ coordinate, e.g.

$$G_x = \frac{G_n}{\delta} \left(\delta - \frac{1}{2} + X \right) \tag{5.7}$$

and the integration of Eqns.(5.2) now gives

$$P_{ss} = \frac{G_n}{2\delta}\left[X^2 + (2\delta - 1)\,X\right] + Y_o - Y$$

and

$$Y = Y_o + \frac{G_n}{2\delta}\left[X^2 + (2\delta - 1)\,X\right] \qquad (5.8)$$

where the coordinate Y_o is taken at X=0, see Fig. 5.5. The four configurations, corresponding to the four different positions of the free surface, are defined similarly as for the case of rectilinear motion, but with one difference: the free surface now has a parabolic shape. The transition from the general solution, Eqns (5.8), to the particular one can be done separately for each configuration by defining the value of Y_o, which is always located at the intersection of the free surface or its continuation with the Y-axis. For this purpose, the system of three equations must be solved. One of those equations is obtained by integration of the free-surface equation (the second of Eqns.(5.8)) with respect to the X-coordinate, i.e. by defining the area occupied by the liquid and equating it to the initial area, and the two remaining equations result from the pressure equation (the first of Eqns.(5.8)) written for two points of intersection of the free surface with the walls where the gage pressure is equal to zero.

As an example, consider the equations for Configuration 2 shown in Fig. 5.5. The area occupied by the liquid can be expressed as:

$$\int_0^{X_A} Y(X)\,dX + (1 - X_A)h = f$$

where the RHS represents the initial area. Using the second equation of

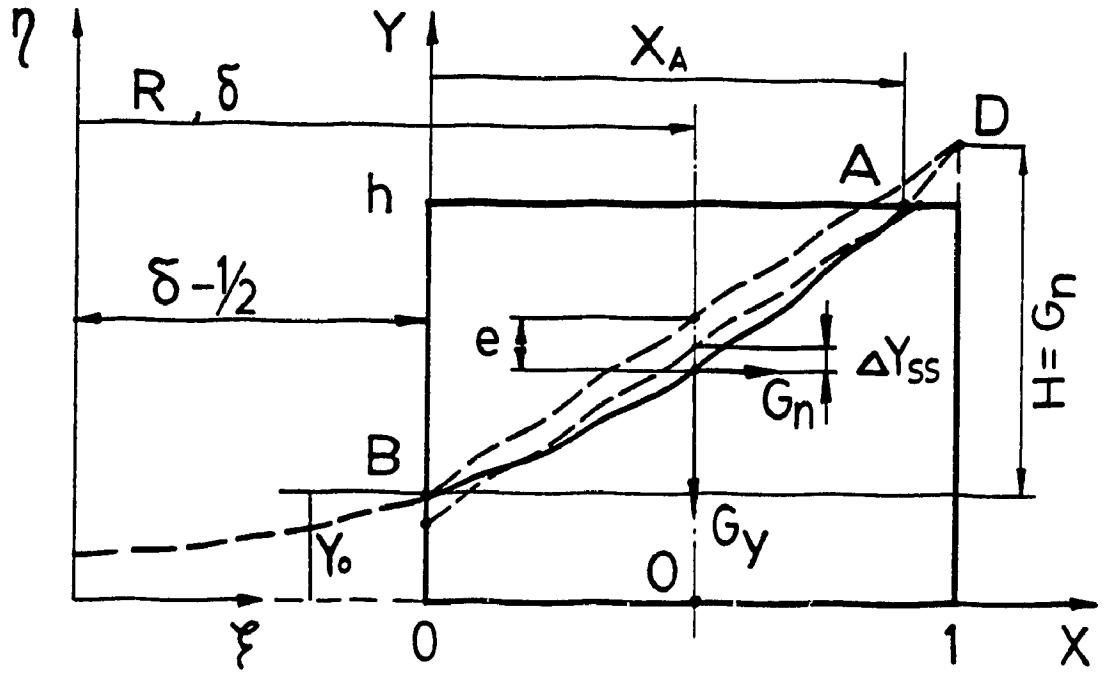

Fig.5.5. Schematics for rotational motion of a rectanqular container

Eqns. (5.8) gives:

$$\int_0^{X_A} Y_o \, dX + \frac{G_n}{2\delta} \int_0^{X_A} \left[X^2 + (2\delta - 1) X \right] dX + (1-X_A) h = f$$

Integrating the last eqation with respect to X yields

$$\frac{G_n}{6\delta} X_A^3 + \frac{G_n (2\delta-1)}{4\delta} X_A^2 + Y_o X_A + h (1-X_A) - f = 0 \qquad (5.9)$$

Since only one limit of integration, X_A, is unknown, only one boundary condition is needed that can be obtained from the pressure equation upon substitution $X = X_A$, $Y = h$, $P_{ss} = 0$ in the form

$$\frac{G_n}{2\delta} X_A^2 + \frac{G_n (2\delta-1)}{2\delta} X_A + Y_o - h = 0 \qquad (5.10)$$

Eqns. (5.9) and (5.10) can be easily solved with respect to X_A using the trigonometric solution of the third-order linear algebraic equation. Parameter Y_o can be found and then substituted into the general solution, Eqn. (5.8). The solutions for Configurations 1, 2 and 3 are given in Table 5.3. For Configuration 4, the original system of equations must be added with the equation for X_B resulting from the pressure boundary condition at X_B. The solution for the resulting system can not be given in an explicit form. In order to obtain an explicit formulation, an approximation will be effected. For steady turns with large radii, the curvature of the free-surface parabola is very small and the parabola may be approximated by a straight line. To validate this approach, the curvature of the parabola must be analyzed and

Table 5.3. Free-surface equations and configurations' definition for steady-state response in rotational motion

Config No.	Free-surface equations, $G_n>0$	Configuration conditions, $G_n>0$
1	$Y_{ss} = f + \frac{G_n}{2\delta}\left[X^2 + (2\delta-1)X - \delta + \frac{1}{6}\right]$	$\begin{cases} f - \frac{G_n}{2} + \frac{G_n}{12\delta} \geq 0 \\ f + \frac{G_n}{2} + \frac{G_n}{12\delta} \leq h \end{cases}$
2	$Y_{ss} = h + \frac{G_n}{2\delta}\left[X^2 + (2\delta-1)X - (\delta - \frac{1}{2})^2 \left(\cos^2\frac{\alpha}{3} + \cos\frac{\alpha}{3} - \frac{3}{4}\right)\right]$ $\cos\alpha = \frac{96\delta\,(h-f)}{G_n(2\delta-1)^3} - 1$	$\begin{cases} 2\delta h - G_n(\delta - \frac{1}{2})^2\left(\cos^2\frac{\alpha}{3} - \cos\frac{\alpha}{3} - \frac{3}{4}\right) \geq 0 \\ 2\delta - (\delta - \frac{1}{2})^2\left(\cos^2\frac{\alpha}{3} + \cos\frac{\alpha}{3} - \frac{3}{4}\right) \geq 0 \end{cases}$
3	$Y_{ss} = \frac{G_n}{2\delta}\left\{X^2 + (2\delta-1)X - (\delta+\frac{1}{2})^2\left[\cos^2\left(\frac{\alpha}{3} - \frac{2\pi}{3}\right) + \cos\left(\frac{\alpha}{3} - \frac{2\pi}{3}\right)\right] + \frac{12\delta^2 - 20\delta + 3}{16}\right\}$. $\cos\alpha = \frac{96\,\delta\,f}{G_n(2\delta+1)^3} - 1$	$\begin{cases} \frac{12\delta^2 - 20\delta + 3}{16} - (\delta+\frac{1}{2})^2\left[\cos^2\left(\frac{\alpha}{3} - \frac{2\pi}{3}\right) + \cos\left(\frac{\alpha}{3} - \frac{2\pi}{3}\right)\right] \leq 0 \\ G_n - \frac{G_n}{2\delta}(\delta+\frac{1}{2})^2\left[\cos^2\left(\frac{\alpha}{3} - \frac{2\pi}{3}\right) + \cos\left(\frac{\alpha}{3} - \frac{2\pi}{3}\right)\right] + \frac{G_n(12\delta^2 - 20\delta + 3)}{32\delta} \leq h \end{cases}$

compared with that of the straight line. In the assumed Y-X Cartesian coordinates, the curvature of the free-surface can be expressed as

$$C = \frac{\left| \frac{d^2Y}{d X^2} \right|}{\left[1 + \left(\frac{dY}{dX} \right)^2 \right]^{3/2}} \tag{5.11}$$

Differentiating the free-surface equation for Configuration 1, for example, and substituting the derivatives into Eqn. (5.11) yields

$$C = \frac{G_n}{\delta \left[4\delta^2 - 4\delta + 2 + 4 G_n X - \frac{2G_n}{\delta} X + \frac{G_n^2}{\delta^2} X^2 \right]^{3/2}} \tag{5.12}$$

The maximum curvature occurs at minimum X, i.e. X=0, then the Eqn. (5.12) simplifies to

$$C_{x=0} = \frac{G_n}{\delta \left(4\delta^2 - 4\delta + 2\right)^{3/2}} \tag{5.13}$$

For the case of road containers, the radius of the track is sufficiently large compared to the container size. Thus, for turns with radii of 10, 50 and 100 times the tank width, the curvature of the parabola is $0.15 \times 10^{-5} G_n$, $0.21 \times 10^{-7} G_n$, and $0.13 \times 10^{-8} G_n$, respectively. Such small values imply very flat parabolas which can be replaced by the corresponding straight lines, and hence the rotational motion of a container can be approximated by the rectilinear motion with the body force G_x equal to the nondimensional centrifugal acceleration, G_n, in

the middle of the container. A brief analysis shows that the ratio of the difference between liquid heights in rotational and rectilinear motions, ΔY_{ss}, at the middle of the container to the total parabola deflection, e, computed between X=0 and 1, is the largest for Configuration 1 and is equal to

$$\frac{\Delta Y_{ss}}{e} = \frac{Y^{rot} - Y^{rec}}{e} = -\frac{1}{3} \quad , \; e = -\frac{G_n}{8\delta}, \tag{5.14}$$

while for Configurations 2 and 3 it is expressed as:

$$\frac{\Delta Y_{ss}}{e} = \frac{8\delta\sqrt{2(h-f)G_n}}{G_n} - 1 - (2\delta-1)^2\left(\cos^2\frac{\alpha}{3} + \cos\frac{\alpha}{3} - \frac{3}{4}\right) \text{ and}$$

$$\frac{\Delta Y_{ss}}{e} = \frac{12\delta^2+12\delta+3}{4} - 1 - (2\delta+1)^2\left[\cos^2\left(\frac{\alpha}{3} - \frac{2\pi}{3}\right) + \cos\left(\frac{\alpha}{3} - \frac{2\pi}{3}\right) - \frac{8\delta\sqrt{2fG_n}}{G_n}\right] \tag{5.15}$$

respectively, with the absolute values of the ratio slightly smaller than for Configuration 1. For Configuration 4, this value must be even smaller. Thus, the solution for a rotational motion, expressed in terms of the free-surface height, can be approximated by the solution of the rectilinear motion with an upper bound on the error, equal to one third of the parabola deflection between X=0 and 1. The straight line approximation of the free surface will give smaller values of the liquid heights at the sides of the container and greater values in the middle with an obsolute error not exceeding

$$E = \frac{G_n}{12\delta} \tag{5.16}$$

The pressure, and hence the overturning moment, will also be affected by this approximation, but the errors will be of the same order as for liquid heights, since the pressure is proportional to the depth of the liquid. Finally, it can be recommended to use the solutions given in the Tables 5.1 and 5.2 for both the rotational and rectilinear motions assuming that G_n is equal to G_x, provided that the radius of road curvature is large.

5.3 Transient Solutions

In this section, the transient response of the liquid sloshing when subjected to a step input acceleration is investigated. The input acceleration can be used to study the longitudinal dynamics of the fluid in the case of braking-accelerating manoeuvres; or the lateral dynamics of the fluid, with some approximations, when the tank negotiates a steady turn. The validity of such approximations have been earlier justified for the case of the steady-state response and it is assumed to be valid for the transient response as well.

The numerical solutions are carried out in accordance with the numerical procedure and definition of the boundary conditions considered in Chapters 3 and 4. The three basic input parameters, namely the fill level, f, the acceleration level, G_x, and the geometry parameter, h, were varied in the range given in Table 5.4, where the framed values correspond to basic values of each parameter, two of which were kept fixed while the remaining parameter was changed within the given range.

Table 5.4. Cases of numerical study for rectangular containers

Fill level, f	Acceleration level, G_x	Geometrical parameter h
0.3 h	0.1	0.15
0.5 h	0.3	0.35
0.7 h	0.5	0.7
0.9 h	0.7	1.4
	1.0	2.1

The influence of the Re-number is studied in the case of a circular cross-section tank and is presented in Chapter 6.

5.3.1 Influence of Fill Level

The fill level is one parameter having a strong influence on the character of liquid motion. Sufficiently small and sufficiently large values of f result in Configurations 3 and 2, respectively (refer to Fig. 5.1), while its intermediate values give Configuration 1, for which the bottom and top walls of the container do not interfere. The results of numerical solutions for different values of f, given in Table 5.5 and Fig. 5.6 a) and b), display the maxima for coefficients of dynamic overturning moment and horizontal force at some values of f occurring between 0.25 and 0.35, and reaching 55% and 44% in surplus with respect to the corresponding steady-state values, see Fig.5.6 a), for h=0.7 and G_x=0.3. The dimensional values of the fill level, corresponding to the maxima of the moment and horizontal force, will be of the order 75-85% of the height of the container. The share of the horizontal force in creating of the moment increases with increase of f due to a relatively smaller displacement of the liquid mass that results in smaller arm of the vertical force. The normalized first natural damped frequency of the horizontal force and moment vibration is approximately the same and is presented in Table 5.5 and plotted in Fig. 5.6 b), where it is compared with the frequency resulting from the linear theory and normalized with respect to the total body force, as shown in Eqn.(5.17):

Table 5.5. Effect of fill level on numerical solution for h=0.7, G_x=0.3, Re=1.29×10^7 (101"×72" container, water)

$\alpha = \frac{f}{h}$	f	Peak value F_H	Peak value M	Steady-state M_{ss}	Dynamic coefficients $\frac{F_H}{F_{HSS}}$	Dynamic coefficients $\frac{M}{M_{ss}}$	Share of F_H in moment generation %	Ω $\frac{rad}{s}$ (Config.1)	K Present Investigation (Config.1)	K Linear theory
0.3	0.21	0.4238	0.2320	0.1540	1.4127	1.5065	31.3	——	——	1.3190
0.5	0.35	0.4308	0.1958	0.1270	1.4360	1.5417	45.9	2.9224	1.4625	1.5519
0.7	0.49	0.4089	0.1650	0.1251	1.3630	1.3191	61.5	3.1416	1.5722	1.6566
0.9	0.63	0.3352	0.1390	0.1290	1.1173	1.0775	76.6	——	——	1.7019
1.0	0.7	0.3	0.105	0.105	1.0	1.0	100	——	——	1.7135

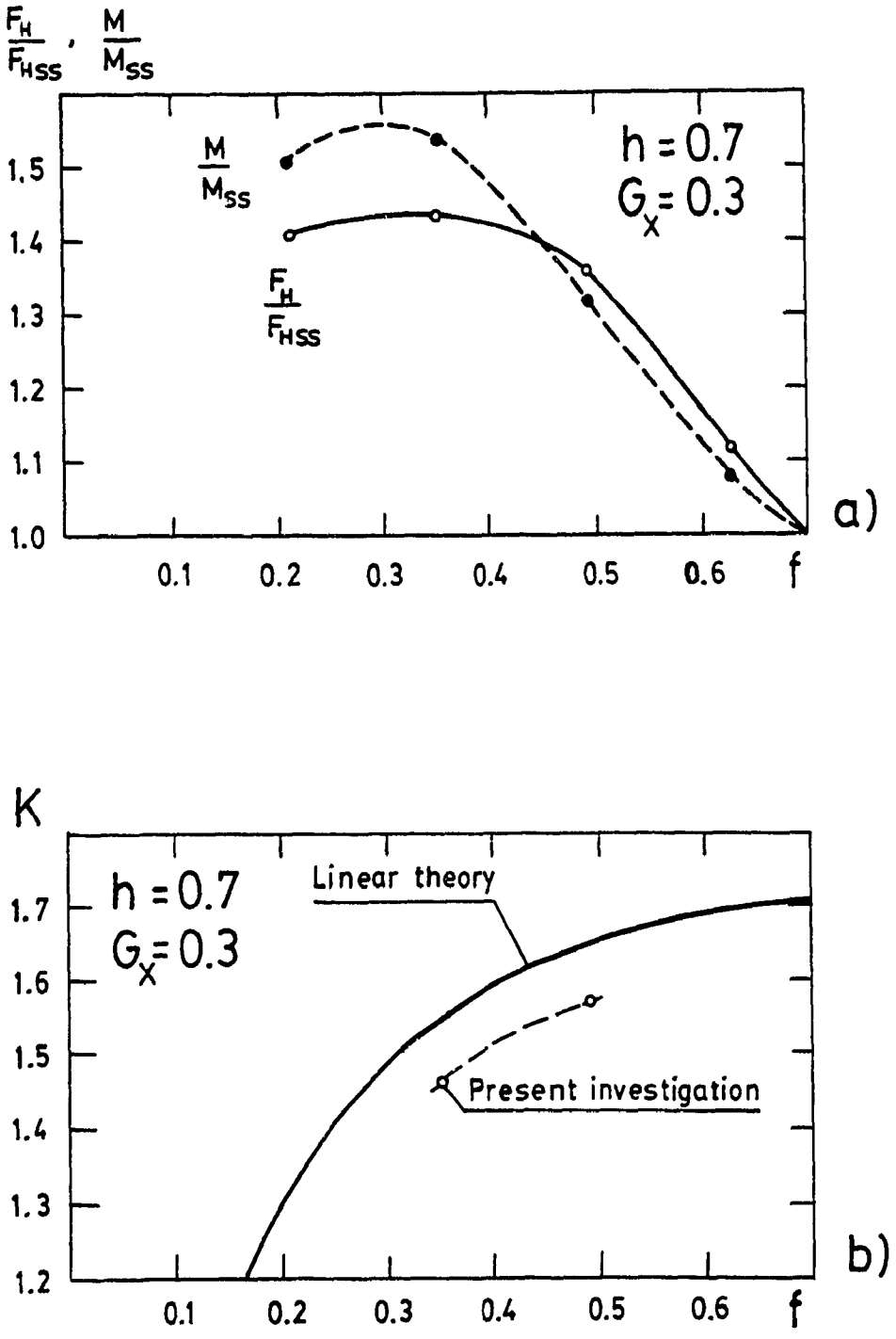

Fig.5.6. Influence of the fill level on dynamic coefficients of the horizontal force and overturning moment, a), and on the frequency of the sloshing oscillation, b)

Present Investigation

$$K = \frac{\Omega}{\sqrt{\frac{g(1 + G_x^2)^{1/2}}{L_o}}} \quad ; \quad \text{Linear Theory} \quad K = \frac{1}{(1 + G_x^2)^{1/4}} \sqrt{\pi \tanh(\pi f)} \quad , \qquad (5.17)$$

where Ω is the circular frequency from the numerical solution. The difference between the linear and the numerically computed frequencies for Configuration 1 is 5.7% and 7.8% for f = 0.35 and 0.49, respectively. For very small or large fill levels, the liquid motion is chaotic and the frequencies are inconclusive. If the horizontal walls do not interfere, the motion of the liquid is sufficiently close to the one given by the linear theory, and it is slightly damped and oscillating with the frequency very slowly increasing in time. If, however, the fill level allows the top horizontal wall to interfere, Configurations 2, then the liquid motion is characterized by a very strong peak at the "first" period, which is followed by some irregular vibrations with smaller amplitudes and higher frequencies. These frequencies could be of higher modes or even their combination.

The behaviour of the dimensional and nondimensional overturning moment in statics (m_{ss}, M_{ss}) and dynamics (m, M) with variation of the fill level is shown in Fig. 5.7 a) for a tank of h = 0.7 and G_x = 0.3. It can be seen that, though the nondimensional moment is decreasing with increase of f, the dimensional moment grows with the fill level and reaches a maximum value at f approximately equal to 0.65 (or 93% filling with respect to the container height) in steady-state and 0.62 (or 88%) in transient.

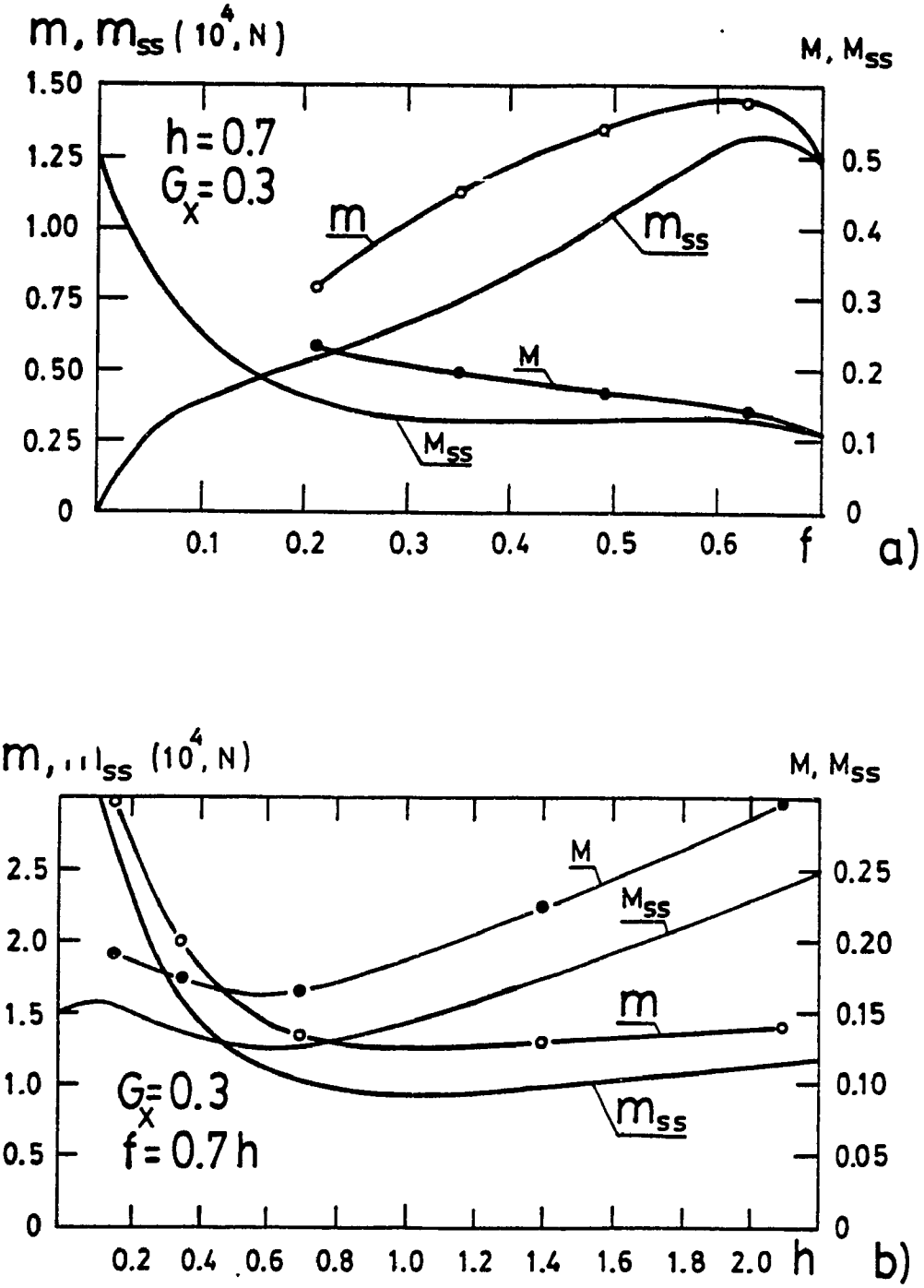

Fig.5.7. Comparison of dimensional, m, and nondimensional, M, moments in steady-state and in transient for container of h=0.7 and G_x=0.3 under fill level variation, a), and under container height variation, b)

The behaviour of the dimensional and nondimensional moments with the container height variation is shown in Fig.5.7 b). It can be seen that dimensionalizing of the moments, both in statics and dynamics, shifts the minima for the dimensional moments to the greater values of the h. In particular, for the fill level of 70%, the minima of the moments fall to the value of h approximately equal to 1, or to a square container, for a tank of 2.565m (101") wide and filled with a crude oil of density 850kg/m^3.

5.3.2 Influence of Input Acceleration

The level of the input acceleration is another factor affecting the dynamics of sloshing. The G_x value was varied between 0.1 and 1.0 and the numerical solutions are given in Table 5.6 and Fig. 5.8 a) and b). It can be seen that the dynamic coefficients of overturning moment and horizontal force decrease with increasing of the input acceleration, at least in the range of G_x between 0 and 1 g's. The normalized frequency is very close to the linear theory for small G_x, below 0.1. However, its deviation from the linear theory increases reaching about 5% for G_x between 0.3 and 0.5. Further increase in G_x results in essential change of the character of the liquid motion, which becomes irregular, similarly to the previous case with high fill level. This means that Configuration 2 is fully developed and the upper wall interference destroys the first mode of the vibration typical to a rectangular tank. The vibrations, again, after the first strong overshoot, are characterized by smaller amplitudes and higher frequencies. The share of the horizontal force in generating the moment is almost constant for

Table 5.6. Effect of input acceleration on numerical solution for h=0.7, f=0.7h, Re=1.29×10^7 (101"×72" container, water)

G_λ	Peak value F_H	Peak value M	Steady-State M_{ss}	Dynamic coefficients $\frac{F_H}{F_{HSS}}$	Dynamic coefficients $\frac{M}{M_{ss}}$	Share of F_H $\frac{\text{Static}}{\text{Dynamic}}$ %	Ω $\frac{\text{rad}}{\text{s}}$ (Config.1)	K Present investigation (Config.1)	K Linear theory
0.1	0.1491	0.0626	0.0416	1.4910	1.5052	61.7	3.2640	1.6649	1.6885
0.3	0.4089	0.1650	0.1251	1.3630	1.3191	61.5	3.1416	1.5722	1.6566
0.5	0.6588	0.2543	0.2182	1.3176	1.1657	78.7	3.1416	1.5193	1.6008
0.7	0.8628	0.3344	0.2978	1.2326	1.1229	81.7	—	—	1.5321
1.0	1.2409	0.4658	0.4199	0.2409	1.1093	87.6	—	—	1.4234

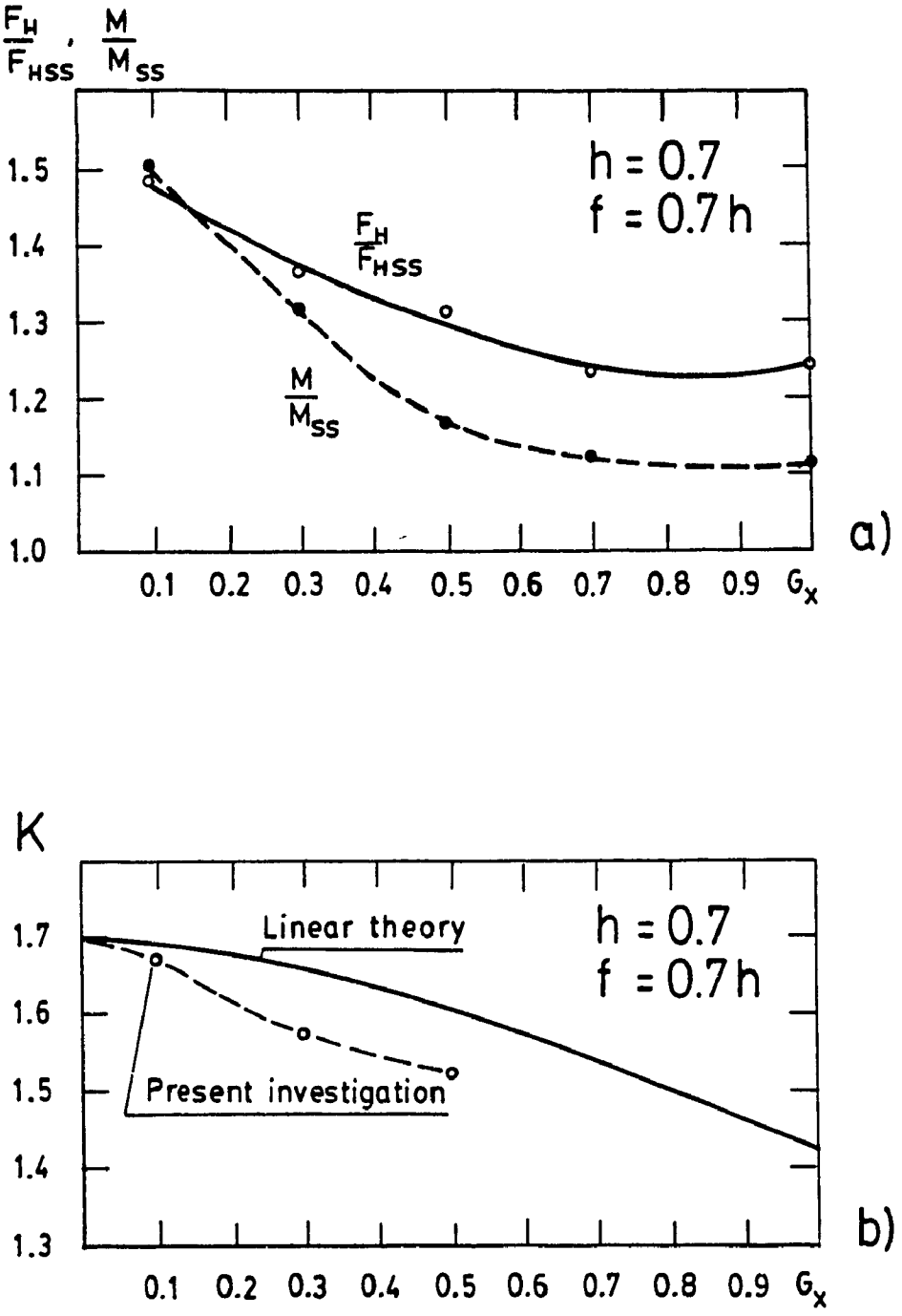

Fig.5.8. Influence of the input acceleration on dynamic coefficients of the horizontal force and overturning moment, a), and on the frequency of the slohing oscillation, b)

G_x below 0.3, and above this value, it increases and tends to 100% for G_x urging to infinity.

5.3.3 Influence of Container Geometry

The geometrical parameter, representing the ratio of the container height to the length of its cross-section, was varied between 0.15 and 2.1. This is the range that covers all possible values of h including plain containers with no separating walls and fully compartmented containers. The high values of h may also be related to longitudinally compartmented containers for analyzing their lateral stability problem. The results of computer study are given in Table 5.7 and Fig. 5.9 a) and b). The dynamic coefficient of the horizontal force decreases with increasing of h and tends to 1.0 for h going to infinity, Fig.5.9 a). This fact shows that the overall damping is higher in containers with large height than in containers with smaller height. The dynamic coefficient of the overturning moment displays maximum at h=1.0 that corresponds to the square container. An unlimited increase in h must bring the coefficient to 1.0 or to the absence of sloshing in tanks with excess height. Thus, the most severe sloshing takes place in a square container. The normalized frequency, shown in Fig. 5.9 b), is compared with that of the linear theory, and this comparison gives 5% to 7% reduction of the damped frequency with respect to the undamped one for container with h between 0.7 and 2.1. For longer containers with h below 0.4, the computed frequency is greater than the one obtained via the linear theory. This happens because Configuration 1 is replaced by Configuration 2 or even 4 and the free surface starts to interact with

Table 5.7. Effect of container height on numerical solution for $f=0.7h$, $G_x=0.3$, $Re=1.29\times10^7$ (101" wide container, water)

h	f	Peak value F_H	Peak value M	Steady-State M_{ss}	Dynamic coefficients $\frac{F_H}{F_{Hss}}$	Dynamic coefficients $\frac{M}{M_{ss}}$	Share of F_H in moment generation %	Ω $\frac{rad}{s}$ (Config.1)	K Present investigation (Config.1)	K Linear theory
0.15	0.105	0.4305	0.1930	0.1550	1.4350	1.2451	13.4	—	—	0.9788
0.35	0.245	0.4255	0.1725	0.1351	1.4183	1.2768	31.6	2.0268	1.4344	1.3950
0.7	0.49	0.4089	0.1650	0.1251	1.3630	1.3191	61.5	3.1416	1.5722	1.6566
1.4	0.98	0.3672	0.2263	0.1728	1.2240	1.3096	87.6	4.5421	1.6074	1.7310
2.1	1.47	0.3505	0.2986	0.2377	1.1683	1.2562	94.4	5.5998	1.6181	1.7345

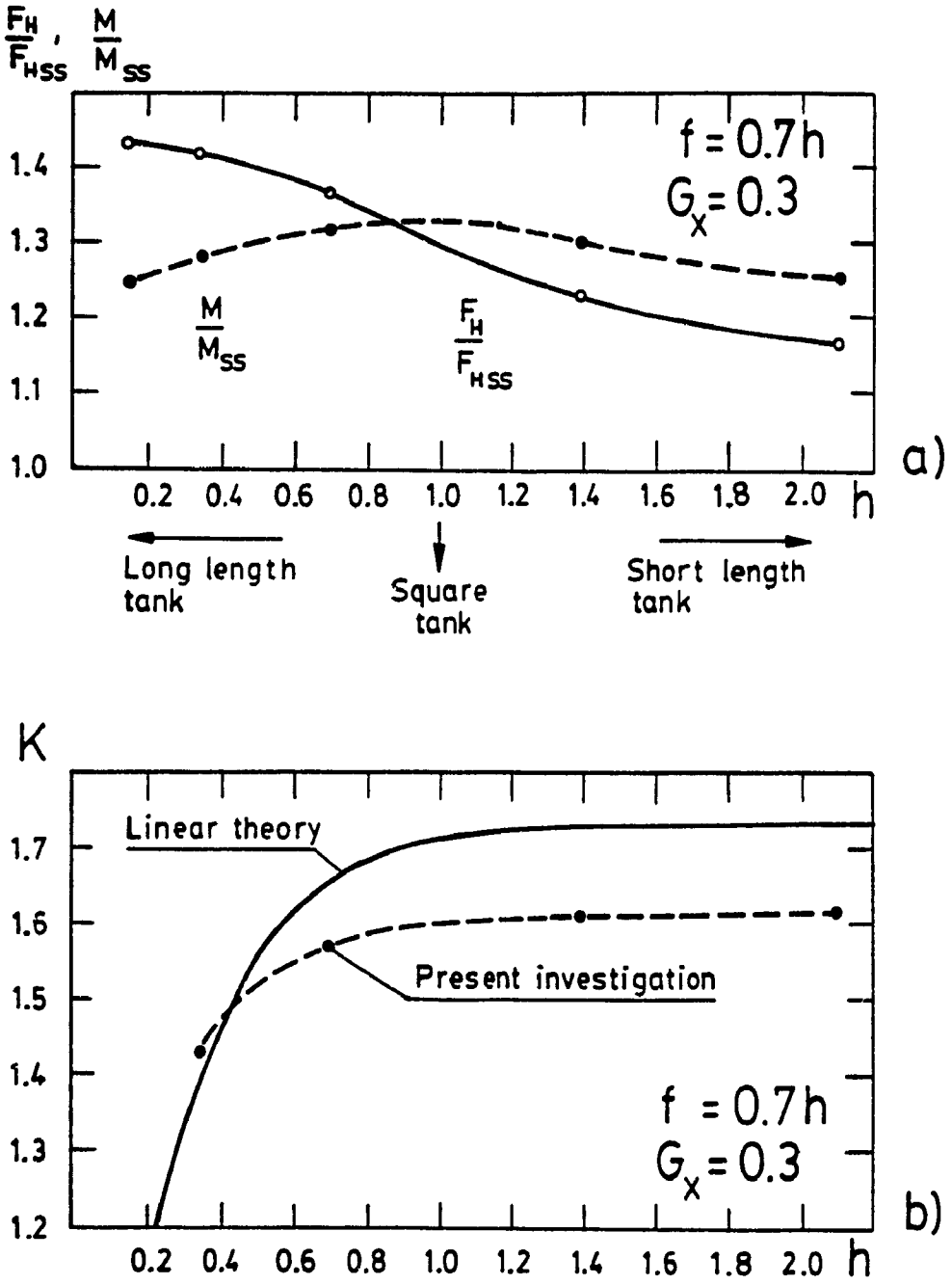

Fig.5.9. Influence of the container height on dynamic coefficients of the horizontal force and overturning moment, a), and on the frequency of the sloshing oscillation, b)

the top and/or bottom wall of the container. In this case, the linear theory can not be applied at all since it does not allow the action of the horizontal walls. For h less than 0.35, the liquid motion becomes irregular and the frequency is inconclusive. The nature of the vibrations, in this case, is similar to those which are usual in the previous cases with very high G_x or with very high or very low f, when the interference of the horizontal walls suppresses the first mode of vibration and essentially changes the characteristic of liquid motion. The share of the horizontal force in the generation of the moment increases asymptotically to 100% for a container with large height underscoring the fact that the horizontal displacement of the liquid is decreasing and tending to zero with h.

5.4 Summary

This chapter deals with the dynamics of liquid motion in rectangular road containers subjected to a step acceleration input simulating the braking-accelerating or steady turn vehicle manoeuvres. The analytical steady-state and numerical transient solutions are obtained in terms of amplitudes and frequencies of the main sloshing parameters such as liquid heights, forces, and overturning moments. From the steady-state solution, it has been shown that a steady turn can be sufficiently accurately simulated by the same set of equations characterizing the braking-acceleration manoeuvre by simply assuming a homogeneous body field in the liquid for the former. The error, introduced by this simplification, is small.

The results and the methodology of the transient response in this

investigation, can be applied both to the lateral and longitudinal dynamics of liquid motion in a tank vehicle. During a steady turn of a vehicle, the lateral stability is of primary concern and the dynamic overturning moment is the major parameter affecting the stability. During the braking-acceleration manoeuvres, the overturning moment is still of some importance since it dictates the loading on the vehicle axles.

The dynamic behaviour of the overturning moment and forces was studied on a sufficiently accurate model of the sloshing process, including most of the nonlinear effects relevant to the problem. The most intense sloshing occurs when f is between 0.2-0.4 or the container filling is approximately between 30-60% with respect to the container height. However, the maximum of the dimensional forces and moments falls between f=0.55-0.65 or at 75-93% of filling depending on the combination of h and G_x. These results correspond to only steady turn or uniform braking/acceleration. For a more complex manoeuvre, the sloshing may lead to a resonance which can further produce very large forces and moments.

The level of input acceleration has maximum effect on the sloshing amplitudes for small G_x. Increase in G_x leads to decreasing of amplitudes, at least up to G_x = 1.0. The range beyond 1.0 was not studied since it is out of the feasible region, but the trend of the dynamic coefficients shows that they may increase again.

The container shape parameter h, produces maximum of sloshing at h≅1, or in a square container, for the overturning moment. The lateral force coefficient, however, increases while the container height is

decreased, and this creates large forces which often lead to skidding of a vehicle in braking.

The natural damped frequencies of the sloshing vibrations are about 5-8% below of those from the linearized theory, if the vibrations do not interact with the top or bottom walls of the container. If the liquid vibrations are affected by the top and bottom walls, the frequencies sharply increase while the amplitude of vibration decreases. The liquid motion becomes irregular. This implies that the linearized theory may not any longer be applicable to the sloshing process. The results obtained in this chapter for the liquid loading at steady-state reveal that there exists an optimal geometrical shape for rectangular containers. The optimization of the container geometry will be presented in Chapter 8.

CHAPTER 6

STEADY-STATE AND TRANSIENT RESPONSES OF LIQUID SLOSHING IN HORIZONTAL CYLINDRICAL CIRCULAR CONTAINERS

6.1 General

In this chapter, the steady-state and transient solutions for liquid sloshing in horizontal cylindrical road containers subjected to a step acceleration input, simulating vehicle manoeuvres such as steady turns, are presented and discussed. The steady-state solution in terms of liquid heights, forces, and their moments is derived analytically from the hydrostatic equations. They are carried out for the rectilinear motion of the container and then applied to the rotational motion to simulate a steady turn. The validity of approximating the rotational motion by the rectilinear motion is illustrated by estimating the resultant error which is small.

The transient responses are obtained by solving the liquid slosh model developed in previous chapters. The mathematical model of the liquid motion includes all essential nonlinear effects due to the nature of the governing equations, shape of curved walls, and the free surface. This allows to obtain the damped natural frequencies of liquid oscillations as well as the magnitudes of forces and moments due to sloshing. From this study, it is possibe to investigate the directional dynamics of a partially filled cylindrical tank vehicle, undergoing different road manoeuvres, by integrating the nonlinear fluid slosh model with an appropriate vehicle stability model.

6.2 Steady-State Solutions

Steady-state solutions, although do not show fluctuations in the

liquid forces as the transient solutions do, may present some interesting result in the case of highly viscous liquid or in the case, when a vehicle undergoes a steady turning manoeuvre for a sufficiently long time, so that all vibrations are almost damped out. Steady-state solutions are obtained by integrating the 2-D momentum equations, reduced for a static case. The input excitations considered correspond to two different motions of the vehicle. The first motion corresponds to the displacement of the container in the lateral direction under a constant acceleration, producing a homogeneous body force field, which is rather a rare case in practice. The second one corresponds to a very common practical case when the vehicle traverses a curved track of constant radius with a constant velocity and when the body force field is not homogeneous.

6.2.1 Rectilinear Motion of a Container

The 2-D hydrostatic equations in the nondimensional form are

$$G_x = \frac{\partial P_{ss}}{\partial X} \quad \text{and} \quad G_y = \frac{\partial P_{ss}}{\partial Y} \tag{6.1}$$

where G_x and G_y are coordinate independent, as shown in Fig.6.1. Equations (6.1) can be easily transformed into the equation for total differential in pressure at static equilibrium and also into the equation of isobars that include the free surface:

$$dP_{ss} = G_x\, dX - G_y\, dY \quad \text{and} \quad G_x dX - G_y dY = 0 \tag{6.2}$$

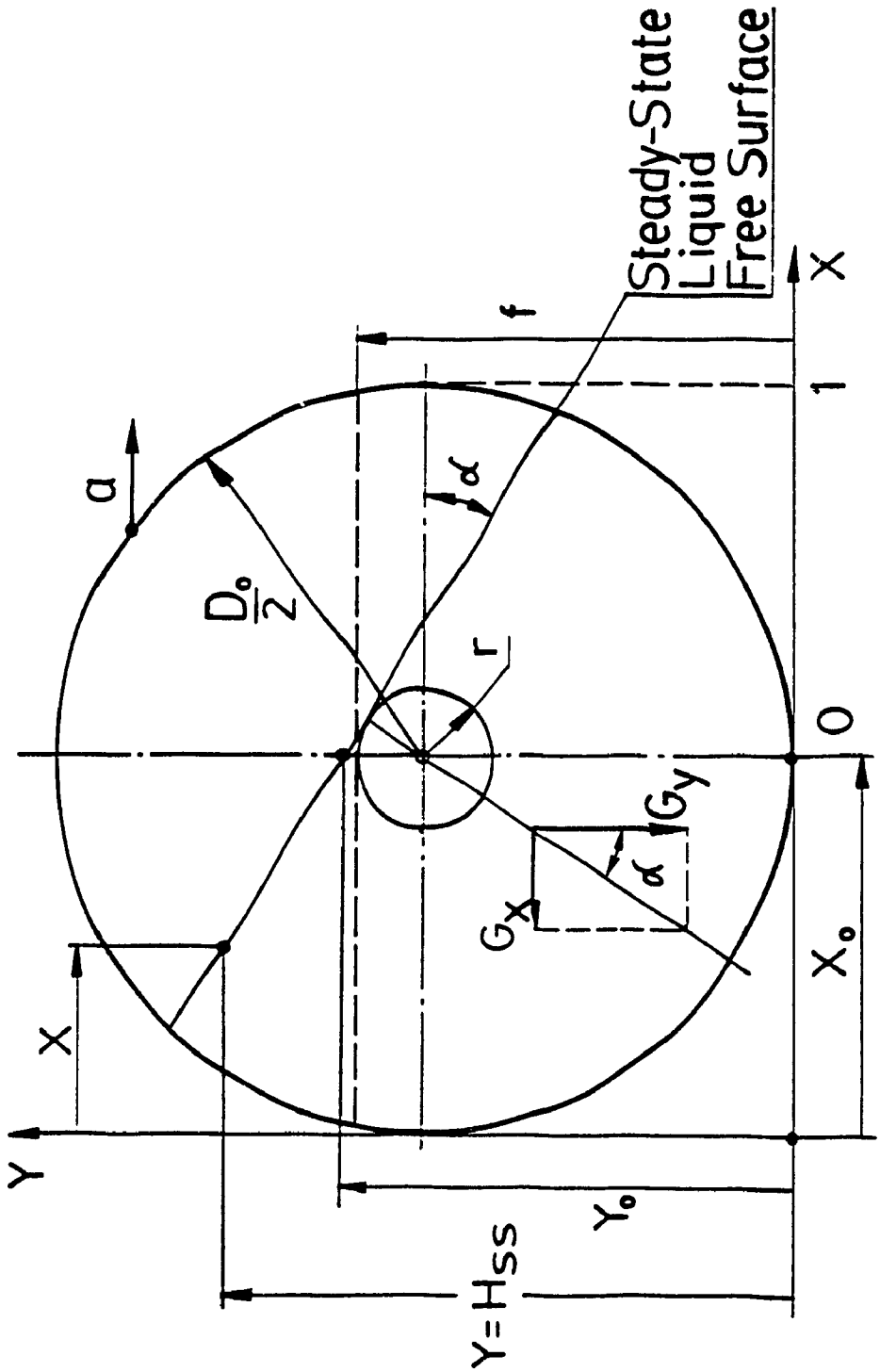

Fig.6.1. Schematics for rectilinear motion of a cylindrical circular container

Integrating Eqns. (6.2) yields:

$$P_{ss} = G_x (X - X_o) - Y + Y_o \quad \text{and} \quad Y = Y_o + G_x (X - X_o)$$

$$Y_o = \frac{1}{2} + (f - \frac{1}{2}) \sqrt{1 + G_x^2} \quad \text{and} \quad X_o = \frac{1}{2} \tag{6.3}$$

The isobars represent a family of straight lines with a slope, $\tan\alpha = G_x$. The free surface is a line tangent to a circle of radius r, see Fig.6.1. This condition is used to find the X_o and Y_o values. Finally, the area of the container, A_o, occupied by the liquid, the steady-state values of the liquid heights, the pressure, the horizontal and vertical forces and the overturning moment around the point 'O' are found to be:

$$A_o = \frac{\pi}{8} + (f - \frac{1}{2}) \sqrt{f (1 - f)} + \frac{1}{4} \sin^{-1} (2f - 1)$$

$$H_{SS} = G_X X + \frac{1}{2} (1 - G_X) + (f - \frac{1}{2}) \sqrt{1 + G_X^2} \tag{6.4}$$

$$P_{SS} = G_X X - Y + \frac{1}{2} (1 - G_X) + (f - \frac{1}{2}) \sqrt{1 + G_x^2}$$

$$F_{HSS} = G_X ; \qquad F_{VSS} = - 1 ; \qquad M_{SS} = \frac{G_x}{2}$$

where the nondimensional forces represent the ratios of their dimensional values to the liquid weight per unit length of the container, and the moment, also per unit length, is positive if it is directed clock-wise around the point 'O'.

For a cylindrical container the dimensionless moment, taken as the ratio of its dimensional value to the product of the liquid weight and of the container diameter, is independent of the container filling and

is a function of G_x alone.

The conversion of the values given by Eqns. (6.4) into the dimensional form can be obtained using the following expressions:

$$a_o = D_o^2 A_o; \qquad h_{ss} = D_o H_{ss};$$
$$f_{Hss} = \rho g a_o b G_x; \qquad f_{vss} = -\rho g a_o b ; \tag{6.5}$$
$$m_{ss} = \frac{1}{2} \rho g a_o b D_o G_x$$

which represent a modification of the general expressions, Eqns.(2.20), to the case of a circular container.

6.2.2 Rotational Motion of a Container

When the vehicle undergoes a steady turn, the free surface takes a parabolic shape and the unit body force is not homogeneous, see Fig.6.2, since its horizontal component is expressed by $G_x = \omega^2 \xi / g$.

By integrating the hydrostatic equations, the following expressions for the liquid height and gage pressure are obtained:

$$Y = Y_o + \frac{G_n}{2\delta} \left[X^2 + (2\delta - 1) X \right]$$
$$P = Y_o - Y + \frac{G_n}{2\delta} \left[X^2 + (2\delta - 1) X \right] \tag{6.6}$$

The shape of the free surface is completely defined by the parameters G_n and δ, and its position may be found from the pressure equation applied to a point where the pressure is known. This involves the definition of the area under the parabola and equating it to the initial area occupied by the liquid. Such a procedure results in a rather lengthy expression for the liquid height. An alternate way to approximate the liquid height uses the assumption that the parabola is shifted downward from the

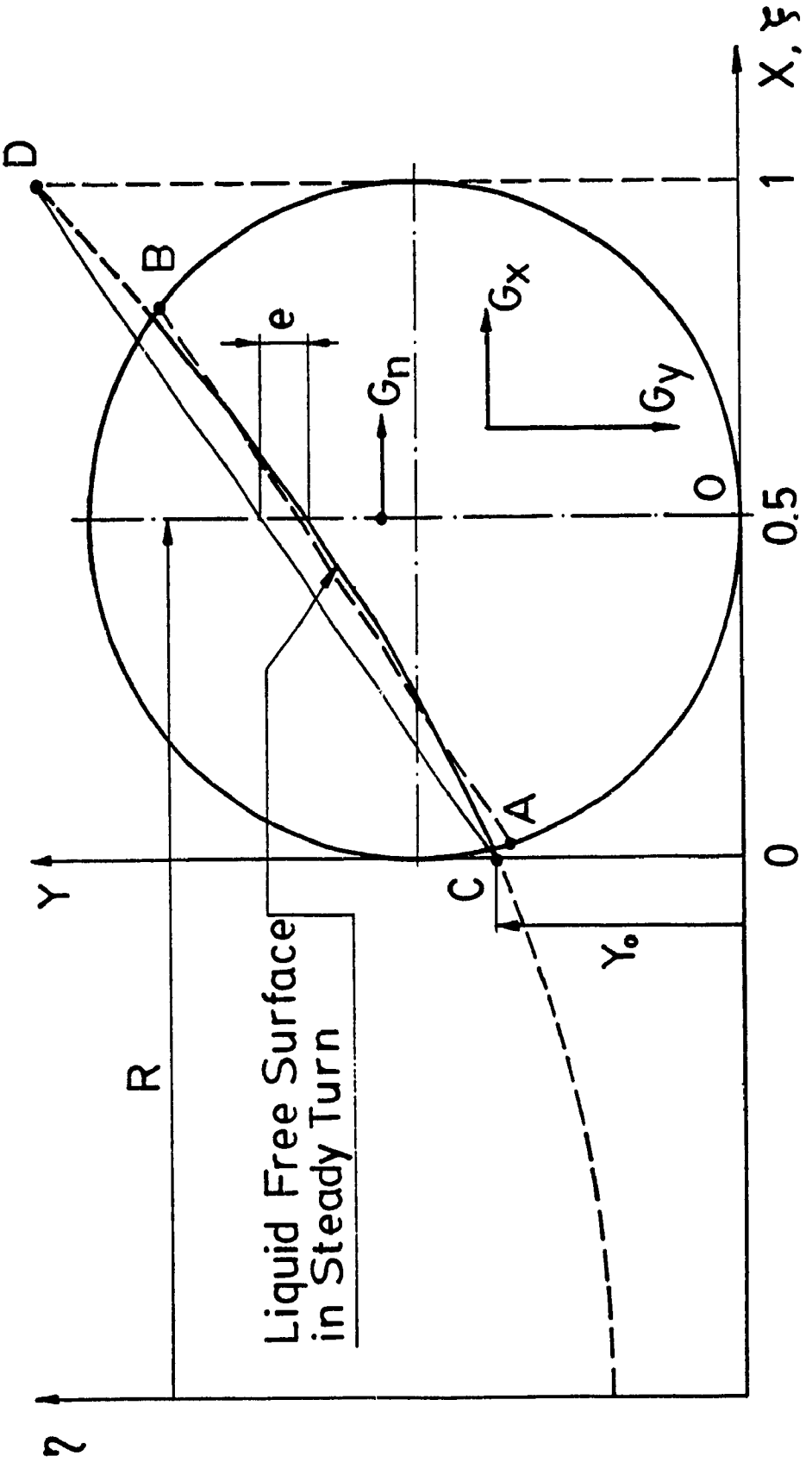

Fig.6.2. Schematics for rotational motion of a cylindrical circular container

straight line AB, see Fig.6.2, representing the free surface of the equivalent rectilinear motion, by a distance equal to one-third of the parabola deflection, e, in the middle of the container, where the nondimensional deflection is given by:

$$e = -\frac{G_n}{8\delta} \quad \text{with} \quad G_n = -\frac{\omega^2 R}{g} \tag{6.7}$$

Based on this assumption, the liquid height may be expressed as

$$H_{ss} = \frac{1}{2} + \left(f - \frac{1}{2}\right)\sqrt{1 + G_n^2} + \frac{G_n}{2\delta}\left[X^2 + X(2\delta - 1) - \delta + \frac{1}{6}\right] \tag{6.8}$$

and the relative error of heights, taken as the ratio of the absolute error to the container diameter, is given by

$$E_H = \frac{G_n}{2\delta}\left(X^2 - X + \frac{1}{6}\right) \tag{6.9}$$

The above expression gives the maximum possible error as a function of G_n, δ, and X-coordinate, with the maximum occurring at X = 0 or 1, and is equal to

$$E_H^{max} = \frac{G_n}{12\,\delta} \tag{6.10}$$

The horizontal force, F_{HSS}, on the container walls may be found by integration of the pressure equation, Eqns. (6.6), along the wetted perimeter where the coordinate X must be substituted by Y from the circle equation of the wall. The simultaneous solution of these two equations with the exact definition of the Y_o-value results in a very complicated expression for F_{HSS} that may be hardly recommended for practical application. Under those circumstances, the horizontal force may be rather estimated from the simpler expression for the translational motion with the definition of the error resulting from

such a simplification. This can be carried out through the comparison of the pressures at similar points for the rotational and rectilinear motions. The difference in dimensionless pressures is found to be

$$\Delta P = P^{rot} - P^{rec} = \frac{G_n}{2\delta}\left(X^2 - X + \frac{1}{6} \right) \tag{6.11}$$

The maximum difference occurs at X=0 or X=1. In some cases, it would be more important to know the error with respect to some real pressure inside a container. The maximum pressure in the container taking place at maximum depth, referenced from the free surface in the direction of the total vector of body forces, may be chosen as the reference pressure. Then, the relative error is

$$E_p = \frac{P^{rot} - P^{rec}}{P^{max}} = \frac{G_n}{12\ \delta\ f \sqrt{1 + G_n^2}} \tag{6.12}$$

Since it is computed for X=0 or 1, this is the maximum possible error. A plot of the percentage error, is given in Fig. 6.3 with a sample calculation shown on the diagram by dotted lines. It can be seen that the error on pressure, resulting from the replacement of the rotational motion by the rectilinear one, is very small for most practical combinations of parameters G_n, δ, and f. It also can be seen from the expression (6.11) that the difference in pressures between the rectilinear and rotational motions is symmetrical with respect to the vertical axis of the container, and therefore it will be partially cancelled while computing the liquid forces. Then, the error of the horizontal force will be even smaller than that of the pressure for all fillings of the container, except f = 1 when the errors coincide.

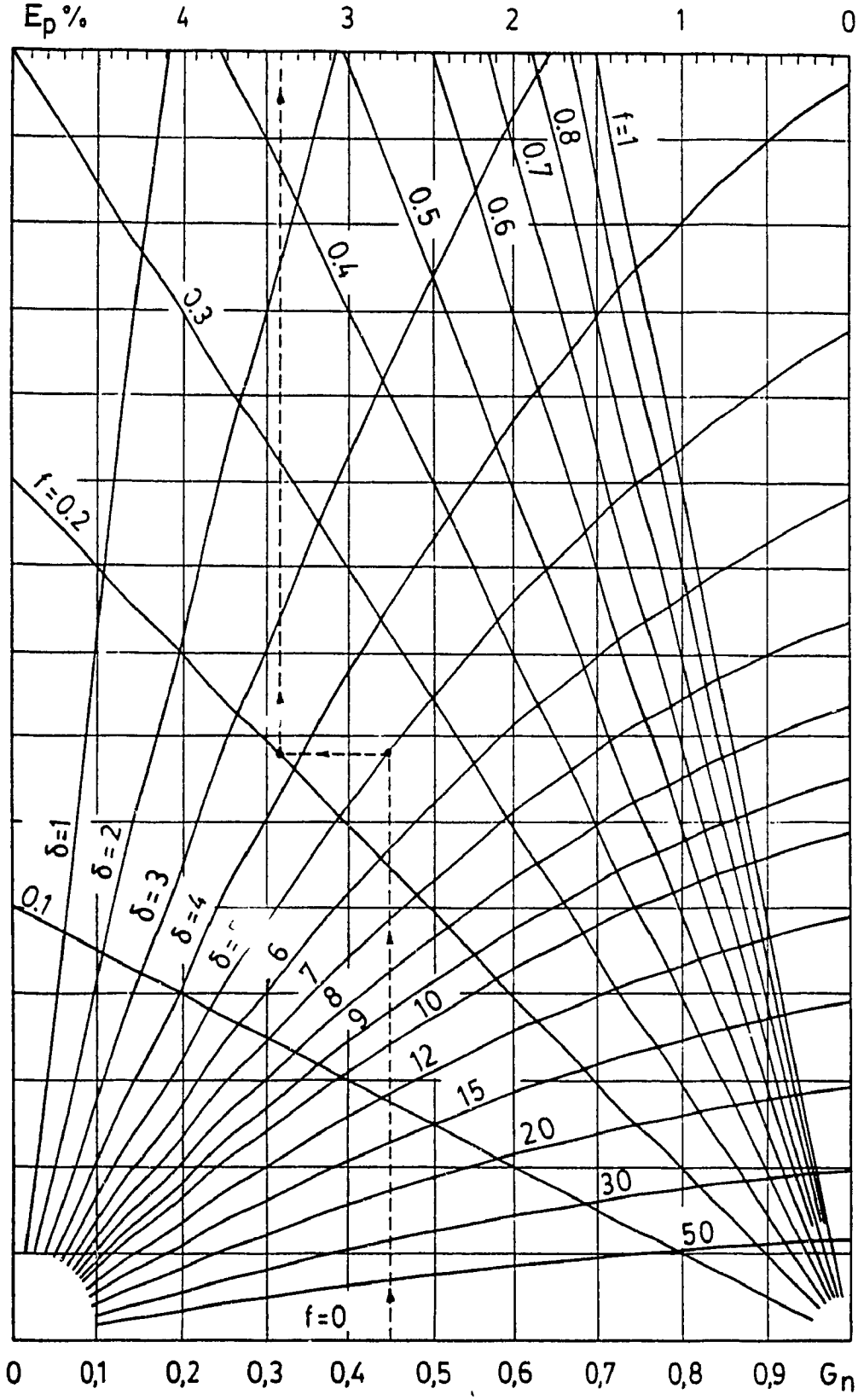

Fig.6.3. Diagram of error of pressure due to replacement of the rotational motion by the rectilinear motion

As an example, consider a tanker container performing a steady turn of radius equal to 5 times the container diameter, $\delta = 5$, filled up to 20%, $f = 0.2$, and subjected to a centrifugal acceleration in the middle of the container of 45% of g, $G_n = 0.45$. The maximum possible error of the pressure, computed for the rectilinear motion, does not exceed 3.4% as it is shown in Fig.6.3 by the dotted lines. The error of the horizontal force will be smaller than the estimated error of 3.4%. For the same parameters, but 60% filled container, the upper bound on the error, E_p, is only 1.2%.

The vertical force at the steady-state is always equal to the liquid weight with its nondimensional value equal to -1. The overturning moment for the rotational motion is slightly increased due to the upward shifting of the horizontal force and to the outward shifting of the vertical force. However, it can be still computed using the expression for the rectilinear motion with the error estimation given by Eqn. (6.12). It has to be noted that this expression becomes invalid when the fill level tends to become zero because of the assumption made above for its derivation, but the small fill levels are unimportant in the case of the road container.

Thus, the considerations above show that the analytical steady-state solution for the rotational motion can be reduced to the solution for equivalent rectilinear uniformly accelerated motion occuring under the step input acceleration of the same magnitude. Such a simplification provides good accuracy if the real values of the steady turn parameters are assumed. Strandberg suggested in his investigation [28] that the threshold of the lateral acceleration may not exceed 0.4 g's for large capacity liquid tankers. On the other hand, the radius

of the turn is also limited, and usually is greater than 50m, or in the nondimensional form, $\delta > 25$. Taking into account those limitations, the expression (6.12) approximates the upper bound of the error on the pressure, forces, and moment in the range 0.4 to 0.12 percent for fill levels between 30 and 100% ,respectively.

6.3 Transient Solutions

In this section, the transient solutions for cylindrical road containers with circular cross-section, undergoing a cornering maneouvre, are presented and discussed. Though the solutions have been obtained with a homogeneous body forces, simulating the rectilinear motion, they can also be applied to the rotational motion characterized by the coordinate dependent centrifugal acceleration as it has been discussed in the previous section.

The three input parameters, namely, the Re-number representing the viscosity, the input acceleration, and the fill level of the container were varied in order to investigate their influence on the transient response of the liquid. The numerical values of these parameters are given in Table 6.1, where the framed values indicate the two fixed parameters while the third one was varying.

6.3.1 Influence of Re-Number

The Re-number was varied in large range, from 10^3 to 10^7, while the remaining parameters were kept constant at $f = 0.6$ and $G_x = 0.306$. These values correspond to a container with diameter $D_o = 2.032$ m (80 inches), a liquid density ρ=850 kg/m^3, and a lateral acceleration a = 3 m/s.^{2} The computational grid was 22 x 22 cells, including the boundary

Table 6.1. Cases of numerical study for cylindrical circular containers

Viscosity variation		Input acceleration variation		Fill level variation
Re	ν, m^2/s	G_x	a, m/s^2	f
1×10^7	0.907×10^{-6}	0.1	- 0.981	0.3
1.52×10^6	0.600×10^{-5}	0.2	- 1.862	0.5
1×10^6	0.907×10^{-4}	0.306	- 3.0	0.6
1×10^5	0.907×10^{-3}	0.4	- 3.924	0.7
1×10^4	0.907×10^{-2}	0.5	- 4.905	0.9
1×10^3				

Table 6.2. Effect of Re-number on numerical solution for f=0.6, G_x=0.306, (light crude oil, ρ=850kg/m^3, ν=0.6x$10^{-5}m^2/s$; 80" container diameter)

Re	Peak values of		Share of F_H in creating of the moment %	First damped natural frequency	Undamped theoretical frequency
	F_H	M			
10^7	0.4053	0.2038		1.151	
10^6	0.4053	0.2038		1.151	
10^5	0.4053	0.2037	≅ 70	1.151	1.201
10^4	0.4031	0.2027		1.143	
10^3	0.4008	0.2016		1.139	

cells, and the time increment was $\Delta T = 0.002$ corresponding to real time of 0.02 sec.

The liquid motion due to a suddenly applied step lateral acceleration is as follows. Under the influence of the body forces, G_x, the liquid begins to move from the right to the left, see Fig.6.4 a) and b). The drag effect of the wall leads to creation of a higher mode wave with its crest initially occurring near the left wall, curve 1 in Fig. 6.4 a), which travels to the right and slowly dissipates, curve 2. The liquid height on the left reaches its maximum sooner (T = 0.8 sec.) than the liquid height on the right reaches its minimum (T = 1.0 sec.). This causes the free surface to bulge and to generate the wave that is superimposed on the lower mode wave. Curve 3 gives the free surface when the height at left reaches a minimum while the wave on right is running up the wall. Fig. 6.4 b) shows the two extreme positions of the free surface at the 4th overshoot; here the presence of the higher mode wave with its considerably smaller amplitude is seen even better.

Time histories of the liquid heights at the left and right walls, H_L and H_R, are given in Fig.6.5 a) and b) and the corresponding plots of F_H, F_V, and M in Fig.6.6 a). The displacement of F_H from the X-axis Y_H, and the displacement of F_V from the point '0', E_V, are shown in Fig.6.6 b); all these correspond to $Re = 10^7$, $G_x = 0.306$, and $f = 0.6$. The peak values of the sloshing parameters are greatest at the first overshoot and they slightly decrease with time. The fundamental frequency varies insignificantly from period to period and the average frequency, computed over the first five periods, show a very weak dependence on the Re-number within the range $10^7 - 10^3$. From the plots of Fig. 6.6, it can be seen that all sloshing parameters, i.e. the

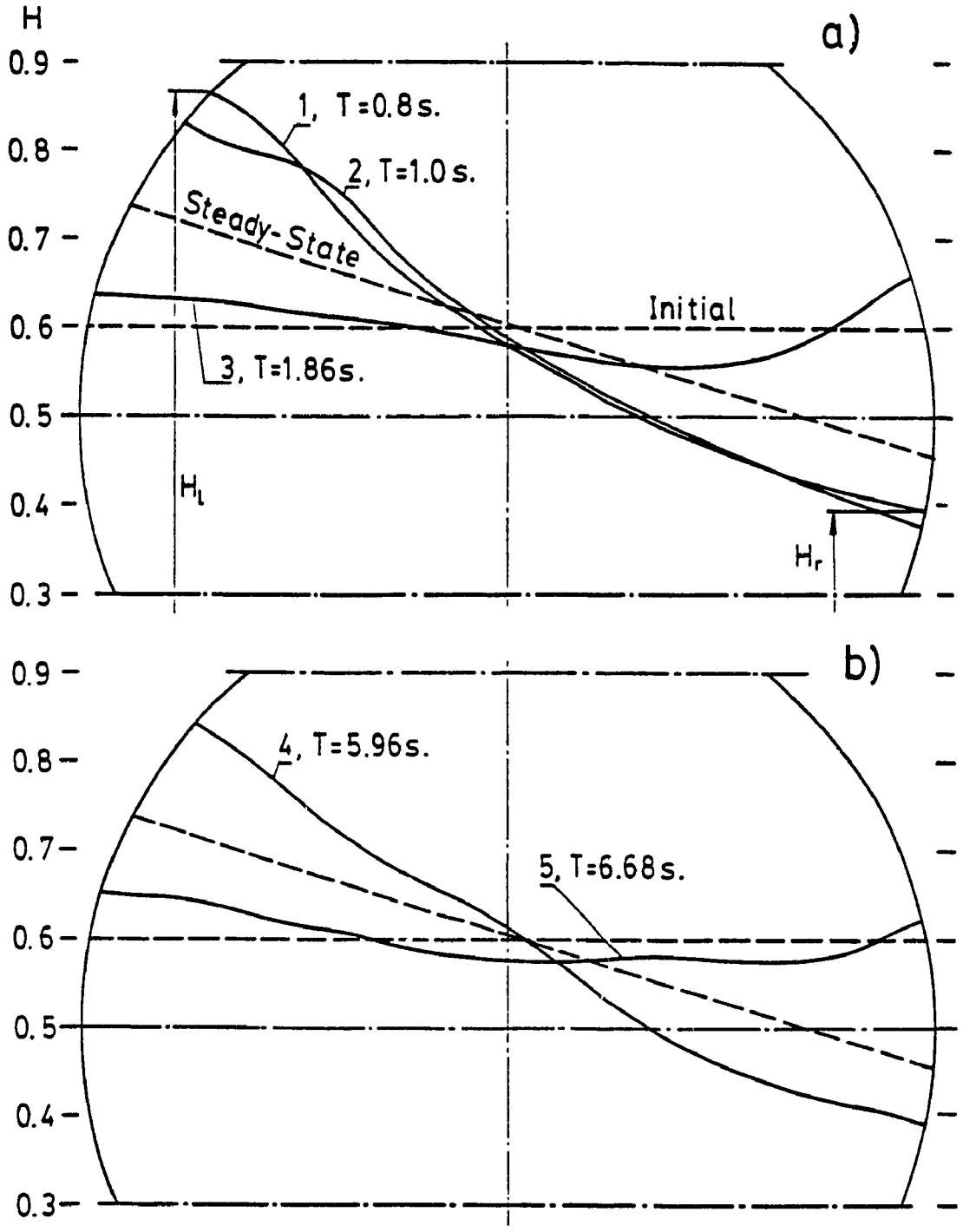

Fig.6.4. Typical shapes of the free surface for $Re=10^7$, $f=0.6$, and $G_x=-0.3$

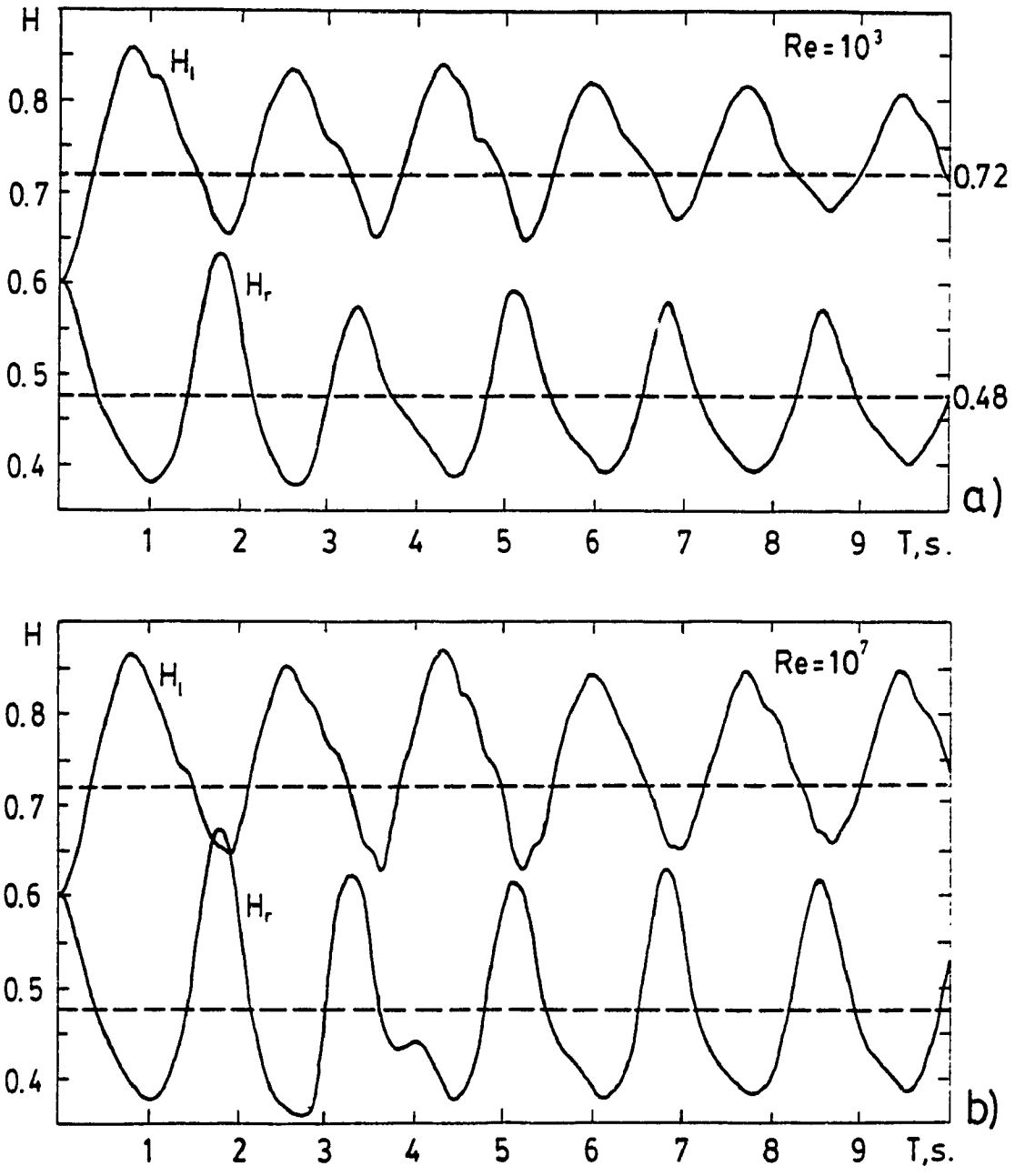

Fig.6.5. Typical liquid height oscillation for f=0.6 and G_x=-0.3 and for Re=10^3, a), and Re≐10^7,b)

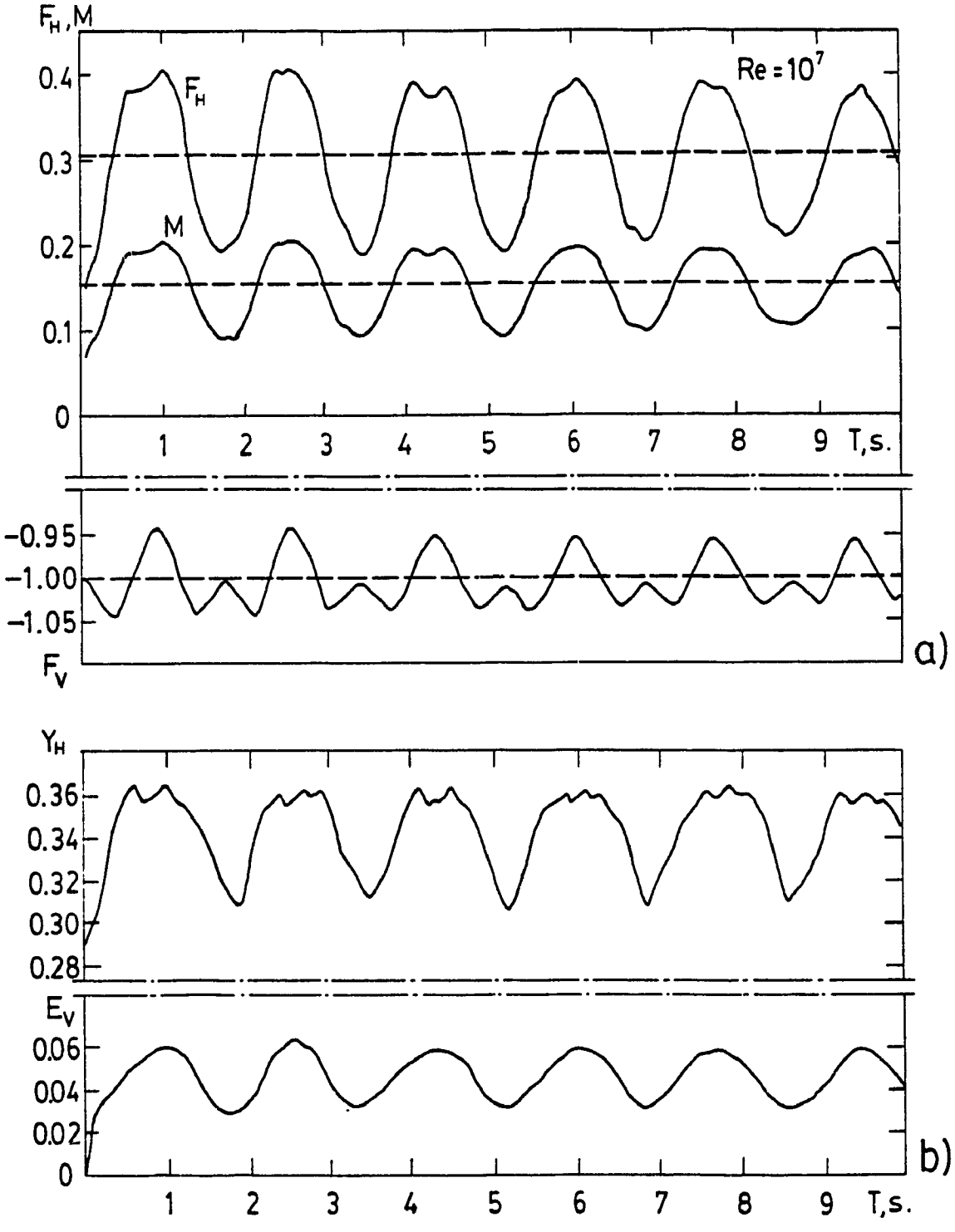

Fig.6.6. Time histories of sloshing parameters for Re=10^7, f=0.6, and G_x=0.3

forces, their coordinates, and the moment, oscillate in phase, and that there is a small decrease in vertical force occurring twice during each period of vibration at the time when the free surface reaches the upper position near the left or the right wall of the container. This means that the inertia force of the part of the liquid directed upward, or against the liquid weight, leads to a temporary decrease of the vertical reaction of the liquid exerted on the container walls. These results are summarized in Table 6.2, where the peak values of the horizontal force and moment are given for the first overshoot. The computed normalized damped natural frequencies, K, are about 5 percent less than the undamped frequencies computed from the Budiansky's linear theory [20]. For the majority of practical cases, which corresponds to Re values from 10^7 to 10^5, the main sloshing parameters are almost independent of the Re-number.

6.3.2 Influence of Input Acceleration

The input acceleration, G_x, was varied from 0.1 to 0.5 which approximately corresponds to the lateral vehicle acceleration between 1 and 5 m/s^2. All remaining parameters were kept constant as they are given in Table 6.1. The results of this investigation are presented in Table 6.3 and Figs. 6.7 and 6.8.

As it can be seen from Fig.6.7 a), the steady-state values of the horizontal force and moment are proportional to the magnitude of the input acceleration, while their dynamic values become relatively smaller with increasing of the G_x due to the nonlinear effects of the wall shape and of the viscosity of the liquid. The dynamic coefficients for the lateral force and moment are given in Fig.6.7 b). The graphs in Fig.6.7

Table 6.3. Effect of input acceleration on numerical solution for f=0.6, $Re=1.52\times10^{6}$, (light crude oil, $\rho=850 kg/m^3$, $\nu=0.6\times10^{-5}\ m^2/s$; 80" container diameter)

G_x	Peak values of		$\frac{F_H}{F_{HSS}}$	$\frac{M}{M_{SS}}$	Share of F_H in creating of M, %	First damped natural frequency	Undamped theoretical frequency
	F_H	M					
0.1	0.1412	0.0871	1.410	1.740	57	1.198	
0.2	0.2811	0.1510	1.405	1.510	68	1.180	
0.306	0.4053	0.2038	1.333	1.392	70	1.151	1.201
0.4	0.5061	0.2613	1.265	1.305	71	1.004	
0.5	0.5952	0.3082	1.190	1.232	71	0.883	

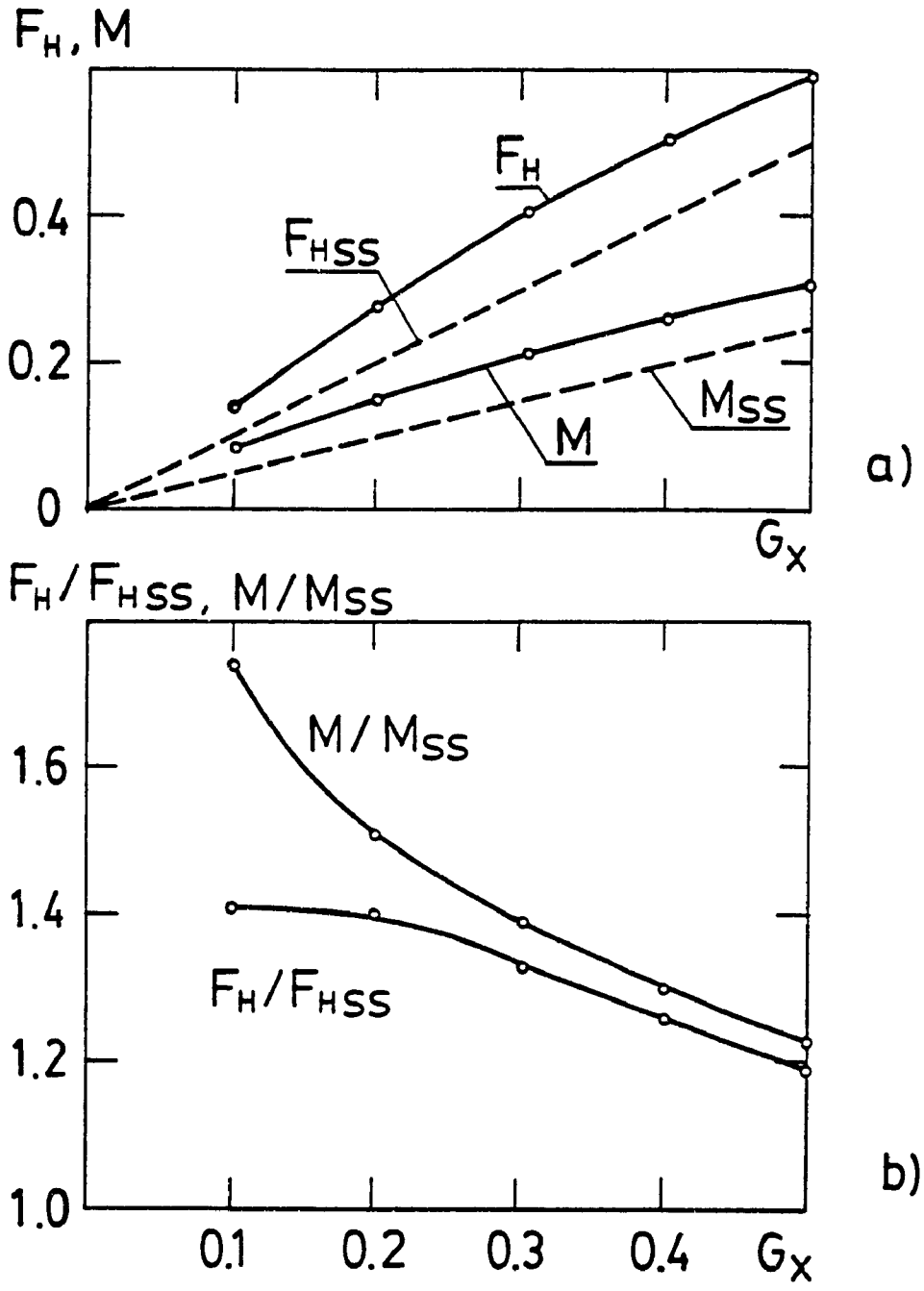

Fig.6.7. Influence of the input acceleration on horizontal force and overturning moment, a), and their dynamic coefficients, b)

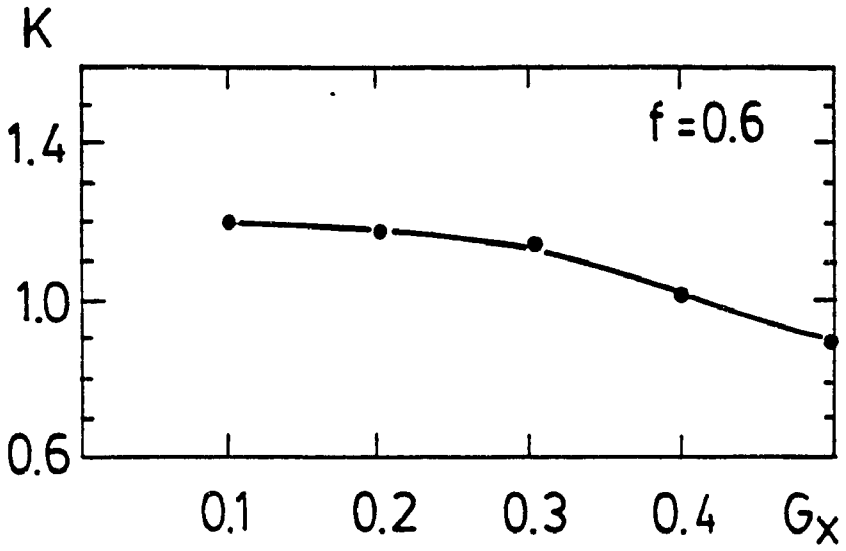

Fig.6.8. Normalized damped frequency as function of lateral input acceleration

a) and b) correspond to the filling of 60% when the contribution of F_H in the generation of the overturning moment varies between 57% and 71% depending upon the G_x. For smaller G_x, the displacement of the liquid mass in the horizontal direction is sufficiently large, however the rate of its further increasing decreases with G_x. Hence, the moment arm of the vertical force increases progressively slow with increasing of G_x and this causes the continuously diminishing contribution of the vertical force to generation of the moment. This effect is stronger for small filling and it tends to zero for the filling of 100%.

The frequencies of the sloshing appear to be dependent on the magnitude of G_x, decreasing with increase of the input acceleration. The plot showing the behaviour of the normalized first damped natural frequency is given in Fig. 6.8. A similar behaviour was observed by Peterson in his experimental investigation [58] for liquid sloshing at low gravity condition. Of course, this phenomena is not related to the low gravity itself, but it is rather produced by damping and, in principal, must be seen under any gravity forces.

6.3.3 Influence of Fill Level

In this study, the fill level of the container was varied from 0.3 to 0.9 with other input parameters fixed. The results are given in Table 6.4 and Figs.6.9 a), b),and c) and 6.10. The last row in Table 6.4 represents the steady-state values of the corresponding parameters for the completely filled container when the sloshing is absent. The peak values of the horizontal force and moment slowly decrease with the fill level as shown in Fig 6.9 a) and tend to reach their steady-state values at f = 1. The fill levels less than 30% were not studied since they

Table 6.4. Effect of fill level on numerical solution for G_x=0.306, $Re=1.52\times10^6$, (light crude oil, ρ=850kg/m^3, $\nu=0.6\times10^{-5}$m^2/s; 80" container diameter)

f	Peak values of		$\frac{F_H}{F_{HSS}}$	$\frac{M}{M_{SS}}$	Share of F_H in creating of the moment, %	First damped natural frequency	Undamped theoretical frequency
	F_H	M					
0.3	0.4671	0.2388	1.526	1.559	43	1.037	1.056
0.5	0.4229	0.2140	1.382	1.400	63	1.098	1.140
0.6	0.4053	0.2038	1.333	1.392	70	1.151	1.201
0.8	0.3720	0.1881	1.216	1.225	81	1.221	1.291
0.9	0.3282	0.1652	1.072	1.076	96	1.555	1.701
1.0	0.3060	0.1530	1	1	100	---	---

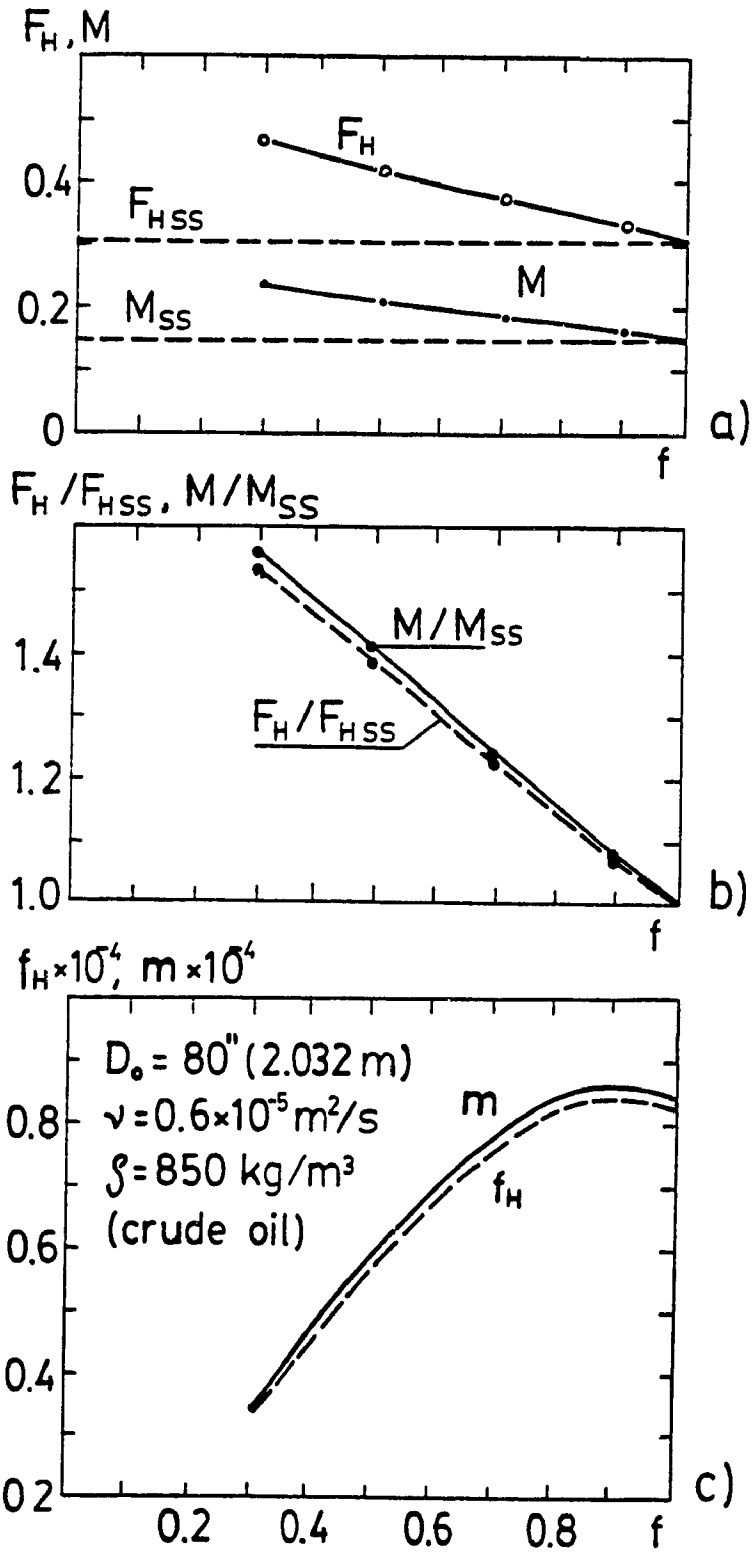

Fig.6.9. Influence of the fill level on horizontal force and overturning moment, a), on their dynamic coefficients, b), and on the dimensional values of the force and moment, c)

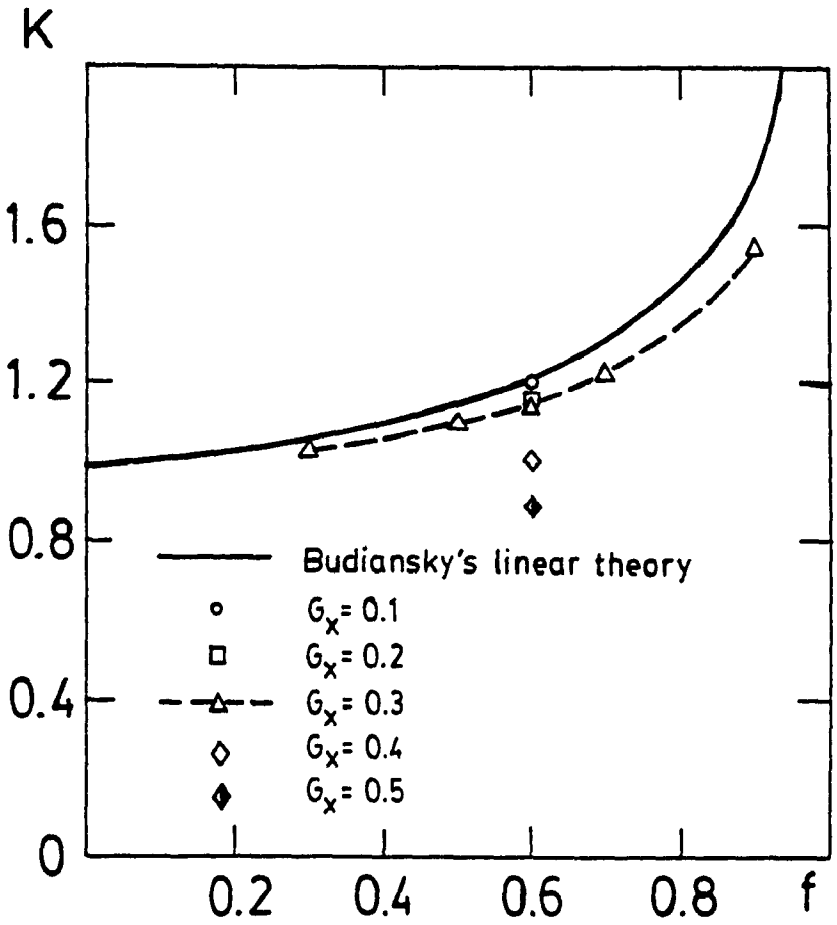

Fig.6.10. Normalized frequencies of sloshing as functions of the fill level

have no importance for practical cases, however at f=0, the forces and moments must vanish. This implies that F_H and M reach a maximum value somewhere between f = 0 and 0.3. Fig.6.9 b) represents the dynamic coefficients for F_H and M and Fig.6.9 c) shows the dimensional values of the horizontal force, f_H, and moment, m, per unit width of the container for the following set of parameters: tank diameter of 2.032 m (or 80 inches), crude oil with density $\delta = 850\ kg/m^3$ and viscosity $\nu = 0.6\times10^{-5} m^2/s$, and input acceleration of the container, $a = -3\ m/s^2$. It can be seen that the maximum loading (f_H,m) occurs for a filling between 80 and 90%. For smaller input acceleration, the maximum values of f_H and m are shifted to smaller values of the fill level.

The fill level has a strong influence on the frequency of liquid oscillation. An increase in fill level implies an increase of the damped natural frequency as shown in Fig. 6.10. The normalized damped natural frequencies are also compared with the results from the linear theory of Budiansky [20]. The good agreement is seen only for small input accelerations and for small fill levels, and the difference progressively grows with increasing of G_x and f. Thus, it can be concluded that the linearized theory holds only for small amplitudes of liquid vibration.

6.4 Summary

The steady-state and transient solutions for liquid sloshing in horizontal cylindrical road containers subjected to a step acceleration input, simulating the steady cornering, have been obtained in terms of amplitudes and damped natural frequencies of the main sloshing parameters such as liquid heights, forces, and overturning moments.

Analytical method for steady-state and numerical solution for transient responses of the liquid are presented.

From the steady-state solution for the liquid response, it has been shown that the non-homogeneous pressure field of the rotational motion may be replaced by the homogeneous one for the rectilinear translational motion with a small error. The same approach of replacing the rotational motion by the rectilinear motion has also been used in transient response since the error is of the same order as in statics. This has been confirmed by comparison of the computer outputs for rotational and rectilinear motions at identical conditions.

The main parameters affecting the liquid motion are the Reynolds number, the level of input acceleration, and the fill level of the container. The Re-number has insignificant influence on the magnitudes and frequencies of the sloshing parameters, at least in the range 10^7-10^3. For Re = 10^3, the frequency is only a half percent smaller than that for Re = 10^7, but for Re < 10^3, the difference in amplitudes and frequencies rapidly increases in such a way that the more viscous liquids vibrate slower, with smaller amplitude, and with stronger decay.

The input acceleration, G_x has a significant influence on the magnitudes and frequencies of sloshing parameters. Increasing of G_x increases the magnitudes of the lateral force and moment and decreases the oscillation frequency. Thus, for G_x = 0.5, the frequency is 25% less than that for G_x = 0.1, while the peak value of the moment is 3.5 times greater.

The fill level is another strong factor influencing the sloshing parameters. Increasing of f leads to the decrease of the amplitude of slosh parameters and oscillating frequency, referring to the

nondimensional form of calculation. However, in the dimensional form, the slosh loads experience maxima which occur at sufficiently high fill levels, i.e., between 80 and 90% depending on the set of input parameters. The normalized damped natural frequencies compared with those from the linearized theory show a good agreement only for small input accelerations and for small fill levels, and the difference progressively grows as G_x and f increase.

CHAPTER 7

STEADY-STATE AND TRANSIENT RESPONSES OF LIQUID SLOSHING IN CONTAINERS WITH SEPARATING WALLS

7.1 General

In this chapter, a study of liquid sloshing behaviour in compartmented and baffled road containers subjected to a step acceleration input are presented and discussed. The analytical steady-state and numerical transient solutions are given in terms of the liquid heights, forces and overturning moments exerted by the liquid on the container body. The influence of the number of separating walls, the size and the location of the baffle orifices is studied for a container with rectangular cross-section. The transient response of the liquid is obtained using numerical solution of the incompressible 2-D Navier-Stokes, the continuity, and the free-surface differential equations as it was discussed in Chapter 3.

The solutions for steady-state and transient responses of the liquid sloshing are obtained for different combinations of the main parameters: the relative height of the container, h; the fill level, f; the horizontal acceleration, G_x; and the number of compartments, n. The study includes uncompartmented (plain), compartmented, and baffled containers with different size of baffle orifices and different number of baffles.

7.2 Steady-State Solutions for Compartmented Containers

Under the influence of the applied lateral acceleration, the free surface of the liquid can take different positions, or configurations,

which are similar to the configurations for an uncompartmented rectangular container described in Chapter 5. The existence of these configurations is defined by the following general conditions:

$$
\left.
\begin{array}{lll}
\text{Conf.1} & \begin{cases} G_x \geq 0 & \begin{cases} Y(X_{k-1}) \geq 0 \\ Y(X_k) \leq h \end{cases} \\ G_x \leq 0 & \begin{cases} Y(X_{k-1}) \leq h \\ Y(X_k) \geq 0 \end{cases} \end{cases} \\
\text{Conf. 2} & \begin{cases} G_x \geq 0 & \begin{cases} Y(X_{k-1}) \geq 0 \\ Y(X_k) \geq h \end{cases} \\ G_x \leq 0 & \begin{cases} Y(X_{k-1}) \geq h \\ Y(X_k) \geq 0 \end{cases} \end{cases} \\
\text{Conf. 3} & \begin{cases} G_x \geq 0 & \begin{cases} Y(X_{k-1}) \leq 0 \\ Y(X_k) \leq h \end{cases} \\ G_x \leq 0 & \begin{cases} Y(X_{k-1}) \leq h \\ Y(X_k) \leq 0 \end{cases} \end{cases} \\
\text{Conf. 4} & \begin{cases} G_x \geq 0 & \begin{cases} Y(X_{k-1}) \leq 0 \\ Y(X_k) \geq h \end{cases} \\ G_x \leq 0 & \begin{cases} Y(X_{k-1}) \geq h \\ Y(X_k) \leq 0 \end{cases} \end{cases}
\end{array}
\right\} \qquad (7.1)
$$

where the subscript k represents the number of a compartment counting from left to right in Fig. 7.1.

The free-surface equations are found separately for each configuration by integrating the differential equation of isobars:

$$G_x dX + G_y dY = 0 \qquad \text{with} \qquad G_y = -1 \qquad (7.2)$$

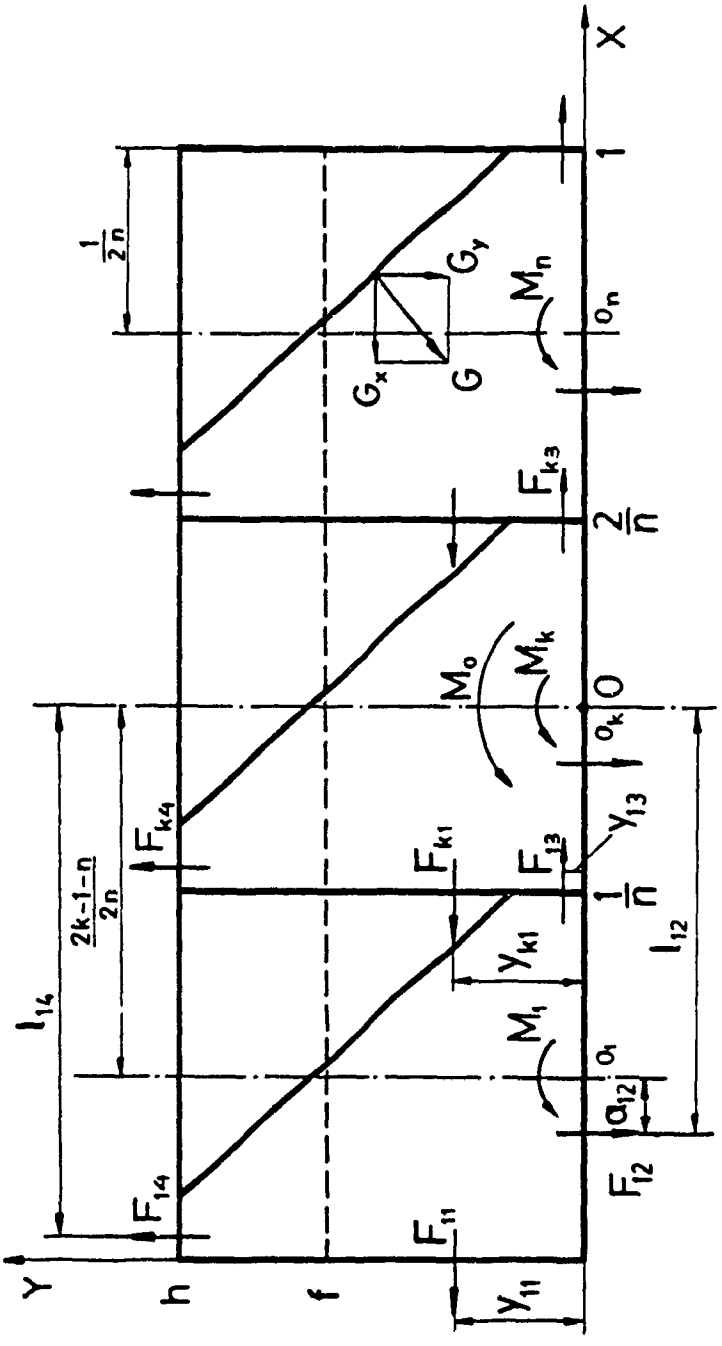

Fig.7.1. Schematics of a compartmented container

Using the condition at the free surface:

$$Y(X_k) - Y(X_{k-1}) = \frac{G_x}{n} \tag{7.3}$$

Maintaining the mass conservation by equating the current cross-sectional area occupied by the liquid to the initial area, and taking into account that the spacing of each compartment from the center of the container is

$$\frac{2k - n - 1}{2n} \tag{7.4}$$

The resulting expressions for the free surface and the configuration conditions are summarized in Table 7.1, where the parameter n in the last column is an integer and must be the nearest superior, for ≥ inequality, or the nearest inferior, for ≤ inequality.

The total horizontal force at steady-state is equal to the algebraic sum of the forces exerted on vertical walls and it must be equal to the force of inertia of the liquid. The total vertical force is equal to the liquid weight. In the non-dimensional form, they may be expressed as

$$F_{Hss} = G_x, \quad \text{and} \quad F_{vss} = G_y = -1 \tag{7.5}$$

for the unit width of the tank and both values are ratios of their dimensional values to the liquid weight. Thus, the separating walls have no influence on the magnitudes of forces in the steady-state, but

they obviously affect the overturning moments, since the moment arms for the forces depend on n. The overturning moment for a compartmented tank, M^c_{ss}, taken around the middle bottom point '0' is computed as the sum of the moments of all forces for each configuration separately. As an example, consider Configuration 2 given in Fig. 7.1. The total moment is found as

$$M^c_{ss} = n\, F_{k1}\, Y_{k1} + F_{k2} \sum_{k=1}^{n} l_{k2} + n\, F_{k3}\, Y_{k3} + F_{k4} \sum_{k=1}^{n} l_{k4} \qquad (7.6)$$

where the nondimensional values are

$$\left.\begin{aligned} F_{k1} &= \frac{h_{k1}\, s_{k1}}{f}\,; \qquad l_{k2} = \frac{2k - n - 1}{n} + \frac{G_x}{12\, n^2 f}\,; \\ l_{k4} &= \frac{2k - n - 1}{2n} + \frac{1}{6n} + \frac{A}{3G_x}\,; \qquad Y_{k1} = \frac{1}{3}(h-A); \\ Y_{k3} &= \frac{h}{2} - \frac{h^2}{12\left(\frac{G_x}{n} + \frac{h}{2} - A\right)} \end{aligned}\right\} \qquad (7.7)$$

and h_{ki} are the depths of the center of gravity of each wetted wall under the free surface, s_{ki} are the wetted wall lengths, the second subscript coming immediately after k, i.e. i=1,2,3,4 refers to the wall of a compartment in the following order: left, bottom, right, top, and A is defined in Table 7.1. After substituting of the expressions (7.7) into (7.6), the equation of the moment becomes

Table 7.1. Free-surface equations and configurations' definition for steady-state response in compartmented containers

Conf.	Free-Surface equations	Conditions from the heignt equa tions	Condition on n
1	For $G_x \gtrless 0$ $Y = G_x X + f - \frac{2k-1}{2n} G_x$	$f - \frac{G_x}{2n} \geq 0$ $f + \frac{G_x}{2n} \leq h$	$n \geq \frac{\lvert G_x \rvert}{2f}$ $n \geq \frac{\lvert G_x \rvert}{2(h-f)}$
2	$Y = G_x X + h - \frac{k-1}{n} G_x - A;\ G_x > 0$ $Y = G_x X + h - \frac{k}{n} G_x - A;\ G_x < 0$ where $A = \sqrt{\frac{2(h-f)\lvert G_x \rvert}{n}}$	$h - A \geq 0$ $\frac{\lvert G_x \rvert}{n} - A \geq 0$	$n \geq \frac{2(h-f)\lvert G_x \rvert}{h^2}$ $n \leq \frac{\lvert G_x \rvert}{2(h-f)}$
3	$Y = G_x X - \frac{k}{n} G_x - B;\ G_x > 0$ $Y = G_x X - \frac{k-1}{2} G_x + B;\ G_x < 0$ where $B = \sqrt{\frac{2f\lvert G_x \rvert}{n}}$	$B - \frac{\lvert G_x \rvert}{n} \leq 0$ $B - h \leq 0$	$n \leq \frac{\lvert G_x \rvert}{2f}$ $n \geq \frac{2f\lvert G_x \rvert}{h^2}$
4	$Y = G_x X + \frac{h}{2} - (\frac{k}{n} - \frac{f}{nh}) G_x;\ G_x > 0$ $Y = G_x X + \frac{h}{2} - (\frac{k-1}{n} + \frac{f}{nh}) G_x;\ G_x < 0$	$\frac{h}{2} - \frac{\lvert G_x \rvert}{2}(1 - \frac{f}{h}) \leq 0$ $\frac{f\lvert G_x \rvert}{nh} - \frac{h}{2} \geq 0$	$n \leq \frac{2f\lvert G_x \rvert}{h^2}$ $n \leq \frac{2(h-f)\lvert G_x \rvert}{h^2}$

$$M_{ss}^{c} = -\frac{n}{6f}(h-A)^3 + \frac{G_x}{12n^2f} + \frac{h^2}{6f}\left(3G_x + nh - 3nA\right) - \frac{1}{6f}\left(\frac{1}{n} - \frac{A}{G_x}\right)^2\left(\frac{G_x}{2} + nA\right) \tag{7.8}$$

This equation, as well as the similar equations for the remaining configurations can be simplified, and in the reduced form, they are given in Table 7.2 together with the expressions for the horizontal and vertical forces and their moment arms. The values of A and B are the same as in Table 7.1. The overturning moment for a compartmented tank, M_{ss}^{c}, is a function of the four nondimensional parameters: h, f, G_x, and n, in general. However, for Configuration 1 the height of the tank has no influence on M_{ss}^{c}.

The behaviour of the moment with variation of number of compartments and the level of acceleration for fixed values of h and f is illustrated in Figs. 7.2 and 7.3 for two different geometries of the tank and for the same filling of 60% with respect to the container height. In particular, Fig. 7.2 can be referred to a long tank (13.5 m x 2 m) and Fig. 7.3 to a short one (2.56 m x 1.83 m). It can be seen that the magnitudes of M_{ss}^{c} rapidly drop from those of uncompartmented tanks and tend asymptotically to $fG_x/2$. The reducing effect due to separating walls is significantly stronger for long tanks. This effect is even better illustrated in Figs. 7.4 - 7.8, where the ratios of the moments of the uncompartmented tank to those of the compartmented one are plotted against G_x, or f, or h. The ratios M_{ss}/M_{ss}^{c} for a long tank are given in Fig.7.4, from where one can read that four separating walls, n=5, can reduce the moment by 12 times for sufficiently small

Table 7.2. Overturning moments and forces for steady-state response in compartmented containers

Conf.	Moments, Forces, and Forces Arms
1	$M^c_{ss} = \frac{G_x}{2}\left(f + \frac{G_x^2}{12\,n^2 f} - \frac{1}{6\,n^2 f}\right)$ $F_H = G_x,\ Y_H = \frac{f}{2} + \frac{G_x^2}{24\,n^2 f}$ $F_V = -1,\ E_V = \frac{G_x}{12\,n^2 f}$
2	$M^c_{ss} = G_x \frac{h-f}{f}\left[-h + \frac{1}{2\,n\lvert G_x\rvert} + \frac{h^2}{2(h-f)} - \frac{A}{3}\left(\frac{1}{G_x^2} - 1\right)\right]$ $F_H = G_x,\ Y_H = \frac{h-f}{f}\left[-h - \frac{h^2}{2(h-f)} + \frac{A}{3}\right]$ $F_V = -1,\ E_V = G_x \frac{h-f}{f}\left(\frac{1}{2n\lvert G_x\rvert} - \frac{A}{3G_x^2}\right)$
3	$M^c_{ss} = G_x\left[\frac{1}{2n\lvert G_x\rvert} - \frac{B}{3}\left(\frac{1}{G_x^2} - 1\right)\right]$ $F_H = G_x,\quad Y_H = \frac{B}{3}$ $F_V = -1,\quad E_V = G_x\left(\frac{1}{2n\lvert G_x\rvert} - \frac{B}{3G_x^2}\right)$
4	$M^c_{ss} = G_x\left[\frac{1}{2n\lvert G_x\rvert} + \frac{h}{2} - \frac{f}{2nn\lvert G_x\rvert} - \frac{nh^3}{12f\lvert G_x\rvert} - \frac{nh^3}{24f\lvert G_x\rvert^3}\right]$ $F_H = G_x,\ Y_H = G_x\left(\frac{h}{2\lvert G_x\rvert} - \frac{nh^3}{12fG_x^2}\right)$ $F_V = -1,\ E_V = G_x\left(\frac{h-f}{2nh\lvert G_x\rvert} - \frac{nh^3}{24f\lvert G_x\rvert^3}\right)$

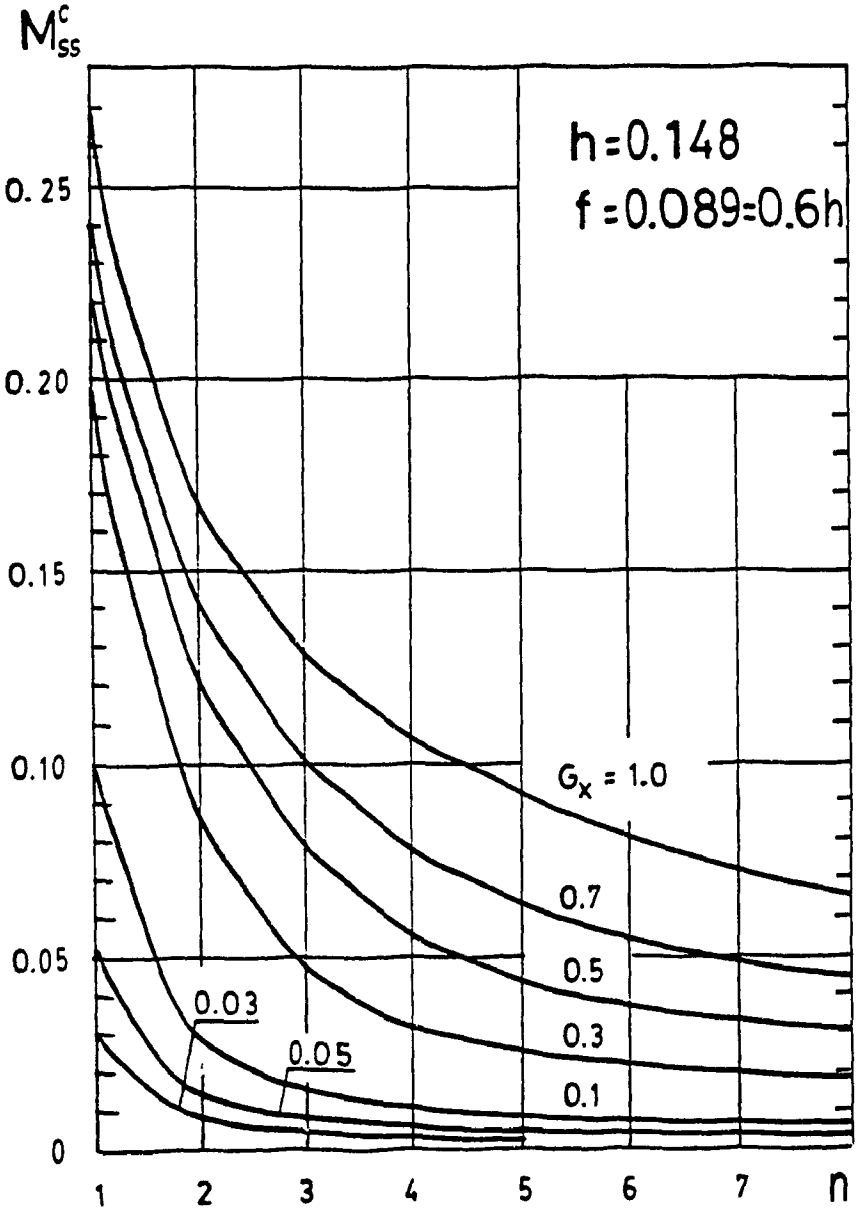

Fig.7.2. Steady-state overturning moment as function of the number of compartments for a long rectangular container

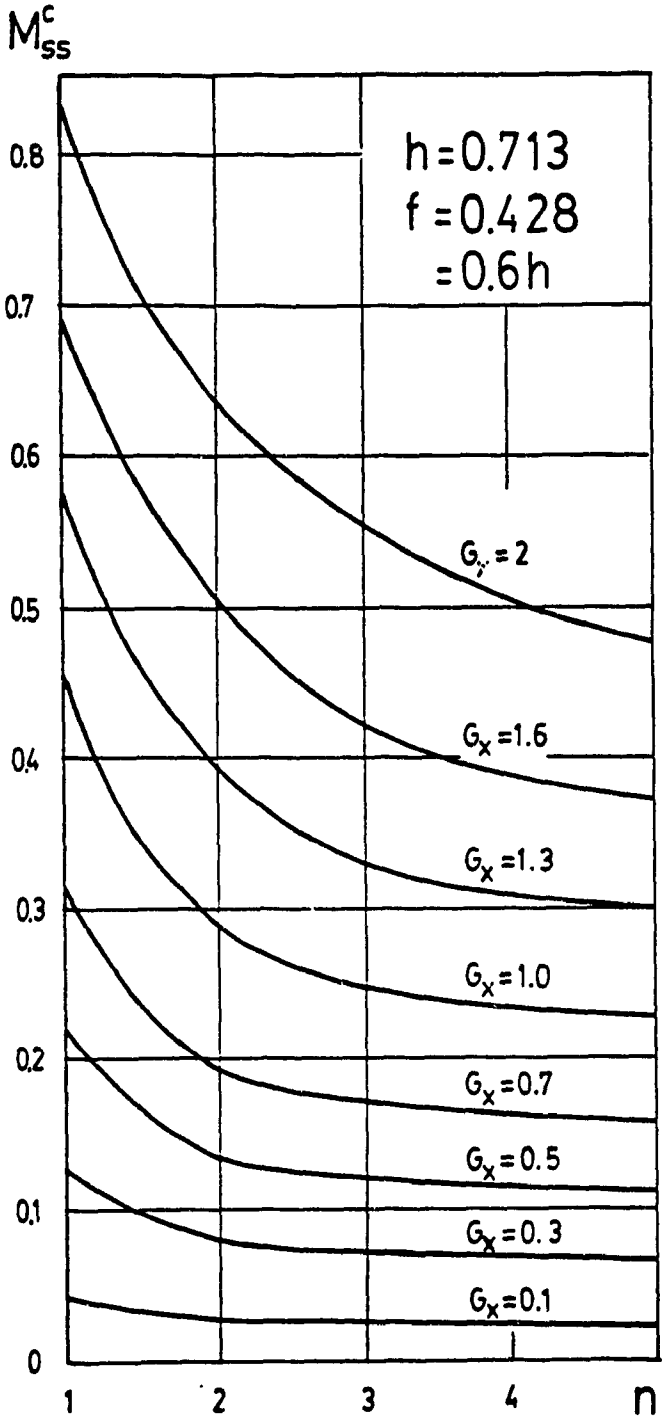

Fig.7.3. Steady-state overturning moment as function of the number of compartments for a short in length container

value of G_x, however this effect decreases with increasing of G_x. The dotted lines in Fig.7.4 define the regions of configurations. The similar plot for a short tank, h = 0.713 in Fig.7.5, displays the smaller influence of partitions. Thus, for the same n = 5, the maximum gain in the moment reduction is slightly above 200%. Figs. 7.6 and 7.7 show the reducing effect of the separating walls as functions of the fill level for two tank geometries. The functions have strongly pronounced maxima occurring at some values of f which decrease with increasing of number of compartments. The moment reducing effect also depends on the geometric parameter h, as shown in Fig.7.8. It can be seen that the effectiveness of separating walls is significantly greater for long tanks, besides, for very long tanks it decreases again. For short tanks, h = 0.6 - 0.8, the reduction is still essential; for example for h = 0.7, one separating wall reduces the moment by 160% for G_x = 0.3 and f = 0.6 h. Relating to the lateral stability of a tanker, the 160% reduction is considerable. Thus, one longitudinal separating wall is quite efficient in reducing of the overturning moment. However, further increasing of the number of walls is not so gainful. For example, for 2 ,3 ,4, and infinite number of separating walls, the reducing effect is 179%, 187%, 191%, and 199%, respectively.

These results are also applicable for baffled containers provided that the baffle orifices are closed during transportation. If this is not the case, then the baffled tank behaves as an uncompartmented tank for all fill levels exceeding (h-d)/2 value, where d is the nondimensional diameter of the baffle orifice. For fill levels less than this value the solution for a baffled tank is quite different.

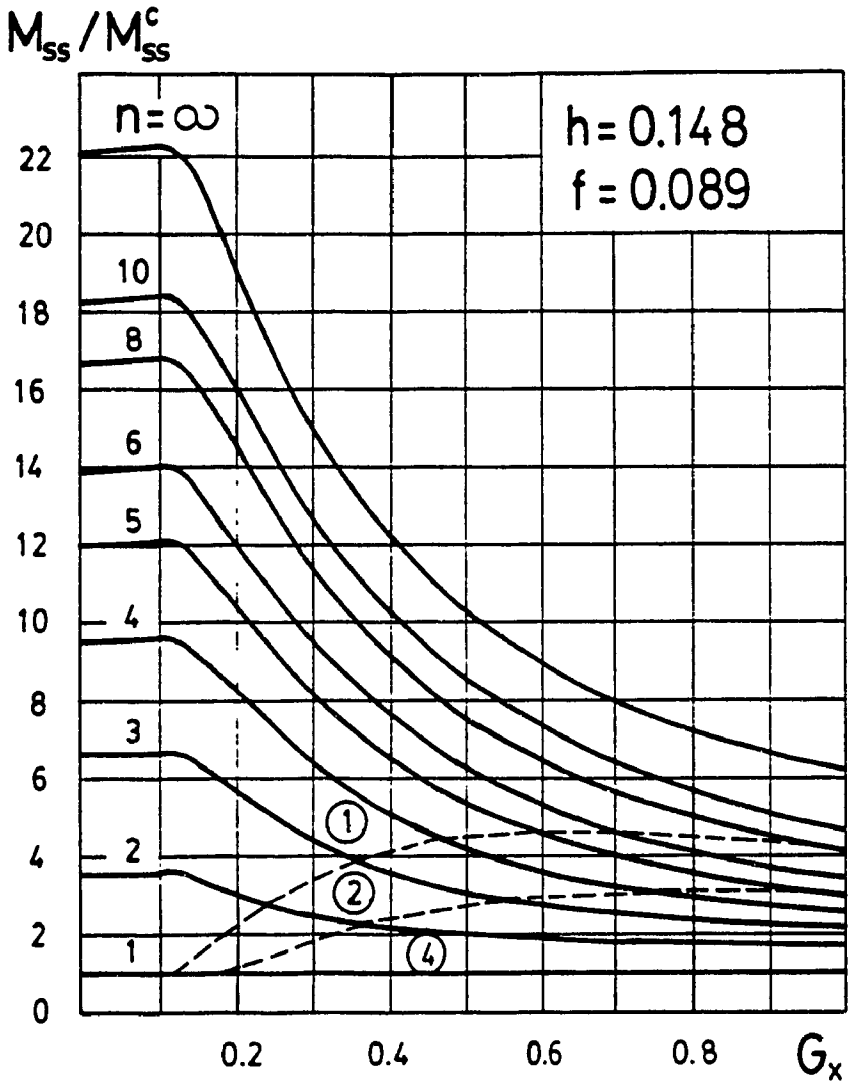

Fig.7.4. Moment reduction factor as function of input acceleration for a long container

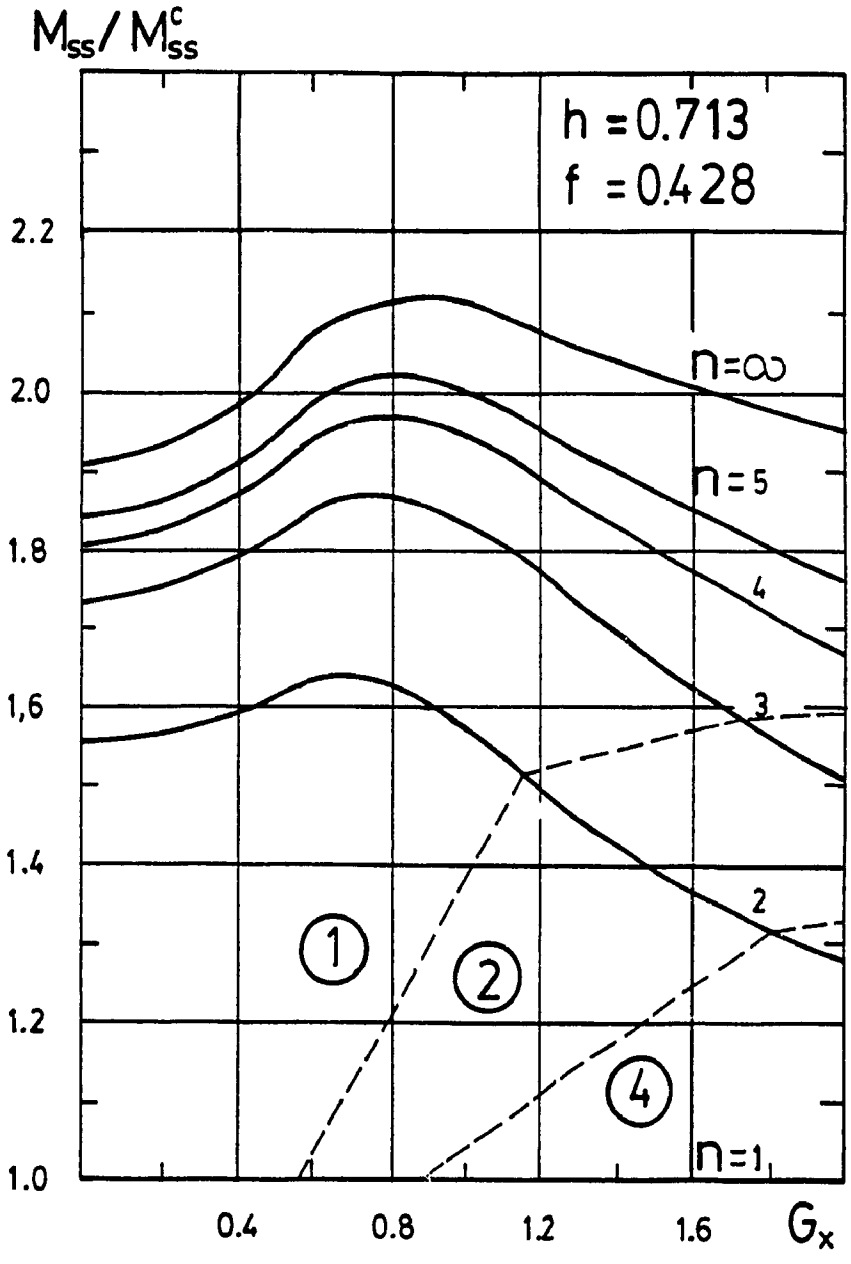

Fig.7.5. Moment reduction factor as function of input acceleration for a short in length container

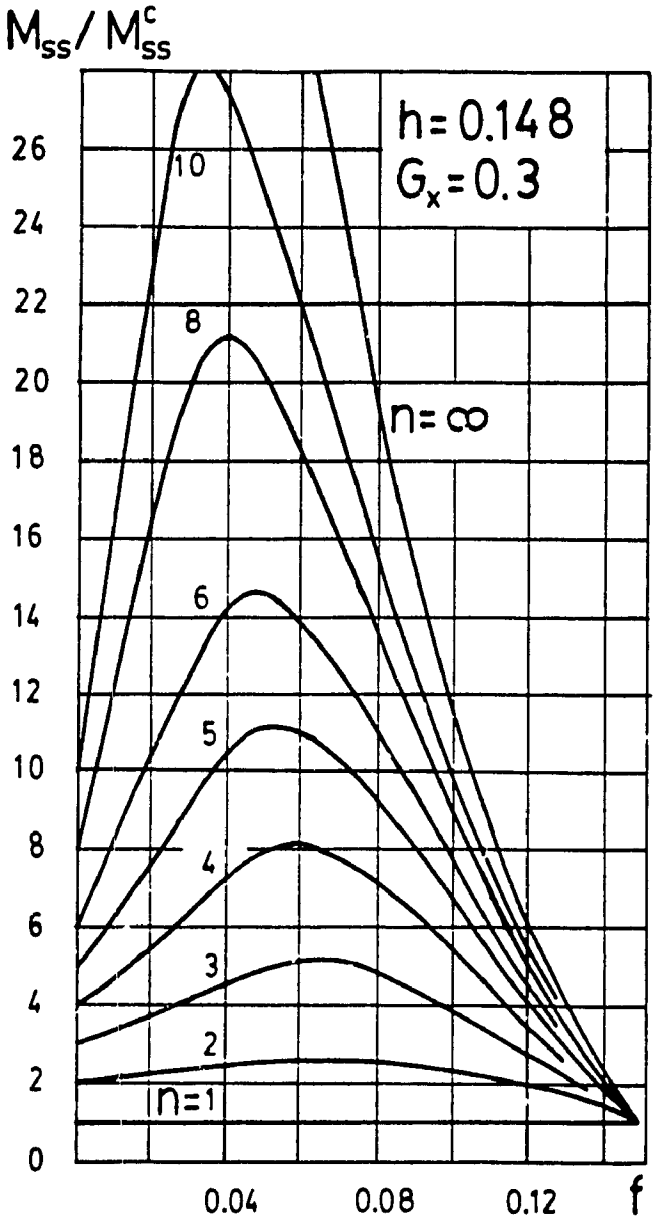

Fig.7.6. Moment reduction factor as function of fill level for a long container

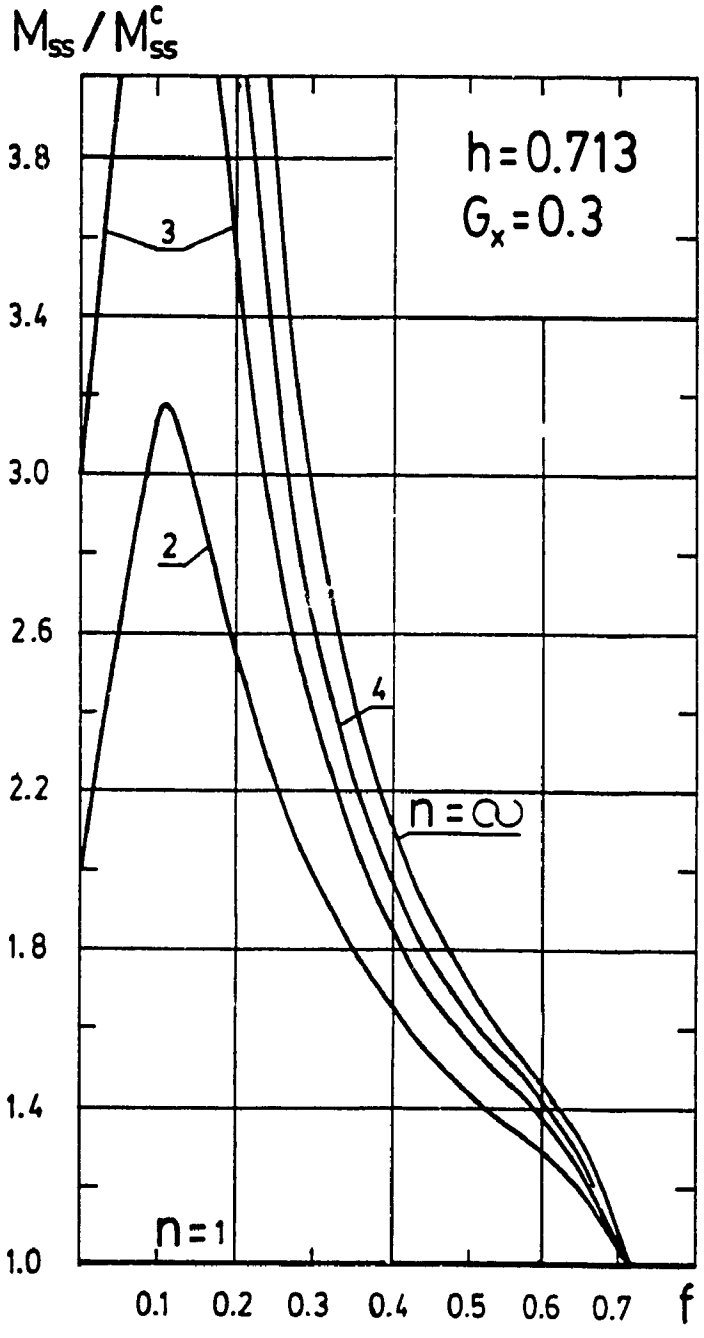

Fig.7.7. Moment reduction factor as function of fill level for a short in length container

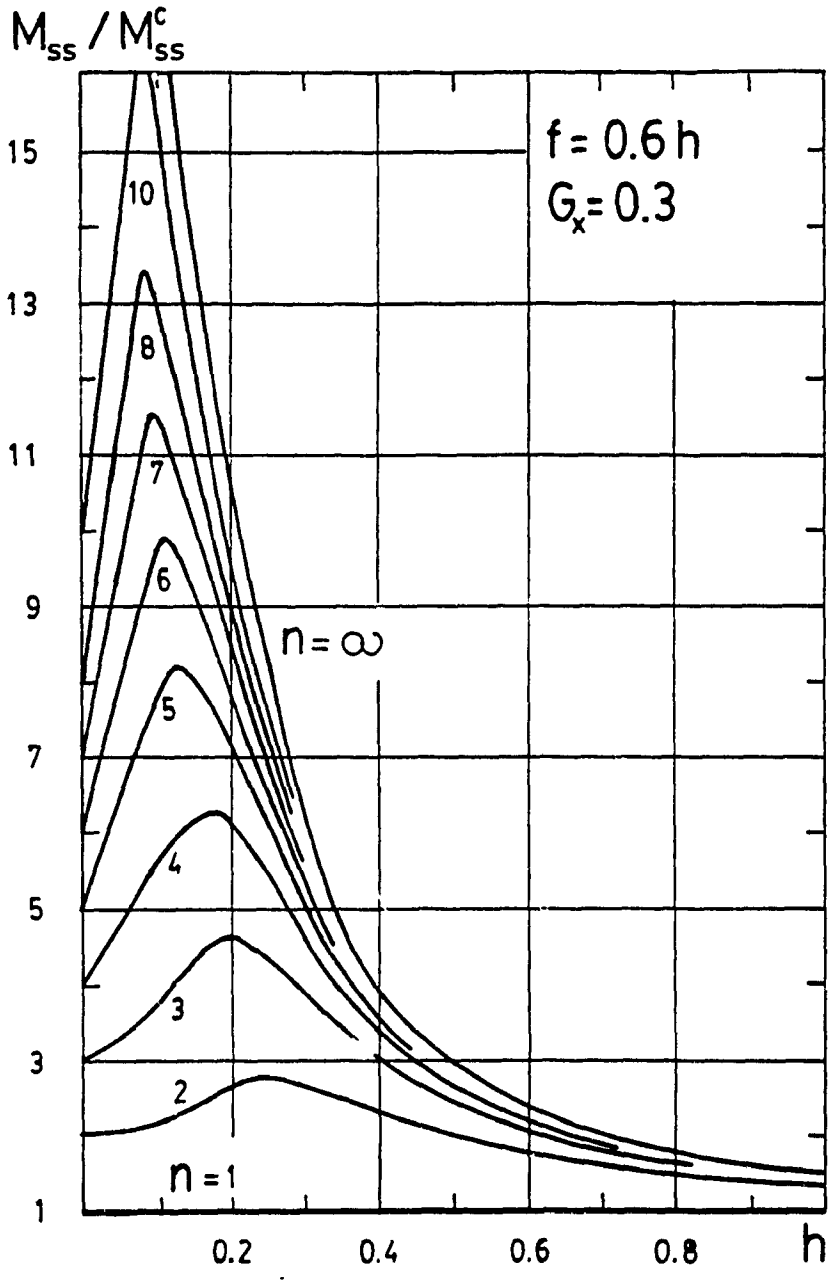

Fig.7.8. Moment reduction factor as function of the container height

7.3 Transient Solutions for Compartmented Containers

The details of the computational procedure for the transient response are described in Chapter 3, however, in this section some computational procedures relevant to the case of baffles are presented. A 3-D array for the velocities and pressures and a 2-D array for liquid heights are used in order to avoid a confusion between the boundary and working values of the flow parameters. Thus, the horizontal velocity array, for example, is expressed in the code as U(k,i,j), where k is referred to the k-th compartment and i and j to the number of the cell in horizontal and vertical directions. If however, the free surface passes through the baffle orifice, then the boundary values are defined as for a continuous flow.

The transient solution for a compartmented tank can be obtained from the solution for a rectangular tank, given in Chapter 5. The vertical and horizontal forces are equal to the sum of the corresponding components of the constituting sections of the container. The total moment is also equal to the sum of the moments of each compartment. The component moments must be translated to a new point, which is the middle bottom point of the compartmented container, point 'O' in Fig. 7.1. The non-dimensionalizing must be done with respect to the value $\rho g L_o^2 h_{in}$, where L_o is the total container length, in contrast to the $\rho g L_k^2 h_{in}$, where L_k is the length of the k-th compartment. Assuming that the compartments are equal in size and the fill level is the same for each section of the tank, the following expressions for a compartmented tank can be obtained:

$$F_H^c = n\, F_{Hk}\,, \qquad F_V^c = n\, F_{Vk}\,, \qquad M^c = \frac{M_k}{n} \tag{7.9}$$

The solutions for a long tank, h = 0.15, and for a short tank, h = 0.7, are given in Table 7.3 for G_x = 0.3 and the fill level corresponding to 70% with respect to the container height. The corresponding plots are shown in Fig.7.9 (long tank) and Fig.7.10 (short tank) as functions of number of compartments. It can be seen that increasing of number of separating walls leads to a strong decrease of the overturning moment both in statics and dynamics, but the sloshing becomes more intense, dotted line, Fig. 7.9 a). An increase in number of separating walls changes the geometry of the compartments from a rectangular cross-section to almost a square cross-section, and a further increase of n leads to a narrow cross-section. Also, it has been shown in Chapter 5 that the most strong sloshing occurs in a square container. Therefore, the further increase in n, producing the narrow compartment, forces the dynamic coefficient for the moment to decrease. The dynamic coefficient of the horizontal force monotonically drops from its maximum value corresponding to an uncompartmented tank (n=1) and, in principle, tends to 1. The damped natural frequency, Fig. 7.9 b), is below of that from the linear theory for number of separating walls equal to 3 and more, however, for n=2 or 1 it is somehow higher than the linear one because, for those compartment shapes, the vibrations occur in a mode that is not accounted by the linear theory.

The plots of Fig. 7.10 a) and b) give the similar quantities for a short container, h = 0.7. This case can be interpreted as the lateral sloshing in a container filled with longitudinal separating walls. The dynamic coefficient of the moment decreases with increase of n and tends

Table 7.3. Influence of number of compartments on numerical solution for h=0.15 and 0.7, G_x=0.3, f=0.7h

n	Compartmented length (m)	M^c_{ss}	Peak Value F^c_h	Peak Value M^c	$\frac{F^c_h}{F^c_{Hss}}$	$\frac{M^c}{M^c_{ss}}$	Ω $(\frac{rad}{s})$	K	K_{th}	Ω_{th}
Long tank, h = 0.15										
1	13.500	0.1550	0.4305	0.1930	1.435	1.2452	--	--	0.979	0.8532
2	6.750	0.0696	0.4266	0.0879	1.422	1.2613	1.7284	1.402	1.319	1.6261
3	4.500	0.0432	0.4227	0.0552	1.409	1.2784	2.2557	1.494	1.510	2.2799
4	3.375	0.0313	0.4158	0.0410	1.386	1.3083	2.6988	1.548	1.615	2.8157
5	2.700	0.0257	0.4053	0.0339	1.351	1.3188	3.0798	1.580	1.672	3.2591
6	2.250	0.0227	0.3960	0.0299	1.320	1.3206	3.4100	1.597	1.702	3.6342
Short tank, h = 0.7										
1	2.565	0.1251	0.4089	0.1650	1.3630	1.3189	3.1442	1.572	1.657	3.3138
2	1.283	0.0864	0.3682	0.1132	1.2273	1.3102	4.5461	1.607	1.731	4.8957
3	0.855	0.0792	0.3505	0.0995	1.1683	1.2563	5.6049	1.618	1.735	6.0098
4	0.641	0.0768	0.3431	0.0933	1.1437	1.2150	6.4775	1.620	1.735	6.9409

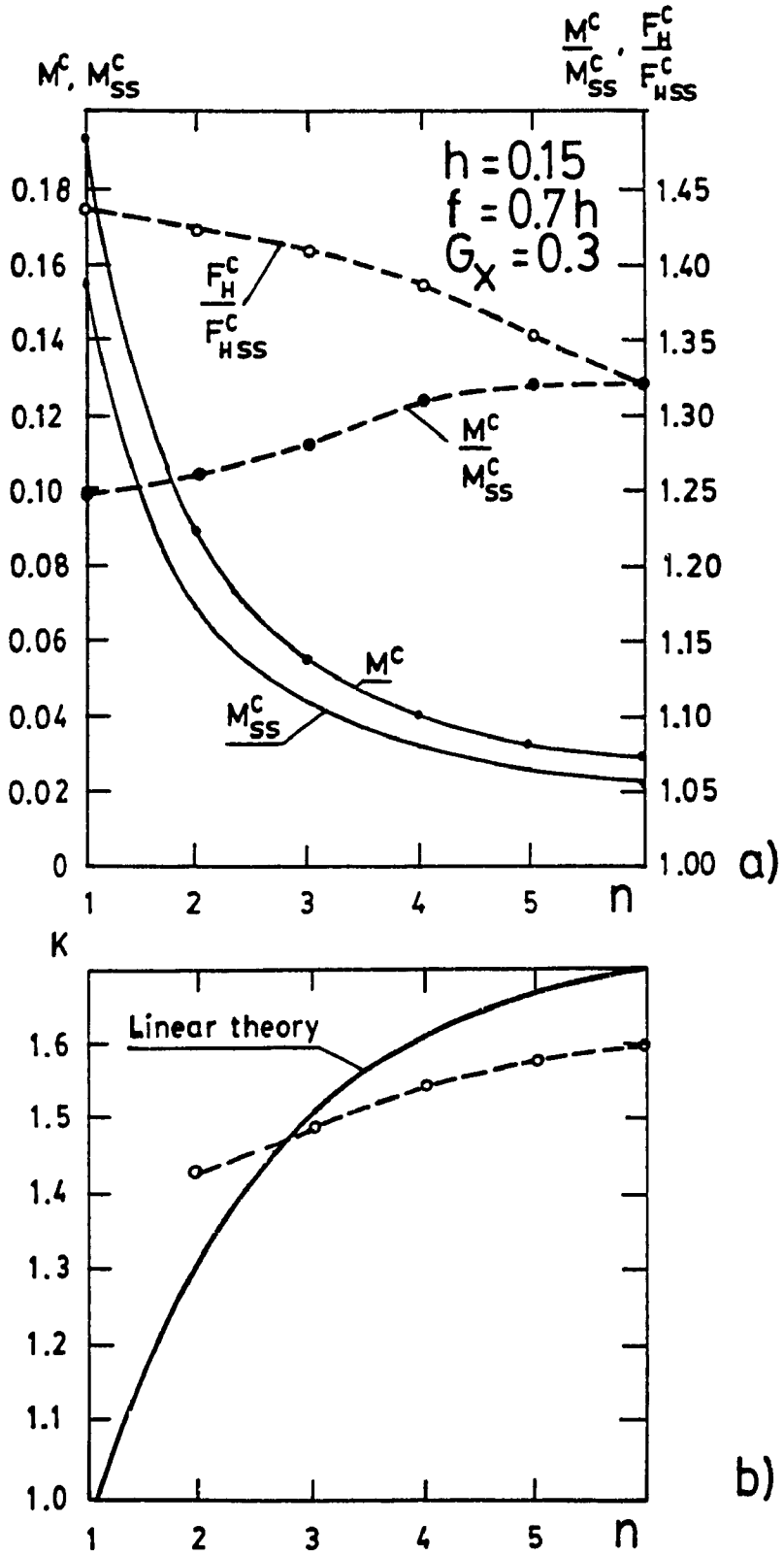

Fig.7.9. Transient solution for a long compartmented container. Moment, horizontal force, and their dynamic coefficients, a), and natural damped frequency, b)

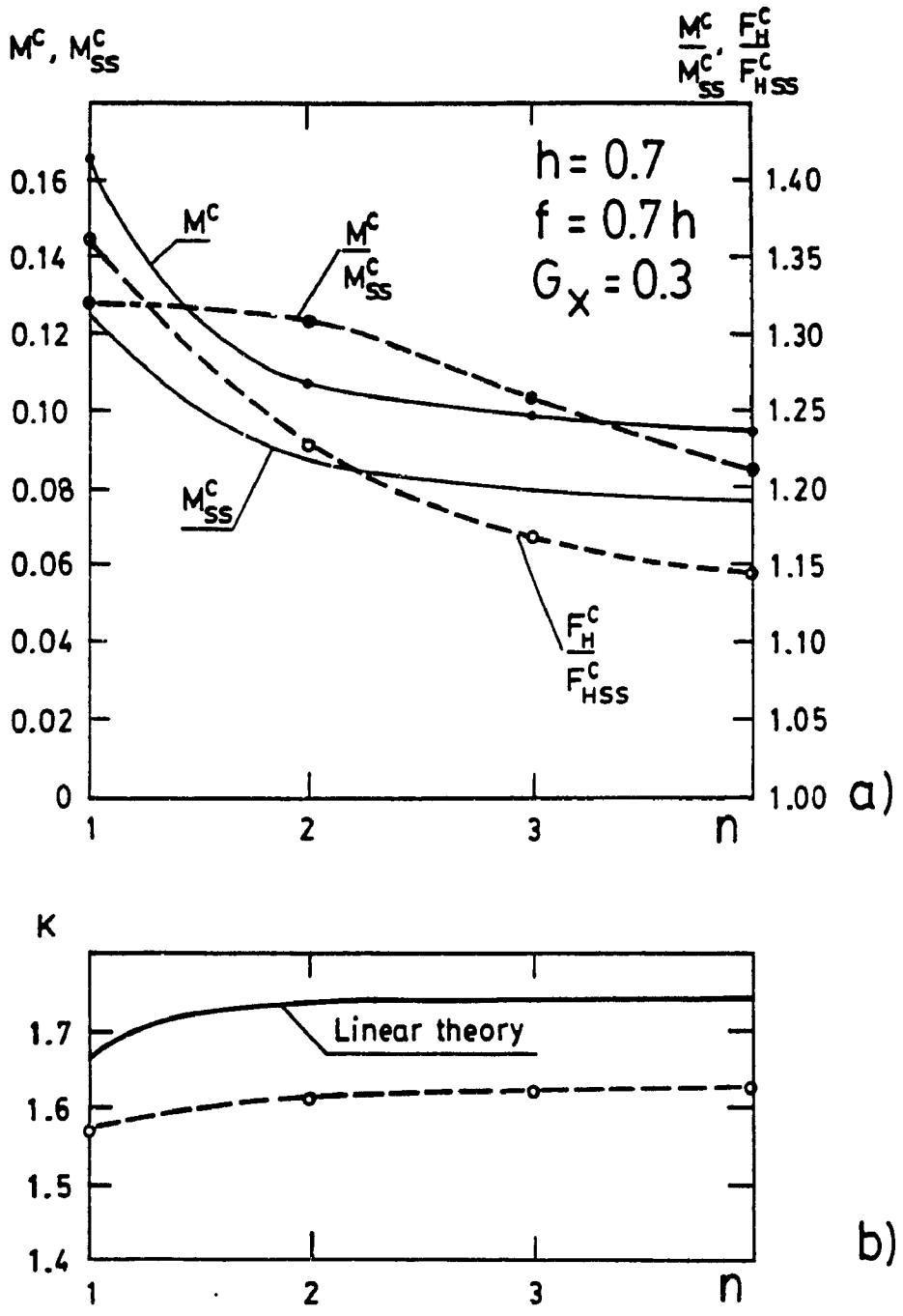

Fig.7.10. Transient solution for a short in length compartmented container. Moments and dynamic coefficients of the moment and horizontal force, a), and natural damped frequency, b)

to reach unity as $n \to \infty$, and so does the coefficient of the lateral force. The damped frequency is always below of the undamped one and, as an average, is about 6% less than the latter.

The circular frequency of liquid vibrations is a function of the container length alone, if the height, input acceleration, and fill level are fixed. In Fig. 7.11, an example of such a functional dependence is shown. Since in the calculations, the heights of the short (1.8 m) and of the long (2.0 m) containers were not equal, a small discrepancy between frequencies appears and can be seen in the overlapping region of the two considered cases. Also, it can be seen that there is the tendency for intersection of the damped and und· · (linear theory) frequencies at the length of compartment approachi: In a compartment of this length, the character of vibration changes because Configuration 1, corresponding to smaller lengths, is replaced by Configuration 2 and the latter is not accounted by the linear theory.

7.4 Transient Solutions for Baffled Containers

The liquid motion in a baffled container significantly differs from that of compartmented one because of the liquid flow from one section to another. This interflowing affects all parameters of the sloshing including the forces, moments, and frequencies of vibrations which become coupled. In the present study, an attempt is made to investigate the role of the location of the baffle orifice, the size of the orifice, and the number of baffles.

The location of the orifice has a negligible effect on the main sloshing parameters, unless the free surface does not pass through the orifice. If, however, it happens, then the interflowing of the liquid

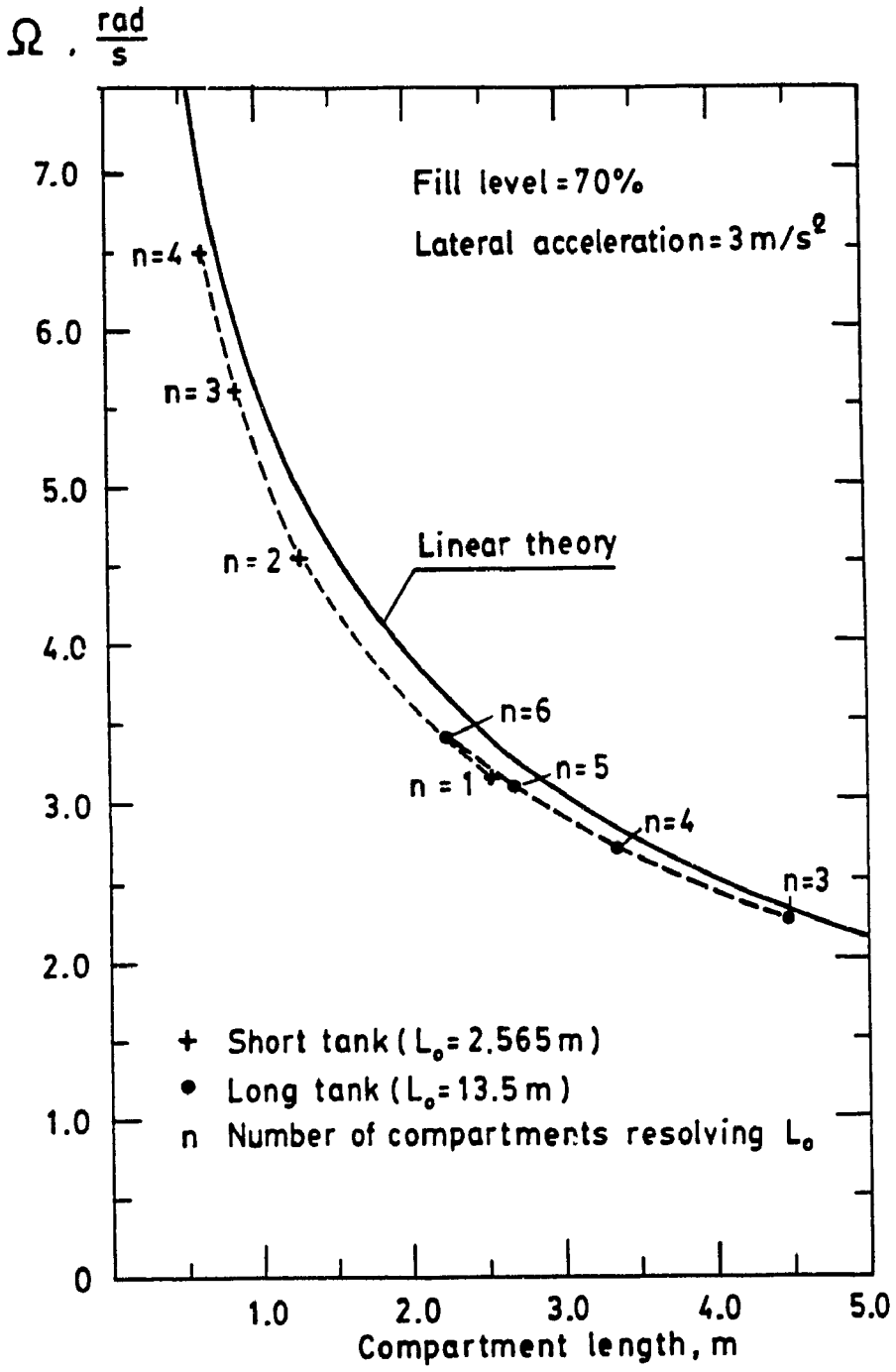

Fig.7.11. Circular frequency of sloshing as function of compartmented length

can be significantly delayed. The two cases with middle and near-bottom location of the orifice, with the area of 5% from the cross-sectional area of the container for both cases, have been considered for a container with one baffle initially filled with a liquid at 70% with respect to the container height. Thus, the orifice situated in the middle of the baffle was initially completely covered by the free surface. During fluid oscillation, this orifice was partly opened and partly closed depending on the phase of oscillation. The difference between those two cases can be seen from Fig. 7.12 a). For the orifice located near-bottom the liquid height at the right wall of the second compartment reaches the top wall (h = 0.7) at the fifth cycle while for the middle orifice it happens at the seventh cycle. After this time, the continuously fed right compartment accumulates such an amount of liquid that it leads to the change of the vibration frequency that becomes higher while the amplitude decreases. The vibrations of the vertical and horizontal forces, as well as the moment, are shown in Fig. 7.12 b). The vertical and horizontal forces, do not depend on the interflowing of the liquid from one compartment to another and they vibrate around the corresponding steady-state values. The moment, in contrast, does depend upon the amounts of liquid in the compartments, and its peak value increases with time until the interflowing is stabilized, that happens approximately at the fifth cycle, in accordance with the liquid height vibrations. It also can be noted, that the vertical force reflects the variation of the pressure field in the container, and the pressure recasts as twice as fast as the velocities and heights do.

The increase of number of baffles affects the flow in such a way

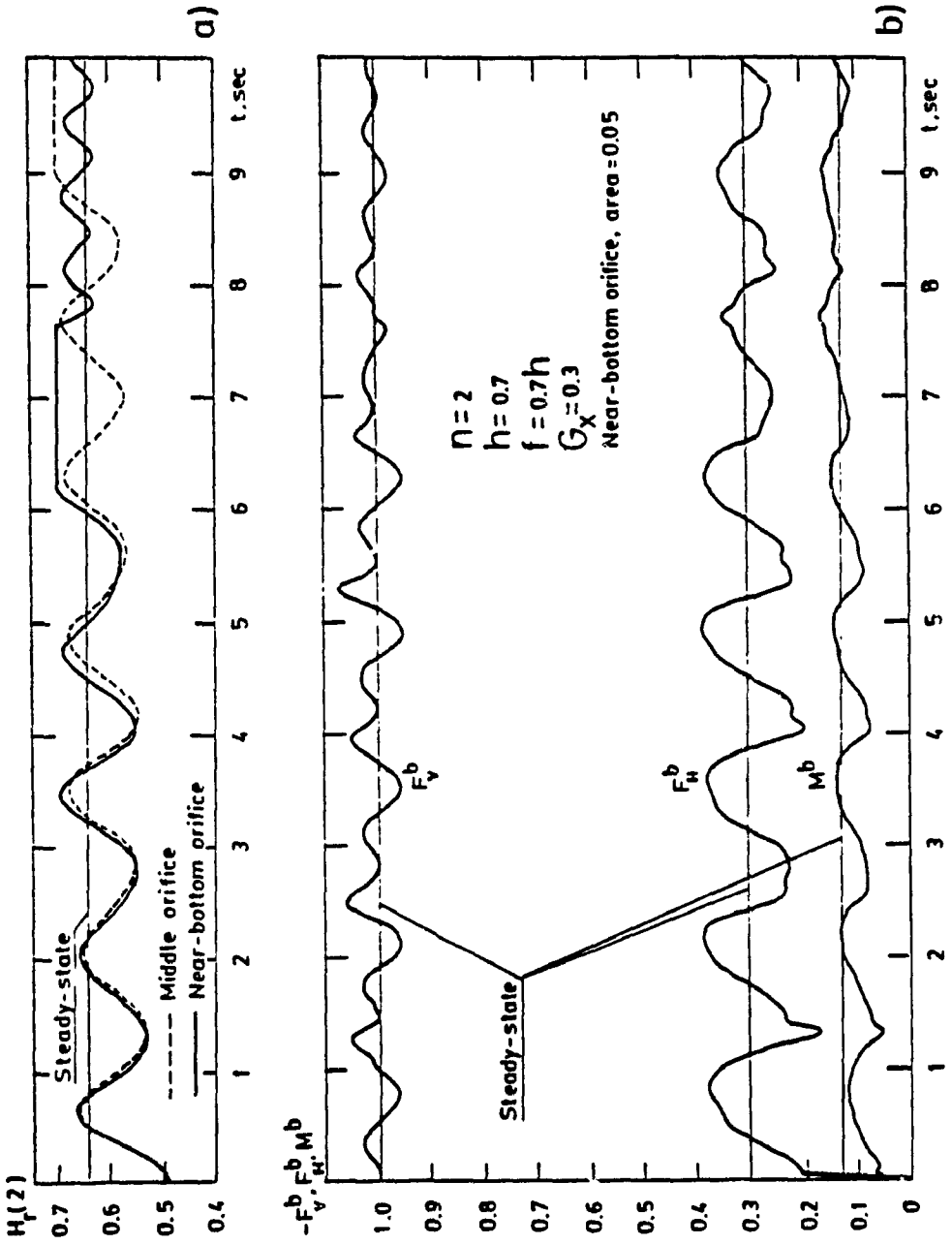

Fig.7.12. Liquid heights time histories for different baffle orifice locations, a), and time histories of sloshing parameters in a short in length baffled container,b)

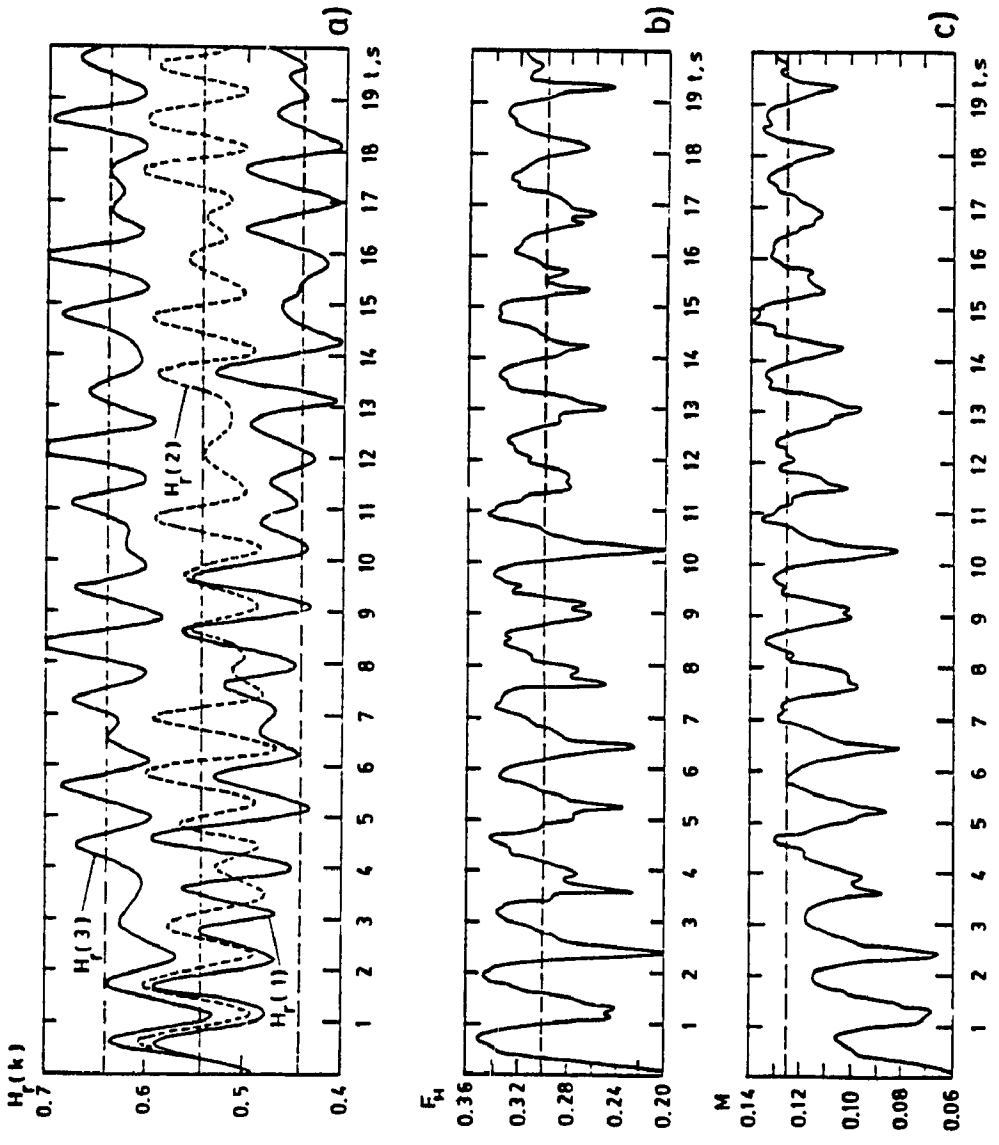

Fig.7.13. Time histories of sloshing parameters oscillations in a container with two baffles, $h=0.7$, $f=0.7h$, $G_x=0.3$, and $n=3$. Liquid heights near the right walls of compartments, a), horizontal force ,b), and overturning moment, c)

that the interflowing of the liquid is delayed. Thus, for two baffles, the time required for the mean value of the moment to reach the steady-state value is almost twice larger compared with one baffle. In Fig. 7.13 c), the stabilizing of the moment occurs at 11th cycle. However, the liquid heights achieve this point at different times, see Fig.7.13 a). In the last, 3rd, compartment, fed from the 2nd and 1st compartments, the mean height reaches its steady-state value at 6th cycle, while in the 1st compartment it takes 11 cycles. The intermediate compartment loses some amount of liquid during the first 8-9 cycles and later it gets it back. This shows that the process of liquid flowing happens with different rate for different compartments and that there is some low frequency vibration of interflowing. The horizontal force oscillations are very similar to those of the moment, Fig.13 b), with one difference: they occur around the steady-state all the time.

The size of the baffle orifice was varied from 5% to 20% of the container cross-sectional area. It has been found that even the smallest orifice has a significant effect on the peak value of the moment, Fig.7.14 a). The shaded area gives the limits for the peak moments, where the lower line corresponds to the first cycle of vibration and the upper line to that cycle when the interflowing is practically ceased. The baffle area of 5% increases the peak value of the moment by 29% compared to a corresponding compartmented tank, and further increase in the orifice area introduces very little change to the moment. The horizontal force is practically independent of the orifice size variation. The dynamic coefficients of the moment and force are shown in Fig.7.14 b). It can be seen that a baffle in a tank

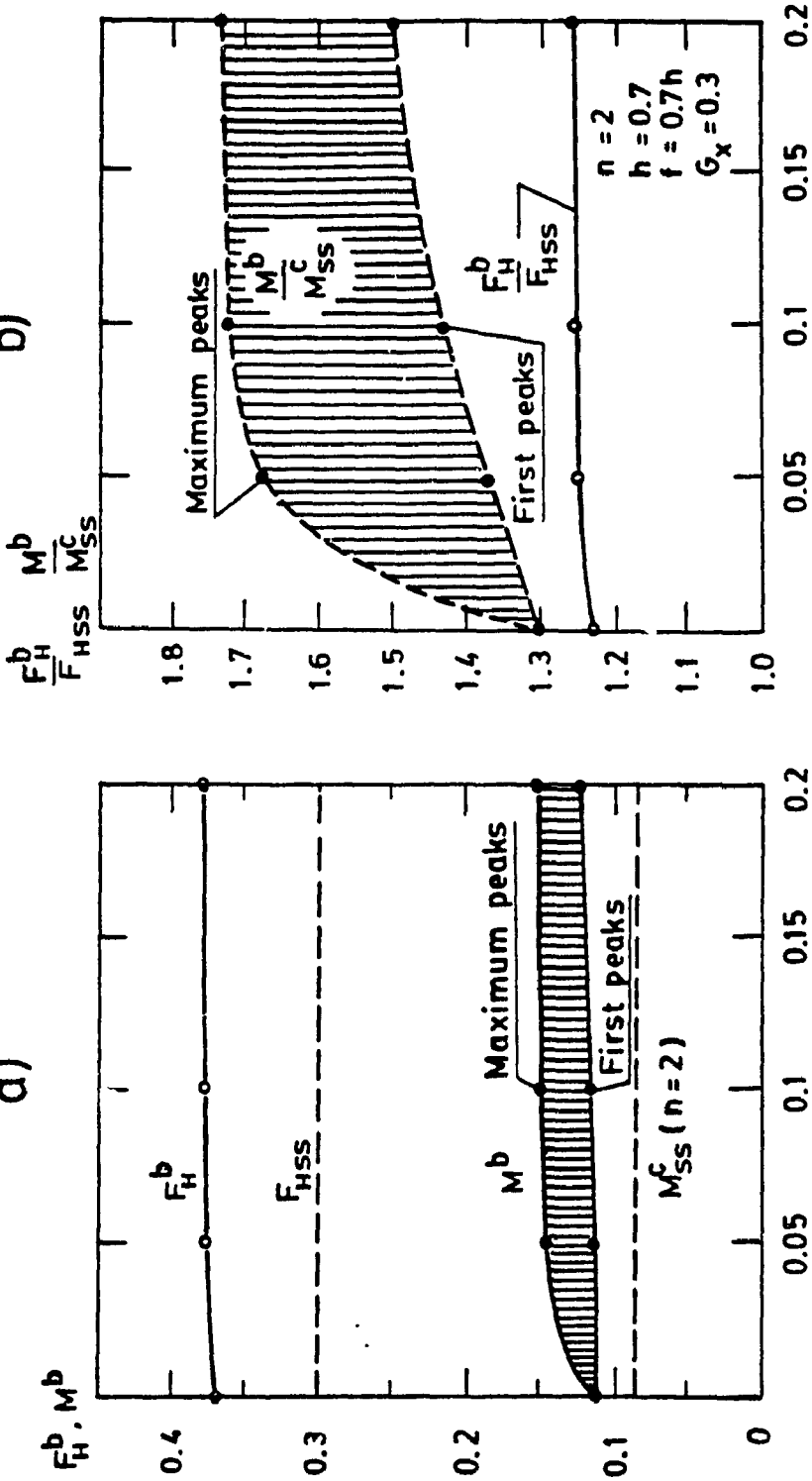

Fig.7.14. Influence of the baffle's orifice size on horizontal force and moment, a), and on their dynamic coefficients, b)

can increase the dynamic moment by 167%, 172%, and 173% with respect to the static moment for the area of the orifice 5, 10, and 20%, respectively.

The number of baffles has a positive effect in reducing of the moment, compared with a container without any baffle. However, the gain is smaller when it is compared with the corresponding compartmented tank. Increasing of number of baffles diminishes the peak values of the moment, Fig.7.15 a). The horizontal force also decreases with increase of number of baffles, approximately by 10, 14, and 17% for one, two, or three baffles, respectively. The relative magnitudes of the force and moment with respect to the corresponding ones of the compartmented tank are shown in Fig.7.15 b).

The comparison of the horizontal forces, F_H, and moments, M, for uncompartmented, compartmented, and baffled tanks is given in Fig. 7.16, where n is the number of vertical sections and corresponds to (n-1) separating walls or baffles. It can be seen that baffles give a smaller reduction in force comparing with a compartmented tank, and this reduction tends to increase with increase of number of separating walls. After $n > 4$ the peak values of the forces are practically identical, Fig.7.16 a). The difference in moments is, however, more significant. The shaded area, Fig.7.16 b), shows the maximum and the first peak values of the moment. The band limiting the peak values of the moment becomes more narrow with increasing of n and asymptotically tends to the line of a compartmented tank. This indicates that a large number of baffles has such a strong damping that orifices have no longer their negative effect and the entire flow behaves like in a compartmented tank.

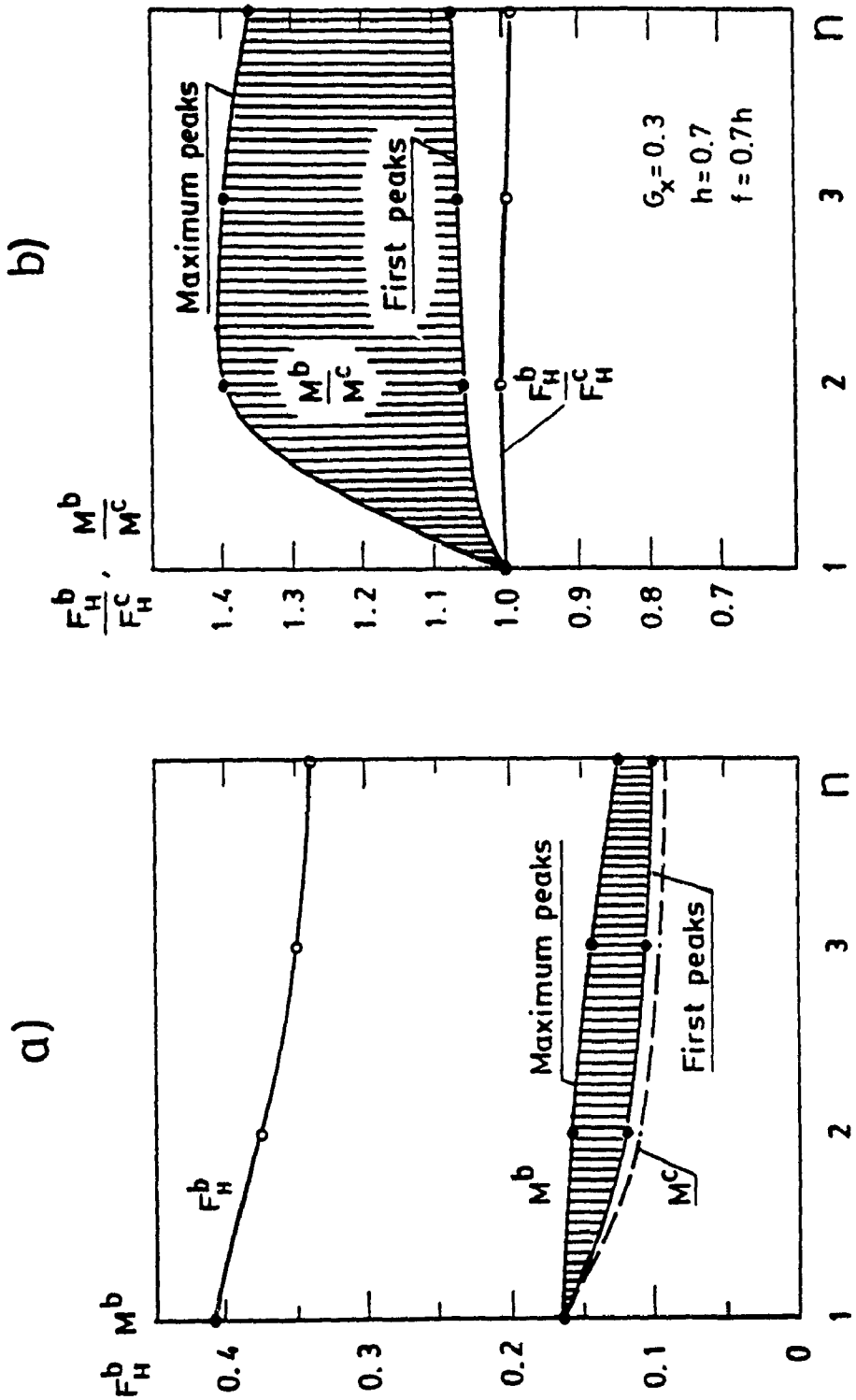

Fig.7.15. Influence of the number of baffles (n-1) on the horizontal force and moment, a), and on their dynamic coefficients, b)

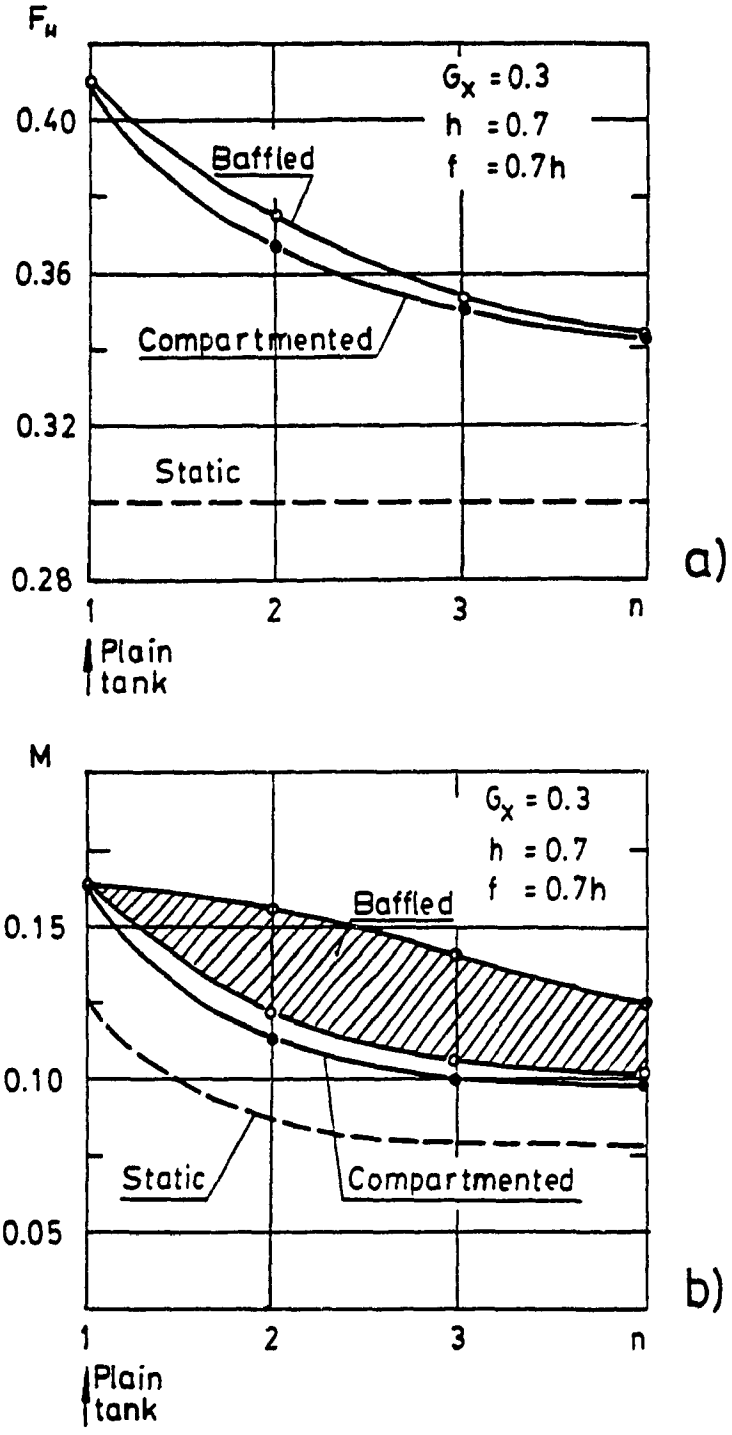

Fig.7.16. Comparison of dynamic horizontal forces, a), and moments, b), in plain, compartmented, and baffled containers

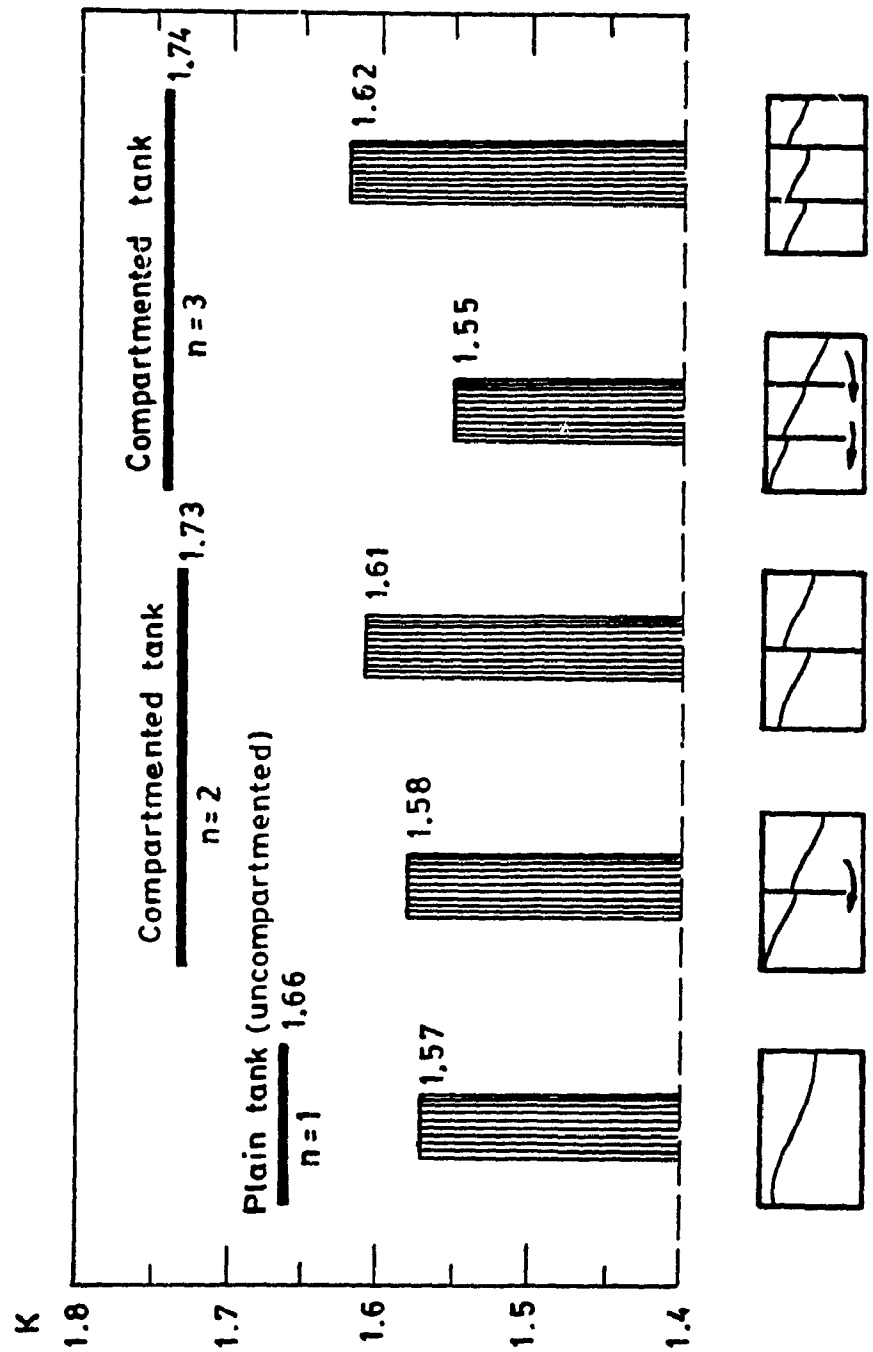

Fig.7.17. Normalized sloshing frequencies diagram for plain, compartmented, and baffled containers with 70% fill level and G_x=0.3

The normalized damped natural frequencies are shown in Fig.7.17, where the upper lines show the undamped natural frequencies resulting from the linear theory and the columns represent the damped frequencies. In compartmented tanks, the frequencies increase with refining of the tank by separating walls. In baffled tanks, the trend is rather inverse: frequencies decrease with increasing of the number of baffles. This is due to the coupling between the baffled compartments and the damping effect of the baffles.

7.5 Summary

In this chapter, the analytical steady-state solutions for compartmented road containers and the transient numerical solutions both for compartmented and baffled containers are presented. The quantitative analysis of the liquid sloshing, provided in this investigation, includes the influence of the main parameters of the liquid container, i.e. number of compartments both isolated and coupled by baffles with orifices, fill level, level of input acceleration, and shape of the rectangular container. The influence of the location, size, and number of baffled orifices has also been included in this study.

It has been found a sufficiently close agreement between the linear theory and the present method results only for such a combination of input parameters for which there is no interaction between the liquid free surface and the top or bottom walls of the container. In such cases, the damped natural frequencies, obtained by numerical integration, are 5 to 7% below of the frequencies resulting from the linear theory. In practice, however, those cases are not often feasible, since the range of most severe loading occurs when the fill

level (between 70 and 90%) and the input acceleration (between 0.3 and 0.5 g's) produce the sloshing with interaction with the top wall. In these cases, the linear theory does not predict the slosh loading parameters, but the present approach does. The study reveals that in these cases the frequency of sloshing becomes higher than it is predicted by the linear theory because of the change in the characteristic of vibration.

The compartment has significant influence in reducing of sloshing amplitudes, while that of the baffle is somewhat less because of the coupling between compartments. The magnitude of the overturning moment decreases by 30% for a tank with one full separating wall comparing with the similar case of one baffle.

The location of the orifice in the baffle is found to be not significant if the free surface does not intersect the orifice area. But if it does so, then the process of interflowing of the liquid may be significantly delayed, and this can happen if the baffled compartments are long enough and the fill level allows the orifices to be partly immersed. In such cases, the baffles can be as beneficial as the compartmented tanks are but only for short duration.

The size of the baffle orifice has a significant influence on the magnitude of sloshing parameters, even if it is sufficiently small, i.e. 5% or less of the cross-sectional area. Practically, the orifices are from 16 to 20 inches in diameter and this constitutes from 4 to 6% of the total cross-section of area of the tank. Further increase in the orifice size has a very little additional influence.

The methodology used in this investigation allows to significantly enlarge the fields of study in the sense of the ranges of input

parameters comparing with the linear theory of sloshing. In many cases it can give the only solution to the sloshing problem when the linear theory does not work, i.e. in the cases of very small or very high fill levels, of high values of the input acceleration, and of course, in baffled containers. An accurate simulation of the rotational motion of a container by the rectilinear one, justified in previous chapters, allows to apply the results, obtained in the present chapter, both for the cases of longitudinal and lateral input acceleration, or for braking-accelerating and steady turning manoeuvres, of rectangular and modified rectangular tanks. In principle, this method can be applied to achieve a solution for any kind of input acceleration and any type of road container.

CHAPTER 8
OPTIMIZATION OF GEOMETRICAL PARAMETERS OF RECTANGULAR CONTAINERS

8.1 General

In this chapter, an optimization study is presented for rectangular liquid tankers subjected to step input acceleration. The optimal geometrical parameter, given by the ratio height/width of a container, is computed based on the nonlinear static analysis of the liquid loading arising during a steady cornering of the vehicle. The objective function is selected to minimize the peak overturning moment around the middle bottom point of the container, described in Chapter 5. For this purpose, the hydrostatic equations are modified in this chapter. The container cross-sectional area is assumed to be a constant and the fill level and the lateral acceleration are considered as parameters. This study introduces a new concept to liquid tanker design and can be, in principle, extended to the dynamic case accounting for magnified amplitudes of slosh loading.

The lateral stability problem, associated with transportation of liquid cargoes, imposes specific requirements for design of liquid tankers, one of which consists in bringing the centre of liquid mass to the lowest position with respect to the road level. This requirement is quite correct, however, it keeps in shadow the question of an optimal container shape. It has been noticed by Strandberg [28] that in some cases, the circular cross-section tank may be more stable in lateral direction than the associated elliptical tank despite the fact that for the latter the CG position is lower than for the former. This is due

to a larger possible displacement of the liquid mass in a wider tank which leads to larger overturning moment compared with a narrow tank. The similar situation exists with rectangular containers, when the excessive reduction of the height with a corresponding increase of the width may give a negative effect in some range of fill levels.

In practice, however, there exists a restriction on the container width dictated by traffic requirements, but actually it is not known if the existing tank widths are in the optimal range. It seems quite reasonable to design a container of optimal shape, if this does not contradict the traffic requirements, and then bring it as low to the ground as the frame and suspension of the vehicle can allow.

The results of this optimization study can be applied, with some degree of accuracy, to the shapes close to rectangular, i.e., modified rectangular and, perhaps, modified oval.

8.2 Recasting of the Moment Equations

The steady-state solutions in terms of overturning moment computed around the middle bottom point of the container, have been obtained in Chapter 5, where the moments are given for four possible configurations constituted by the free surface with the container walls. The behaviour of the overturning moment, is illustrated in Fig. 5.4 where the M_{ss} function is plotted against the container height with fill level as a parameter and for a fixed value of the lateral acceleration of 0.3 g. It can be seen that for fill levels below 0.8, these functions display the minima occurring at different values of the container height. A comparison of two containers having h's equal to 0.5 and 2.0 is made to clarify the behaviour of the moment. For small fill levels, see circles

on the vertical lines at h = 0.5 and 2.0, it is advantageous to have a container with greater height, while for high fill levels, for example f = 0.9, see squares on the figure, a tank smaller in height but wider is preferable. The transition from an advantageous to a disadvantageous container happens at the fill level of approximately 0.6 for $G_x = 0.3$. For greater G_x's this transition shifts to smaller values of f. This effect is due to larger displacement of the liquid mass in transversal direction in containers with smaller h. The dimensionalizing of the functions for M_{ss} will affect the positions of minima and hence the optimization of the container shape is a feasible problem.

The solutions, given in Table 5.2, were derived in the most general form with no restriction placed on the container size. In practical design, however, the problem of searching of the optimal form becomes more meaningful if the cross-sectional area of the container is kept constant. This puts an additional constraint of the form

$$a_o = h\, L_o^2 = \text{const} \tag{8.1}$$

Then, introducing the new fill level definition as

$$\alpha = \frac{f}{h} \tag{8.2}$$

and incorporating expressions (8.1) and (8.2) into the moment equations, given in Table 5.2, the new form solutions, taking into account the condition of the constant area, can be obtained in the form given in Table 8.1. It should be noted that the configuration conditions are written with respect to the container height. The dimensionalizing of

Table 8.1. Steady-state overturning moments for rectangular containers of fixed cross-sectional area

Configuration	Configuration conditions	Overturning moment (cw direction is positive; sign + for $G_x > 0$; sign − for $G_x < 0$)
1	$h \geq \dfrac{\lvert G_x \rvert}{2(1-\alpha)}$ $h \geq \dfrac{\lvert G_x \rvert}{2\alpha}$	$M_{ss}^{\circlearrowright} = \dfrac{G_x}{2}\left(\alpha^2\sqrt{h} + \dfrac{G_x^2+2}{12h\sqrt{h}}\right)$
2	$h \leq \dfrac{\lvert G_x \rvert}{2(1-\alpha)}$ $h \geq 2\lvert G_x \rvert (1-\alpha)$	$M_{ss}^{\circlearrowright} = (1-\alpha)\left[\pm\dfrac{1}{2\sqrt{h}} - \dfrac{(1-2\alpha)G_x\sqrt{h}}{2(1-\alpha)} - \dfrac{\sqrt{2(1-\alpha)\lvert G_x \rvert}}{3}\left(\dfrac{1}{G_x} - G_x\right)\right]$
3	$h \geq \alpha \lvert G_x \rvert$ $h \leq \dfrac{\lvert G_x \rvert}{2\alpha}$	$M_{ss}^{\circlearrowright} = \pm\dfrac{\alpha}{2\sqrt{h}} - \dfrac{\alpha\sqrt{2\alpha\lvert G_x \rvert}}{3}\left(\dfrac{1}{G_x} - G_x\right)$
4	$h \leq \alpha \lvert G_x \rvert$ $h \leq 2\lvert G_x \rvert (1-\alpha)$	$M_{ss}^{\circlearrowright} = \pm\left[\dfrac{\alpha(1-\alpha)}{2\sqrt{h}} - \dfrac{h\sqrt{h}}{12} - \dfrac{h\sqrt{h}}{24 G_x^2}\right] + \dfrac{\alpha G_x \sqrt{h}}{2}$

the new expressions for the moment and its relationship with previously defined moment are given by

$$m_{ss} = \delta\, g\, a_o^{3/2}\, M^o_{ss} \qquad \text{and} \qquad M^o_{ss} = \frac{\alpha\, M_{ss}}{\sqrt{h}} \tag{8.3}$$

8.3 Search for the Optimal Parameters of the Container

Considering the overturning moment, M^o_{ss}, as the objective function, the general optimization problem can be formulated as follows:

$$\left.\begin{array}{l} \text{Minimize } M^o_{ss} = f_i\,(h\ ,\ \alpha,\ G_x)\ ,\ i = 1,\ 2,\ 3,\ 4 \\ \\ \begin{array}{cccccccc} & i=1 & & i=2 & & i=3 & & i=4 \end{array} \\ \text{Subject to: } h \begin{cases} \geq a \\ \geq b \end{cases} ;\ h \begin{cases} < a \\ \geq c \end{cases} ;\ h \begin{cases} \geq d \\ < b \end{cases} ;\ h \begin{cases} < d \\ < c \end{cases} \\ \\ a,\ b,\ c,\ d = f_j\,(\alpha,\ G_x),\ j = 1,\ 2,\ 3,\ 4 \\ \\ 0 \leq \alpha \leq 1 \\ \\ G_x \geq 0 \end{array}\right\} \tag{8.4}$$

where the objective functions are given for each configuration in Table 8.1, integer i accounts for the configuration number, constraints on h are expressed in terms of a, b, c and d which represent the limits for each configuration and are encountered twice in the column corresponding to configuration conditions in Table 8.1, and integer j is the number of each of the four pairs of the configuration conditions.

The solution of this optimization problem appears to be very cumbersome, either carried out analytically or numerically. Moreover, there exists some pitfalls due to the fact that the objective function

may not have minimum at all or may have it on the boundary as, for example, for $\alpha = 0$ or $\alpha = 1$ when the optimal value of the container height tends to infinity or to zero, respectively. This problem, however, can be simplified by making a preliminary analysis of the moment equations and reconsidering the status of the variables involved. The standard optimization technique, once being accomplished, fixes the optimal values of variables which provide with the minimum of the objective function. In this specific problem, there is only one such a variable, namely the container height, while the fill level and input acceleration may not be specified since they are uncontrollable variables. Refering to Fig. 8.1, where the fill level is considered as a parameter and the lateral acceleration is fixed at $G_x = 0.5$, the analysis of the functions for the overturning moment can be made based on the behaviour of the corresponding plots. It can be seen, that for each fill level there exists a local minimum of M^o_{ss} which shifts from infinity to zero while the fill level is varied from 0 to 1. The line composed by circles shows positions of the local minima. It is obvious that a properly designed tank must have the height corresponding to the crest of this line, which is a saddle point. In this case, the small variation of the fill level will give sufficiently small magnification of the moment limited by the line of $\alpha = 1$ from the right and by lines, corresponding to smaller fill levels, from the left. Increasing of the h from the value lying on the crest results in a moderate increase of the moment, corresponding to the line of $\alpha = 1$, while decreasing of h results in a very large augmentation of the moment since all those curves tend to infinity with h going to zero. The overturning moment for 100% filled container, corresponding to the case of rigid cargo, is

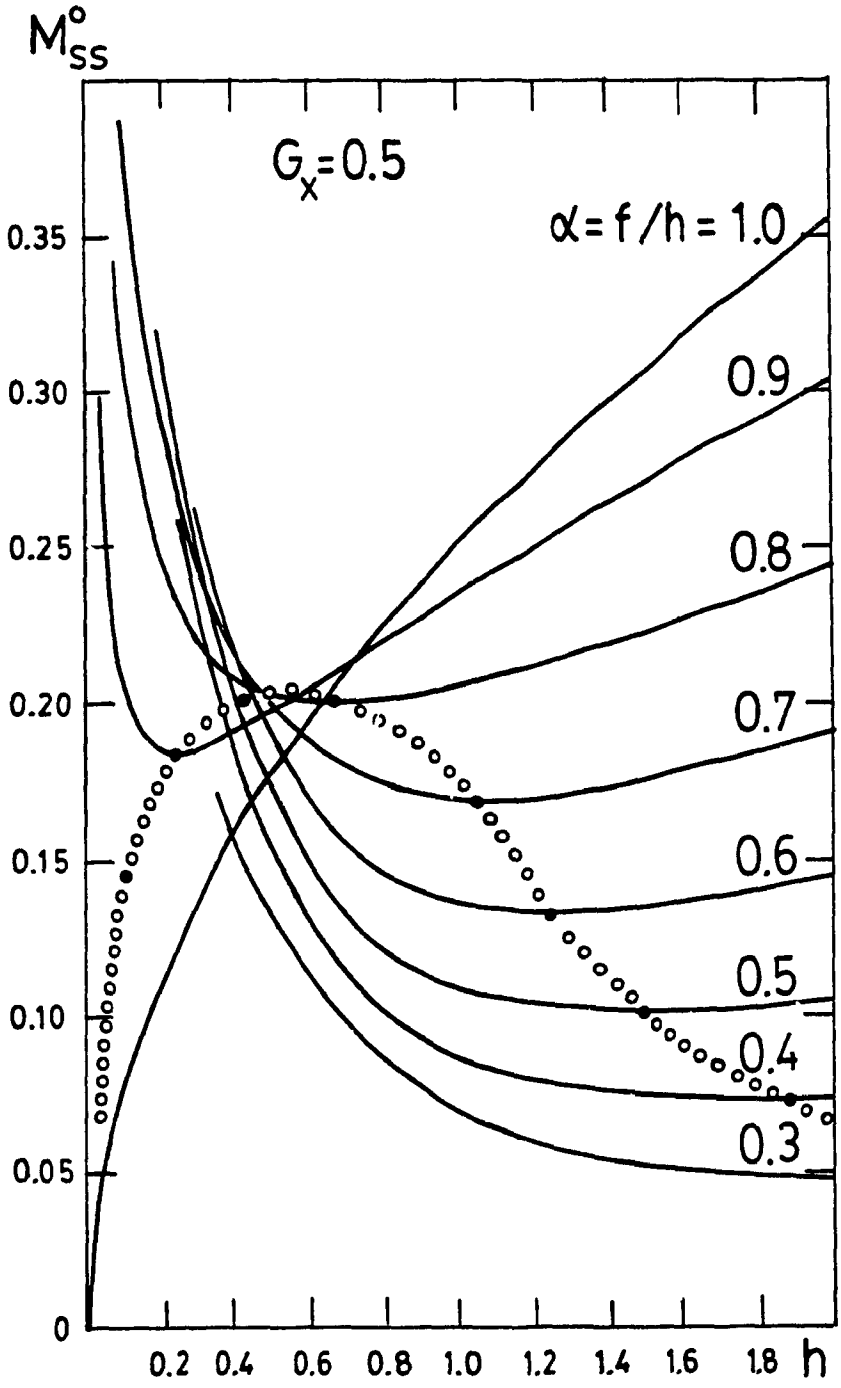

Fig.8.1. Behaviour of the overturning moment with the container height and fill level variations

given by

$$M^{o}_{ss} = \frac{G_x \sqrt{h}}{2} \tag{8.5}$$

From Fig. 8.1, it can also be seen, that the global minimum of the function M^{o}_{ss}, with fixed G_x, does not exists in the strict meaning of the word and the limiting minimal values of the function are lying on the boundary, i.e., at $h = 0$ for $\alpha = 1$ and at $h = \infty$ for $\alpha = 0$.

By virtue of the reasoning above, the optimization problem can be restated in the following manner: search for the saddle points of the functions $M^{o}_{ss} = f_1 (h , \alpha)$ considering the G_x as threshold of the lateral acceleration. This can be done separately for each of the four configurations satisfying the conditions of their existence. The necessary condition for the stationary points, saddle points in question, is

$$\frac{\partial M^{o}_{ss}}{\partial h}\bigg|_{h^*,\, \alpha^*} = 0 \quad , \quad \frac{\partial M^{o}_{ss}}{\partial \alpha}\bigg|_{h^*,\, \alpha^*} = 0 \tag{8.6}$$

The sufficient condition is

$$\left| \frac{\partial^2 M^{o}_{ss}}{\partial h^2} \frac{\partial^2 M^{o}_{ss}}{\partial \alpha^2} - \left(\frac{\partial^2 M^{o}_{ss}}{\partial h \partial \alpha} \right)^2 \right|_{h^*,\alpha^*} < 0 \tag{8.7}$$

where the stationary points are designated as (h^*, α^*), and $G_x \geq 0$ is considered in the analysis of the corresponding equations.

Configuration 1

The necessary condition, Eqn. (8.6) applied to the moment equation for Configuration 1, gives:

$$\begin{cases} \alpha^2 - \dfrac{G_x^2 + 2}{4\,h^2} = 0 \\ G_x\,\alpha\,\sqrt{h} \quad\quad = 0 \end{cases} \tag{8.8}$$

with the two stationary points

$$\begin{cases} h_1^* = \infty \\ \alpha_1^* = 0 \end{cases} \quad \text{and} \quad \begin{cases} h_2^* = 0 \\ \alpha_2^* = \infty \end{cases} \tag{8.9}$$

which are both infeasible. Thus, in the practical range of the variables, there is no stationary point.

Configuration 2

For Configuration 2, the stationary points can be found from the solution of the following equations:

$$\begin{cases} \alpha - 1 + h\,G_x\,(2\,\alpha - 1) = 0 \\ 2\,h\,G_x + c\,\sqrt{h}\,(1-\alpha)^{1/2} - 1 = 0 \end{cases} \qquad c = (1 - G_x^2)\,\sqrt{\frac{2}{G_x}} \tag{8.10}$$

Eliminating α from this system of equations, leads to the cubic algebraic equation for the h:

$$h^3 - \frac{1 + G_x^4}{4\,G_x^3}\,h^2 - \frac{1}{4\,G_x^2}\,h + \frac{1}{8\,G_x^3} = 0 \tag{8.11}$$

The analysis of this equation shows that two of the three roots are

complexe-conjugate and the third one is real. The real root has been computed numerically and the results are given in Table 8.2 where the corresponding α^* is found from the expression

$$\alpha^* = \frac{1 + G_x h^*}{1 + 2 G_x h^*} \tag{8.12}$$

The calculation also shows that the determinant for the sufficient condition, Eqn.(8.7), is negative in the feasible range of Configuration 2, that is, the stationary point is the saddle point. If the h^* is varied, Configuration 2 may lead to Configuration 1 or Configuration 4, but never to Configuration 3. Thus, the region for h^*, when Configuration 2 may lead to other configurations, is defined by the corresponding inequalities from Table 8.1, as

$$\begin{aligned} h^* &\leq \frac{G_x}{2(1 - \alpha^*)} \qquad \text{with Config. 1} \\ h^* &\geq 2 G_x (1 - \alpha^*) \quad \text{with Config. 4} \end{aligned} \tag{8.13}$$

Substitution of numerical values for the stationary point into the constraints, Eqns.(8.13), shows that Configuration 2 may be replaced by Configuration 1 only at $G_x = 0$ while the change for Configuration 4 occurs at $G_x = 1$. Hence, in the range of G_x from 0 to 1, Configuration 2 is taking place, and for $G_x > 1$ it is replaced by Configuration 4.

Configuration 3

The necessary condition for a stationary point in this configuration is given by the equations

Table 8.2. Stationary points (h^*, α^*) and optimal container height (h^*) for Configurations 2 and 4 as functions of G_x

Configuration 2			Configuration 4		
G_x	h^*	α^*	G_x	h^*	α^*
0	$\sqrt{2}/2$	1	1	0.5	0.75
0.01	0.702	0.993	1.01	0.486	0.745
0.1	0.660	0.942	1.1	0.397	0.718
0.3	0.587	0.871	1.2	0.339	0.703
0.4	0.560	0.846	1.5	0.246	0.685
0.5	0.539	0.825	2.0	0.175	0.675
0.7	0.513	0.791			
0.9	0.502	0.763			
1.0	0.5	0.75			

$$\begin{cases} \dfrac{\alpha}{h\sqrt{h}} = 0 \\ 1 - c\sqrt{\alpha\, h} = 0 \end{cases} \tag{8.14}$$

where c is given in Eqn. (8.10).

These equations yield the only stationary point with $\alpha^* = 0$ and $h^* = \infty$ which is not in the range of practical interest and, therefore, its nature is not examined. Thus, Configuration 3 is not in the study.

Configuration 4

Differentiation of the moment equation with respect of h and α gives the following system of equations for stationary points:

$$\begin{cases} \alpha^2 + \alpha\,(h\,G_x - 1) - h^2\,\dfrac{1 + 2G_x^2}{4G_x^2} = 0 \\ 2\,\alpha - 1 - hG_x = 0 \end{cases} \tag{8.15}$$

The solution of this system yields two roots for h^* one of which is infeasible since it gives a negative value for the container height. Then, the feasible stationary point is given by

$$\begin{cases} h^* = \dfrac{-G_x^3 + G_x\sqrt{4\,G_x^4 - 2\,G_x^2 - 1}}{3\,G_x^4 - 2\,G_x^2 - 1} \\ \alpha^* = \dfrac{1 + G_x h^*}{2} \end{cases} \tag{8.16}$$

The analytical solution of Eqns.(8.15) is shown in Table 8.2. Substitution of the expressions (8.16) into Eqn.(8.7) reveals that, in

the feasible region of the variables, this stationary point is the saddle point. The feasible region for the stationary point is defined by the inequalities which bound Configuration 4 from Configurations 2 and 3 in the following way:

$$\begin{cases} h^{\bullet} \le 2\, G_x\, (1 - \alpha^{\bullet}) & \text{with Config. 2} \\ h^{\bullet} \le \alpha^{\bullet}\, G_x & \text{with Config. 3} \end{cases} \tag{8.17}$$

The boundary with Configuration 2 has already been investigated, where the saddle point was found to be located at $G_x=1$. The boundary with Configuration 3, as it follows from the second expression of Eqn. (8.17) may be lying only at $G_x<1$ or in the region physically infeasible for Configuration 4. Thus, practically, in an optimized container, Configuration 4 is never replaced by Configuration 3.

It has been shown above that the saddle point can belong either to Configuration 2 or to Configuration 4 depending upon the level of the lateral acceleration. The plot of the optimal container height, $h^{\bullet}$, as a function of the G_x is given in Fig. 8.2. This height is here called optimal conventionally: it does provide with minimum of the overturning moment in presence of the arbitrary varying fill level, however, it has nothing to do with mathematical global minimum which does not exist. It can be seen from Fig. 8.2, that increasing of the threshold acceleration requires decreasing of the container height if the cross-section area is kept constant. The breaking point of the $h^{\bullet}$ curve corresponds to the change of configurations and, for Configuration 4, the optimal height drops monotonically to 0 with G_x tending to infinity.

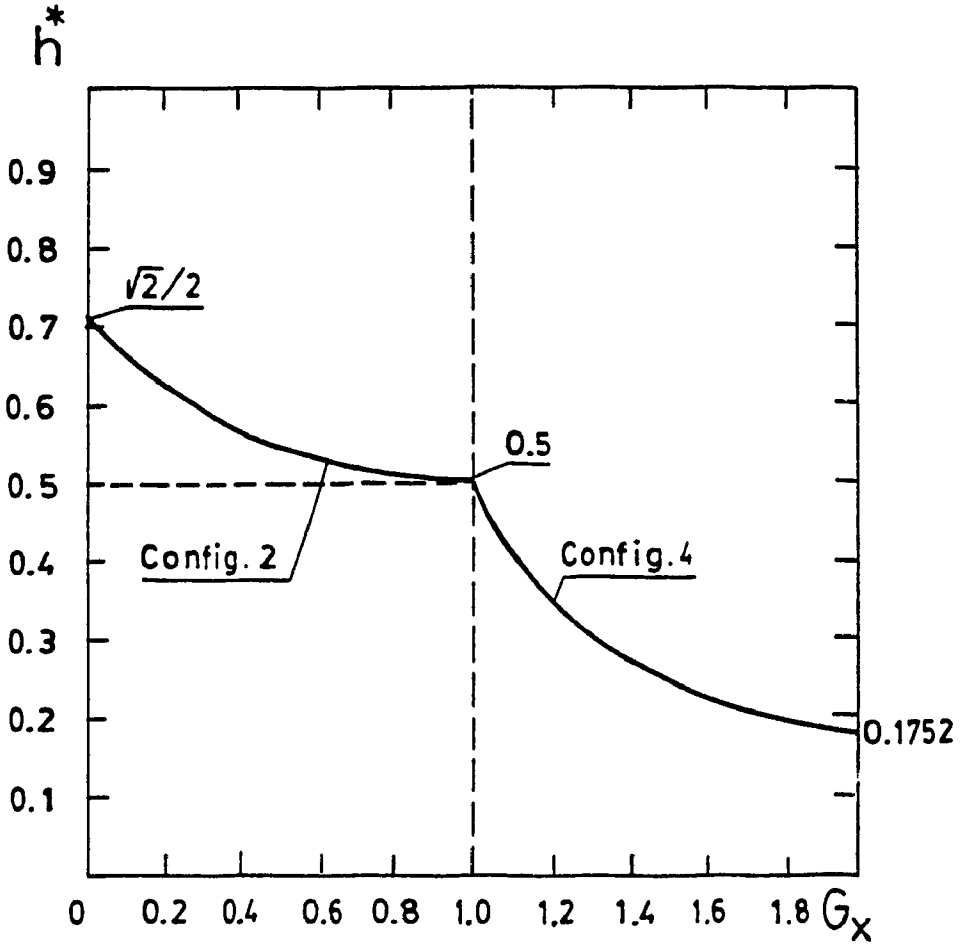

Fig.8.2. Optimal container height, h*, as function of lateral acceleration

8.4 Sensitivity of the Objective Function to the Container Height Variation

For some reason, if the container height does not correspond to its optimal value, then it would be interesting to know what is its influence on the overturning moment. For this purpose, a sensitivity analysis of the overturning moment to the deviation of the container height from its optimal value is here investigated in the following manner. The height variation is expressed as the ratio of the real height to its optimal value, i.e.,

$$\bar{h} = \frac{h}{h^*} \tag{8.18}$$

and the ratio of the moment, corresponding to real h, to the minimum moment, corresponding to h^*, is designated as:

$$\bar{M} = \frac{M^o_{ss}}{M^{o*}_{ss}} \tag{8.19}$$

Then, the post optimal analysis of the function

$$\bar{M} = f(\bar{h}, G_x) \tag{8.20}$$

is formulated. The moment is computed for that value of the fill level which provides the maximum expected moment for the chosen h and fixed G_x, by finding the local maximum of the M^o_{ss} function. For Configurations 2 and 4, the expressions for this fill level are found as:

$$\alpha = 1 - \frac{(1 - 2 h G_x)^2}{c^2 h} \quad \text{and} \quad \alpha = \frac{1 + h G_x}{2} \tag{8.21}$$

For Configuration 2, however, the first expression above may not work for all h's of interest. This can be seen from Fig.8.1, for example, where the region to the right from the saddle point can be split into two parts. The first part is understood between the boundary between Configurations 4 and 2 and the point of intersection of the α^* with the $\alpha=1$, where the corresponding container height, called here critical, can be found from the first expression of Eqn.(8.21) by setting $\alpha=1$. This results in the following expression for the critical height:

$$h_{cr} = \frac{1}{2G_x} \tag{8.22}$$

For the h exceeding h_{cr}, α is maintained equal to 1 for Configuration 2.

The plots of the function $\bar{M}$ are given in Figure 8.3, where G_x is considered as a parameter. It can be seen that increase in moment is significantly larger if the height is taken smaller than the optimal one, i.e., when $\bar{h}<1$. This is true for sufficiently small values of G_x. However, with increase of G_x, the trend is rather reverse; i.e., increasing of the container height generates larger moment with increase in G_x. It also can be noted that a small increase of the height, within 20% for example, gives a sufficiently small augmentation of the moment, i.e., about 10% for $G_x=1$ and about 5% for smaller values of G_x. A quantitative example for the container of typical height, h=0.7, shows that in this case of $\bar{h}^*=0.559$ and $\bar{h}=1.252$ the increase of the moment is of the order of 4% comparing with the optimal container for the threshold of acceleration equal to 0.4 g. If the acceleration is increased to 1 g then, for the same container, the moment increases by 13.8%.

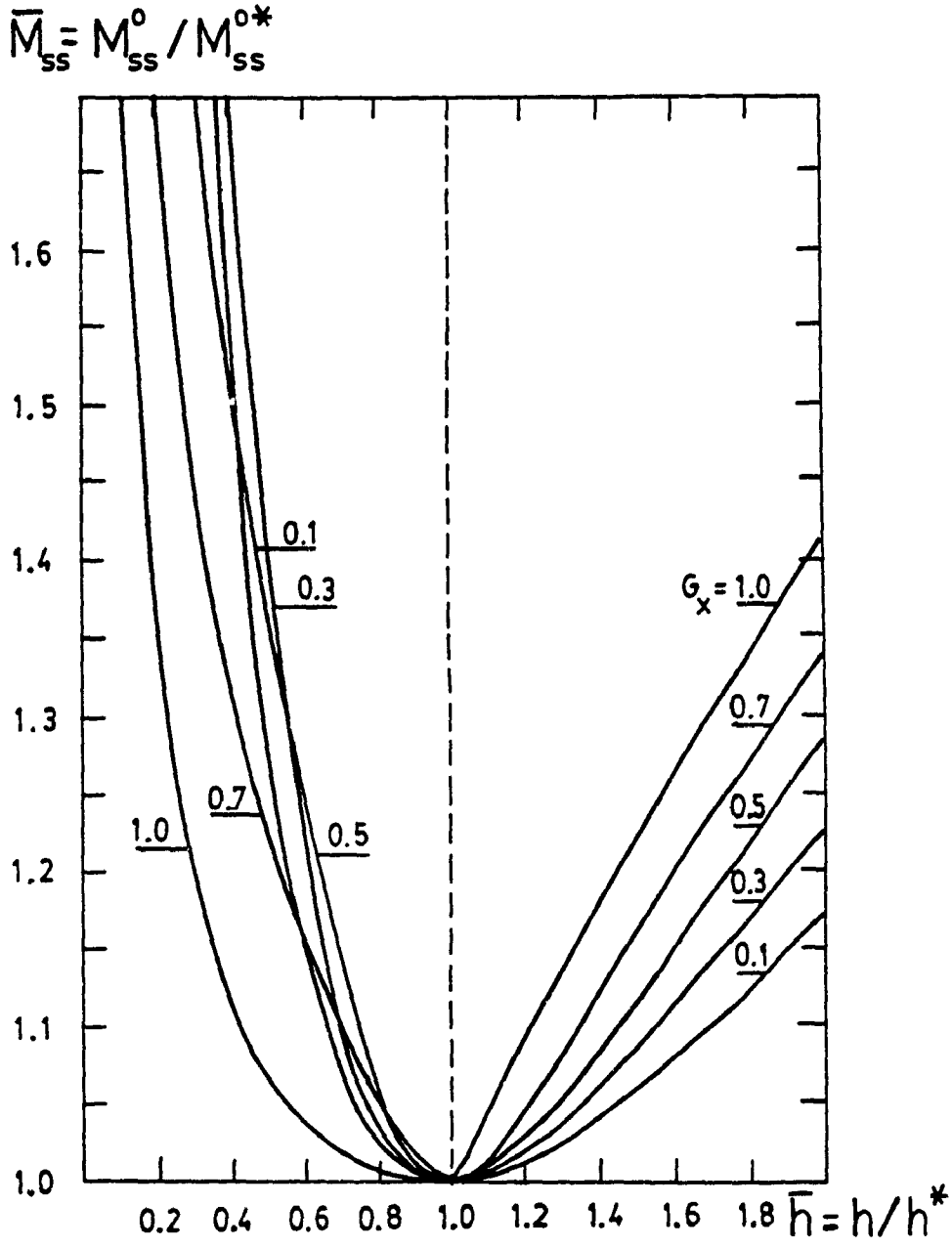

Fig.8.3. Sensitivity of the overturning moment to height variation

8.5 Summary

This study provides an optimization of the geometrical shape of rectangular liquid road tankers for the simplest case of static liquid load, and represents a first step towards more complicated cases related to dynamic loading due to liquid sloshing. It has been found that there exists an optimal height of the container which corresponds to the minimum overturning moment for a particular fill level and input lateral acceleration. It is also shown that increase of the threshold acceleration requires a reduction of the optimal height of the container if the cross-sectional container area is maintained constant. These results can be used for a practical implementation in the liquid tanker design, in order to improve the container characteristics.

CHAPTER 9

CONCLUSIONS AND RECOMMENDATIONS

9.1 Highlights of the Investigation

The present investigation attempts to show that certain practical solutions to the nonlinear sloshing problem in road containers can be achieved, prior to full scale testing, using analytical and computer simulation techniques. The analytical approach yields the steady-state responses of the liquid in different shape containers subjected to input acceleration simulating such vehicle manoeuvres as straight-line braking-acceleration and steady turn. The practical importance of steady-state solutions is that they can serve as a basis for determining of the dynamic slosh loading during the liquid tanker design by simple introduction of the necessary corrections obtained from corresponding transient solutions.

The transient responses are achieved by numerical solution of the Navier-Stokes, continuity, and free-surface equations using the modified Marker-and-Cell method developed in this study in a general form suitable for solving the sloshing problem for containers of arbitrary shape and subjected to arbitrary input acceleration. Further, the dynamic responses of the liquid are found in terms of the main sloshing parameters, such as heights of the free surface, forces and overturning moment exerted on the container body, which allows the linking of the developed slosh model with an appropriate vehicle dynamics model to study the coupled dynamics of the "tank-vehicle" system. Such an attempt has been made in [33] and has shown a good efficiency and adequate accuracy.

In this investigation, special attention was given to development of the boundary conditions for the numerical solution in conjunction with the coarse computational grid that provides a great saving of the computer time without excessive loss of accuracy. The boundary conditions were derived based on the assumption of the reflection principle and checked by laboratory testing which has shown a good correlation between the theory and experiment.

The validation of the computer slosh model has been carried out with a rectangular container and a specially created experimental set-up in the laboratory. It has been assumed that the method of calculation of the boundary conditions, verified for a rectangular tank, can be extended to other container shapes since the boundary conditions is a matter of general nature.

The results for transient solutions have been compared, wherever it was possible, with those from the linear sloshing theory. This comparison reveals a sufficiently close agreement between the two approaches but only within the applicability of the linear theory, which is limited by the assumption of small oscillations and simplified shape of the container. Thus, this investigation confirms the applicability of the linear theory within some limits and, on the other hand, gives the solutions beyond of these limits that is an essential contribution to the fluid sloshing problems.

Finally, the optimal geometrical shape, yielding the minimum overturning moment, has been defined for rectangular containers utilizing the standard multivariable optimization technique. Although the optimization was made for the steady-state, it can be extended to the transient solutions provided that the parametric study is done in a

full form.

The original aspects of this work can be summarized in the following statements:

i) An effective mathematical model of the sloshing phenomena, developed in this investigation, combines both adequate accuracy and complexity to reflect the actual dynamic behaviour of the sloshing liquid. The accuracy is sustained by including the most essential nonlinearities of the problem due to the nature of the governing equations and to the boundary including rigid walls and free surface. In order to eliminate an excessive computing time, the coarse computational grid has been used in conjunction with appropriate boundary conditions that provides a sufficient accuracy.

ii) The computer model includes a careful calculation of the boundary condition compatible with adopted coarse grid and derived in a general way suitable for implementation for a large class of sloshing problems.

iii) The analytical steady-state solutions for circular and rectangular containers as well as for containers with separating walls were developed.

iv) The transient responses in terms of slosh loading have been obtained for road containers of rectangular and circular cross-sections and for compartmented and baffled containers. The influence of the number of baffles and of the size and location of the baffle orifices has been studied. All this provides with a new information about liquid behaviour and can be used in the liquid tanker design.

v) Available analytical optimization technique was applied to rectangular containers to specify the optimal geometrical shape that

would minimize the overturning moment in steady turn.

9.2 Discussion of the Results

In this section, the most important results and general conclusions are summarized to reflect the findings of the present investigation.

Comparison of the solutions obtained from the developed computer model hardly can be done in a direct way because of lack of experimental data. An indirect comparison, however, was done by other authors, [57] and [33], who investigated a coupled "liquid-vehicle" system and verified their quasi-dynamic model against the field testing results and the results given by this slosh model incorporated into the considered system. The present model correlates well with the experimental results in terms of the vehicle roll angle and axle loads, and hence, demonstrates a high degree of confidence in the slosh model employed in this investigation.

The analysis of the steady-state solutions reveals that the input lateral acceleration for a steady turn, being a function of the instantaneous radius of the track curvature, can be replaced with high degree of accuracy by the coordinate-independent equivalent lateral acceleration. The error arising from such a simplifying procedure is very small and estimated for most practical cases of road containers subjected to steady cornering. However, it can be dangerous to use this recommendation in the case of evasive manoeuvres when the radius of turn is relatively small and underestimating of the loading becomes essential.

The transient solutions obtained for circular and rectangular cross-section containers indicate both similarities and non-similarities

of the liquid behaviour under identical input conditions. The response in a compartmented baffled container, however, displays a significant damping effect of the baffles. The main parameters, strongly affecting the liquid response in terms of amplitudes and frequencies of the sloshing forces and overturning moments, are the fill level, the magnitude of input acceleration, and the container geometry and also the number of separating walls, the number, location, and the size of baffle orifices for compartmented and baffled containers. The influence of the Reynolds number, or of the liquid viscosity, was found negligible for most practical cases covered by the Re number above 10^5, sufficiently small for Re lying in diaposon 10^5 - 10^3, and essential for Re below 10^3. The practical significance of this result is that the liquid vibrations can be considered as undamped for such liquids as gasoline, light crude oils, and other liquids close in viscosity to these ones. This leads to the conclusion that for these liquids a strong resonance can be expected in the case of a periodic input disturbance, while for very viscous liquids like heavy mineral oils at low temperature and tars, the vibrations are strongly damped. Thus, for most of transported liquids, some artificial measures to suppress the excessive sloshing such as longitudinal and transversal baffles are needed.

The fill level is one of the most important factors influencing the output slosh parameters. Comparison of the slosh responses for circular and rectangular containers shows that manifestation of the container's form nonlinearity is stronger in rectangular tanks due to the stronger damping effect of the horizontal walls. In rectangular containers, the dynamic force and moment coefficients display maxima for medium values of the nondimensional fill level while such maxima for circular

containers fall to smaller filling. In the range of fill levels of practical interest, i.e., between 50 and 100%, the dynamic coefficients are sufficiently close in values for both types of container. The natural damped frequencies, in these two cases, behave differently. In circular containers, the frequencies are much closer to those predicted from linear theory and always lower than the latter, while in rectangular containers, the frequencies behave similarly only in a sufficiently narrow region of fill levels when the interference of the horizontal walls is absent. If, however, the horizontal walls are involved, then the frequencies increase but the amplitudes decrease and the liquid motion is becoming chaotic. The decreasing of the amplitude, in this case, happens only for cycles following the very first one which is characterized by a large amplitude. Practically, this fact means that the rectangular shape is preferable since the resonance, if it appears, happens in a different mode than the fundamental mode and therefore the expecting loading must be smaller. As for the loading due to the first overshoot, the rectangular container has no advantage. The peak values of the load, recomputed to the dimensional form, shows that the most dangerous fill levels fall to 80 - 90% with respect to the container height. It is also known, from the different sources, based on experimental investigations, that the critical fill level is somewhere between 60 and 75%. This difference is explained by the fact that the mentioned experimental results were obtained for vehicle tankers where the vibration of the suspension induced a partial resonance which can develop stronger for relatively smaller fill levels, while in this investigation the resonant phenomena has not been considered.

The magnitude of the input acceleration is another factor affecting the liquid response in road containers. The results of this part of parametric study indicate that the horizontal force and overturning moment are monotonically and almost linearly increasing with increase of the input acceleration while their dynamic coefficients decrease in the practical range of the acceleration displaying a relatively weaker sloshing. This fact is due to a greater allowable displacement of the liquid occurring under smaller horizontal acceleration, especially in circular containers. The damped frequencies branch below from the theoretical undamped frequencies for rectangular and circular containers in the range of the input acceleration between 0 and 0.5 g's and they sharply increase for the rectangular containers only above this range leading to an irregular liquid sloshing due to interaction of the upper wall. In such a case, the liquid behaviour becomes somehow similar to the case when the fill level allows the horizontal walls to interact with the free surface. This fact leads to the following important conclusion: the damped natural frequency of liquid oscillation, being a function of many parameters, depends the most on the length of the free surface. Thus, in circular containers, the free surface length is weakly dependent on its orientation, while in rectangular containers, when the horizontal walls interfere with the free surface, its length becomes shorter and this affects the frequencies. This statement fully explains the behaviour of the frequencies that can not be made on the basis of the linear theory.

The liquid response in rectangular containers strongly depends on the container form expressed in this study as ratio of the height to the width or length. It has been found that the more intense sloshing, in

terms of the dynamic moment coefficient, happens in a square container, while the maximum of the dynamic horizontal force coefficient falls to the smallest value of the ratio. The practical significance of this fact is that for good lateral dynamics of a vehicle, associated with lateral stability, the height/width ratio must be smaller than 1.0, but not too small according to the results of optimization study, while for longitudinal dynamics, the separating walls are strongly advisable in order to diminish the excessive horizontal force often leading to skidding or jack-knifing. Besides the instability modes related to longitudinal dynamics, the separating walls are also beneficial in the sense of the reduction of the overturning moment which can produce excessive loading on the axles, suspension elements, and tires of the vehicle. Thus, for a tanker of 13 m in length the arrangement of five evenly distributed separating walls reduces the dynamic overturning moment by approximately 6.5 times and the dynamic horizontal force by 1.34 times which is, of course, a great reduction. In practical designing there can be encountered the recommendation to install the separating walls at the distance not less than 64" which corresponds to eight compartments or seven separating walls for the container in question. This will give a very small additional gain, about 7 times, comparing with five separating walls (6.5 times) because of the exponential character of the moment as a function of the number of partitions. Hence, the design concepts may be reconsidered in the light of the present investigation.

The study of baffled tanks has shown that the effect of partitions with orifices is reduced comparing with full separating walls because of interflowing of the liquid from one compartment to another. For

example, the overturning moment for a tank with one opened baffle can be reduced up to 30% by closing the baffle. Therefore, the requirement to keep baffle orifices closed during the transportation is important. It has also been found that the location of an open orifice has no effect on the sloshing parameters unless the free surface does not pass through the orifice. In the opposite case, the interflowing of the liquid is delayed and the baffling effect is increased. The size of the orifice affects the magnitude of sloshing parameters suddenly, when even a small opening between compartments is arranged. However, the increase of the orifice size from 16" to 20", that is in practical range of existing orifices, has a very little additional effect. Thus, if the orifices are intended for use, they may be of the full size, i.e., 20", for practical commodity and without losing too much of their efficiency. The influence of the number of baffles on the horizontal force is sufficiently small and manifests stronger only for tanks with 1 or 2 baffles. If their number is 3 or more then their effect is vanishing and the peak force values are almost equal to the corresponding cases with closed baffles. As for the overturning moment, the large number of baffles makes the flow behave like full partition are installed instead of baffles. The small number of baffles has a strong effect for a few first cycles of oscillations and this effect is loosing with time due to the liquid interflowing. The summarized effect of baffles can be formulated in the following statement: the container baffles delay the interflowing of the liquid and increase the overall damping which is a positive effect; however this effect may become negative in the case of longitudinal baffles when after a short duration turn the vehicle performs a second turn in the same direction. In this case, the liquid

has no time to come to the equilibrium state and the second manoeuvre can result in larger loading.

The optimization of the rectangular container shape, carried out for the steady-state response of the liquid, has shown that the favourable ratio height/width is lying in the range 0.7 - 0.5 for the input acceleration from 0 to 1 g, respectively, and equal to 0.56 for the threshold acceleration of 0.4 g. Since the maximum of sloshing intensity falls to a square shape container, the optimal ratio will be slightly decreased in dynamics. The expected difference in optimal values in statics and dynamics should be sufficiently small because of relatively small and smooth variation of the dynamic moment coefficient with the container's shape ratio. The more accurate optimization study can be easily extended to the dynamic case provided that the full parametric study data is available.

Finally, the present investigation has confirmed the applicability of the linear sloshing theory for small amplitude of liquid oscillation which are induced by relatively small input acceleration, not exceeding 0.2 g's, in presence of narrow range of fill level centered around the 50% filling, and for containers with medium values of the ratio "height/width" also centered around the square container, in the case of rectangular tankers. For a large number of practical cases, when those conditions are not satisfied, the present approach gives solutions for a complicated sloshing problem essentially extending the knowledge of this important phenomena.

9.3 Recommendations for Future Work

The investigation presented in this work provides new information

on the dynamics of liquid sloshing arising under specific conditions of the cornering or braking manoeuvres. The nonlinear mathematical and computer two-dimensional models and the analytical methods used for the solutions obtained in this study may be easily extended to study the lateral dynamics in containers of other shapes of interest such as elliptical, superelliptical, modified rectangular, and lately introduced into the design T-shape. The two-dimensional model of sloshing, in the form as it is presented in this investigation, can also be applied to evasive manoeuvre of the tank vehicle, while the combination of turning and braking-acceleration can be only solved by means of the three-dimensional slosh model.

The methodology, used for development of the 2-D model, can be applied to create the three-dimensional slosh model which will allow to solve more complicated problems characterized by the coupling of liquid motions in the transversal and longitudinal directions. As an example of such an important problem, the liquid response for cornering-braking manoeuvre can be considered. Because of the generality of the approach employed here, especially with respect to the definition of boundary conditions, such an implementation is seen as a straightforward procedure.

One of the most important problems associated with dynamics of liquid carrying vehicles is the coupled sloshing problem considering the behaviour of the complete "liquid-vehicle" system. The present 2-D slosh model has been tested in combination with a vehicle model, separately from this investigation by other researchers, and has shown a high degree of confidence. As a logical extension of this direction of study, the coupling of the 3-D slosh model with a reasonably simplified

vehicle model can be considered in the future; the results obtained could be hardly overestimated.

The accumulation of results for transient liquid responses for an exhaustive number of combinations of input parameters, made through detailed parametric studies, will allow to radically simplify the liquid tanker design procedure by eliminating of complex and time consuming solutions of dynamic slosh models. Instead, the steady-state model results, duly adjusted by the coefficients accounting for sloshing effect due to variation of the main input parameters involved, can be used for estimation of the slosh loading. Such an approach becomes especially beneficial for coupled problems.

The resonant phenomena due to periodic or repeating input disturbance often arises during transportation of liquids. It was not the subject of study in this investigation, however, the developed mathematical models allows, with minor alterations, to obtain the frequency responses which would essentially extend the knowledge about this practical and important problem. The above-mentioned topics form a continuing spectrum of research efforts in this vital field of engineering.

REFERENCES

1. U.S. Department of Transportation. *Hazardous Material Transportation*. Tenth Annual Report, 1980.

2. University of Michigan, Transportation Research Institute. *Institute Report No.* UMITRI-89-1, Jan. 1989.

3. Rakheja, S., and Sankar, S. "Tank Vehicle Accidents: A Survey of Reports on File." *CONCAVE Report No.* 14-87, Concordia University, October 1987.

4. Hutton, R.E. "An Investigation of Resonant, Nonlinear, Nonplanar Free Surface Oscillations of a Fluid." *NASA TND* - 1870, May 1963.

5. Abramson, H.N. "The Dynamic Behaviour of Liquids in Moving Containers." *NASA SP-106*, 1966.

6. Abramson, H.N., and Ransleben G.E. "Simulation of Fuel Sloshing Characteristics in Missile Tanks by Use of Small Models." *ARS Journal*, Vol. 30, No. 7, 1960, pp. 603-612.

7. Abramson, H.N., Gaza, L.R., and Kana, D.D. "Liquid Sloshing in Compartmented Cylindrical Tanks." *ARS Journal*, Vol. 32, No. 6, 1962, pp. 978-980.

8. Abramson, H.N. "Dynamic Behaviour of Liquids in Moving Containers." *Applied Mechanics Reviews*, Vol. 16, No. 7, 1963, pp. 501-506.

9. Abramson, H.N., and Garza L.R. "Some Measurements of Liquid Frequencies and Damping in Compartmented Cylindrical Tanks." *AIAA Journal of Spacecraft and Rockets*, Vol. 2, No.3, 1965, pp. 453-455.

10. Abramson, H.N., Chu, W.H., and Kana, D.D. "Some Studies of Nonlinear Lateral Sloshing in Rigid Containers." *Journal of Applied Mechanics*, Dec. 1966, pp. 777-784.

11. Moiseyev, N.N. "Theory of Nonlinear Vibrations of a Liquid of Finite Volume." *Journal of Applied Math. Mech. (PMM)*, Vol. 22, No. 5, 1958, pp. 860-870.

12. Shimizu, T., and Hayama, S. "Nonlinear Responses of Sloshing Based on the Shallow Water Wave Theory." *JSME Int. Journal*, Vol. 30, No. 263, 1987, pp. 806-813.

13. Milne-Thompson, L.M. *Theoretical Hydrodynamics*. 4th ed. London: MacMillan. 1960, ch. 14.

14. Kochin, N.E., Kibel, I.A., Rose, N.V., "*Theoretical Hydrodynamics*." (in Russian) 6th ed. Moscow: Gosizdat Phys. Math. Liter., 1963, ch.8.

15. Bauer, H.F. "Dynamic Behaviour of an Elastic Separating Wall in Vehicle Containers." Part 1, *Int. Journal of Vehicle Design,* Vol. 2, No. 1, 1981, pp. 44-77.

16. Bauer, H.F. "Dynamic Behaviour of an Elastic Separating Wall in Vehicle Containers." Part 2, *Int. Journal of Vehicle Design,* Vol. 3, No. 3, 1982, pp. 307-332.

17. Bauer, H.F. and Villaneuve, J. "Theory of Liquid Sloshing in a Rectangular Container with Numerical Examples for C5 Wing." *Lockheed-Georgia Company Report,* No. ER 8390, 1967.

18. Bauer, H.F. "On the Destabilizing Effect of Liquids in Various Vehicles." *Vehicle System Dynamics,* No. 1, 1972, pp. 227.

19. Lamb, M. *Hydrodynamics.* New York: Dover, 1945, sects. 257 and 259.

20. Budiansky, B. "Sloshing of Liquids in Circular Canals and Spherical Tanks." *Journal of The Aero/Space Sciences*, Vol. 27, No. 3, 1960, pp. 161 - 173.

21. Graham, E.W., and Rodriguez, A.M. "The Characteristics of Fuel Motion which Affect Airplane Dynamics." *Journal of Applied Mechanics,* Vol. 19, No. 3, 1952, pp. 381-388.

22. McCarty, J., and Stephens, D. "Investigation of Natural Frequencies of Fluids in Spherical and Cylindrical Tanks." *NASA TND* - 252, 1960.

23. Khandelwal, R.S., and Nigam, N.C. "Parametric Stabilities of a Liquid Free Surface in a Flexible Container under Vertical Periodic Motion." *Journal of Sound and Vibration,* Vol. 74, No. 2, 1981, pp. 243-249.

24. Miles, J.W. "On the Sloshing of Liquid in a Flexible Tank." *Journal of Applied Mechanics,* Vol. 25, 1958, pp. 277-284.

25. Natyshkin, V.F., and Rakhimov, I.S. "Oscillations of a Cylindrical Shell Partially Filled with a Liquid." (in Russian) *Aviatzionnay Technika,* Vol. 17, No. 3, 1964.

26. Lindholm, U.S., et al. "Bending Vibrations of a Circular Cylindrical Shell with an Internal Liquid Having a Free Surface." *AIAA Journal,* Vol. 1, No.9, 1963, pp. 2092-2099.

27. Partom, I.S. "Numerical Calculation of Equivalent Moment of Inertia for a Fluid in a Cylindrical Container with Partitions." *Int. Journal for Numerical Methods in Fluids,* Vol. 5, 1985, pp. 25-42.

28. Strandberg, L. "Lateral Stability of Road Tankers." *Nat. Road and Traffic Res. Institute,* Sweden, Report No. 138A, 1978.

29. Aslam, M., Godden, W.G., and Scalise, D.T. "Earthquake Sloshing in Annular and Cylindrical Tanks." *Journal of Engineering Mechanics Division,* ASCE, No. 105, June 1979, pp. 371-389.

30. "Computer Simulation of the Effect Shifting on Articulated Vehicles Performing Braking and Cornering Maneuvers." *Johns Hopkins University,* Technical Rep. FHWA/RD - 80/143, Vol. 2, May 1981.

31. Lindström, M. "Road Tankers' Overturning Limit - The Steady - State Case." (in Swedish) *National Road and Traffic Res. Institute, Sweden, Working paper* No. 1976-12-17.

32. Sankar, S., Rakheja, S., and Ranganathan, R. "Directional Response of Partially Filled Tank Vehicles." SAE Technical Paper No. 892481, *Truck and Bus Meeting and Exposition,* Charlotte, N.C., November 6-9, 1989.

33. Ranganathan, R. "Stability Analysis and Directional Response Characteristics of Heavy Vehicles Carrying Liquid Cargo" Ph.D. Thesis, Concordia University, Montreal, Canada, 1990.

34. Warner, R.W., and Caldwell, J.T. "Experimental Evaluation of Analytical Models for the Inertia and Natural Frequencies of Fuel Sloshing in Circular Cylindrical Tanks." *NASA TND* - 856, 1961.

35. Abramson, H.N., Chu, W.H., and Ransleben, G.E. "Representation of Fuel Sloshing in Cylindrical Tanks by an Equivalent Mechanical Model." *ARS Journal,* Vol. 31, Dec. 1961, pp. 1697-1705.

36. Miles, J.W. "Stability of Forced Oscillations of a Spherical Pendulum." *Quarterly of Applied Mathematics,* Vol. 20, No. 1, April 1962, pp. 21-32.

37. Sumner, I.E., Stofan, A.J., and Shramo, D.J. "Experimental Sloshing Characteristics and a Mechanical Analogy of Liquid Sloshing in Scale-Model Centaur Liquid Oxygen Tank." *NASA TM* X-999, 1964.

38. Sayar, B.A. "Fluid Slosh Dampers." Ph.D. Thesis, Georgia Institute of Technology, 1971, pp. 1-36.

39. Bauer, H.F. "Nonlinear Mechanical Model for Description of Propellant Sloshing." *AIAA Journal,* Vol. 4, No. 9, Sept. 1966, pp. 1662-1668.

40. Sayar, B.A., and Baumgarten, J.R. "Pendulum Analogy for Nonlinear Fluid Oscillations in Spherical Containers." *Journal of Applied Mechanics,* Vol. 48, Dec. 1981, pp. 769-772.

41. Nichols, B.D., and Hirt, C.W. "Improved Free Surface Boundary Conditions for Numerical Incompressible-Flow Calculations" *Journal of Computational Physics,* Vol. 8, No. 3, Dec. 1971, pp. 434-448.

42. Peacemen. D.W., and Rachford, H.H. "The Numerical Solution of Parabolic and Elliptic Differential Equations." *J. Soc. Ind. Appl. Mathematics,* Vol. 3, No. 1, 1955, pp. 28-41.

43. Fox, L. "A Short Account of Relaxation Methods." *Quarterly J. Mechanics and Applied Mathematics,* Vol. 1, 1948, pp. 253-280.

44. Roach, P.J. *Computational Fluid Dynamics.* Albuquerque, N.M.: Hermosa, 1976, Sect. 3.1.16.

45. Anderson, D.A., Tannehill, J.C., Pletcher, R.H. *Computational Fluid Mechanics and Heat Transfer.* (series in Computational Methods in Mechanics and Thermal Sciences) New York: Hemisphere, 1984, sect. 9-3-1.

46. Harlow, F.H., and Amsden, A.A. "A Numerical Fluid Dynamics Calculation Method for All Flow Speeds." *Journal of Computational Physics,* Vol. 8, No. 2, Oct. 1971, pp. 197-213.

47. Harlow, F.H., and Welch, J.E. "Numerical Calculation of Time-Dependent Viscous Incompressible Flow of Fluid with Free-Surface." *Physics of Fluids,* Vol. 8, No. 12, 1965, pp. 2182-2189.

48. Amsden, A.A., and Harlow, F.H. "The SMAC Method: A Numerical Technique for Calculating Incompressible Fluid Flows." Los Alamas Sc. Laboratory, Report LA - 4370, Los Alamos, N.M.

49. Viecelli, T.A. " A Method for Including Arbitrary External Boundary in the MAC Incompressible Fluid Computing Technique." *Journal of Computational Physics,* Vol 4, 1969, pp. 543-551.

50. Chan, R.K. - C, and Street R.L. "SUMMAC - A Numerical Model for Water Waves." Dept. Civil Eng., Stanford University, Technical Report No. 135, 1970.

51. Patankar, S.V. *Numerical Heat Transfer and Fluid Flow.* New York: Hemisphere, 1980, p. 118.

52. Strang, G., and Fix, J. "An Analysis of the Finite Element Method." Prentice - Hall, 1973.

53. Hutton, A.G. "Incompressible Viscous Flow Modelling by the Method of Finite Elements." Ed. B. Hunt. *Numerical Method in Applied Fluid Mechanics.* New York: Academic Press, 1980.

54. Washizu, K. "Some Application of Finite Element Techniques to Nonlinear Free Surface Fluid Flow Problems." *Proceedings of the 4th Int. Symposium on Finite Element Methods in Flow Problems.* Tokyo, Chuo University, July 1982.

55. Wu, J.C., "Fundamental Solutions and Numerical Methods for Flow Problem." *International Journal for Numerical Methods in Fluids,* Vol. 4, 1984, pp. 185-201.

56. Hirt, C.W., Nichols, B.D., Romero, N.C. "SOLA - A Numerical Solution Algorithm for Transient Fluid Flows." *Los Alamos Sci. Lab. Report* No. LA-5852, 1975.

57. Sankar, S.,et al. "Liquid Tanker Stability." Final Report, TDC July 1990, CONCAVE Res. Centre, Concordia University, Montreal, Canada.

58. Peterson, L.D. "Experimental Observation of Low and Zero Gravity Nonlinear Fluid-Spacecraft Dynamics." *Proceedings of the 59th Shock and Vibration Symposium,* October 18-20, 1988, Albuquerque, N.M., Vol. II., pp. 269-291.

APPENDIX I

THE WEIGHTING COEFFICIENTS FOR RIGID WALL VELOCITY BOUNDARY CONDITIONS

In Chapter 3, the general expressions for interpolation of the boundary conditions were derived in terms of the weighting coefficients accounting for the contribution of nearest cell velocities. In this appendix, these coefficients are derived for different configurations of the cell velocities involved by using the Newton's interpolation technique for unequal distribution of the nodes, see Fig. 3.4. These derivations are carried out through the use of divided differences written to express a liquid velocity as a function of the distance along the n-axis, Fig. 3.5. Considering maximum second-order extrapolation, the two nodes, 1 and 2, and the node lying on the wall are needed. Hence, the argument (distances), functions (normal velocities), and first and second-order divided differences can be expressed as it is given in the table below:

n	V_n	First order divided differences	Second order divided differences
$n_0 = 0$	$V_{nw} = 0$	$[n_0, n_1] = \frac{V_{n1} - V^{\nearrow 0}_{nw}}{b}$	$[n_0, n_1, n_2] = \frac{[n_1, n_2] - [n_0, n_1]}{b+c}$
$n_1 = b$	V_{n1}	$[n_1, n_2] = \frac{V_{n2} - V_{n1}}{c}$	$= \frac{V_{n2}}{c(b+c)} - \frac{V_{n1}}{bc}$
$n_2 = b+c$	V_{n2}		

where the normal velocity components account both for U and V velocities

and for simplicity are designated as V_n. The normal component of the boundary velocity can be expressed by reflecting the V'_{nB} into the fictitious flow, i.e. $V_{nB} = - V'_{nB}$ as:

$$V_{nB} = - V_{nw}^{\rightarrow 0} - \frac{V_{n1}}{b} (a-0) - \left[\frac{V_{n2}}{c(b+c)} - \frac{V_{n1}}{bc} \right] (a-0) (a-b) \qquad (I.1)$$

where the distance a is positive for the point B located both inside or outside of the wall. The normal and tangential components of nodal velocities are

$$\begin{aligned} V_{n1} &= V_1 \sin \alpha \qquad \text{and} \quad V_{n2} = V_2 \sin \alpha \\ V_{\tau 1} &= V_1 \cos \alpha \qquad \text{and} \quad V_{\tau 2} = V_2 \sin \alpha \end{aligned} \qquad (I.2)$$

The interpolation of the V_1 and V_2 between the cell velocities, shown in Fig. 3.4, is made by the linear interpolation formula, which can be written in the form

$$V = \mu_i \, V_i + \mu_{i+1} \, V_{i+1} \qquad (I.3)$$

where the interpolation length μ_i is from the side of velocity V_{i+1}, μ_{i+1} is from the side of velocity V_i, and the velocity of interest, V, is located between V_i and V_{i+1}. The distance between V_i and V_{i+1} may be equal either to δX or δY depending on the considered case and the subscripts i and (i+1) have no relationship with the computational mesh but rather serve to express the nearest cell velocities both in horizontal and vertical directions. The expression (I.3) is also used to linearly interpolate the tangential component $V_{\tau B}$, in which case the interpolation lengths and the tangential boundary velocity are

$$\mu_1 = 1 + \frac{b-a}{c}\ ,\quad \mu_2 = \frac{a-b}{c}\ ,\quad V_{\tau B} = \mu_1 V_{\tau 1} + \mu_2 V_{\tau 2} \qquad (I.4)$$

I.1 Configuration 1. V velocity

In this case, the normal line, n-axis, intersects the mesh lines between points 3 and 6 for V_1 and between points 4 and 7 for V_2. Defining the value m as

$$m = \frac{\delta Y}{\delta X \tan\alpha}\ , \qquad (I.5)$$

the interpolation lengths lying on the n-axis as

$$a = -\frac{\ell}{\cos\alpha}\ ,\ b = \frac{\delta X + \ell}{\cos\alpha}\ ,\ c = \frac{\delta X}{\cos\alpha} \qquad (I.6)$$

rearranging the expression (I.1) for linear and quadratic extrapolation as

$$V_{nB} = -\frac{a}{b} V_{n1} \text{ and } V_{nB} = -\frac{a}{b}\left(1 + \frac{b-a}{c}\right) V_{n1} - \frac{a(a-b)}{c(b+c)} V_{n2} \qquad (I.7)$$

and expressing the V_1 and V_2 velocities through the factor m as

$$V_1 = \frac{m-1}{m} V_3 + \frac{1}{m} V_6$$
$$V_2 = \frac{m-2}{m} V_4 + \frac{2}{m} V_7, \qquad (I.8)$$

the expressions for the normal components of the velocity are obtained, for the first and second-order interpolation respectively, in the form:

$$V_{nB} = \left[\frac{\ell\,(m-1)}{m(\delta X+\ell)} V_3 + \frac{\ell}{m(\delta X+\ell)} V_6\right] \sin\alpha \qquad (I.9)$$

$$V_{nB}=\left[\frac{2\ell\ (m-1)}{m\ \delta X}V_3+\frac{2\ell}{m\delta X}\ V_6-\frac{\ell(m-2)(\delta X+2\ell}{m\delta X(2\delta X+\ell)}V_4\ -\ \frac{2\ell(\delta X+2\ell)}{m\delta X(2\delta X+\ell)}V_7\right]\ \sin\ \alpha$$

where complexes accompanying the cell velocities are referred as η's weighting coefficients in Tables 3.2 and 3.3.

For the tangential components of the V velocity zero and first-order interpolation is carried out. In the first case, the boundary tangential velocity is set equal to the tangential velocity at the node 1, in the second case, it is linearly interpolated using the formula (I.4), i.e.

$$V_{\tau B} = V_{\tau 1} \quad \text{and} \quad V_{\tau B} = \left(1 + \frac{b-a}{c} \right) V_{\tau 1} - \frac{b-a}{c}\ V_{\tau 2} \qquad (I.10)$$

where

$$V_{\tau 1} = V_1\ \cos\alpha \quad \text{and} \quad V_{\tau 2} = V_2\ \cos\alpha \qquad (I.11)$$

and V_1 and V_2 velocities are given in Eqn. (I.8).

Substitution of Eqn. (I.6) and (I.11) into the Eqns (I.10) yields:

$$V_{\tau B} = \left(\frac{m-1}{m}\ V_3 + \frac{1}{m}\ V_6 \right)\ \cos\alpha$$

$$V_{\tau B} =\left[\frac{2(m-1)(\delta X+\ell)}{m\delta X}\ V_3- \frac{(m-2)(\delta X+2\ell)}{m\delta X}\ V_4+ \frac{2(\delta X+\ell)}{m\delta X}\ V_6- \frac{2(\delta X+2\ell)}{m\delta X}V_7 \right]\cos\alpha \qquad (I.12)$$

for zero and first-order interpolation respectively.

For Configurations 2, 3 and 4 the boundary V velocity is derived similarly but the interpolation lengths and the velocities at nodes 1 and 2 are defined differently.

I.2 Configuration 2. V velocity

For this configuration, the cell velocities involved are V_3 and V_6 for V_1 and V_6 and V_7 for V_2. The interpolation lengths are

$$a = -\frac{\ell}{\cos\alpha}, \quad b = \frac{\delta X+\ell}{\cos\alpha}, \quad c = \frac{\delta Y}{\sin\alpha} - \frac{\delta X}{\cos\alpha} \tag{I.13}$$

The nodal velocities can be expressed by means of the m factor as:

$$\begin{aligned} V_1 &= \frac{m-1}{m} V_3 + \frac{1}{m} V_6 \\ V_2 &= (2-m)\, V_6 + (m-1)\, V_7 \end{aligned} \tag{I.14}$$

Since the expressions for a, b, and V_1 are similar to those of Configuration 1 and c and V_2 do not affect the first-order interpolated velocity, exactly the same expressions can be obtained for the normal and tangential components of the V boundary velocity in the case of linear interpolation, i.e. the first expressions in Eqns. (I.9) and (I.12). For quadratic interpolation, substitution of Eqns. (I.13) and (I.14) into Eqn.(I.7) for the normal component and into Eqn. (I.10) for the tangential component gives:

$$V_{nB} = \left\{ \frac{\ell(m\delta X+2\ell)}{m\delta X(\delta X+\ell)} V_2 + \frac{\ell}{\delta X(m-1)} \left[\frac{m\delta X+2\ell}{m(\delta X+\ell)} - \frac{(2-m)(\delta X+2\ell)}{m\delta X+\ell} \right] V_6 - \frac{\ell(\delta X+2\ell)}{\delta X(m\delta X+\ell)} V_7 \right\} \sin\alpha$$

$$V_{\tau B} = \left\{ \frac{m\delta X+2\ell}{m\delta X} V_3 + \frac{m\delta X-m(2-m)(\delta X+2\ell)+2\ell}{m(m-1)\delta X} V_6 - \frac{\delta X+2\ell}{\delta X} V_7 \right\} \cos\alpha \tag{I.15}$$

I.3 Configuration 3. V velocity

For this configuration, the initial quantities needed for derivation, are defines as:

$$a = -\frac{\ell}{\cos\alpha}\ ,\ b = \frac{\delta Y}{\sin\alpha} + \frac{\ell}{\cos\alpha}\ ,\ c = \frac{\delta X}{\cos\alpha} - \frac{\delta Y}{\sin\alpha}\ ,$$
$$V_1 = m\ V_6 + (1-m)\ V_5,$$
$$V_2 = \frac{2m-1}{m}\ V_6 + \frac{1-m}{m}\ V_9 \qquad (I.16)$$

The solutions for the boundary velocity components are obtained in the following form:

$$V_{nB} = \left[\frac{\ell(1-m)}{m\delta X+\ell}\ V_5 + \frac{m\ell}{m\delta X+\ell}\ V_6\right]\sin\alpha$$
$$V_{\tau B} = \left[(1-m)\ V_5 + m\ V_6\right]\cos\alpha \qquad (I.17)$$

for the linear interpolation of V_{nB} and zero-order interpolation of $V_{\tau B}$, and

$$V_{nB} = \left\{\frac{\ell(\delta X+2\ell)}{\delta X(m\delta X+\ell)}\ V_5 + \frac{\ell}{\delta X(1-m)}\left[\frac{m(\delta X+2\ell)}{m\delta X+\ell} - \frac{(2m-1)(m\delta X+2\ell)}{m(\delta X+\ell)}\right] V_6 - \frac{\ell(\delta X+2\ell)}{m\delta X(\delta X+\ell)}\ V_9\right\}\sin\alpha \qquad (I.18)$$

$$V_{\tau B} = \left\{\frac{m\delta X+2\ell}{m\delta X}\ V_3 + \frac{m^2(\delta X+2\ell)-(2m-1)(m\delta X+2\ell)}{m(1-m)\delta X} V_6 - \frac{m\delta X+2\ell}{m\delta X}\ V_9\right\}\cos\alpha$$

for the quadratic interpolation of V_{nB} and linear interpolation of $V_{\tau B}$.

I.4 Configuration 4. V velocity

Configuration 4, for the case of the first-order interpolation, is identical to Configuration 3, therefore, the boundary velocity

components are given by Eqn. (I.17). For the second-order interpolation, the interpolation lengths and nodal velocities are

$$a = -\frac{\ell}{\cos\alpha}\ ,\ b = \frac{\delta Y}{\sin\alpha} - \frac{\ell}{\cos\alpha}\ ,\ c = \frac{\delta Y}{\sin\alpha}$$

$$V_1 = (1-m)\ V_5 + m\ V_6 \qquad (I.19)$$

$$V_2 = (1-2m)\ V_8 + 2\ m\ V_9$$

Then, the transformations, similar as for Configuration 1, lead to the following expressions for the boundary velocity components by the second-order interpolation of the normal component:

$$V_{nB} = \left[\frac{2\ell(1-m)}{m\delta X} V_5 + \frac{2\ell}{\delta X} V_6 - \frac{\ell(1-2m)(m\delta X+2\ell)}{m\delta X(2m\delta X+\ell)} V_8 - \frac{2\ell(m\delta X+2\ell)}{\delta X(2m\delta X+\ell} V_9 \right] \sin\alpha \qquad (I.20)$$

$$V_{\tau B} = \left[\frac{2(1-m)(m\delta X+\ell)}{m\delta X} V_5 + \frac{1(m\delta X+\ell)}{\delta X} V_6 - \frac{(1-2m)(m\delta X+2\ell)}{m\delta X} V_8 - \frac{2(m\delta X+2\ell)}{\delta X} V_9 \right] \cos\alpha$$

The expression for the first-order interpolation coincides with those of Configuration 3, i.e. with Expr. (I.17).

I.5 U boundary Velocities

The derivation of U boundary velocities is quite similar to that of V velocities. However, the nodal velocity components, given by Eqn. (I.2) for the V velocity, in this case, will be expressed as:

$$U_{n1} = U_1 \cos\alpha \quad \text{and} \quad U_{n2} = U_2 \cos\alpha$$

$$U_{\tau 1} = U_1 \sin\alpha \quad \text{and} \quad U_{\tau 2} = U_2 \sin\alpha \qquad (I.21)$$

Taking into account that the interpolation lengths, a, b, and c, and the nodal velocities, U_1 and U_2, are expressed by the same equations as for the V velocity, the weighting coefficients will also be expressed by the same formulas where the length ℓ must be computed for U velocity in U-velocity grid. Also, the $\sin\alpha$ and $\cos\alpha$ will be interchanged in the expressions for U_{nB} and $U_{\tau B}$, as it is shown in Eqns.(I.21). The listing of the weighting coefficients for U boundary velocities is given in Tables 3.2 and 3.3.

APPENDIX II

THE REFLECTION TYPE BOUNDARY CONDITION ON THE LIQUID HEIGHT FOR A VERTICAL WALL

The boundary liquid height for a vertical wall can be derived from the Eqn. (2.1) rewritten in the following form

$$\frac{\partial H}{\partial t} = \frac{1}{St}\left(\bar{V} - \bar{U}\frac{\partial H}{\partial X} \right) \tag{II.1}$$

where the barred velocities are the free-surface velocities.

The symmetry of the real and fictitious flows, see Fig. 3.6, assumes for the no-slip velocity condition the following:

$$\begin{aligned} \bar{U}_B^k &= -\bar{U}_2^k \\ \bar{V}_B^k &= -\bar{V}_2^k \\ H_B^k &= H_2^k \\ \left(\frac{\partial H}{\partial X}\right)_B &= -\left(\frac{\partial H}{\partial X}\right)_2 \end{aligned} \tag{II.2}$$

From the Eqn. (II.1) written for the boundary point B in the fictious flow and for the point 2 in the real flow, the heights at the next time level (k+1), upon the substitution of the last expression of (II.2), are

$$\begin{aligned} H_B^{k+1} &= H_B^k + \frac{\delta T}{St}\left(\bar{V}_B^k + \bar{U}_B^k \frac{H_3^k - H_2^k}{\delta X} \right) \\ H_2^{k+1} &= H_2^k + \frac{\delta T}{St}\left(\bar{V}_2^k - \bar{U}_2^k \frac{H_3^k - H_2^k}{\delta X} \right) \end{aligned} \tag{II.3}$$

where the spatial and time derivatives are both approximated by forward differences. Subtracting the second equation of Eqn. (II.3) from the first one and substituting the first three expressions of (II.2) yield the following expression for the boundary height:

$$H_B^{k+1} = H_2^k - \frac{2\delta T}{St} \bar{V}_2^k \qquad \text{(II.4)}$$

For the free-slip velocity condition, the second expression of (II.2) becomes

$$\bar{V}_B^k = \bar{V}_2^k$$

and the similar procedure of derivation leads to the boundary height in the following form:

$$H_B^{k+1} = H_2^{k+1} \qquad \text{(II.5)}$$